

# **Structural and Molecular Insight of Naturally Available Small Molecule Modulators for Their Anticancer Activity *via* Targeting G-quadruplex DNA**

**Ph.D. Thesis**

By  
**ARPITA TAWANI**



**CENTRE FOR BIOSCIENCES AND BIOMEDICAL ENGINEERING  
INDIAN INSTITUTE OF TECHNOLOGY INDORE**

**FEBRUARY 2017**



# **Structural and Molecular Insight of Naturally Available Small Molecule Modulators for Their Anticancer Activity *via* Targeting G-quadruplex DNA**

**A THESIS**

*Submitted in partial fulfillment of the requirements for the award of the degree*

*of*

**DOCTOR OF PHILOSOPHY**

*by*

**ARPITA TAWANI**



**CENTRE FOR BIOSCIENCES AND BIOMEDICAL ENGINEERING  
INDIAN INSTITUTE OF TECHNOLOGY INDORE**

**FEBRUARY 2017**





# INDIAN INSTITUTE OF TECHNOLOGY INDORE

## CANDIDATE'S DECLARATION

I hereby certify that the work which is being presented in the thesis entitled **Structural and Molecular Insight of Naturally Available Small Molecule Modulators for Their Anticancer Activity via Targeting G-quadruplex DNA** in the partial fulfillment of the requirements for the award of the degree of **DOCTOR OF PHILOSOPHY** and submitted in the **CENTRE FOR BIOSCIENCES AND BIOMEDICAL ENGINEERING, Indian Institute of Technology Indore**, is an authentic record of my own work carried out during the time period from JANUARY, 2013 to FEBRUARY, 2017 under the supervision of Dr. Amit Kumar, Assistant Professor.

The matter presented in this thesis has not been submitted by me for the award of any other degree of this or any other institute.

Signature of the student with date  
(**ARPITA TAWANI**)

-----  
This is to certify that the above statement made by the candidate is correct to the best of my/our knowledge.

Signature of Thesis Supervisor with date  
(**DR. AMIT KUMAR**)

-----  
**ARPITA TAWANI** has successfully given his/her Ph.D. Oral Examination held on

Signature of Chairperson (OEB)  
Date:

Signature of External Examiner  
Date:

Signature(s) of Thesis Supervisor(s)  
Date:

Signature of PSPC Member #1  
Date:

Signature of PSPC Member #2  
Date:

Signature of Convener, DPGC  
Date:

Signature of Head of Discipline  
Date:

-----

## ACKNOWLEDGEMENTS

First and foremost, I would like to thank God, the Almighty, for His showers of blessings throughout my research work to complete the research successfully.

I would like to express my sincere gratitude to my supervisor Dr. Amit Kumar for providing me this wonderful opportunity to pursue Ph.D. in exciting field of Cancer Biology. His valuable guidance, unfailing support, motivation and immense knowledge helped me to complete this journey successfully. I am deeply indebted to him for his attention, his confidence and the freedom he gave me to do this work. Despite of his busy schedule, he was always there to listen, to understand and to give advice. His meticulous suggestions and astute criticism during the experiments helped me in developing critical thinking and made me a better researcher. He showed me various ways to approach a research problem and to be persistent for research. He taught me to write academic papers, to express my ideas and had confidence in me when I doubted myself. I would like to pay sincere thanks for his inexhaustible patience during the correction phase of my academic writing. I am really honored to be his first Ph.D. student and I could not have imagined having a better advisor and mentor for my Ph.D. study. His enthusiasm for new ideas and dedication for research has always inspired me. He is not only my Ph.D. advisor but he also took lectures in course work. I could not have found a better teacher like him who helps us in developing the basic concepts and uncovers the real world research from a confinement of classroom. I will not forget our very frequent teleconferences during which he gave me advice and encouragement. Without his coherent and illuminating instruction, this thesis would not have reached its present form.

Further, I would like to thank my PSpC members Dr. Debasis Nayak and Dr. Sharad Gupta for their valuable suggestions and support. I wish to express my sincere gratitude to Prof. Pradeep Mathur, Director, Indian Institute of Technology, Indore for his continuous encouragement, help and support in every aspect. I am deeply grateful to all members of the jury for agreeing to read the manuscript and to participate in the defense of this thesis. I am grateful to Dr. Suman Mukhopadhyay (Head, Center of Biosciences and Biomedical Engineering, IIT Indore) for his kind support in various aspects. I extend my sincere thanks to all faculty members of IIT Indore for their direct or indirect contributions to this study. I would like to express my sincere gratitude all faculty members of Centre of Biosciences and Biomedical Engineering, IIT Indore. In particular, I extend my heartfelt gratitude to Dr.

Prashant Kodgire for his insightful suggestions and encouragement that incentivize me to widen my research from various perspectives. He has always shown up as wonderful teacher during course work lectures. His lectures clear various doubts and make basis of various concepts that were utilized in research. I wish to express my gratitude to Dr. Debasis Nayak for his help in confocal microscopy experiments.

I would also like to thank technical staff from Sophisticated Instrumentation Center (SIC), IIT Indore, Ms. Sarita Batra, Mr. Kinny Pandey, Mr. Ghanshyam Bhavsar and Mr. Manish Kushwaha for their patience and timely technical support without which it was impossible to continue with my work. In particular, I want to extend my thanks to Mr. Kinny Pandey for his friendly and supportive nature and his help in the time of difficulties. I would like to extend my sincere thanks to Mr. Amit Mishra (Deputy Lab manager, BSBE, IIT Indore) for his kind nature and help in dealing with various issues regarding instruments. I would also like to thank academic authorities of IIT Indore, library staff of IIT Indore, Ms. Jaya Vakade, Mr. Prahalad Singh Panwar, Mr. Subu Jana, Mr. Nithin Bhate, and other technical and non-technical staff for their constant help, whenever required.

I personally want to extend my thanks to my batch mates and friends Ms. Camellia Sarkar, Ms. Deepika Tyagi, Mr. Rohit Kumar Rai, Mr. Bharat Parajapati, Mr. Sandeep Tiwari and Dr. Vaibhav Jain who were always there and never let me down during these Ph.D. days. I would like to thank my seniors Dr. Sonali Bhagwat, Dr. Ajai Tripathi, Mr. Anupam Das, Mr. Taksen Jhadav for their generous co-operation and help. I would like to record my thanks to my labmates Mr. Subodh Kumar Mishra, Mr. Eshan Khan, Mr. Arun Kumar Verma, Ms. Richa Agrawal, Ms. Nirali Pandya and Ms. Prativa Majee.

I would like to take an opportunity to express my respect; love and gratitude to all the teachers from Shri J.G.H.S School, Govt. Holkar Science College, School of Biotechnology, DAVV, Indore. I would express my gratitude to mentors of my previous work place Dr. H.S Parmar, Dr. D.D. Kulkarni and Dr. C.G. Joshi.

Most importantly, I owe a lot to my family. Without the support of all members of my family, I would never find the courage to finish this thesis. I deeply express my love and gratitude to my lovable father Mr. Nandkishor Tawani and my mother Mrs. Ranjna Tawani for their confidence and love and support during all these years. I would especially like to express my gratitude to my sisters Mrs. Apurva Tawani Maheshwari, Ms. Oshin Tawani, Ms. Shreya Lalawat and my brother Mr. Ishaan Tawani who were always been my strengths. I am thankful to my uncles Dr. O.P. Tawani, Dr. N.K. Dad and Mr. Praveen Lalawat for their generous suggestions, love and care. I must have to mention youngest members of our family

Ms. Ananya Maheshwari for her smiley support. I also owe to my supervisor family, in particular his wife Mrs. Amita Hiwase. She always supported me and encourages me throughout the years. I extend my love to his both of kids Mr. Shiven Kartikeya and Mr. Deven Kartikeya for their sweet love and affection.

I would like to express my thanks to IIT Indore for infrastructure and Ministry of Human Resource Development for my Fellowship and all others who helped and supported me directly or indirectly.

**ARPITA TAWANI**



*DEDICATED TO MY  
BELOVED PARENTS AND  
RESPECTED TEACHERS*

**ARPITA TAWANI**



In the last few decades, several strategies have been developed to design specific drugs for potentially malefic diseases like cancer to target them at DNA level. G-quadruplexes are secondary structures of DNA formed by a square planar arrangement of guanosines held together by Hoogsteen hydrogen bonding and stabilized by a central cation. These structures are known to be formed at various regions of human genome such as telomeres, promoter regions of certain oncogenes, immunoglobulin switch regions etc. Altogether, it could be suggested that these structures play significant roles in various biological processes including cancer. One of the mechanisms by which cancer cells reaches immortalization is the maintenance of their telomere length. This length is maintained by activity of a reverse transcriptase enzyme, telomerase, which is found to be overexpressed in cancer cells. Several lines of evidence suggested that stabilization of G-quadruplex structure at telomere could inhibit the telomerase activity of DNA elongation and subsequently lead to cellular death. Moreover, it is well-known that in 80% of cancers, there is an overexpression of various proto- oncogenes. The promoter regions of several proto-oncogenes, such as, *c-myc*, *bcl2*, *k-ras*, *ckit*, etc., are found to be enriched in guanine bases that form G-quadruplex structures. Stabilization of G-quadruplex structure at the promoter region of these proto-oncogenes could down-regulate the gene expression. Thus, the significance of these G-quadruplex structures in cancer treatment drives the exploration of small molecules that induce the formation of G-quadruplexes or that stabilize them. Over the several years, efforts have been made in the exploration of small molecules containing planar polyaromatic core that aid in stabilization of these G-quadruplexes structures and regulate the cellular processes. Till date, numerous G-quadruplex selective ligands having antitumor activity have been developed, such as anthraquinones and its derivatives, trisubstituted acridines with cationic side chains, etc. Many of these ligands have been shown to bind G-quadruplex structures and are found to be effective in inhibiting telomerase activity. As large number of these molecules is synthetic in nature, therefore, major limitations with these molecules are cytotoxicity to normal cells, other side-effects and bio-availability. Nature has provided us prodigious chemically diverse scaffolds of molecules. These naturally occurring small molecules are less toxic than synthetic molecules and have better bio-availability. However, very few natural molecules have been explored for targeting G-quadruplex structure such as telomestatin, berberine derivatives, etc. Exploring the potential of naturally available small

molecules that are readily available in our daily diets and have been known for their propitious effects on human health will lead us to enter into a new era of cancer therapy. Such group of molecule includes flavonoids, alkaloids, etc. Flavonoids are one of the major components of human diets and are widely present in the citrus fruits. They have been known to exhibit various beneficial effects on human health such as anti-oxidant, antiviral, anti-cancer, etc. Similarly, alkaloids are highly diverse group of natural compounds that have a wide distribution in the plant kingdom and these are amongst the most important active components in natural herbs. These alkaloids are known to exhibit anti-proliferative and anti-metastatic effects on various types of cancers both *in vitro* and *in vivo*.

Despite a lot of studies on these naturally available small molecules, the major cellular target of their action remains elusive. A substantial body of research has been directed towards understanding the molecular and structural basis of action and DNA sequence specificity for binding, by identifying the preferred binding sequences of many key drugs with DNA. Structural tools such as NMR spectroscopy, coupled with molecular modelling techniques have considerable impact in advancing our understanding of the microscopic structural homogeneity of DNA and the molecular basis for drug-DNA interactions.

The main objectives of present study are:

- ❖ To target the interaction of naturally available dietary small molecules with various G-quadruplex forming DNA sequences found in human genome.
- ❖ To explore the potential of these molecules as a potent anti-cancer drug candidate.

The Ph.D. thesis work has been reported in the form of six chapters.

Chapter 1 contains introduction of the subject, a comprehensive review of the literature and scope of thesis.

Chapter 2 deals with materials and methods used in the study. Basic principles of the methods used in this study were also described such as fluorescence titration experiment to understand the DNA binding for their sequence specificity and selectivity. UV-melting spectroscopy and Circular Dichroism (CD) spectroscopy were mentioned that revealed the stability of G-quadruplex structure upon binding of ligand. Time correlated single photon counting spectroscopy (TSCPC) and Isothermal Titration Calorimetry (ITC) was also discussed that provides details about mode of binding and other binding parameters. Nuclear

Magnetic Resonance Spectroscopy- 1D NMR,  $^1\text{H}$  -  $^1\text{H}$  NOESY for the proton assignment and the strategies used for energy minimization and restrained Molecular Dynamics were also discussed. Further, basis for evaluation of cytotoxicity of molecules and molecular insights for their cytotoxic effects were discussed including apoptosis assays by employing FACS and confocal microscopy.

Chapter 3 deals with the interaction of four representative flavonoids: Luteolin, Quercetin, Rutin and Genistein with human telomeric DNA  $(5'\text{-T}_2\text{AG}_3\text{T-3}')_4$  forming G-quadruplex structure. Various biophysical techniques were employed like steady-state, time-resolved fluorescence spectroscopies and circular dichroism spectroscopy to understand the various parameters of their interaction. Further, NMR spectroscopy was performed to deduce the solution structure of complex formed between human telomeric DNA forming intermolecular parallel G-quadruplex structure and Quercetin. This study aimed to achieve the structural basis for interaction and stabilization of human telomeric DNA  $(5'\text{-T}_2\text{AG}_3\text{T-3}')_4$  forming G-quadruplex structure with flavonoids. Our study revealed that all of the flavonoids used in this study bind to G-quadruplex DNA with  $\sim 100\text{-}1000$  fold higher selectivity as compared to duplex DNA. Furthermore, detailed structural studies revealed that Quercetin binds to  $(5'\text{-T}_2\text{AG}_3\text{T-3}')_4$  G-quadruplex DNA via end-stacking at the T1pT2 and G6pT7 steps. We have reported the first solution structure for the flavonoid Quercetin complexed with human telomeric G-quadruplex DNA. The coordinates of NMR model of Quercetin and  $(5'\text{-TTAGGGT-3}')_4$  complex have been deposited in the PDB as 2MS6.

Chapter 4 is focused on the interaction of 24 nucleotide c-myc promoter G-quadruplex sequence Pu24T  $(5'\text{-TGAGGGTGGTGGAGGGTGGGGAAGG-3}')$  comprising of central guanine tracks of c-myc with nine representative flavonoids: Luteolin, Quercetin, Rutin, Genistein, Kaempferol, Hesperidin, Daidzein, Myricetin and Puerarin. The binding properties of flavonoids with c-myc DNA gives Quercetin as a lead molecule showing highest affinity for c-myc DNA among other flavonoids and high specificity for G-quadruplex DNA structure over duplex DNA. Steady-state, time-resolved fluorescence spectroscopy and isothermal titration calorimetry results suggested that Quercetin binds to Pu24T DNA in 2:1 stoichiometry. Our study highlighted the structural aspects of binding of Quercetin to c-myc promoter sequence forming G-quadruplex structure. Herein, we report the first solution structure of Quercetin-c-myc G-quadruplex complex in which Quercetin stacks at 5' and 3' G-tetrads of Pu24T G-quadruplex DNA structure and stabilize it via  $\pi\text{-}\pi$  stacking. The coordinates of NMR model of Quercetin and Pu24T complex have been deposited in the

PDB as 2N6C. Moreover, the stabilization of G-quadruplex structure upon binding of Quercetin was validated by PCR stop assay that shows the inhibition of *Taq Polymerase* activity. Further, the biological activity of Quercetin was assessed in HeLa cells that showed its subcellular localization in nucleus. It inhibits the cell growth by inducing apoptosis and down-regulates c-myc gene expression in cancer cell.

Chapter 5 deals with interaction of Piperine with three biologically significant DNA sequence forming G-quadruplex structure viz. human telomeric DNA tel22, (d-5'-AGGGTTAGGGTTAGGGTTAGGG-3'), promoter region of c-kit21 (d-5'-CGGGCGGGCGCGAGGGAGGGG-3') and c-myc promoter G-quadruplex sequence Pu24T (5'-TGAGGGTGGTGGAGGGTGGGGAAGG-3'). In order to understand this interaction, various biophysical techniques were employed such as circular dichroism, DNA melting studies, steady-state and time-resolved fluorescence spectroscopy. The binding parameters suggested that Piperine has highest affinity for c-myc DNA, with specificity and it stabilizes the G- quadruplex structure. This study is further supported by proton NMR spectroscopy, docking and molecular modelling analysis to understand the dynamics of Piperine-Pu24T DNA interaction that suggested that Piperine stacks at 5' and 3' G-tetrads of Pu24T G-quadruplex DNA structure and stabilize it via  $\pi$ - $\pi$  stacking and hydrogen bonding. Furthermore; *in vitro* studies were employed to understand the cytotoxic effects of Piperine on various cancer cell lines, explored its mechanism of action on human lung carcinoma (A549) cell lines and established its potential to down-regulate c-myc gene expression in cancer cells. This is the first study for the interaction of ding of Piperine, a natural alkaloid, with various human G-quadruplex DNA sequences. Altogether this study gives us an idea of anti-proliferative and pro-apoptotic nature of Piperine and suggested that Piperine could exert its anti-cancer activity by stabilizing G-quadruplex structure formed at c-myc promoter region and down regulates its expression in cancer cells.

Chapter 6 contains the conclusions of the work done in the thesis and future prospective of the study.

### List of Publications from Thesis:

1. **Arpita Tawani** and Amit Kumar\*, (2016) Structural insight for the recognition of G-quadruplex structure at human c-myc promoter sequence by flavonoid Quercetin, *Sci. Rep.*, *x*, 38192. (Under revision)
2. **Arpita Tawani**, Ayeman Amanullah, Amit Mishra and Amit Kumar\*, (2016) Evidences for Piperine inhibiting cancer by targeting human G-quadruplex DNA sequences, *Sci. Rep.*, *6*, 39239 (DOI: :10.1038/srep39239)
3. **Arpita Tawani** and Amit Kumar\*, (2015) Structural Insight into the interaction of Flavonoids with Human Telomeric Sequence, *Sci. Rep.*, *5*, 17574 (DOI: 10.1038/srep17574)

### List of other publications:

4. Subodh Kumar Mishra, **Arpita Tawani**, Amit Mishra, and Amit Kumar\*, (2016) G4IPDB: A database for G-quadruplex structure forming nucleic acid interacting proteins, *Sci. Rep.*, *6*, 38144 (DOI: 10.1038/srep38144).
5. **Arpita Tawani** and Amit Kumar\*, (2015) Structural Insights Reveal the Dynamics of the Repeating r(CAG) Transcript Found in Huntington's Disease (HD) and Spinocerebellar Ataxias (SCAs), *PloS one*, *10*, e0131788 (DOI: 10.1371/journal.pone.0131788. eCollection 2015).

### List of structures submitted to PDB:

1. **2MS6**: Human Telomeric G-quadruplex DNA sequence (TTAGGGT)<sub>4</sub> complexed with Flavonoid Quercetin.
2. **2MS5**: Structural dynamics of double-helical RNA having CAG motif.
3. **4YN6**: Structural Insight reveals dynamics in repeating r(CAG) transcript found in Huntington's disease (HD) and Spinocerebellar ataxias (SCAs).
4. **2N6C**: Solution structure for quercetin complexed with c-myc G-quadruplex DNA.

### List of Conference (Oral/Poster) Presentations:

**Arpita Tawani**, Ritvija Agrawal and Amit Kumar\*. Oral Presentation on “Structural Insight reveals dynamics in repeating r(CAG) transcript found in Huntington’s disease (HD) and Spinocerebellar ataxias (SCAs)” at the International Conference on Biomolecular Simulations and Dynamics 2013, being organized by IIT Madras from 28<sup>th</sup> - 30<sup>th</sup> November 2013.

# TABLE OF CONTENTS

<b>1. List of Figures</b>	<b>xvii</b>
<b>2. List of Tables</b>	<b>xxvii</b>
<b>3. Acronyms</b>	<b>xxix</b>
<b>4. Nomenclatures</b>	<b>xxxiii</b>
<b>Chapter 1. Introduction and Literature review</b>	<b>1-42</b>
1.1 Nucleic Acids	1
1.2 G-quadruplex DNA	3
1.2.1 G-quadruplex Structure	3
1.2.2 Topologies of G-quadruplex DNA	4
1.2.3 Presence and significance of G-quadruplex DNA in human Genome	6
1.2.3.1 In-silico evidences for the presence of G-quadruplex DNA structures	6
1.2.3.2 Human telomeres	7
1.2.3.3 Promoter regions of genes	9
1.2.4 G-quadruplex DNA as target for anticancer drugs	10
1.3 Drug- DNA interaction	14
1.3.1 Different class of drugs that interact with DNA	15
1.3.2 Basis of DNA- Drug interactions	22
1.3.3 Modes of binding	23
1.3.3.1 Covalent DNA binding	23
1.3.3.2 Non-covalent DNA binding	23
1.3.4 Forces governing Drug-DNA interaction	25
1.3.4.1 Hydrogen bonding	25
1.3.4.2 Electrostatic forces: Salt bridge	25
1.3.4.3 Entropic Forces: Hydrophobic effect	25
1.3.4.4 Base stacking: Dispersion forces	26
1.4 Aim of thesis	26
1.5 Organization of thesis	27
1.6 Scope of thesis	28

1.7 References	29
<b>Chapter 2. Material, methods and instrumentation</b>	<b>43-72</b>
2.1 Material	43
2.2 Preparation of samples	44
2.2.1 Sample preparation for UV-melting, steady state and time resolved fluorescence spectroscopy, circular dichroism studies and isothermal calorimetry	44
2.2.2 Sample preparation for NMR studies	44
2.3 Methodology and instrumentation	49
2.3.1 Fluorescence spectroscopy	49
2.3.2 Time Correlated Single-Photon Counting	51
2.3.3 Circular Dichroism spectroscopy	53
2.3.4. Thermal melting experiments using absorption spectroscopy	53
2.3.5. Isothermal Titration Calorimetry	54
2.3.6 NMR spectroscopy	55
2.3.6.1 Two-dimensional NMR techniques	59
2.3.6.1.1 Nuclear Overhauser Effect spectroscopy	59
2.3.6.1.2 Determination of three-dimensional structure	60
2.3.7 Restrained molecular dynamics and simulated annealing	62
2.3.8. Docking studies and molecular modelling simulation	63
2.3.9 Polymerase Chain Reaction stop assay	63
2.3.10 Gel mobility shift assay	65
2.3.11 Cytotoxicity test with MTT	66
2.3.12 Semi-quantitative RT PCR analysis	66
2.3.13 DNA Fragmentation, TUNEL assay, morphological evaluation and FACS analysis of apoptosis	68
2.4 References	69
<b>Chapter 3. Structural Insight into the interaction of Flavonoids with Human Telomeric Sequence</b>	<b>73-116</b>
3.1 Introduction	73
3.2 Results and Discussion	76
3.2.1 Fluorescence spectroscopic studies	76

3.2.1.1 Steady state fluorescence studies	76
3.2.1.2 Time resolved fluorescence studies	82
3.2.2 Circular Dichroism spectroscopy	86
3.2.3 Nuclear Magnetic Resonance spectroscopy	86
3.2.3.1 One dimensional proton NMR studies	86
3.2.3.1.1 Assessment of G-quadruplex structure formation	89
3.2.3.1.2 One –Dimensional proton NMR titration studies	89
3.2.3.1.2.1 Temperature dependent one–dimensional proton NMR studies	91
3.2.3.2 Two dimensional NMR spectroscopy	95
3.2.3.3 Restrained molecular dynamics studies	101
3.3 Conclusion	106
3.4 Material and methods	107
3.4.1 Reagents	107
3.4.2 Fluorescence titrations	108
3.4.3 Circular Dichroism	108
3.4.4 Time-resolved fluorescence measurements	109
3.4.5 Nuclear Magnetic Resonance	109
3.4.6 Restrained molecular dynamics studies	110
3.5 References	110
<b>Chapter 4. Structural insight for the recognition of G-quadruplex Structure at human c-myc promoter sequence by flavonoid Quercetin</b>	<b>117-172</b>
4.1 Introduction	117
4.2 Results and Discussion	118
4.2.1 Steady state fluorescence spectroscopic studies	118
4.2.2 Isothermal Titration Calorimetry studies	126
4.2.3 Time resolved fluorescence studies	131
4.2.4 Circular Dichroism studies	134
4.2.5 Nuclear Magnetic Resonance studies	134
4.2.5.1 One dimensional proton NMR studies	134
4.2.5.1.1 Assessment of G-quadruplex structure formation	136

4.2.5.1.2 One –Dimensional proton NMR titration studies	136
4.2.5.2 Two dimensional proton NMR studies	141
4.2.5.3 Restrained molecular dynamics studies	147
4.2.4 Assessment of biological activity of Quercetin	156
4.2.4.1 Evaluation of cytotoxicity and mechanism of action	156
4.2.4.2 Semi quantitative reverse transcriptase PCR	157
4.2.4.3 PCR stop assay	157
4.2.4.4 Luciferase assay	162
4.3 Conclusions	162
4.4 Material and methods	163
4.4.1 Reagents and cell lines	163
4.4.2 Fluorescence titrations	163
4.4.3 Isothermal titration calorimetry experiment	164
4.4.4 Time-resolved fluorescence measurements	164
4.4.5 Circular Dichroism	165
4.4.6 Nuclear Magnetic Resonance	165
4.4.7 Restrained molecular dynamics studies	165
4.4.8 PCR stop assay	166
4.4.9 MTT assay	166
4.4.10 Confocal microscopy for localization of Quercetin in cells	167
4.4.11 Semi-quantitative RT PCR analysis	167
4.5 References	167

## **Chapter 5. Evidences for Piperine inhibiting cancer by targeting human**

<b>G-quadruplex DNA sequences</b>	<b>173-225</b>
5.1 Introduction	173
5.2 Results and Discussion	176
5.2.1 Fluorescence spectroscopic studies	176
5.2.1.1 Steady state fluorescence studies	176
5.2.1.2 Time-resolved fluorescence studies	179
5.2.2 UV -Thermal denaturation studies	183
5.2.3 Circular Dichroism studies	186
5.2.4 Nuclear Magnetic Resonance studies	189
5.2.4.1 One dimensional proton NMR studies	189

5.2.4.1.1 Assessment of G-quadruplex structure formation	189
5.2.4.1.2 Temperature dependent one –dimensional proton NMR studies	189
5.2.4.1.3 One –dimensional proton NMR titration studies	191
5.2.5 Docking and modelling studies	197
5.2.6 Assessment of biological activity of Piperine	203
5.2.6.1 Gel retardation assay	203
5.2.6.2 PCR stop assay	205
5.2.7 Cytotoxic effects of Piperine on cancer cells	205
5.2.7.1 Evaluation of apoptosis	205
5.2.7.2 Semi- quantitative RT-PCR	212
5.3 Conclusion	212
5.4 Methods	214
5.4.1 Reagents and cell lines	214
5.4.2 Fluorescence titrations	215
5.4.3 Time-resolved fluorescence measurements	216
5.4.4 DNA thermal denaturation experiments	216
5.4.5 Circular Dichroism	216
5.4.6 Nuclear Magnetic Resonance	216
5.4.7 Docking and molecular dynamics simulation	217
5.4.8 Gel mobility shift assay	217
5.4.9 Cell culture, DNA fragmentation, TUNEL assay, morphological evaluation and FACS analysis of apoptosis	218
5.5 References	218
<b>Chapter 6. Conclusion and scope for future work</b>	<b>227-230</b>
6.1 Conclusions	227
6.2 Future prospective	229

# LIST OF FIGURES

## Chapter 1. Introduction and Literature review

- Figure 1.1. Molecular structure of (a) purines (b) pyrimidines (c) five membered furanose ring of ribose and deoxyribose sugar 2
- Figure 1.2. G-quadruplex structures (a) G-quartets or G-tetrads formed by square planar arrangement of four guanines bonded by Watson-Crick as well as Hoogsteen hydrogen bonding (N1–N6 and N2–N7) (b) G-quartets stack on top of one another (c) Schematic presentation of formation of G-quadruplex structure 4
- Figure 1.3. Structural polymorphism of G-quadruplex structures showing parallel and anti-parallel G-quadruplex topologies 5
- Figure 1.4. Location of G-quadruplex structures forming DNA sequences in various regions of human genome (a) telomeric region (b) promoter region of gene (c) NHEIII1 region of c-myc promoter gene 8
- Figure 1.5. Schematic representation of stabilization of G-quadruplex structure formed at telomere by G-quadruplex binding ligands (yellow) 12
- Figure 1.6. Schematic representation of stabilization of G-quadruplex structure formed at promoter region G-quadruplex binding ligands (yellow) 13
- Figure 1.7. Chemical structure of various DNA binders 17
- Figure 1.8. Chemical structure of (a) Flavonoids (b) Piperine 20

## Chapter 2. Material, methods and instrumentation

- Figure 2.1. Jablonski diagram showing the excitation of molecule and a time scale of photophysical processes for fluorophore 50
- Figure 2.2. Principle of TCSPC showing histogram for start and stop signals 52
- Figure 2.3. (a) Energy levels for a nucleus with spin quantum number  $\frac{1}{2}$  (b) Precessional motion by the nucleus spinning on its axis in presence of the external magnetic field (c) Flipping of the magnetic moment on absorption of the radiations 57
- Figure 2.4. Principle of PCR stop assay 64
- Figure 2.5. Principle of MTT assay 67

### Chapter 3. Structural Insight into the interaction of Flavonoids with Human Telomeric Sequence

- Figure 3.1. Chemical structure of flavonoids (a) Luteolin, Quercetin, Rutin (b) Genistein 75
- Figure 3.2. Fluorescence titration curve of flavonoids as a function of Tel7G-quadruplex DNA concentration (a) Luteolin (b) Quercetin (c) Rutin (d) Genistein. Solid lines represent fit according to the ligand binding two site saturation. Value of Binding constant(s) ( $K_d$ ) are indicated at the top left side of the plot. The normalized data was plotted for Genistein, as it shows quenching 77
- Figure 3.3. Fluorescence titration curve of flavonoids as a function of CT-DNA concentration (a) Luteolin (b) Quercetin (c) Rutin (d) Genistein. Solid lines represent fit according to the ligand binding two site saturation. Value of Binding constant(s) ( $K_d$ ) are indicated at the top left side of the plot. The normalized data was plotted for Genistein, as it shows quenching 78
- Figure 3.4. Fluorescence titration curve of Quercetin as a function of various G-quadruplex DNA concentration (a) tel22 DNA (b) c-myc DNA (c) c-kit21 DNA. Solid lines represent fit according to the ligand binding two site saturation. Value of Binding constant(s) ( $K_d$ ) are indicated at the top left side of the plot 80
- Figure 3.5. Fluorescence lifetime decay curve of flavonoids and their complex with Tel7 G-quadruplex DNA at D/N = 2.0 for (a) Luteolin (b) Quercetin (c) Rutin (d) Genistein 85
- Figure 3.6. Circular Dichroism titration spectrum for free DNA (straight line) and in the presence of (a) Luteolin (b) Quercetin (c) Rutin (d) Genistein (dotted line); at D/N = 2.0 ratio 87
- Figure 3.7. One dimensional proton NMR spectra of 200  $\mu$ M flavonoids and their titration with increasing concentration of Tel7 DNA (a) Luteolin (b) Quercetin (c) Rutin (d) Genistein 88
- Figure 3.8. NMR spectra for Quercetin and Tel7 DNA complex monitored by imino region as a function of ligand/DNA ratio at 298 K 90
- Figure 3.9. One dimensional proton NMR spectra for Quercetin and Tel7 DNA complex monitored by base proton and H1' region as a function of

- (a) increasing concentration of Quercetin upto D/N = 1.0 ratio at 298 K (b) temperature at D/N = 1.0 ratio. Proton resonances from Quercetin are marked with asterisk 92
- Figure 3.10. NMR spectra for Quercetin and Tel7 DNA complex monitored by imino region as a function at temperature at (a) D/N = 0.0 (b) D/N = 2.0 ratio 93
- Figure 3.11. Portion of 200ms NOESY spectrum of Quercetin - Tel7 DNA complex showing (a) NH-NH NOEs between adjacent G-tetrads at 298 K at D/N = 1.0 (b) Free and bound NH signals due to Drug-DNA complex formation at 318 K at D/N = 1.0 ratio 96
- Figure 3.12. Expansion of NOESY spectrum of (a) unbounded Tel7 DNA showing good stacking interactions of G4NH-A3H2 (b) Quercetin complexed with Tel7 DNA at D/N = 1.0 showing the absence of G4NH-A3H2 NOE and presence of G5NH-G6H8 NOE illustrating perturbations in stacking interaction of G and A-tetrads 97
- Figure 3.13. Expansion of NOESY spectrum of Tel7 DNA complexed with Quercetin showing loss of sequential connectivity between T1H1'-T2H6 in drug-DNA complex at D/N = 1.0 ratio 98
- Figure 3.14. Portion of 200ms NOESY spectrum of Quercetin – Tel7 DNA complex at D/N=2.0 ratio showing intramolecular cross peak within Quercetin and intermolecular cross peaks of Quercetin H2', H6', H8, H6 with Tel7 G-quadruplex DNA 99
- Figure 3.15. Quercetin and Tel7 DNA complex at D/N = 2.0 ratio. (a) Schematic representation showing Quercetin (yellow) stacking at the T1pT2 and G6pT7 steps. Potassium ions (orange) are bound at the GpG steps (PDB Code: 2MS6) (b) Energy minimised model of Quercetin and Tel7 DNA complex showing Quercetin end-stacks at the T1pT2 and G6pT7 steps. The four strands of Tel7 DNA are shown in red, green, cyan and magenta color (c) Ensemble of five lowest energy structures after restrained molecular dynamics (rMD) simulation showing the position of Quercetin at the T1pT2 (top) and G6pT7 steps (bottom) of Tel7 G-quadruplex DNA. The four strands of Tel7 DNA are shown in red, green, cyan and orange color 102

Figure 3.16. Interaction of Quercetin at (a) T1/T2 (b) G6/T7 base steps of Tel7 G-quadruplex DNA. Green dots represent the hydrogen bonds 103

#### **Chapter 4. Structural insight for the recognition of G-quadruplex structure at human c-myc promoter sequence by flavonoid Quercetin**

Figure 4.1. Chemical structure of flavonoids showing flavones, flavonols, flavanones (left side) and isoflavanols (Right side). Ring A- benzoyl system, Ring B- cinnamoyl system 119

Figure 4.2. Fluorescence titration curve of flavonoids as a function of Pu24T G-quadruplex DNA concentration (a) Quercetin (b) Luteolin (c) Rutin (d) Kaempferol (e) Puerarin (f) Hesperidin (g) Myricetin (h) Daidzein. Solid lines represent best fit according to the ligand binding two site saturation. Values of binding constant(s) ( $K_d$ ) are indicated at the bottom right side of the plot 121

Figure 4.3. Fluorescence titration curve of flavonoids as a function of CT-DNA concentration (a) Quercetin (b) Luteolin (c) Rutin (d) Kaempferol (e) Puerarin (f) Hesperidin (g) Myricetin (h) Daidzein. Solid lines represent best fit according to the ligand binding two site saturation. Values of binding constant(s) ( $K_d$ ) are indicated at the bottom right side of the plot 122

Figure 4.4. Fluorescence titration curve of Quercetin as a function of various G-quadruplex DNA concentration (a) c-kit21 DNA (b) T<sub>2</sub>AG<sub>3</sub>T DNA (in presence of Na<sup>+</sup> ions forming anti –parallel structure). Solid lines represent best fit according to the ligand binding two site saturation. Values of binding constant(s) ( $K_d$ ) are indicated at the bottom right side of the plot 124

Figure 4.5. (a-d) Isothermal Titration Calorimetry data (points) for various flavonoids binding to Pu24T G-quadruplex DNA at 25°C (a) Quercetin (b) Luteolin (c) Rutin (d) Kaempferol. Solid line represents the fitted data results from two site binding mode 127

Figure 4.5. (e-h) Isothermal Titration Calorimetry data (points) for various flavonoids binding to Pu24T G-quadruplex DNA at 25°C (e) Puerarin (f) Hesperidin (g) Myricetin (h) Daidzein. Solid line represents the fitted data results from two site binding mode 128

- Figure 4.6. Fluorescence life time decay curve of 40.0  $\mu\text{M}$  free Quercetin (Blue) and its complex with Pu24T DNA at D/N ratio = 2.0 (Red). D= Quercetin; N= Pu24T 132
- Figure 4.7. Circular Dichroism titration spectrum for free Pu24T (Red) and in the presence of Quercetin as a function of Quercetin concentration at D/N ratio = 0.5 to D/N ratio = 2.0. D= Quercetin; N= Pu24T 135
- Figure 4.8. One dimensional proton NMR spectra of 200  $\mu\text{M}$  Quercetin and its titration with increasing concentration of Pu24T DNA from D: N = 100: 0 to 100:1 137
- Figure 4.9. One dimensional proton spectra for Quercetin - Pu24T complex monitored by imino region as a function of D/N ratio at 298 K (Changes in the chemical shift for G4, G13, G24, G17 were followed by blue dotted lines from D/N = 0.0 to D/N = 2.0 and broadening of G20 was marked as asterisk) 139
- Figure 4.10. One dimensional proton spectra for Quercetin - Pu24T complex monitored by base (a) as a function of D/N ratio at 298 K (Changes in the chemical shift for G4, G2, G24 were followed by blue dotted lines from D/N = 0.0 to D/N = 2.0 (b) Interaction of Quercetin with Pu24T showing proton resonances from Quercetin (LH6' and LH8) 140
- Figure 4.11. Portion of NOESY spectrum of Quercetin – Pu24T complex showing NH-NH NOEs between adjacent G-tetrads at 298 K at D/N ratio = 0.0 (top) and 2.0 (bottom). (Dash lines show the sequential connectivity) 144
- Figure 4.12. NOE cross peaks of Quercetin – Pu24T complex at D/N = 2.0. Various regions of NOESY spectrum showing intermolecular cross-peaks between Quercetin and Pu24T DNA 145
- Figure 4.13. (a-b) Quercetin and Pu24T complex at D/N = 2.0 (a) Lowest potential energy model of the complex after rMD simulation. Black dashes showing hydrogen bond formed between Quercetin (red) and Pu24T DNA. All the three G-tetrads are shown in blue and rest nucleotides are shown in cyan color, DNA backbone is shown in worm-representation. (b) Ensemble of ten lowest energy

structures after restrained molecular dynamics simulation (PDB Code: 2N6C)	150
Figure 4.13. (c) Schematic representation showing Quercetin (red) stacking at 5' G-tetrad and the 3' G-tetrad of Pu24T G-quadruplex DNA	151
Figure 4.14. Quercetin interacting with Pu24T c-myc G-quadruplex DNA via $\pi$ - $\pi$ stacking interaction with 5' G-tetrad (a) top view (b) side view	152
Figure 4.15. Quercetin interacting with Pu24T G-quadruplex DNA via $\pi$ - $\pi$ stacking interaction with 3' G-tetrad (a) top view (b) side view	153
Figure 4.16. Quercetin interacting with Pu24T G-quadruplex DNA by formation of hydrogen bonds with (a) G-20 (b) A12	154
Figure 4.17. Quercetin interacting with Pu24T c-myc G-quadruplex DNA by stacking (a) above the top G-tetrad (b) below the bottom G-tetrad	155
Figure 4.18. Cell viability was measured by MTT assay after 48 h (a) HeLa cells (b) HEK cells (c) Morphological changes observed under confocal microscope for Quercetin (100 $\mu$ M for 4 hr) treated HeLa cells followed by DAPI staining (Arrow indicates the apoptotic cells) (d) Morphological changes in Quercetin treated HeLa cells as compared to control cells monitored under phase contrast microscope	158
Figure 4.19. Confocal images of control HeLa cells stained with DAPI for monitoring co-localization of Quercetin inside nucleus of the cell detected by its autofluorescence (a) Quercetin treated cells (b) Control cells.	159
Figure 4.20. (a) Representative semi-quantitative RT-PCR analysis. $\beta$ -actin was used as internal control (b) Polymerase stop assay for determination of the effect of Quercetin on stabilization of Pu24T G-quadruplex DNA with increasing concentrations of Quercetin as shown	160
Figure 4.21. Luciferase activity assay for monitoring the effect of Quercetin on c-MYC promoter activity	161

## **Chapter 5. Evidences for Piperine inhibiting cancer by targeting human G-quadruplex DNA sequences**

Figure 5.1. Chemical structure of Piperine	175
Figure 5.2. Fluorescence titration curve of Piperine as a function of various DNA concentration; Red: Pu24T; Blue: tel22; Green: c-kit21; Black: CT-DNA. Solid lines represent fit according to the ligand binding two site saturation	177
Figure 5.3. (a) Fluorescence life time decay curve of 40.0 $\mu$ M Piperine (Black) and its complex with Pu24T G-quadruplex DNA at D/N ratio = 1.0 (Red) and D/N ratio = 2.0 (Green)	180
Figure 5.3. (b) Fluorescence life time decay curve of 40.0 $\mu$ M Piperine (Black) and its complex with tel22 G-quadruplex DNA at D/N ratio = 1.0 (Red) and D/N ratio = 2.0 (Green)	180
Figure 5.3. (c) Fluorescence life time decay curve of 40.0 $\mu$ M Piperine (Black) and its complex with ckit21 G-quadruplex DNA at D/N ratio = 1.0 (Red) and D/N ratio = 2.0 (Green)	181
Figure 5.3. (d) Fluorescence life time decay curve of 40.0 $\mu$ M Piperine (Black) and its complex with CT-DNA at D/N ratio = 1.0 (Red) and D/N ratio = 2.0 (Green)	181
Figure 5.4. UV- thermal denaturation profile of (a) Pu24T G-quadruplex DNA, (b) tel22 G-quadruplex DNA (c) c-kit21 G-quadruplex DNA in the absence (black) and presence of Piperine upto D/N = 2.0	184
Figure 5.5. Circular Dichroism titration spectrum for free G-quadruplex DNA (Red) (a) Pu24T (b) tel22 (c) c-kit21 and in the presence of Piperine as a function of increasing concentration of Piperine up to D/N ratio = 2.0	187
Figure 5.6. Induced Circular Dichroism spectrum for free Pu24T (Black) and in the presence of Piperine as a function of increasing concentration of Piperine up to D/N ratio = 10.0. Bottom image showing magnified ICD signals	188
Figure 5.7. One dimensional proton NMR titration of 400 $\mu$ M of Piperine with increasing concentration of Pu24T. Changes in perturbation of resonances were marked with asterisk. Chemical structure of Piperine is shown above the NMR spectra with numbered assigned protons	190

Figure 5.8. <sup>1</sup> H NMR spectra showing interaction of Piperine with Pu24T monitored by imino region as a function of temperature at various D/N ratio (a) 0.0 (b) 1.0 (c) 2.0	192
Figure 5.9. <sup>1</sup> H NMR spectra showing interaction of Piperine with Pu24T monitored by base region as a function of temperature at various D/N ratio (a) 0.0 (b) 1.0 (c) 2.0	193
Figure 5.10. One dimensional proton spectra for Piperine and Pu24T complex as a function of ligand/DNA (D/N) ratio at 298 K monitored by (a) Imino region (b) Base region	194
Figure 5.11. Expansion of NOESY spectra showing imino region for Piperine and Pu24 DNA as a function of D/N ratio (a) D/N = 0.0 (b) D/N = 2.0 at 298 K	195
Figure 5.12. Expansion of NOESY spectra showing base region for Piperine and Pu24 DNA as a function of D/N ratio (a) D/N = 0.0 (b) D/N = 2.0 at 298 K	196
Figure 5.13. Stable conformation of Piperine with Pu24T obtained from docking by Autodock 4.0 in which Piperine is shown in yellow color as ball stick representation. Black dotted lines showing hydrogen bonds between Piperine and Pu24T DNA	198
Figure 5.14. Representation of docked structure of complex obtained from docking by Autodock 4.0 showing $\pi$ - $\pi$ interactions (orange colored line) between Piperine (cyan) and G-tetrads (green) of Pu24T for both the sites (a) Top (b) Bottom	199
Figure 5.15. Representation of hydrogen bond (green) formation between G18 nucleotide and Piperine molecule (Yellow) as obtained from molecular dynamic simulation studies	200
Figure 5.16. (a) Lowest potential energy model of the complex obtained after molecular dynamic simulation. Black dashes showing hydrogen bond formed between Piperine (yellow) and Pu24T (G-tetrads are shown in blue color) (b) Ensemble of ten lowest energy structures after molecular dynamics simulation (Piperine: yellow color, Pu24T: ice blue color)	201

Figure 5.16. (c) Schematic representation showing Piperine (yellow) stacking at the top G-tetrad and below the bottom G-tetrad of Pu24T DNA sequence forming G-quadruplex structure	202
Figure 5.17. Native PAGE image for gel retardation assay of (a) Pu24T (b) ckit21 DNA (c) tel22 G-quadruplex DNA incubated with increasing concentration of Piperine	204
Figure 5.18. Gel retardation assay of complimentary sequence of Pu24T that does not forms G-quadruplex structure incubated with increasing concentration of Piperine. No significant shift in the mobility of DNA bands was observed	204
Figure 5.19. PCR stop assay for Pu24T incubated with increasing concentration of Piperine	206
Figure 5.20. (a-d) Exposure to Piperine results in reduced cell viability and apoptosis in A549 cells. (a-b) Bright field images for cells treated with Piperine in (a) concentration (b) time dependent manner. (c-d) Quantitative analysis of cell counting done using bright field images of cells treated with Piperine in (c) concentration (d) time dependent manner	207
Figure 5.20. (e-h) Apoptosis was assessed in A549 cells, by flow cytometry analysis, using Annexin V-FITC and Propidium Iodide double staining. Cells were treated with 250 $\mu$ M Piperine for (e) 24 hrs (f) 48 hrs (g) DMSO was used as control (h) Apoptosis analysis shown in bar graphs	208
Figure 5.20. (i-k) (i) Nuclear morphology of Piperine treated cells was observed using DAPI staining. (j-k) DNA fragmentation was assessed in Piperine treated cells as shown in agarose gel (j) TUNEL assay (k) DNA fragmentation confirmation	209
Figure 5.21. (a) Cytotoxic effect of Piperine on MCF-7 cancer cell line. IC <sub>50</sub> value is mentioned at the bottom of plot	210
Figure 5.21. (b) Cytotoxic effect of Piperine on PC3 cancer cell line. IC <sub>50</sub> value is mentioned at the bottom of plot	210
Figure 5.21. (c) Cytotoxic effect of Piperine on HepG2 cancer cell line. IC <sub>50</sub> value is mentioned at the bottom of plot.	

Figure 5.21. (d) Cytotoxic effect of Piperine on HeLa cancer cell line. IC <sub>50</sub> value is mentioned at the bottom of plot	211
Figure 5.22. Representative of semi-quantitative RT-PCR analysis. $\beta$ -actin was used as internal control	213

# LIST OF TABLES

## Chapter 1. Introduction and Literature review

Table 1.1. Classification of bioflavonoids with their dietary source	21
--	----

## Chapter 2. Material, methods and instrumentation

Table 2.1. List of oligonucleotides with their molar extinction coefficient	45
Table 2.2. Various concentration ratios (D/N) for the complex formed between Quercetin and d-(T <sub>2</sub> AG <sub>3</sub> T) <sub>4</sub>	46
Table 2.3. Various concentration ratios (D/N) for the complex formed between Quercetin and Pu24T DNA	47
Table 2.4. Various concentration ratios (D/N) for the complex formed between Piperine and Pu24T DNA	48

## Chapter 3. Structural Insight into the interaction of Flavonoids with Human Telomeric Sequence

Table 3.1. Binding constant ( $K_d$ , (M)) values of flavonoids with G-quadruplex DNA in comparison to CT-DNA	79
Table 3.2. Binding constant ( $K_d$ , (M)) values of Quercetin with various G-quadruplex forming DNA sequences	81
Table 3.3. Life time fluorescence decay parameters for flavonoids and their D/N = 2:1 complex with Tel7G-quadruplex DNA at 298 K	85
Table 3.4. Relative intensity of intermolecular NOE connectivity between Tel7 DNA and Quercetin in the complex at D/N=2.0 from NOESY spectra at 298K	100
Table 3.5. NMR statistics for complex formed between Quercetin and Tel7G-quadruplex DNA	104
Table 3.6. Energy terms (kcal mol <sup>-1</sup> ) for initial structure and final rMD structure	105

## Chapter 4. Structural insight for the recognition of G-quadruplex structure at human c-myc promoter sequence by flavonoid Quercetin

Table 4.1. Binding constant ( $K_d$ , (M)) values of flavonoids with G-quadruplex DNA in comparison to CT-DNA	123
---	-----

Table 4.2. Binding constant ( $K_d(M)$ ) values of Quercetin with various G-quadruplex DNA	125
Table 4.3. Thermodynamic and energetics data for the interaction flavonoids with Pu24T DNA as obtained from ITC experiment	129
Table 4.4. Detailed thermodynamic and energetics data for the interaction Quercetin with Pu24T DNA as obtained from ITC experiment	130
Table 4.5. Life time fluorescence decay parameters for Quercetin and its D/N = 2:1 complex with Pu24T DNA at 298 K	133
Table 4.6. Proton chemical shift table for Pu24T-c-myc DNA and Quercetin complex at D/N = 2.0	143
Table 4.7. Relative intensity of intermolecular NOE connectivity between Pu24T and Quercetin in complex at D/N=2.0 from NOESY spectra at 298K	146
Table 4.8. Energy terms ( $kcal\ mol^{-1}$ ) for starting structure and final rMD structure	148
Table 4.9. Statistics of the solution structure of Quercetin- Pu24T complex	149

## **Chapter 5. Evidences for Piperine inhibiting cancer by targeting human G-quadruplex DNA sequences**

Table 5.1. Binding constant ( $K_d(M)$ ) values of Piperine with DNA	178
Table 5.2. Life time fluorescence decay parameters for Piperine and its complex with various DNA at D/N = 2:1 collected at 298K	182
Table 5.3. Values of melting temperature of G-quadruplex DNA in absence and presence of Piperine	185

## ACRONYMS

DNA	Deoxyribonucleic acid
RNA	Ribonucleic acid
A	Adenine
G	Guanine
C	Cytosine
T	Thymine
U	Uracil
PQS	Putative quadruplex sequences
TSS	Transcription start sites
DHS	Dnase I hypersensitive sites
hTERT	Human Telomerase reverse transcriptase
NMR	Nuclear magnetic resonance
PDB	Protein data bank
NHE	Nuclear hypersensitive element
GIST	Gastrointestinal stromal tumors
PDC	Pyridodicarboxamide
$T_m$	Melting temperature
$t_m$	Mixing time
CHD	Coronary heart diseases
CPT	Camptothecin
HRT-18	Human rectal adenocarcinoma
NOESY	Nuclear overhauser spectroscopy
MTT	3-(4,5-dimethylthiazol-2-yl)-2,5-diphenyltetrazolium bromide
PCR	Polymerase chain reaction
FACS	Fluorescence-activated cell sorting
CT-DNA	Calf thymus DNA
tel7	Human telomeric DNA sequence (short)
tel22	Human telomeric DNA sequence (long)
Pu24T	Human c-myc promoter DNA sequence
ckit21	Human c-kit promoter DNA sequence
EDTA	Ethylenediaminetetraacetic acid
DMSO	Dimethyl sulphoxide

DAPI	4',6-diamidino-2-phenylindole
PI	Propidium iodide
HPLC	High-performance liquid chromatography
A549	Human lung cancer cell lines
PC3	Human prostate cancer cell lines
HepG2	Human liver cancer cell line
HeLa	Human cervical cancer cell line
MCF-7	Human breast cancer cell lines
HEK	Human embryonic kidney cell line
NCCS	National Centre for Cell Science
DMEM	Dulbecco's modified Eagle's medium
MEM	Minimum essential media Eagle
FBS	Fetal bovine serum
PBS	Phosphate buffer saline
TCSPC	Time correlated single-photon counting
D/N	Drug/ nucleotide or drug/ DNA
PMT	Photo multiplier tube
CFD	Constant fraction discriminator
TAC	Time-to-amplitude converter
MCA	Multi-channel analyser
CD	Circular dichroism
UV	Ultra violet
PTP	Peltier temperature programmer
ITC	Isothermal titration calorimetry
NOE	Nuclear Overhauser effect
1D	One-dimensional
2D	Two-dimensional
COSY	Correlation spectroscopy
TOCSY	Total Correlation spectroscopy
HMBC	Heteronuclear multiple bond correlation
HSQC	Heteronuclear single quantum correlation
NOESY	Nuclear Overhauser effect spectroscopy
ROESY	Rotating frame nuclear Overhauser effect spectroscopy

MD	Molecular dynamics simulations
DS	Discovery studio
rMD	Restrained molecular dynamic simulation studies
LGA	Lamarckian genetic algorithm
EtBr	Ethidium bromide
TBE	Tris borate edta
IC <sub>50</sub> value	Inhibitory concentration value
RT-PCR	Reverse transcription-polymerase chain reaction
cDNA	Complimentary DNA
TUNEL	Terminal deoxynucleotidyl transferase (tdt) dutp Nick-End Labeling



## NOMENCLATURE

$\lambda$	Wavelength
$\epsilon$	Extinction coefficient
$\pi$	Pi
$\text{\AA}$	Angstrom
nm	Nanometer
cm	Centimeter
ps	Picosecond
ns	Nanosecond
ms	Millisecond
M	Molar
nM	Nanomolar
$\mu$ M	Micromolar
mM	Millimolar
pmol	Picomole
nmol	Nanomole
L	Liter
mL	Milliliter
$\mu$ L	Microliter
$^{\circ}$	Degree
$^{\circ}$ C	Degree centigrade

# Chapter 1

## Introduction and Literature review

---

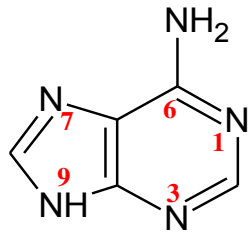
---

### 1.1 Nucleic Acids

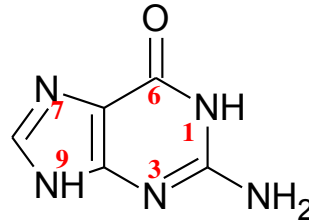
Nucleic acids are composed of series of basic units called nucleotides that are linked to each other by phosphodiester bonds.<sup>[1]</sup> Each nucleotide is constituted of a nucleoside formed by covalent linkage of nitrogenous bases to a pentose sugar through glycosidic bond and a phosphate group. There are majorly two groups of nitrogenous bases that are purines and pyrimidines. Purine ring is composed of two different heterocyclic aromatic bases while pyrimidine consists of single heterocyclic ring.<sup>[2]</sup> Two nitrogenous bases of purines are Adenine (A) and Guanine (G). Adenine has amino group ( $-\text{NH}_2$ ) at C6 position of the purine ring. In Guanine, this C6 position is occupied by carbonyl group ( $-\text{CO}$ ) while amino group is present at C2 position of purine ring (Figure 1.1a). Pyrimidines consist of Thymine, Cytosine and Uracil nucleobases. In Thymine, the C5 position has a methyl group ( $-\text{CH}_3$ ) and carbonyl group at C4 and C2 positions. Cytosine contains an amino group at C4 position of pyrimidine ring. In DNA, primarily, two pyrimidines were present: Cytosine (C), and Thymine (T), while in RNA, thymine is substituted by Uracil (U). Uracil is demethylated form of thymine (Figure 1.1b). Besides these, minor bases like inosine, 7-methyl guanosine, etc. are also found as components of nucleic acids. Sugar present in nucleic acids is pentose sugar. Ribose sugar is found in all RNA molecules while  $\beta$ -D-2-deoxyribose is found in DNA. This is a derivative of  $\beta$ -D-ribose in which the hydroxyl ( $-\text{OH}$ ) the 2' position is replaced by hydrogen ( $-\text{H}$ ) (Figure 1.1c). The sugar combined with base forms nucleoside unit that got phosphorylated at one of the free sugar hydroxyls and forms nucleotide. These nucleotides are basic unit of nucleic acids.<sup>[3]</sup>

In 1953, Watson and Crick discovered the first double helix DNA structure that is called as B form of DNA.<sup>[4]</sup> Nevertheless, the B form is not the only base pairing arrangement that can occur between bases, rather, other forms of duplex DNA also occurs that is A form and Z form of DNA. DNA is known to exhibit structural polymorphism that means it does not occurs in only duplex form, but also present in other forms such as Hairpin structures, triplex DNA as well as quadruplex forms.<sup>[5]</sup>

a.

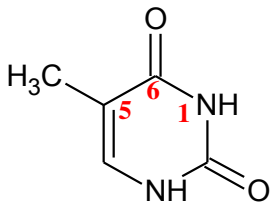


Adenine

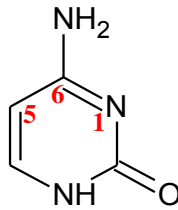


Guanine

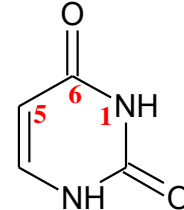
b.



Thymine

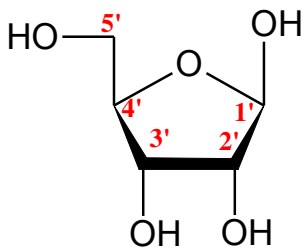


Cytosine

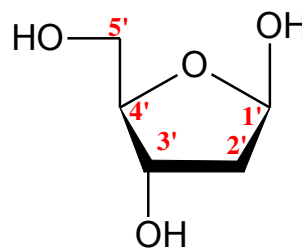


Uracil

c.



Ribose



Deoxy ribose

*Figure 1.1. Molecular structure of (a) purines (b) pyrimidines (c) Five membered furanose ring of ribose and deoxyribose sugar.*

## 1.2 G-quadruplex DNA

G-quadruplex DNA structures are non-canonical secondary structures of DNA that are formed by square planar arrangement of tetrameric guanine bases.<sup>[6-7]</sup> These guanine bases are held together by Hoogsteen hydrogen bonding and forms G-tetrads/quartets<sup>[8]</sup> (Figure 1.2a). The presence of monovalent cations stabilizes these G-tetrads and they stacked on to each other to form G-quadruplex structure<sup>[9]</sup> (Figure 1.2b-c).

### 1.2.1 G-quadruplex Structure

The basic unit of G-quadruplex structure is G-tetrads in which the guanines are linked by two types of Hydrogen bonds.<sup>[8-10]</sup> In the first type, hydrogen bonds are formed between the oxygen of carbonyl group in position 6 (O6) and the hydrogen of imino group in position 1 (N1), while the second type of hydrogen bonds are established between the nitrogen in position 7 (N7) and the hydrogen of amino group in position 2 (N2). G-tetrads are stabilized by monovalent cations such as  $K^+$  that interacts with four oxygen atoms belonging to the carbonyl group (O6) of the four guanines that forms G-quartets.<sup>[11]</sup> In this G-quartets, the sugar pucker of the guanines is usually in *C2'-endo/C3'-exo* conformation, but, the glycosidic bond angles can adopt two different orientations that is *syn* and *anti*. This *syn/anti*-conformations of guanines defines the groove dimension between two adjacent guanines and categorized them as wide, narrow or medium grooves.<sup>[12]</sup> The combination of these different conformations leads to structural polymorphism of G-quadruplexes; that are composed of two or more G-quartets arranged in intermolecular or intra-molecular structures along with different orientation of the strands.<sup>[13-14]</sup>

### 1.2.2 Topologies of G-quadruplex DNA

The invariant core of all G-quadruplex structures is G-quartet and their association with each other by formation of hydrogen bonds, dipole interactions and  $\pi$ - $\pi$  stacking interactions. These interactions play a significant role in defining the structural diversity of G-quadruplex structures. Some other parameters are also involved in explaining their structural diversity that includes number of strands and their orientation, loop conformations and nature of cations.<sup>[15]</sup> Depending upon the number of DNA strands involve formation of G-quadruplex structure, they are categorized in two main categories namely, intramolecular G-quadruplex structure and intermolecular G-quadruplex structure.<sup>[16]</sup> Intramolecular G-quadruplex structures are composed of

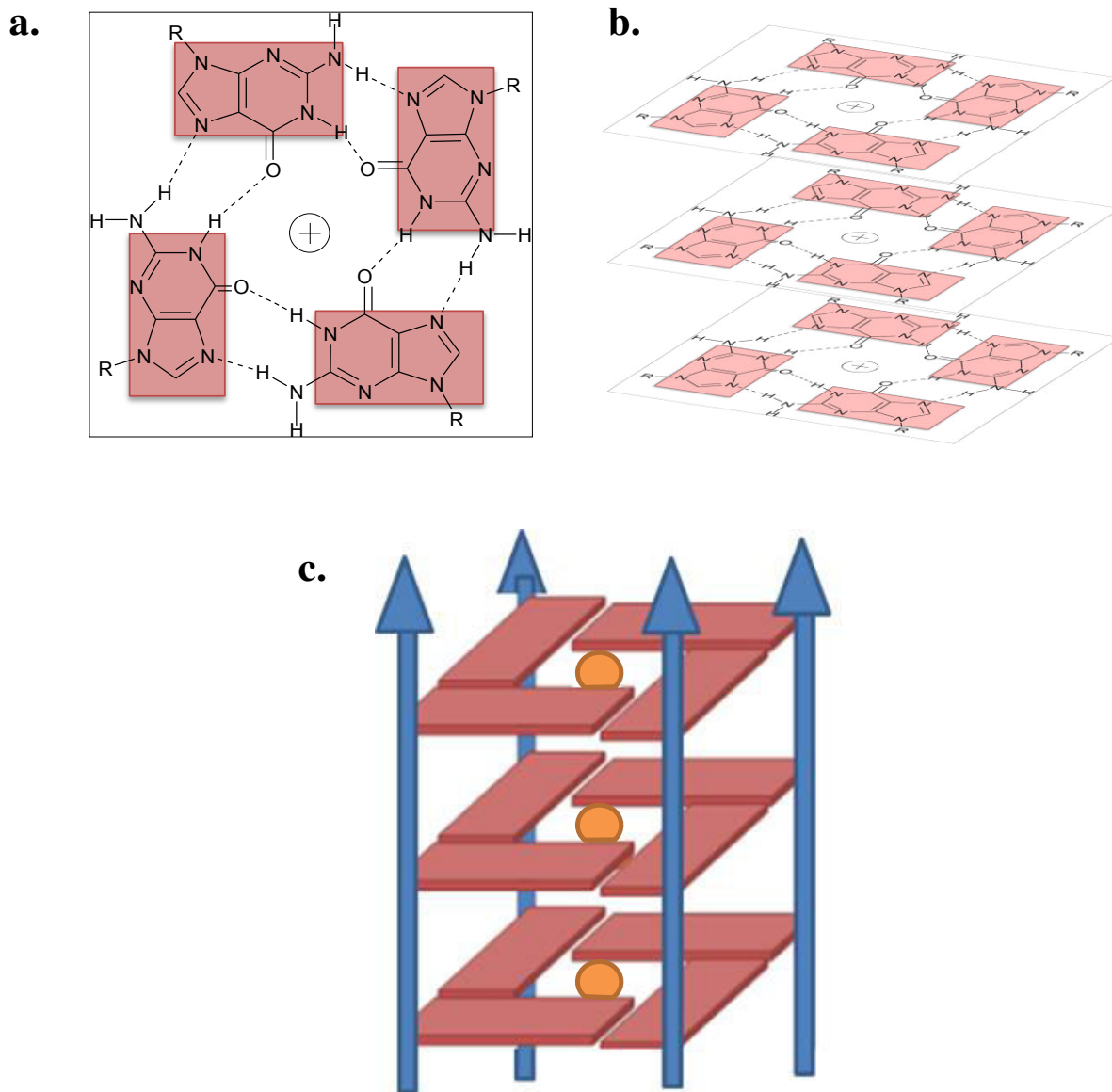
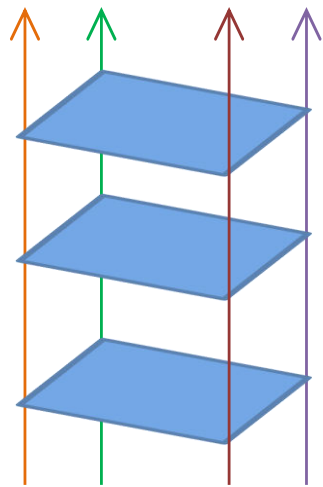
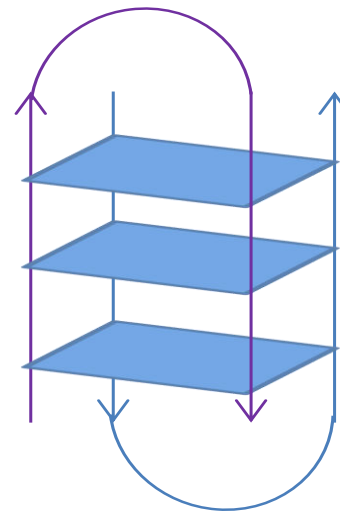


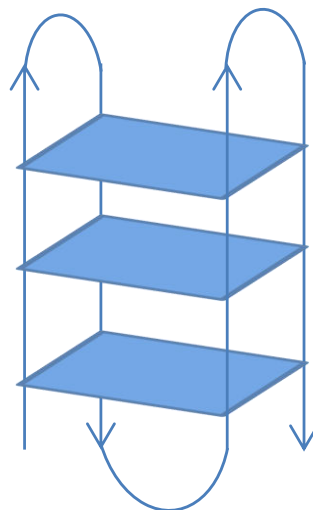
*Figure 1.2. G-quadruplex structures (a) G-quartets or G-tetrads formed by square planar arrangement of four guanines bonded by Watson-Crick as well as Hoogsteen hydrogen bonding (N1–N6 and N2–N7). (b) G-quartets stack on top of one another (c) Schematic presentation of formation of G-quadruplex structure.*



**Tetra-molecular Parallel**



**Bi-molecular Anti-Parallel**



**Unimolecular Anti-Parallel**

*Figure 1.3. Structural polymorphism of G-quadruplex structures showing parallel and anti-parallel G-quadruplex topologies.*

single strand of DNA that folds to form G-quadruplex structures. Intermolecular G-quadruplex structures are formed by association of two or more strands of DNA, thus they are categorized as follows: (a) Tetra-molecular: composed of four strands, (b) Tri-molecular: composed of three strands and (c) Bimolecular: composed of two strands. The orientation of guanines (*syn* and *anti*-conformation) in these strands defines their polarity that could be of same type or of different types.<sup>[17]</sup> When all the guanines are present in same conformation, G-quadruplex structure attains parallel form with all the strands of same polarity. But, if these guanines exhibit different glycosidic bond angles, theoretically, it could give rise to 16 conformations that are categorized in 4 major groups: (a) a parallel conformation composed of 4 strands oriented in same direction (b) a hybrid conformation (3+1) in which 3 strands are in same direction and 4<sup>th</sup> strand is in opposite direction (c) an anti-parallel conformation with 2 adjacent stands oriented in the same direction and the others in the opposite direction, and (d) another anti-parallel conformation where 2 adjacent stands are oriented in the opposite direction<sup>[18]</sup> (Figure 1.3). Sequences that connect G-quartets with each other are called as loops and plays important role in providing structural polymorphism to G-quadruplex structures and its stability. These loops are of various conformations as follows: (a) diagonal loops: connecting two anti-parallel strands, (b) propeller or chain reversal loop connecting two parallel adjacent strands, (c) lateral or edgewise loop connecting two anti-parallel adjacent strands, and (d) snap back or V-shaped loop connecting the wedges of G-quartets.<sup>[19]</sup> Moreover, the conformation of loops is dependent on the length of their sequences. Short loops are favors a stable parallel conformation, however, longer loops give rise to anti-parallel conformation but with reduced stability of G4. Besides the length of loops, the type of nucleotide it is composed of also plays in providing stability to G-quadruplex structure. For example, presence of pyrimidines increases the stability as compare to the presence of adenines. These diversities of G-quadruplex structures could be used to enhance selectivity of ligands toward particular loops and grooves of DNA.<sup>[20]</sup>

### **1.2.3 Presence and significance of G-quadruplex DNA in human genome**

#### **1.2.3.1 *In-silico* evidences for the presence of G-quadruplex DNA structures**

Computational studies have been reached to a level where we could determine the possibility of formation of G-quadruplex structure within genomes of different species. Various algorithms have been developed like Quadparser algorithm,<sup>[21]</sup> its extension or other algorithm

based on pattern searching aid in identification of sequences capable of forming G-quadruplex structures and gives information of putative quadruplex sequences (PQS) present in human genome<sup>[22-23]</sup> (Figure 1.4). Recent analysis showed that the density of PQS is higher in promoters close to the transcription start sites (TSS). The PQS density and the potential of forming G-quadruplex structure (GQP) are correlated with the presence of GC contents of genome as well as the presence of DNase I hypersensitive sites (DHS) and gene function. For example, the tumor suppressor genes are characterized by low GQP while high GQP have been reported for proto-oncogenes. Altogether, these studies suggested that G-quadruplex could play dynamic roles within the cell.<sup>[24]</sup>

### 1.2.3.2 Human telomeres

Telomeres are a nucleoprotein complex located at the end of human chromosomes and plays significant roles in protection of genetic material from recombination, degradation by nucleases, double-strand breaks, etc.<sup>[24-26]</sup> Human telomeric DNA consists of ~2–10 kb of double stranded sequence and approximately 50 - 100 deoxynucleotides of single stranded 3' overhang consist of tandem repeats that are rich in guanines.<sup>[27]</sup> This overhang is capable of folding into a quadruplex structure.<sup>[28]</sup> The importance of human telomeric ends having the sequence d-(TTAGGG)<sub>n</sub> is evident in somatic cells in which telomeres reach a critical limit (Hayflick limit), leading to the shortening of chromosomes and lead to cellular senescence.<sup>[29-30]</sup> Indeed, in 80–85% of tumors, the aberrant cell proliferation and immortalization is due to reactivation of a mechanism of telomere elongation that generally occurs due to over-expression of a ribonucleozyme called telomerase.<sup>[31]</sup> Telomerase utilizes this single stranded end as primer for its reverse transcriptase (hTERT) activity, using its own hRNA component as a template for DNA synthesis and maintains the telomere length.<sup>[32-33]</sup> This fact makes telomerases as a privileged target for cancer treatment. Several lines of evidences suggested that folding of telomeric ends into stable G-quadruplex structure could inhibits the enzymatic activity of telomerase.<sup>[34]</sup> Therefore, the immortalization of cancer cells via elongation of telomeric ends could be interrupted by stabilization of G-quadruplex structure; thereby, suggesting this mechanism as a potent therapeutics for cancer treatment.<sup>[35-36]</sup> Subsequently with the demonstration that telomeres could be promising target for cancer treatment, the structural features of the telomeric G-quadruplex structure is of great interest. Numerous high resolution

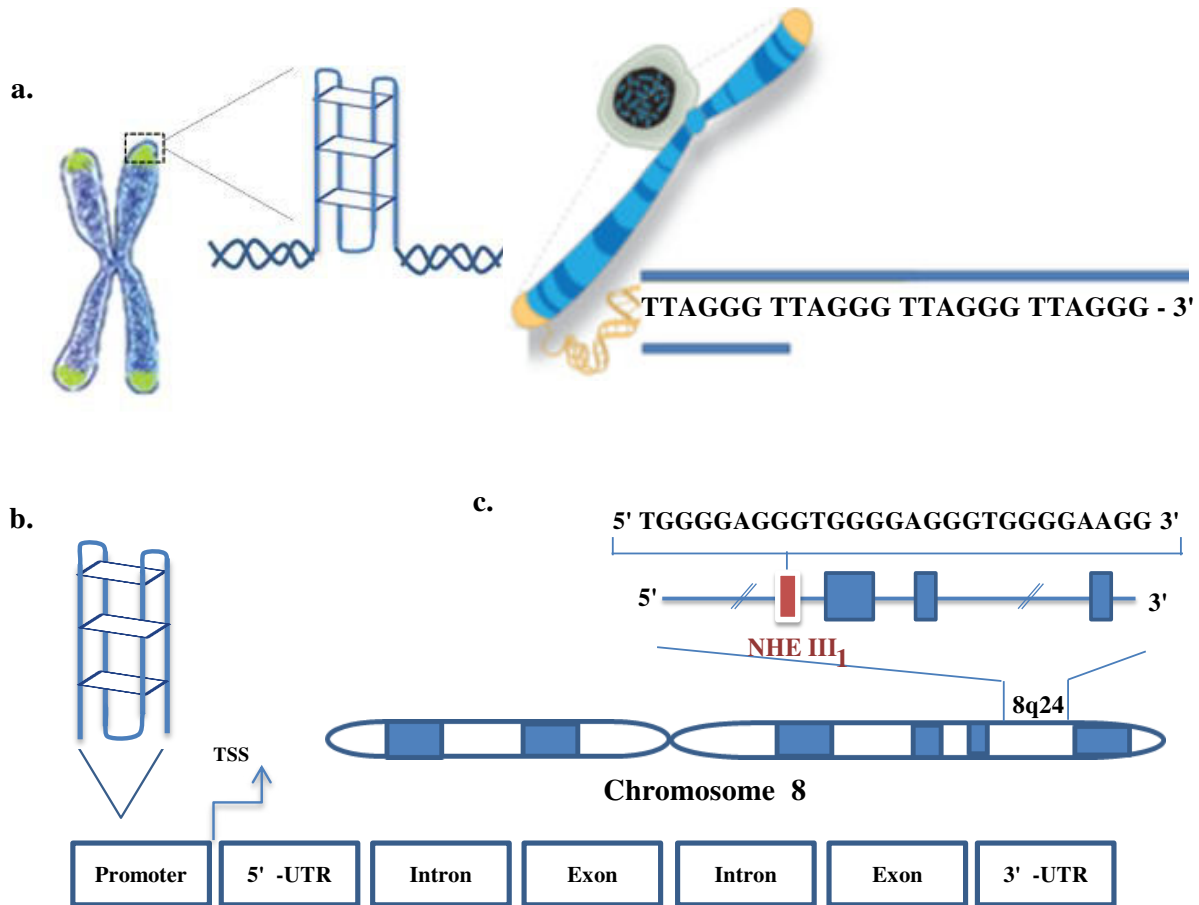


**Figure 1.4.** Location of G-quadruplex structures forming DNA sequences in various regions of human genome (a) telomeric region (b) promoter region of gene (c) NHEIII<sub>1</sub> region of c-myc promoter gene.

structures have been resolved both by NMR and X-ray crystallography. Truncated human telomeric DNA sequence d(AG<sub>3</sub>(T<sub>2</sub>AG<sub>3</sub>T)<sub>4</sub>) in presence of sodium solution forms anti-parallel G-quadruplex structure composed of basket-like folding with one diagonal loop and two lateral loops was obtained by NMR (PDB: 143D).<sup>[37]</sup> Another study shows that anti-parallel (2+2) structure consist of a core arrangement from the known topology (PDB: 2MBJ). However, low structural polymorphism was observed in presence of sodium ions, while, a large set of polymorphic structures were observed in presence of potassium ions that mimics physiological conditions. For example, d(A<sub>3</sub>G<sub>3</sub>(T<sub>2</sub>AG<sub>3</sub>)A<sub>2</sub>) and d(T<sub>2</sub>AG<sub>3</sub>(T<sub>2</sub>AG<sub>3</sub>)<sub>3</sub>T<sub>2</sub>) forms hybrid structures differing in loops arrangements and strands orientation. Two different (3+1) hybrid G-quadruplex structures were observed with the sequences d(TAG<sub>3</sub>(T<sub>2</sub>AG<sub>3</sub>)<sub>3</sub>) and d(TAG<sub>3</sub>(T<sub>2</sub>AG<sub>3</sub>)<sub>3</sub>T<sub>2</sub>) composed of G-tetrad core having two edgewise loops and one double-chain-reversal, although they differ in the successive order of loop arrangements within the G-quadruplex.<sup>[38]</sup> While two edgewise loops and two double-chain reversal loop was observed with (3+1) strand fold topology for T<sub>2</sub>G<sub>3</sub>(T<sub>2</sub>AG<sub>3</sub>). In addition to these folding observed in presence of sodium or potassium ions, another parallel propeller-type G-quadruplex structure was also obtained under molecular crowding conditions (PDB: 2LD8).<sup>[39]</sup> Such a huge structural diversity of human telomeric DNA sequence suggested that the formation of certain conformation does not dependent only on external factors, but number of loops, their orientations and their sequences are also crucial. Unlikely to the various types of G-rich sequences found in the promoter regions of genes, the telomeric DNA sequence is composed of same tandem repeat of d(TTAGGG). This special type of sequence with its structural polymorphism could have been evolved so as to provide it as an attractive means for targeting by small molecules. As it will easily beat the small energy barrier between various forms and subsequently change the dynamics of the structure.

### 1.2.3.3 Promoter region of genes

The upstream location to the transcription site is promoter region of the gene. After the telomeres, these regions are most studied for their potential to form G-quadruplex structures. Computational analysis shows that there is presence of at least one G-quadruplex motif within promoter region of more than 40% of human genes.<sup>[24]</sup> Commonly, formation of stable G-quadruplex structures at promoter regions were demonstrated in cancer-associated genes. The

presence of these quadruplexes marginalized the genes expression involved in regulating the normal cellular processes. Some of the well-studied gene promoters in which G-quadruplex formation has been described includes c-MYC,<sup>[40-41]</sup> BCL-2,<sup>[42-43]</sup> h-RAS,<sup>[44]</sup> KRAS,<sup>[45]</sup> c-KIT,<sup>[45-47]</sup> androgen receptor,<sup>[48]</sup> VEGF,<sup>[49]</sup> etc. Most of these putative promoter quadruplex forming DNA sequences are tend to lie within 1 kb, immediately upstream and/or close to the transcription start site in these genes. In contrast to simple repeats in human telomeric G-quadruplex sequence, the G-quadruplex forming regions of gene promoters are highly diverse in terms of sequence, numbers and lengths of G-tracts and intervening bases. Some quadruplexes simply consists of just four G-tract repeats, notably the two quadruplexes in the c-KIT gene that is 21-mers present between -87 and -109 bp upstream of the transcription initiation site.<sup>[50-51]</sup> In contrast, the well-studied 27-mer NHE III<sub>1</sub> element of the cMYC promoter contains five short G-tracts, and both four-tract quadruplexes (1234- and 2345-G-tract) can be formed.<sup>[52]</sup> Further in BCL-2 promoter, there are six G-tracts and as it is a 39-mer sequence so theoretically up to 15 distinct four-tract intramolecular quadruplexes are possible.<sup>[53]</sup> Thus, they provide higher structural polymorphism using different combinations of G-tracts. c-MYC is the first and most extensively studied system of promoter G-quadruplex formation and majorly it forms a parallel stranded structure with two G3NG3 single nucleotide strand-reversal loops.<sup>[54]</sup> However, some of the genes that were overexpressed in certain cancers, have been targeted with small molecules at protein level, for example, b-RAF, c-KIT, MET, BCL-2, etc. But, many of proteins encoded by genes have long been considered to be undruggable, for example, c-MYC and RAS proteins.<sup>[55]</sup> Quadruplex targeting at the gene level, could provide the possibility of bypassing such roadblocks. Thus, existence of quadruplex sequences in the promoter region of a particular gene has been developed as a potential therapeutic quadruplex-targeting strategy in human cancers <sup>[40-56]</sup>. However, this notion was initially articulated as a simple inhibition of function due to induction of a stabilizing quadruplex-small molecule complex. But today, it is under deliberation, and this quadruplex-small molecule complex would be an effective impediment to RNA polymerase transcription.

#### **1.2.4 G-quadruplex DNA as target for anticancer drugs**

Several lines of evidence suggested that G-quadruplex structures play a significant role in regulation of gene expression and genome stability. The elevated activity of telomerase

enzyme has been found to be associated with 85% of cancers.<sup>[31-57-58]</sup> As the formation of G-quadruplex structure inhibits the telomerase activity, therefore, agents that stabilize the G-quadruplex structures could act as a potent chemotherapeutic agent.<sup>[34]</sup> Ends of human chromosomes consist of non-coding DNA that involves multiple tandem repeats of TTAGGG and terminate in a 3' protruding single-stranded DNA overhang. During replication, telomeres get shorten by 50–200 bp because the 'end replication problem', and cell undergoes replicative senescence.<sup>[59-60]</sup> Under some conditions, cell could escape this process and attains immortalization by maintaining the length of its telomeres. This could be achieved by the activation of the enzyme telomerase. Telomerase is a unique ribonucleoprotein enzyme that incorporates telomeric repeats onto the 3' ends of chromosomes. It has two major components that are required for its proper functioning, the first is a functional or template RNA and second component is its reverse transcriptase (hTERT) catalytic subunit.<sup>[61]</sup> As telomerase activity has been found in ~85–90% of all human tumors but not in normal cells, thus it could be postulated that activation of telomeres is required for a tumor cell to achieve proliferation beyond the limits of cellular senescence. Thus, it makes telomerase a potential target for cancer diagnosis and would help in development of novel therapeutic agents.<sup>[62]</sup> Besides direct targeting the activity of telomerase enzyme, indirect targeting of telomerase gives fruitful results. Telomerase requires an unfolded single-stranded substrate, so sequestration of this primer could inhibit reverse transcriptase activity of this enzyme. The single stranded substrate could be folded into G-quadruplex structure and therefore, no single stranded primers will be available for telomerase activity and this could inhibit telomerase activity. For the first time it was demonstrated that the presence of  $K^+$  facilitates the inhibition of telomerase activity and it could occur probably due to folding of single-stranded telomeric DNA into a G-quadruplex structure.<sup>[34]</sup> Ligands that selectively bind to and stabilize G-quadruplex structures may interfere with telomere conformation and telomere elongation<sup>[35-36]</sup> (Figure 1.5).

Further, biological significance of G-quadruplex structures is also emphasized by the observation that expression of the c-Myc oncogene is implicated with a number of human malignancies. Up to 80% of all solid tumors overexpress MYC, including gastrointestinal, ovarian, cervix, breast cancer etc., so it has attracted considerable interest as a potential therapeutic target.<sup>[40]</sup> Deregulation of MYC gene could be due to altered gene amplification, ploidy, translocations etc. However, it is important to mention that as the control of MYC gene

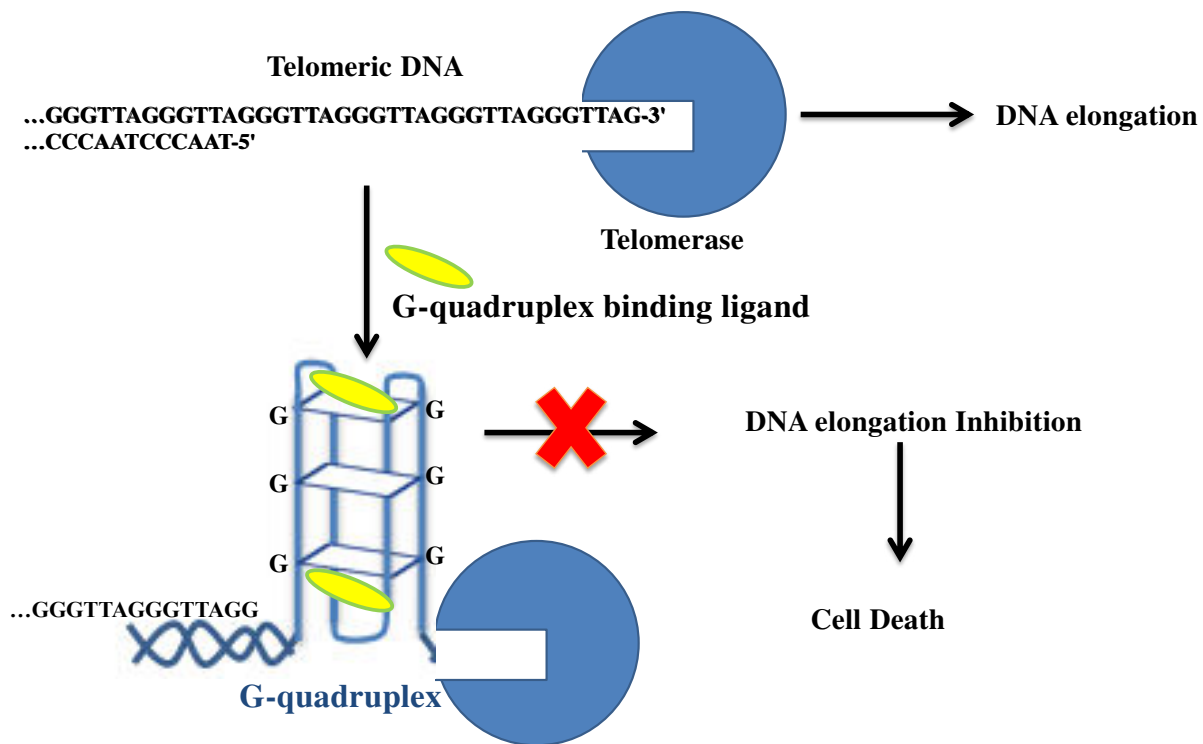


*Figure 1.5. Schematic representation of stabilization of G-quadruplex structure formed at telomere by G-quadruplex binding ligands (yellow).*

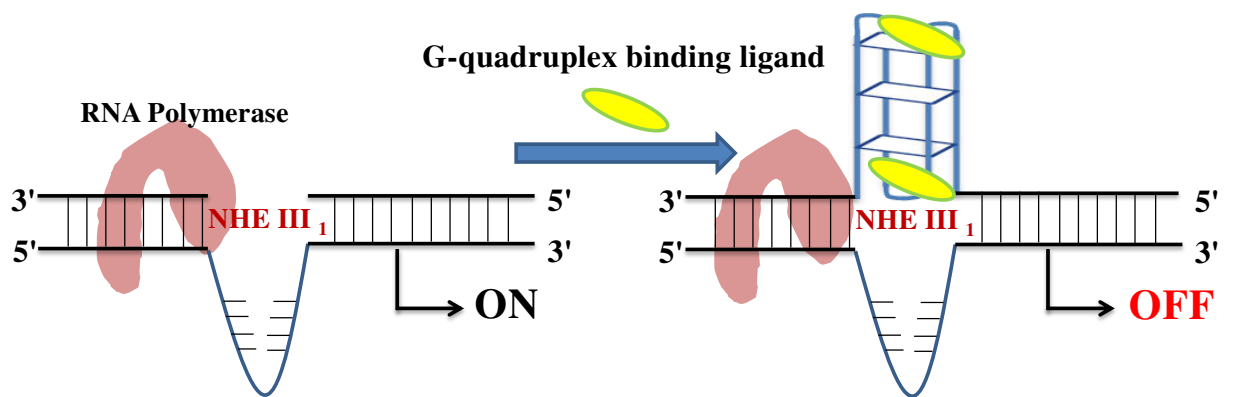


*Figure 1.6. Schematic representation of stabilization of G-quadruplex structure formed at promoter region by G-quadruplex binding ligands (yellow).*

expression is extremely complex, other pathways and mechanisms that may be used to target the over-expression of this gene. Promoter region of MYC gene consists of seven nuclear hypersensitive elements (NHEs) of which, NHEIII<sub>1</sub> is 33-nucleotide G-rich sequence, (TGG GGA GGG TGG GGA GGG TGG GGA AGG TGG GGA).<sup>[63]</sup> This is composed of six G-tracts of unequal length that could form a mixture of G-quadruplex structures in solution. In 2002, it was demonstrated for the first time small molecule mediated stabilization of G-quadruplex structure in the MYC promoter element act as silencer element and down regulates the gene expression.<sup>[64]</sup> Further, more studies have been conducted and demonstrated the effect of ligands mediated stabilization of G-quadruplex structure on MYC transcription. Thus, stabilization of G-quadruplex structures present in promoter regions of this gene, function as transcriptional repressors in cancer condition (Figure 1.6).

Moreover, the KIT proto-oncogene encodes a receptor tyrosine kinase that, upon activation stimulates cell proliferation, differentiation and survival. This activation or overexpression causes oncogenic cellular transformation in various cells of Cajal lineages for example, mast cells, melanocytes, interstitial cells, myeloid cells and germ cells.<sup>[65]</sup> In gastrointestinal stromal tumors (GIST), the constitutive activation of KIT is considered to be the primary pathogenic event that makes KIT protein as a major molecular target for GIST therapy.<sup>[66]</sup> However, due to mutations in the KIT protein, it is requisite of an alternative approaches to target not only GISTs but also those malignancies in which KIT expression has been found to be elevated. The core promoter of KIT is composed of two G-quadruplex-forming sequences, namely, KIT1 and KIT2. These sequences occur between position -87 and -109 base pairs (KIT1) and between -140 and -160 base pairs (KIT2) relative to transcription start site.<sup>[67-68]</sup> It has been demonstrated that both of these sequences are capable of forming stable G-quadruplexes *in vitro*. A study on patient-derived GIST882 cells showed that naphthalene diimide (G-quadruplex binder) causes cell growth arrest in a dose-dependent fashion and suppression of KIT mRNA and KIT protein levels was also demonstrated.<sup>[69]</sup>

Furthermore, the polypurine tract found at the proximal region of VEGF gene promoter consists of four arrays of 3–5 contiguous guanines separated by one or more bases. Thus, formation of G-quadruplex structure at this region increases the chances of ligand mediated regulation of gene expression.<sup>[70-71]</sup>

### 1.3 Drug- DNA interaction

### 1.3.1 Different class of drugs that interact with DNA

Development of G-quadruplex ligands that stabilize or induce G4 formation from the 3' single-stranded overhang may prevent telomerase activity of telomeres elongation and could be a possible therapeutic approach for cancer treatment. Similarly, down-regulation of gene expression could also be attained by stabilization of G-quadruplex structure formed at promoter regions of the genes. Generally, ligands bind to G-quadruplex motifs by  $\pi$ - $\pi$  stacking, formation of hydrogen bonds, electrostatic interactions and stabilize the structure. Usually, G4 ligands have polycyclic planar moiety with positively charged substituents that allows the stacking of these compounds on the planar G-tetrads. Moreover, the planar aromatic core of these molecules should be larger than that of duplex DNA binders which could provide selectivity towards G-quadruplex structures over duplex DNA. Not only the planar G-quartet could be targeted, the grooves and loops of G-quadruplex structures should be taken into account. Thus, on the basis of mode of interactions, G4 ligands could be categorized into different groups: interactions mediated by  $\pi$ - $\pi$  stacking and interaction mediated by grooves and/ or loops. The large hydrophobic surface of G-quartets provides favorable conditions for molecules with large aromatic surfaces. This binding is governed by  $\pi$ - $\pi$  stacking interactions between  $\pi$  electronic orbital of aromatic groups of ligand and G-quartets.

Further, the solubility of molecules could be enhanced by introducing positive charges that will strengthen the G-quadruplex stabilization by interacting with negatively charged grooves. Protons can be added in the side chain around aromatic core by adding amine groups at neutral pH. Many G-quadruplex binders were developed using this method for example, PIPER,<sup>[72]</sup> BRACO-19,<sup>[73]</sup> Quindoline,<sup>[74]</sup> telomestatin derivatives.<sup>[75]</sup> Other method of protonation is to use N-methylated ligands, that will provide better solubility and it also reduces electronic density around aromatic part thereby enhancing the  $\pi$ - $\pi$  stacking ability of the ligand. For example, 360A,<sup>[76]</sup> PhenDC3<sup>[77]</sup> and RHPS4<sup>[78]</sup> are ligands that are synthesized by employing this approach.

For the first time, interaction of G-quadruplex ligand BSU-1051 (2,6-diamidoanthraquinone)<sup>[79]</sup> with human telomeric DNA was reported and this ligand has been shown to inhibit telomerase activity. This study motivates the scientific world to work further on this line and since then plethora of drugs have been studied that interacts with other G-quadruplex structures such as porphyrin - TMPyP4, berberine, dibenzophenanthrolines,

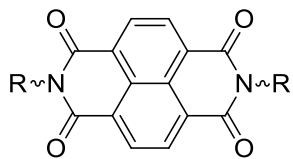
pentacyclic acridines like RHPS4, trisubstituted acridines like BRACO19, ethidium derivative, triazines such as 12459 and 115405, fluoroquinophenoxazines such as QQ58, coronene derivatives like CORON,<sup>[80]</sup> quindoline derivatives like SYUIQ-5, perylenes such as PIPER, etc.

The end stacking mode of binding was observed in solution structure of complex formed between tetramolecular G-quadruplex structure formed by human telomeric DNA sequence and PIPER and RHPS4 individually.<sup>[81]</sup> This interaction is favored by  $\pi$ - $\pi$  stacking on 3' terminal of G-quartet and has been showed to provide inhibitory effect on telomerase enzyme. RHPS4 is a pentacyclic acridine molecule that was found to interacts in 2:1 stoichiometry with parallel telomeric G4 d(TTAGGGT)<sub>4</sub> via  $\pi$ - $\pi$  stacking.<sup>[82]</sup> Another scaffold of molecule that was also explored as G4 binders is PDC (bisquinolinium pyridodicarboxamide). One of the best example for this molecules is 360A that was known to confers stabilization of 23°C in melting experiment for intermolecular telomeric G4 structure.<sup>[83]</sup> It also has high affinity for the telomeric G4 d(AG<sub>3</sub>(T<sub>2</sub>AG<sub>3</sub>)<sub>3</sub>) and 20 folds higher specificity over duplex DNA.

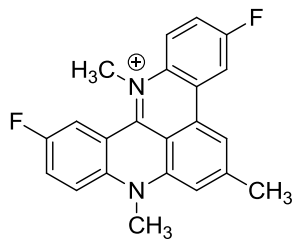
Another example of molecule in this category is PhenDC3 family compounds and these have better selectivity PDC ligands.<sup>[84]</sup> Very recently, Chung *et al* has determined the solution structure of the complex formed by PhenDC3 and c-myc promoter sequence forming G-quadruplex structure. This study revealed that Phen-DC3 interacts with the c-myc quadruplex structure by  $\pi$ - $\pi$  stacking with guanine bases of the top G-tetrad.<sup>[77]</sup>

MMQ1 (Meta-quinacridine n-propylamine) is a popular for its crescent shape that provides an aid to maximize its overlapping with G-quartets. Solution structure shows that MMQ1 interacts with tetramolecular G-quadruplex structure formed by telomeric repeat d(TTAGGGT)<sub>4</sub> in 2:1 stoichiometry on terminal G-quartets. This interaction is also favored by  $\pi$ - $\pi$  stacking and electrostatic interactions with loops of G- quadruplex structure.<sup>[85]</sup>

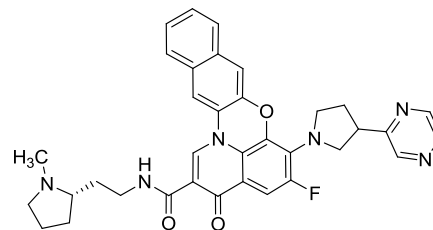
BRACO-19 was found to stabilize human telomeric G-quadruplex structure as reported from increased melting temperature ( $T_m$ ) of DNA upon its binding along with thirty folds higher selectivity over duplex DNA.<sup>[86]</sup> TMPyP4 is a tetra-cationic porphyrin and a potent inhibitor of telomerase activity. X-ray structure of complex formed between TMPyP4 and human telomeric G-quadruplex structure showed that it externally stacks to telomeric G-quadruplex structure onto TTA loop. This porphyrin is also known to interact with G-quadruplex structure formed in the promoter of c-Myc oncogene, leading to down-regulation of c-Myc which in turn leads to the reduced transcription in cancer cells.<sup>[87]</sup>



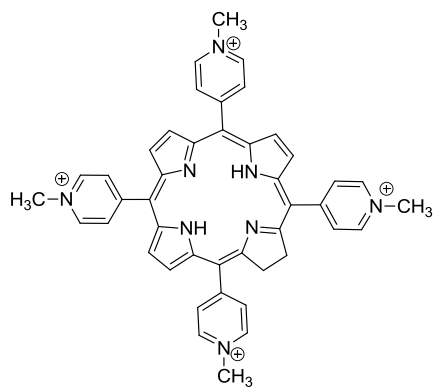
**Naphthalene Diimide**



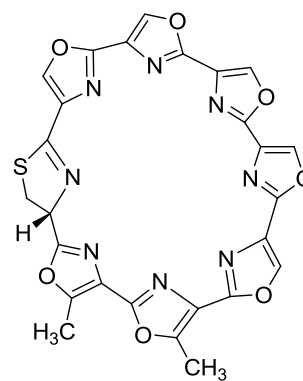
**RHPS4**



**Quarfloxacin**



**TyMPP4**



**Telomestatin**

*Figure 1.7. Chemical structure of various DNA binders.*

Other group of molecules includes macrocyclic compounds for example, telomestatin. It is a natural compound obtained from *Streptomyces annulatus*. Telomestatin has been shown to inhibit telomerase activity by stabilizing G-quadruplex structure formed by human telomeric DNA with higher selectivity for G-quadruplex motifs.<sup>[88]</sup> Solution structure for the interaction of c-myc G-quadruplex structure and quindoline compound suggested that two quindoline molecules bind to c-myc G4 by  $\pi$ - $\pi$  stacking and stabilizes G-quadruplex structure by increasing its melting temperature by 15 °C at a stoichiometry of 2:1 as showed by 1D NMR-melting.<sup>[88]</sup>

Majority of these molecules are synthetic in nature that causes various side effects to human health. Nature has provided us ample source of scaffolds of molecules containing planar aromatic ring systems.<sup>[89]</sup> Those natural molecules that are readily available in our diets could provide us candidate with a potential to act as G-quadruplex binder. Flavonoids, alkaloids are amongst such molecules that are of natural origin and are a part of our daily diets. Molecules with natural origin are less toxic to normal cells as compared to synthetic compounds and have least side effects.

Flavonoids are dietary compounds synthesized by plants sharing a common chemical structure as shown in Figure 1.8 (Table1.1)<sup>[90]</sup> They are categorized into various sub-groups on the basis of the distribution of hydroxyl group on phenyl and benzopyran ring in flavonoids. The functionalization of these chemical groups on the basic moiety of flavonoids yield different structure and is responsible for their various functions <sup>[91-92]</sup>.

Since decades, scientists have shown their interest to explore the potential for several dietary flavonoids in order to explain some of the health benefits like cancer prevention etc. Flavonoids exert various biological activities, like antioxidant activity. Anti-oxidants defend the cells against the effects of reactive oxygen species, such as hydroxyl radicals, singlet oxygen, superoxide, etc. An inequity between antioxidants and reactive oxygen species causes cellular damage due oxidative stress.<sup>[93]</sup> This oxidative stress has known to be associated with atherosclerosis, cardiac dysfunction, inflammation, aging, cancer, neurodegenerative diseases etc. Flavonoids plays a role in providing protection against these diseases by contributing to the total antioxidant defense system of the human body.<sup>[94]</sup> It has been found that higher intake of flavonoid is linked with significant reductions in the risk of in coronary heart diseases (CHD).<sup>[95-96]</sup> Flavonoids also plays important role in improvement of endothelium-dependent vasodilation in patients with coronary artery disease. Vascular endothelial promotes arterial relaxation by

generating nitric oxide and helps in maintaining the cardiovascular health.<sup>[97-99]</sup> Also, it has been observed that relatively high intakes of foods and beverages that are rich in flavonoids like black tea, cocoa, etc. may help in improving vascular endothelial function.

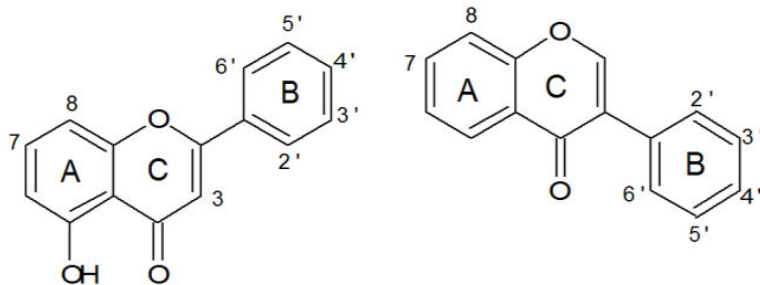
Generally, inflammation, accumulation of transition metal and oxidative stress plays an important role in the pathology of some neurodegenerative diseases such as Alzheimer's disease, Parkinson's disease, etc. Flavonoids have been shown to have protective roles against neurodegenerative diseases.<sup>[100-102]</sup> They reduce the neuro-inflammation by inhibiting the production of cytokines, lipid mediators, etc. They have also been known to increase cerebral blood flow by stimulating the production of nitric oxide (NO).<sup>[103-104]</sup>

Flavonoids have also been known to modulate cell-signaling pathways and help in prevention of cancer. They stimulate the enzymes that promote the excretion of potentially toxic or carcinogenic chemicals,<sup>[105]</sup> regulation of normal cell cycle that otherwise lead cell death (apoptosis) if the damage is irreparable and contributed to the development of cancer.<sup>[106-107]</sup> They also inhibit the proliferation of cancer cells and induce apoptosis in cancer cells.<sup>[108-109]</sup>

Although various flavonoids have been reported to inhibit the chemically-induced cancers development in many in animal models of oral cancer,<sup>[110]</sup> lung cancer,<sup>[111]</sup> breast cancer,<sup>[112]</sup> colon<sup>[113]</sup> prostate<sup>[114-115]</sup> However, there is partial indications for low intakes of flavonoids and their association with increased risk of certain cancers. Although it is uncertain how flavonoids work to protect against cancer, many of their biological actions have been attributed to their antioxidant activity. Flavonoids have also been known for their anti-cancer activity in various *in vitro* and animal model studies. It suggested that they impart effects on important cellular and molecular mechanisms related to carcinogenesis, but their exact target in cell is still unclear.

Another group of naturally available small molecule present in human diets is alkaloids. These groups of phytochemicals possess high diversity in terms of their structure and contains basic core moiety formed composed of a ring structure and a nitrogen atom. They have wide distribution among plant kingdom and chiefly exist in higher plants belonging to Ranunculaceae, Leguminosae, Papaveraceae, Menispermaceae, and Loganiaceae.<sup>[116]</sup> Besides, these alkaloids are the chief active components in natural herbs, and some of these compounds have already been successfully developed into chemotherapeutic drugs, such as camptothecin (CPT) and vinblastine. One of molecule belonging to this group is Piperine. It is a chief alkaloid from black

a.



Quercetin: 3' = OH, 4' = OH, 5' = H, 3 = OH, 7 = OH

Rutin: 3' = OH, 4' = OH, 5' = H, 3 = Rutinose, 7 = OH

Luteolin: 3' = OH, 4' = OH, 5' = H, 3 = H, 7 = OH

Kaempferol: 3' = H, 4' = OH, 5' = H, 3 = H, 7 = OH

Hesperidin: 3' = OH, 4' = OCH<sub>3</sub>, 5' = H, 3 = H, 7 = O-Sugar

Myricetin: 3' = OH, 4' = OH, 5' = OH, 3 = OH, 7 = OH

Genistein: 5 = OH, 7 = OH, 4 = OH, 8 = H

Daidzein: 7 = OH, 4' = OH, 8 = H

Puerarin: 4' = OH, 8 = C-glycoside

b.

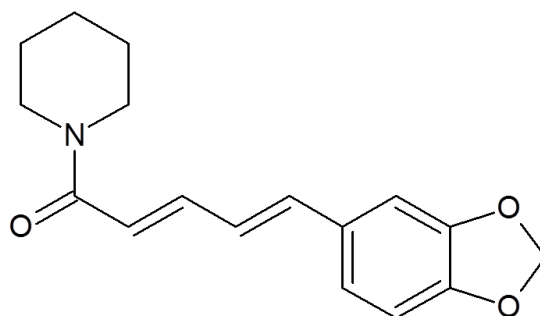


*Figure 1.8. Chemical structure of (a) Flavonoids (b) Piperine.*

*Table 1.1. Classification of bioflavonoids with their dietary source.*

<b>Flavonoid Subclass</b>	<b>Dietary Flavonoids</b>	<b>Some Common Food Sources</b>
<b>Flavanols</b>	<b>Catechin, Epicatechin, Epigallocatechin gallate Theaflavins, Thearubigins, Proanthocyanidins Quercetin, Kaempferol, Myricetin,</b>	<b>Teas, chocolate, grapes, berries, apples, red wine , yellow onions, scallions, kale, broccoli.</b>
<b>Flavanones</b>	<b>Hesperetin, Naringenin, Eriodictyol</b>	<b>Citrus fruits and juices, e.g., oranges, grapefruits, lemons</b>
<b>Flavones</b>	<b>Apigenin, Luteolin</b>	<b>Parsley, thyme, celery</b>
<b>Isoflavones</b>	<b>Daidzein, Genistein, Glycitein</b>	<b>Soybeans, soy foods, legumes</b>

pepper (*Piper nigrum* L.). This bioactive phytochemical is popular since the times of Ayurveda for its various pharmacological and physiological properties. Piperine has been shown to act as antimicrobial, antidepressant, antipyretic, anti-oxidant,<sup>[117]</sup> anti-inflammatory and anti-apoptotic agents.<sup>[118-119]</sup> It has also been demonstrated that in Ehrlich ascites tumor transplanted mice, oral administration of black pepper extract reduces the tumor and increases the life span by 65%. It has also been reported that Piperine enhances the bioavailability other phytochemicals and drugs, for example, rifampicin,<sup>[120]</sup> resveratrol,<sup>[121]</sup> etc. Piperine also inhibits Akt phosphorylation and reduces angiogenesis as well as it also inhibits CREB, NF- $\kappa$ B, c-Fos activities<sup>[122]</sup> in cancer cells. It also suppresses the expression of matrix metalloproteinase-9 (MMP-9) and shows inhibitory effect of invasion and migration in human fibrosarcoma HT-1080 cells. Piperine also showed cytotoxic effect on HRT-18 human rectal adenocarcinoma cells via cell cycle progression and directed towards apoptosis.<sup>[123]</sup> Despite of these studies, the molecular mechanism for action of Piperine with biologically significant macromolecules is not fully studied yet.

### **1.3.2 Basis of DNA- Drug interactions**

DNA is a major target for the action of various drugs including anti-tumor, antiviral and antimicrobial agents. These drugs exert their activity by binding to DNA and modulating its structure or function. Thus, the potential activity of a drug could be assessed by detecting the DNA binding location and fit of the drug candidate. The designing of a potent therapeutic candidate that could identify and binds to DNA requires multi-disciplinary approach. This will led to the determination of its preferred binding sequences, binding sites, modes of binding and thermodynamic parameters governing the complex formation between drug and DNA. High resolution structural data is required to precisely define the way this complex exists in space. This information was further supported by computational approaches that could be used predicatively in further rational designing of drugs. Thus, the mode of DNA/drug interaction is important for rational designing of drugs that specifically and selectively binds to its target. There are several modes of DNA binding are found for anti-cancer drugs as mentioned below.

### **1.3.3 Modes of binding**

#### **1.3.3.1 Covalent DNA binding**

Covalent binding requires the chemical modification of specific nucleotides by binding of drugs that will interfere with DNA function and causes damage to DNA. This group of

interacting molecules includes alkylating agents. There are two types of alkylating agents: mono-functional (one reactive group) that causes single-strand breaks in DNA or damage bases and bi-functional (two reactive groups) that form cross-links. Plethora of molecules was categorized in first generations of anti - cancer drugs were designed to combine this alkylating function.<sup>[124]</sup> These molecules exert their effect by transferring alkyl group to DNA base and causes alkylation of DNA at N7 or N2 position of guanine. Several molecules of this group possess selective anti-tumor activity, attributed to their specificity for DNA binding. For example, Anthramycin, it is an antibiotic that binds to minor groove of DNA by covalently linking to N2 of guanine base.<sup>[125]</sup> Another example is Cisplatin, a transition metal complex cis-diamine-dichloro-platinum. This anticancer drug platinates N7 of guanine nucleotide present in the major groove of DNA double helix.<sup>[126]</sup> These drugs usually form a reactive intermediate ethyleneimmonium ion. Poly-functional alkylating drugs provides resistance against cancer by increasing DNA repair activity, decreasing cellular permeability of drugs, increases glutathione synthesis that in turn inactivates alkylating agents through conjugation reactions. Mitomycin C is another well-known anti-tumor drug that forms covalent interaction with DNA after enzymatic reductive activation of its quinone to alkylate DNA. In activated form, this antibiotic inhibits the formation of single stranded DNA that is required for DNA replication as well as m-RNA transcription. It does this by formation of cross-linking structure between guanine bases on adjacent strands of DNA.<sup>[127]</sup>

### **1.3.3.2 Non-covalent DNA binding**

There are three major modes of non-covalent interactions between Drug and DNA. These are intercalative binding, groove binding and electrostatic interactions. In intercalative mode, small molecule intercalate within the bases of nucleic acid. Groove binding mode is further categorized into two categories that are major groove binders and minor groove binder. Groove binding involves hydrogen bonding or Vander Waal interactions of drug and DNA. While in electrostatic mode of binding, interaction takes place between the positively charged ends of small molecules and negatively charged phosphate backbone of DNA.

#### **Intercalators**

Majority of DNA binders interacts by intercalating with DNA base pairs of double helical DNA.

DNA. They involve antibiotics, anticancer drugs currently used for the treatment of ovarian and breast cancers and acute leukemia, while many others are in different phases of clinical trials. Intercalating agents have a common feature in their structure that is presence of planar poly-aromatic ring system. This scaffold aids in inserting themselves in between DNA base-pairs. These intercalators might exert anti-tumor activity by stabilizing a ternary complex formed by DNA-intercalator-topoisomerase II. These molecules usually have basic chains linked to the chromophore that also helps in providing the affinity and selectivity of these compounds.<sup>[128]</sup> In bis-intercalators, there occur two intercalating ring systems that are connected by linkers varying in length as well as rigidity. One potential mechanism is based on the ability of these agents to take part in electron-transfer processes and generates free radicals. It occurs due to presence of two different types of redox-active groups, that is, quinone and hydroquinone moieties, as present in daunomycin and adriamycin. In daunomycin, this Quinone moiety undergoes one electron reduction to a semiquinone radical. In the presence of oxygen, this radical generates superoxide other reactive oxygen species.<sup>[129]</sup>

### **Groove Binders**

As DNA has two types of groove and both of these grooves are recognized by small molecules, therefore, there are two types of groove binders. One is major groove binders and other is minor groove binders. As both of these grooves differs significantly in their electrostatic potential, hydrogen bonding characteristics, steric effects and hydration, therefore, this aids in selectivity of molecules for their preferential binding. In general, minor groove binding molecules consist of simple aromatic rings connected by bond having torsional freedom. It provides compounds with the appropriate twist that could be fitted into the helical curve of the minor groove *via* forming Van der Waals interactions.<sup>[130]</sup> Furthermore specificity in binding generated from the interactions between the bound molecule and the edges of the base pairs present on the base of the groove. Thus, the aromatic rings of many groove binding molecules form close contact with AH<sub>2</sub> protons in the minor grooves of DNA. Pullman and coworkers have shown that the negative electrostatic potential is greater in the A.T minor groove than G.C rich regions, and this provides an additional important source for A.T specific minor groove binding of cations.<sup>[131]</sup> Examples of minor groove binding drugs are netropsin and distamycin.

### **1.3.4 Forces governing Drug-DNA interaction**

#### **1.3.4.1 Hydrogen bonding**

Various chemical moieties present in nucleic acids such as phosphate group, sugar, bases and hydrophilic groups of drug participates the formation of hydrogen bonds with water. Since all linear hydrogen bonds have similar free energies, they make little net contribution to the favorable free energy change when drug and nucleic acid interact in solution. By contrast, formation of poorly aligned hydrogen bonds, or absence of some of them on the complex formation, carries a free energy penalty of about  $4 \text{ KJ mol}^{-1}$ . Thus hydrogen bonds are one of the most important means of making sequence specific interaction of nucleic acid with drug.

#### **1.3.4.2 Electrostatic forces: Salt bridges**

The electrostatic interactions between groups of opposite charges led to formation of Salt bridges. These are relatively long-range forces and provide about  $40 \text{ KJ mol}^{-1}$  of stabilization per salt bridge. In drug-DNA complexes, with the increase in concentration of salt, the strength of salt bridges decreases. They become stronger if no water molecules are present in between the ionized groups.<sup>[132]</sup>

#### **1.3.4.3 Entropic forces: Hydrophobic effect**

The behavior of water molecules present at the interface produces hydrophobic effects. A water molecule creates a curved shaped interface and makes a layer of water molecules around itself. When these molecules aggregate, there occurs a release of the ordered water molecules at interface which subsequently become part of the disordered bulk water. In this way, the entropy of system increases due to aggregation. Polar surfaces, where the enthalpy loss tends to offset the entropy gain or desolvation are less likely to aggregate than non-polar ones. Molecules of water left at the interface between the drug and the nucleic acid indeed decrease the entropy of the system. Therefore, the surfaces of the non-planar aromatic chromophore of drug molecule are preferred to be complementarily as to avoid excessive water molecules when the complex formation takes place.<sup>[133]</sup>

#### **1.3.4.4 Base stacking: Dispersion forces**

Stacking of DNA bases occurs due to two kinds of interaction: the hydrophobic effect as

mentioned above and dispersion forces. Molecules that have no net dipole moment tend to attract each other by a short dipole–induced–dipole interaction. Such dispersion forces decrease with the inverse sixth power of the distance separating the two dipoles, and so are very sensitive to the thermal motion of the molecules involved. Despite their extreme distance dependence, dispersion forces are important in keeping the structure of double stranded nucleic acids because they help to cause base stacking. Besides they allow aromatic ring of the drug to intercalate between bases and stabilize it by base stacking.<sup>[134]</sup>

#### **1.4 Aim of thesis**

This thesis is focused on understanding the interaction of G-quadruplex DNA formed at various region of human genome with naturally available small molecules readily available in human diet. These non-canonical secondary structures of DNA have been considered as a potent target for anti-cancer therapeutics. Previously, many small molecules have been reported to bind to G-quadruplex DNA structures formed at telomeres and promoter regions of various oncogenes; and they have been known to exhibit anti-cancer activity. Perhaps these small molecules are synthetic in nature, it is obvious that they will exert cytotoxicity to normal cells and imparts other side effects. But, small molecules of natural origin and readily available in human diets could overcome the problem of systemic cytotoxicity and other side effects. However, such small molecules have been exploited very less and their potential to exert anti-cancer activity need to be explore yet.

I have chosen such group of molecules that is flavonoids and alkaloids and targeted their interaction with various G-quadruplex forming DNA sequences and explored their potential to act as a potent anti-cancer drug. The major work of my thesis is inspired by the fact that those DNA sequences that are capable of forming these non-canonical secondary structures are found to be over expressed in majority of all cancers. Further, stabilization of these structures could aid in inhibition of telomerase activity that will results in inhibition of telomere elongation, as well as, inhibition of RNA polymerase activity that will lead to down regulation of gene expression.

Thus, I started my work by understanding the interaction of naturally available small molecules with G-quadruplex structure forming DNA sequences. For this, I have chosen flavonoids as small molecule scaffold and human telomeric DNA forming G-quadruplex structure as its target. Further, the other targets have also been explored with flavonoids as well

as other small molecule that is alkaloid. The interactions were probed by employing various biophysical techniques that will provide detailed information of their interaction. These include multiple spectroscopic techniques such as steady state and time resolved fluorescence spectroscopy, UV- spectroscopy and Circular Dichroism spectroscopy. These will provide the binding parameters governing drug-DNA interaction that includes binding site, mode of binding and its stoichiometry. Once the interaction of small molecule with target is confirmed, the thermodynamic parameter governing interaction was determined by performing isothermal calorimetry titrations were performed. Also, the stabilization effect of ligand on G-quadruplex structure is also determined that makes the small molecule of choice. Selectivity of molecule and its specificity for G-quadruplex DNA was crucial in this study.

Furthermore, for detailed understanding the drug-DNA interaction, it is requisite to precisely know the structure of drug-DNA complex in space. To achieve this goal, I have carried out two- dimensional Nuclear Magnetic Resonance (NMR) spectroscopy that is Nuclear Overhauser Spectroscopy (NOESY). Solution structure of the complex will tell the exact binding site of ligand on G-quadruplex DNA, and their protons that are involved in this interaction.

Moreover, it is indispensable to understand the cytotoxicity of these molecules on cancer cell lines and to get some idea for their mechanism of action. This is achieved by performing various cell culture experiments. The cytotoxic effect of ligands was computed by performing MTT assays. Downregulation of gene expression and its effect on gene expression was determined by performing semi-quantitative PCR and Luciferase assay. The localization of ligand inside cell was also seen and its mechanism of action was determined by performing FACS studies.

This study thus provides a complete story for the exploring the potential of dietary natural molecules to act as anti-cancer agents by targeting G-quadruplex structures formed at various regions on human genome.

## **1.5 Organization of thesis**

**Chapter 1** gives detailed introduction of the basic of targeting G-quadruplex DNA and historic development of drugs that binds and stabilizes these structures. This includes a comprehensive review of the literature and scope of thesis.

**Chapter 2** summarizes the instrumentation and general methods used in this study.

In **Chapter 3**, interaction of flavonoids with human telomeric DNA (5'-T<sub>2</sub>AG<sub>3</sub>T-3')<sub>4</sub> forming G-quadruplex structure was mentioned. This study provides us the first solution structure of complex formed between human telomeric DNA forming intermolecular parallel G-quadruplex structure and Quercetin.

In **Chapter 4**, we have extended the exploration of flavonoids with biologically significant sequence of human c-myc promoter regions forming G-quadruplex structure. We have deduced the first solution structure of Quercetin-c-myc G-quadruplex complex in which Quercetin and suggested its mode of binding. Further, the biological activity of Quercetin was assessed in HeLa cells that showed its subcellular localization in nucleus. It inhibits the cell growth by inducing apoptosis and down-regulates c-myc gene expression in cancer cell.

**Chapter 5** deals with interaction of Piperine with three biologically significant DNA sequences forming G-quadruplex structure and suggested that Piperine stacks at 5' and 3' G-tetrads of c-myc G-quadruplex DNA structure and stabilize it via  $\pi$ - $\pi$  stacking and hydrogen bonding. Its cytotoxic effects on various cancer cell lines were explored and its mechanism of action on human lung carcinoma (A549) cell lines was determined. This is the first study for the interaction of Piperine, a natural alkaloid, with various human G-quadruplex DNA sequences.

**Chapter 6** contains the conclusions of the work done in the thesis and future prospective of the study.

## 1.6 Scope of thesis

G-quadruplex DNA structures are higher ordered structure of DNA found in various regions of human genome like telomeric regions, oncogene promoter regions, immunoglobulin switch regions, etc. There has been increasing knowledge of importance of DNA sequences forming G-quadruplex structures in proliferation and maintenance of cancer. With this interest, it becomes essential to target these G-quadruplex DNA structures by small molecules as potential therapy for cancer treatment. As delineated in the earlier sections that various small molecules have been previously used to target G-quadruplex DNA structure found in human genome. But majority of them are of synthetic in origin therefore they must be associated with several side effects. Natural molecules offer advantage over synthetic molecules by providing low

cytotoxicity to normal cells. The overall theme of the present work mentioned in this thesis is the exploration of naturally available small molecule for targeting various DNA sequences forming G-quadruplex structures. These small molecules are available in our daily diets and have been known for providing several benefits to human health. The interactions of these molecules were probed by employing different biophysical techniques to know their binding and reveal the binding mode. Further, the work is centralized to deduce structure of complex formed by ligand and G-quadruplex DNA. As NMR offers benefit over other spectroscopic techniques in providing the thorough knowledge about structural and dynamic information; thereby it provides the exact binding site, mode and information about structural basis of complex formation. Moreover, the potential of these molecules to stabilize G-quadruplex structure and their effect on regulation of gene expression was also determined. Furthermore, their cytotoxic effect on cancer cells and mechanism of this cytotoxicity were explored. Quite remarkably, we were able to correlate their anti-cancer effect by stabilizing G-quadruplex structure. Our study highlighted the importance of using dietary natural molecules (Flavonoids and Piperine) to act as anti-cancer agents and by targeting G-quadruplex structures formed at various regions on human genome. This structural information will aid in synthesis of new drug candidates utilizing these molecules as basic pharmacophore moiety.

## 1.7 References

1. Krieger M.S.M., Matsudaira P.T, Lodish H.F, Darnell J.E, Lawrence Z, Kaiser C, Berk A (2004), "Section 4.1: Structure of Nucleic Acids". Molecular cell biology. New York: W.H. Freeman and CO. (ISBN 0-7167-4366-3).
2. Alberts B.J.A., Lewis J, Raff M, Roberts K, Wlaler P ( (2002)), Molecular Biology of the Cell (4th ed.), New York NY: Garland Science. , (ISBN 0-8153-3218-1.).
3. Katsuyuki A.K., Murayama; Hu, Ning-Hai (2016), Nucleic Acid Constituent complexes", (DOI:10.1007/978-3-319-21756-7\_3).
4. Watson J.D., Crick F.H.C. (1953), Molecular Structure of Nucleic Acids: A Structure for Deoxyribose *Nucleic Acid*, *Nat.*, 171, 737-738 (DOI: 10.1038/171737a0).
5. Chou S.-H., Chin K.-H., Wang A.H.J. (2003), SURVEY AND SUMMARY: Unusual DNA duplex and hairpin motifs, *Nucleic Acids Res.*, 31, 2461-2474 (DOI: 10.1093/nar/gkg367).
6. Qin Y., Hurley L.H. (2008), Structures, folding patterns, and functions of intramolecular

- DNA G-quadruplexes found in eukaryotic promoter regions, *Biochimie.*, 90, 1149-1171 (DOI: 10.1016/j.biochi.2008.02.020).
7. Huppert J.L. (2008), Hunting G-quadruplexes, *Biochimie.*, 90, 1140-1148 (DOI: 10.1016/j.biochi.2008.01.014).
  8. Gellert M., Lipsett M.N., Davies D.R. (1962), Helix formation by guanylic acid, *Proc. Natl. Acad. Sci. U S A*, 48, 2013-2018.
  9. Hud N.V.P.J. (2006), The role of cations in determining quadruplex structure and stability, In: Neidle S, editor. *Quadruplex Nucleic Acids*. Royal Society of Chemistry Publishing; Cambridge UK: 2006. pp. 100–130., ; Cambridge UK: 2006. pp. 100–130 (ISBN: 978-0-85404-374-3).
  10. Burge S., Parkinson G.N., Hazel P., Todd A.K., Neidle S. (2006), Quadruplex DNA: sequence, topology and structure, *Nucleic Acids Res.*, 34, 5402-5415 (DOI: 10.1093/nar/gkl655).
  11. Keniry M.A. (2000), Quadruplex structures in nucleic acids, *Biopolymers*, 56, 123-146 (DOI: 10.1002/1097-0282(2000/2001)56:3<123::aid-bip10010>3.0.co;2-3).
  12. Wang Y., Patel D.J. (1992), Guanine residues in d(T2AG3) and d(T2G4) form parallel-stranded potassium cation stabilized G-quadruplexes with anti glycosidic torsion angles in solution, *Biochemistry*, 31, 8112-8119 (DOI: 10.1021/bi00150a002).
  13. Simonsson T. (2001), G-quadruplex DNA structures--variations on a theme, *Biol. Chem.*, 382, 621-628 (DOI: 10.1515/bc.2001.073).
  14. Gilbert D.E., Feigon J. (1999), Multistranded DNA structures, *Curr. Opin. Struct. Biol.*, 9, 305-314 (DOI: 10.1016/s0959-440x(99)80041-4).
  15. Crnugelj M., Sket P., Plavec J. (2003), Small change in a G-rich sequence, a dramatic change in topology: new dimeric G-quadruplex folding motif with unique loop orientations, *J. Am. Chem. Soc.*, 125, 7866-7871 (DOI: 10.1021/ja0348694).
  16. Burge S., Parkinson G.N., Hazel P., Todd A.K., Neidle S. (2006), Quadruplex DNA: sequence, topology and structure, *Nucleic Acids Res.*, 34, 5402-5415 (DOI: 10.1093/nar/gkl655).
  17. Guédin A., Gros J., Alberti P., Mergny J.-L. (2010), How long is too long? Effects of loop size on G-quadruplex stability, *Nucleic Acids Res.*, 38, 7858-7868 (DOI: 10.1093/nar/gkq639).

18. Wang Y., Patel D.J. (1993), Solution structure of a parallel-stranded G-quadruplex DNA, *J. Mol. Biol.*, 234, 1171-1183 (DOI: 10.1006/jmbi.1993.1668).
19. Ikebukuro K., Okumura Y., Sumikura K., Karube I. (2005), A novel method of screening thrombin-inhibiting DNA aptamers using an evolution-mimicking algorithm, *Nucleic Acids Res.*, 33, e108-e108 (DOI: 10.1093/nar/gni108).
20. Rachwal P.A., Brown T., Fox K.R. (2007), Sequence effects of single base loops in intramolecular quadruplex DNA, *FEBS Lett.*, 581, 1657-1660 (DOI: 10.1016/j.febslet.2007.03.040).
21. Huppert J.L., Balasubramanian S. (2005), Prevalence of quadruplexes in the human genome, *Nucleic Acids Res.*, 33, 2908-2916 (DOI: 10.1093/nar/gki609).
22. Wong H.M., Stegle O., Rodgers S., Huppert J.L. (2010), A Toolbox for Predicting G-Quadruplex Formation and Stability, *J. Nucleic Acids*, 2010, (DOI: 10.4061/2010/564946).
23. Todd A.K., Johnston M., Neidle S. (2005), Highly prevalent putative quadruplex sequence motifs in human DNA, *Nucleic Acids Res.*, 33, 2901-2907 (DOI: 10.1093/nar/gki553).
24. Huppert J.L., Balasubramanian S. (2007), G-quadruplexes in promoters throughout the human genome, *Nucleic Acids Res.*, 35, 406-413 (DOI: 10.1093/nar/gkl1057).
25. Zakian V.A. (1995), Telomeres: beginning to understand the end, *Science*, 270, 1601-1607 (DOI: 10.1126/science.270.5242.1601).
26. Bochman M.L., Paeschke K., Zakian V.A. (2012), DNA secondary structures: stability and function of G-quadruplex structures, *Nat. Rev. Genet.*, 13, 770-780 (DOI: 10.1038/nrg3296).
27. McElligott R., Wellinger R.J. (1997), The terminal DNA structure of mammalian chromosomes, *EMBO J.*, 16, 3705-3714 (DOI: 10.1093/emboj/16.12.3705).
28. Wright W.E., Tesmer V.M., Huffman K.E., Levene S.D., Shay J.W. (1997), Normal human chromosomes have long G-rich telomeric overhangs at one end, *Genes Dev.*, 11, 2801-2809 (DOI: 10.1101/gad.11.21.2801).
29. Hayflick L., Moorhead P.S. (1961), The serial cultivation of human diploid cell strains, *Exp. Cell Res.*, 25, 585-621 (DOI: 10.1016/0014-4827(61)90192-6).
30. Chai W., Shay J.W., Wright W.E. (2005), Human telomeres maintain their overhang length at senescence, *Mol. Cell. Biol.*, 25, 2158-2168 (DOI: 10.1128/mcb.25.6.2158-2168.2005).
31. Kim N.W., Piatyszek M.A., Prowse K.R., Harley C.B., West M.D., Ho P.L., Coviello G.M., Wright W.E., Weinrich S.L., Shay J.W. (1994), Specific association of human telomerase

- activity with immortal cells and cancer, *Science*, 266, 2011-2015(DOI: 10.1126/science.7605428).
32. Bodnar A.G., Ouellette M., Frolkis M., Holt S.E., Chiu C.P., Morin G.B., Harley C.B., Shay J.W., Lichtsteiner S., Wright W.E. (1998), Extension of life-span by introduction of telomerase into normal human cells, *Science*, 279, 349-352(DOI: 10.1126/science.279.5349.349).
33. Reddel R.R. (2014), Telomere Maintenance Mechanisms in Cancer: Clinical Implications, *Curr. Pharm. Des.*, 20, 6361-6374 (DOI: 10.2174/1381612820666140630101047).
34. Zahler A.M., Williamson J.R., Cech T.R., Prescott D.M. (1991), Inhibition of telomerase by G-quartet DNA structures, *Nature*, 350, 718-720 (DOI: 10.1038/350718a0).
35. Ou T.M., Lu Y.J., Tan J.H., Huang Z.S., Wong K.Y., Gu L.Q. (2008), G-quadruplexes: targets in anticancer drug design, *ChemMedChem*, 3, 690-713 (DOI: 10.1002/cmdc.200700300).
36. De Cian A., Lacroix L., Douarre C., Temime-Smaali N., Trentesaux C., Riou J.F., Mergny J.L. (2008), Targeting telomeres and telomerase, *Biochimie.*, 90, 131-155 (DOI: 10.1016/j.biochi.2007.07.011).
37. Wang Y., Patel D.J. (1993), Solution structure of the human telomeric repeat d[AG<sub>3</sub>(T<sub>2</sub>AG<sub>3</sub>)<sub>3</sub>] G-tetraplex, *Structure*, 1, 263-282 (DOI: 10.1016/0969-2126(93)90015-9).
- d[AG<sub>3</sub>(T<sub>2</sub>AG<sub>3</sub>)<sub>3</sub>] G-tetraplex, *Structure*, 1, 263-282 (DOI: 10.1016/0969-2126(93)90015-9).
38. Luu K.N., Phan A.T., Kuryavyi V., Lacroix L., Patel D.J. (2006), Structure of the human telomere in K<sup>+</sup> solution: an intramolecular (3 + 1) G-quadruplex scaffold, *J. Am. Chem. Soc.*, 128, 9963-9970 (DOI: 10.1021/ja062791w).
39. Heddi B., Phan A.T. (2011), Structure of Human Telomeric DNA in Crowded Solution, *J. Am. Chem. Soc.*, 133, 9824-9833 (DOI: 10.1021/ja200786q).
40. Balasubramanian S., Hurley L.H., Neidle S. (2011), Targeting G-quadruplexes in gene promoters: a novel anticancer strategy?, *Nat. Rev. Drug Discov.*, 10, 261-275 (DOI: 10.1038/nrd3428).
41. Phan A.T., Modi Y.S., Patel D.J. (2004), Propeller-type parallel-stranded G-quadruplexes in the human c-myc promoter, *J. Am. Chem. Soc.*, 126, 8710-8716 (DOI: 10.1021/ja048805k).
42. Dai J., Dexheimer T.S., Chen D., Carver M., Ambrus A., Jones R.A., Yang D. (2006), An

- intramolecular G-quadruplex structure with mixed parallel/antiparallel G-strands formed in the human BCL-2 promoter region in solution, *J. Am. Chem. Soc.*, 128, 1096-1098 (DOI: 10.1021/ja055636a).
43. Dai J., Chen D., Jones R.A., Hurley L.H., Yang D. (2006), NMR solution structure of the major G-quadruplex structure formed in the human BCL2 promoter region, *Nucleic Acids Res.*, 34, 5133-5144 (DOI: 10.1093/nar/gkl610).
  44. Cogoi S., Shchekotikhin A.E., Xodo L.E. (2014), HRAS is silenced by two neighboring G-quadruplexes and activated by MAZ, a zinc-finger transcription factor with DNA unfolding property, *Nucleic Acids Res.*, 42, 8379-8388 (DOI: 10.1093/nar/gku574).
  45. Cogoi S., Xodo L.E. (2006), G-quadruplex formation within the promoter of the KRAS proto-oncogene and its effect on transcription, *Nucleic Acids Res.*, 34, 2536-2549 (DOI: 10.1093/nar/gkl286).
  46. Phan A.T., Kuryavyi V., Burge S., Neidle S., Patel D.J. (2007), Structure of an unprecedented G-quadruplex scaffold in the human c-kit promoter, *J. Am. Chem. Soc.*, 129, 4386-4392 (DOI: 10.1021/ja068739h).
  47. Todd A.K., Haider S.M., Parkinson G.N., Neidle S. (2007), Sequence occurrence and structural uniqueness of a G-quadruplex in the human c-kit promoter, *Nucleic Acids Res.*, 35, 5799-5808 (DOI: 10.1093/nar/gkm609).
  48. Mitchell T., Ramos-Montoya A., Di Antonio M., Murat P., Ohnmacht S., Micco M., Jurmeister S., Fryer L., Balasubramanian S., Neidle S., Neal D.E. (2013), Downregulation of androgen receptor transcription by promoter g-quadruplex stabilization as a potential alternative treatment for castrate-resistant prostate cancer, *Biochemistry*, 52, 1429-1436 (DOI: 10.1021/bi301349c).
  49. Sun D., Guo K., Rusche J.J., Hurley L.H. (2005), Facilitation of a structural transition in the polypurine/polypyrimidine tract within the proximal promoter region of the human VEGF gene by the presence of potassium and G-quadruplex-interactive agents, *Nucleic Acids Res.*, 33, 6070-6080 (DOI: 10.1093/nar/gki917).
  50. Abbaspour Babaei M., Kamalidehghan B., Saleem M., Huri H.Z., Ahmadipour F. (2016), Receptor tyrosine kinase (c-Kit) inhibitors: a potential therapeutic target in cancer cells, *Drug Des. Dev. Ther.*, 10, 2443-2459 (DOI: 10.2147/DDDT.S89114).
  51. Wei D., Parkinson G.N., Reszka A.P., Neidle S. (2012), Crystal structure of a c-kit promoter

- quadruplex reveals the structural role of metal ions and water molecules in maintaining loop conformation, *Nucleic Acids Res.*, 40, 4691-4700 (DOI: 10.1093/nar/gks023).
52. Yang D., Hurley L.H. (2006), Structure of the biologically relevant G-quadruplex in the c-MYC promoter, *Nucleosides Nucleotides Nucleic Acids*, 25, 951-968 (DOI: 10.1080/15257770600809913).
  53. Agrawal P., Lin C., Mathad R.I., Carver M., Yang D. (2014), The Major G-Quadruplex Formed in the Human BCL-2 Proximal Promoter Adopts a Parallel Structure with a 13-nt Loop in K<sup>+</sup> Solution, *J. Am. Chem. Soc.*, 136, 1750-1753 (DOI: 10.1021/ja4118945).
  54. Ambrus A., Chen D., Dai J., Jones R.A., Yang D. (2005), Solution structure of the biologically relevant G-quadruplex element in the human c-MYC promoter. Implications for G-quadruplex stabilization, *Biochemistry*, 44, 2048-2058 (DOI: 10.1021/bi048242p).
  55. Yan C., Higgins P.J. (2013), Drugging the Undruggable: Transcription Therapy for Cancer, *Biochim. Biophys. Acta*, 1835, 76-85 (DOI: 10.1016/j.bbcan.2012.11.002).
  56. Onel B., Lin C., Yang D. (2014), DNA G-quadruplex and its potential as anticancer drug target, *Sci. China Chem.*, 57, 1605-1614 (DOI: 10.1007/s11426-014-5235-3).
  57. Greider C.W. (1996), Telomere length regulation, *Annu. Rev. Biochem.*, 65, 337-365 (DOI: 10.1146/annurev.bi.65.070196.002005).
  58. Stewart S.A., Weinberg R.A. (2006), Telomeres: cancer to human aging, *Annu. Rev. Cell Dev. Biol.*, 22, 531-557 (DOI: 10.1146/annurev.cellbio.22.010305.104518).
  59. Cech T.R., Lingner J. (1997), Telomerase and the chromosome end replication problem, *Ciba. Found. Symp.*, 211, 20-28.
  60. Shay J.W., Wright W.E. (2000), Hayflick, his limit, and cellular ageing, *Nat. Rev. Mol. Cell Biol.*, 1, 72-76 (DOI:10.1038/35036093).
  61. Zvereva M.I., Shcherbakova D.M., Dontsova O.A. (2010), Telomerase: structure, functions, and activity regulation, *Biochemistry (Mosc)*, 75, 1563-1583 (DOI: 10.1134/S0006297910130055).
  62. Sharma S., Doherty K.M., Brosh R.M., Jr. (2005), DNA helicases as targets for anti-cancer drugs, *Curr. Med. Chem. Anticancer Agents*, 5, 183-199 (DOI: 10.2174/1568011053765985).
  63. Marcu K.B., Bossone S.A., Patel A.J. (1992), myc function and regulation, *Annu. Rev. Biochem.*, 61, 809-860 (DOI: 10.1146/annurev.bi.61.070192.004113).
  64. Siddiqui-Jain A., Grand C.L., Bearss D.J., Hurley L.H. (2002), Direct evidence for a G-

- quadruplex in a promoter region and its targeting with a small molecule to repress c-MYC transcription, *Proc. Natl. Acad. Sci.*, 99, 11593-11598 (10.1073/pnas.182256799).
65. Al-Sajee D., Huizinga J.D. (2012), Interstitial Cells of Cajal: Pathology, injury and repair, *Sultan Qaboos. Univ. Med. J.*, 12, 411-421.
66. Klein S., Seidler B., Kettenberger A., Sibaev A., Rohn M., Feil R., Allescher H.-D., Vanderwinden J.-M., Hofmann F., Schemann M., Rad R., Storr M.A., Schmid R.M., Schneider G., Saur D. (2013), Interstitial cells of Cajal integrate excitatory and inhibitory neurotransmission with intestinal slow-wave activity, *Nat. Commun.*, 4, 1630 (DOI: 10.1038/ncomms2626)
67. Fernando H., Reszka A.P., Huppert J., Ladame S., Rankin S., Venkitaraman A.R., Neidle S., Balasubramanian S. (2006), A conserved quadruplex motif located in a transcription activation site of the human c-kit oncogene, *Biochemistry*, 45, 7854-7860 (DOI: 10.1021/bi0601510).
68. Rankin S., Reszka A.P., Huppert J., Zloh M., Parkinson G.N., Todd A.K., Ladame S., Balasubramanian S., Neidle S. (2005), Putative DNA quadruplex formation within the human c-kit oncogene, *J. Am. Chem. Soc.*, 127, 10584-10589 (DOI: 10.1021/ja050823u).
69. Gunaratnam M., Swank S., Haider S.M., Galesa K., Reszka A.P., Beltran M., Cuenca F., Fletcher J.A., Neidle S. (2009), Targeting Human Gastrointestinal Stromal Tumor Cells with a Quadruplex-Binding Small Molecule, *J. Med. Chem.*, 52, 3774-3783 (DOI: 10.1021/jm900424a).
70. Agrawal P., Hatzakis E., Guo K., Carver M., Yang D. (2013), Solution structure of the major G-quadruplex formed in the human VEGF promoter in K<sup>+</sup>: insights into loop interactions of the parallel G-quadruplexes, *Nucleic Acids Res.*, 41, 10584-10592 (DOI: 10.1093/nar/gkt784).
71. Cammas A., Dubrac A., Morel B., Lamaa A., Touriol C., Teulade-Fichou M.P., Prats H., Millevoi S. (2015), Stabilization of the G-quadruplex at the VEGF IRES represses cap-independent translation, *RNA Biol.*, 12, 320-329 (DOI: 10.1080/15476286.2015.1017236).
72. Han H., Cliff C.L., Hurley L.H. (1999), Accelerated assembly of G-quadruplex structures by a small molecule, *Biochemistry*, 38, 6981-6986 (DOI: 10.1021/bi9905922).
73. Campbell N.H., Parkinson G.N., Reszka A.P., Neidle S. (2008), Structural basis of DNA quadruplex recognition by an acridine drug, *J. Am. Chem. Soc.*, 130, 6722-6724 (DOI:

- 10.1021/ja8016973).
74. Dai J., Carver M., Hurley L.H., Yang D. (2011), Solution Structure of a 2:1 Quindoline-c-MYC G-Quadruplex: Insights into G-Quadruplex-Interactive Small Molecule Drug Design, *J. Am. Chem. Soc.*, 133, 17673-17680 (DOI: 10.1021/ja205646q).
75. Rezler E.M., Seenisamy J., Bashyam S., Kim M.Y., White E., Wilson W.D., Hurley L.H. (2005), Telomestatin and diseleno saphyryin bind selectively to two different forms of the human telomeric G-quadruplex structure, *J. Am. Chem. Soc.*, 127, 9439-9447 (DOI: 10.1021/ja0505088).
76. Granotier C., Pennarun G., Riou L., Hoffschir F., Gauthier L.R., De Cian A., Gomez D., Mandine E., Riou J.-F., Mergny J.-L., Mailliet P., Dutrillaux B., Boussin F.D. (2005), Preferential binding of a G-quadruplex ligand to human chromosome ends, *Nucleic Acids Res.* 33, 4182-4190 (DOI: 10.1093/nar/gki722).
77. Chung W.J., Heddi B., Hamon F., Teulade-Fichou M.P., Phan A.T. (2014), Solution structure of a G-quadruplex bound to the bisquinolinium compound Phen-DC(3), *Angew. Chem. Int. Ed. Engl.*, 53, 999-1002 (DOI: 10.1002/anie.201308063).
78. Lagah S., Tan I.L., Radhakrishnan P., Hirst R.A., Ward J.H., O'Callaghan C., Smith S.J., Stevens M.F.G., Grundy R.G., Rahman R. (2014), RHPS4 G-Quadruplex Ligand Induces Anti-Proliferative Effects in Brain Tumor Cells, *PLoS ONE*, 9, e86187 (DOI: 10.1371/journal.pone.0086187).
79. Sun D., Thompson B., Cathers B.E., Salazar M., Kerwin S.M., Trent J.O., Jenkins T.C., Neidle S., Hurley L.H. (1997), Inhibition of human telomerase by a G-quadruplex-interactive compound, *J. Med. Chem.*, 40, 2113-2116 (DOI: 10.1021/jm970199z).
80. Franceschin M., Alvino A., Casagrande V., Mauriello C., Pascucci E., Savino M., Ortaggi G., Bianco A. (2007), Specific interactions with intra- and intermolecular G-quadruplex DNA structures by hydrosoluble coronene derivatives: a new class of telomerase inhibitors, *Bioorg. Med. Chem.*, 15, 1848-1858 (DOI: 10.1016/j.bmc.2006.11.032).
81. Fedoroff O.Y., Salazar M., Han H., Chemeris V.V., Kerwin S.M., Hurley L.H. (1998), NMR-Based model of a telomerase-inhibiting compound bound to G-quadruplex DNA, *Biochemistry*, 37, 12367-12374 (DOI: 10.1021/bi981330n).
82. Gavathiotis E., Heald R.A., Stevens M.F., Searle M.S. (2003), Drug recognition and stabilisation of the parallel-stranded DNA quadruplex d(TTAGGGT)<sub>4</sub> containing the human

- telomeric repeat, *J. Mol. Biol.*, 334, 25-36 (DOI: 10.1016/j.jmb.2003.09.018).
83. Granotier C., Pennarun G., Riou L., Hoffschir F., Gauthier L.R., De Cian A., Gomez D., Mandine E., Riou J.F., Mergny J.L., Mailliet P., Dutrillaux B., Boussin F.D. (2005), Preferential binding of a G-quadruplex ligand to human chromosome ends, *Nucleic Acids Res.*, 33, 4182-4190 (DOI: 10.1093/nar/gki722).
  84. De Cian A., DeLemos E., Mergny J.-L., Teulade-Fichou M.-P., Monchaud D. (2007), Highly Efficient G-Quadruplex Recognition by Bisquinolinium Compounds, *J. Am. Chem. Soc.*, 129, 1856-1857 (DOI: 10.1021/ja067352b).
  85. Hounsou C., Guittat L., Monchaud D., Jourdan M., Saettel N., Mergny J.L., Teulade-Fichou M.P. (2007), G-quadruplex recognition by quinacridines: a SAR, NMR, and biological study, *ChemMedChem*, 2, 655-666 (DOI: 10.1002/cmdc.200600286).
  86. Mergny J.-L., Maurizot J.-C. (2001), Fluorescence Resonance Energy Transfer as a Probe for G-Quartet Formation by a Telomeric Repeat, *ChemBioChem*, 2, 124-132 (DOI: 10.1002/1439-7633(20010202)2:2<124::AID-CBIC124>3.0.CO;2-L).
  87. Gaynutdinov T.I., Neumann R.D., Panyutin I.G. (2008), Structural polymorphism of intramolecular quadruplex of human telomeric DNA: effect of cations, quadruplex-binding drugs and flanking sequences, *Nucleic Acids Res.*, 36, 4079-4087 (DOI: 10.1093/nar/gkn351).
  88. Dai J., Carver M., Hurley L.H., Yang D. (2011), Solution structure of a 2:1 quindoline-c-MYC G-quadruplex: insights into G-quadruplex-interactive small molecule drug design, *J. Am. Chem. Soc.*, 133, 17673-17680 (DOI: 10.1021/ja205646q).
  89. Efferth T., Li P.C., Konkimalla V.S., Kaina B. (2007), From traditional Chinese medicine to rational cancer therapy, *Trends. Mol. Med.*, 13, 353-361 (DOI: 10.1016/j.molmed.2007.07.001).
  90. Beecher G.R. (2003), Overview of dietary flavonoids: nomenclature, occurrence and intake, *J. Nutr.*, 133, 3248s-3254s.
  91. Heim K.E., Tagliaferro A.R., Bobilya D.J. (2002), Flavonoid antioxidants: chemistry, metabolism and structure-activity relationships, *J Nutr Biochem*, 13, 572-584).
  92. Heim K.E., Tagliaferro A.R., Bobilya D.J. (2002), Flavonoid antioxidants: chemistry, metabolism and structure-activity relationships, *J. Nutr. Biochem.* 13, 572-584 (DOI: 10.1016/S0955-2863(02)00208-5).

93. Pietta P.G. (2000), Flavonoids as antioxidants, *J. Nat. Prod.*, 63, 1035-1042(DOI: 10.1021/np9904509).
94. Sroka Z. (2005), Antioxidative and antiradical properties of plant phenolics, *Z. Naturforsch. C.*, 60, 833-843(DOI: 10.1515/znc-2005-11-1204).
95. Hertog M.G., Feskens E.J., Hollman P.C., Katan M.B., Kromhout D. (1993), Dietary antioxidant flavonoids and risk of coronary heart disease: the Zutphen Elderly Study, *Lancet*, 342, 1007-1011 (DOI: 10.1016/0140-6736(93)92876-U).
96. Huxley R.R., Neil H.A.W. (0000), The relation between dietary flavonol intake and coronary heart disease mortality: a meta-analysis of prospective cohort studies, *Eur. J. Clin. Nutr.*, 57, 904-908(DOI: 10.1038/sj.ejcn.1601624).
97. Grassi D., Aggio A., Onori L., Croce G., Tiberti S., Ferri C., Ferri L., Desideri G. (2008), Tea, Flavonoids, and Nitric Oxide-Mediated Vascular Reactivity, *J. Nutr.*, 138, 1554S-1560S).
98. Duarte J., Perez Vizcaino F., Utrilla P., Jimenez J., Tamargo J., Zarzuelo A. (1993), Vasodilatory effects of flavonoids in rat aortic smooth muscle. Structure-activity relationships, *Gen. Pharmacol.*, 24, 857-862(DOI: 10.1016/0306-3623(93)90159-U).
99. Perez A., Gonzalez-Manzano S., Jimenez R., Perez-Abud R., Haro J.M., Osuna A., Santos-Buelga C., Duarte J., Perez-Vizcaino F. (2014), The flavonoid quercetin induces acute vasodilator effects in healthy volunteers: Correlation with beta-glucuronidase activity, *Pharmacol. Res.*, 89, 11-18 (DOI: 10.1016/j.phrs.2014.07.005).
100. Ramassamy C. (2006), Emerging role of polyphenolic compounds in the treatment of neurodegenerative diseases: a review of their intracellular targets, *Eur. J. Pharmacol.*, 545, 51-64 (DOI: 10.1016/j.ejphar.2006.06.025).
101. Magalingam K.B., Radhakrishnan A.K., Haleagrahara N. (2015), Protective Mechanisms of Flavonoids in Parkinson's Disease, *Oxid. Med. Cell Longev.*, 2015, 14 (DOI: 10.1155/2015/314560).
102. Bhullar K.S., Rupasinghe H.P.V. (2013), Polyphenols: Multipotent Therapeutic Agents in Neurodegenerative Diseases, *Oxid. Med. Cell Longev.*, 2013, 18 (DOI: 10.1155/2013/891748).
103. Solanki I., Parihar P., Mansuri M.L., Parihar M.S. (2015), Flavonoid-Based Therapies in the Early Management of Neurodegenerative Diseases, *Adv. Nutr.*, 6, 64-72 (DOI: 10.1093/advn/nvz001).

- 10.3945/an.114.007500).
104. Sokolov A.N., Pavlova M.A., Klosterhalfen S., Enck P. (2013), Chocolate and the brain: neurobiological impact of cocoa flavanols on cognition and behavior, *Neurosci. Biobehav. Rev.*, 37, 2445-2453 (DOI: 10.1016/j.neubiorev.2013.06.013).
  105. Hodges R.E., Minich D.M. (2015), Modulation of Metabolic Detoxification Pathways Using Foods and Food-Derived Components: A Scientific Review with Clinical Application, *J.Nutr. Metab.*, 2015, 23 (DOI: 10.1155/2015/760689).
  106. Moskot M., Jakobkiewicz-Banecka J., Smolinska E., Piotrowska E., Wegrzyn G., Gabig-Ciminska M. (2015), Effects of flavonoids on expression of genes involved in cell cycle regulation and DNA replication in human fibroblasts, *Mol. Cell Biochem.*, 407, 97-109 (DOI: 10.1007/s11010-015-2458-3).
  107. Woo H.H., Jeong B.R., Hawes M.C. (2005), Flavonoids: from cell cycle regulation to biotechnology, *Biotechnol. Lett.*, 27, 365-374 (DOI: 10.1007/s10529-005-1521-7).
  108. Kim J.A., Lee S., Kim D.-E., Kim M., Kwon B.-M., Han D.C. (2015), Fisetin, a dietary flavonoid, induces apoptosis of cancer cells by inhibiting HSF1 activity through blocking its binding to the hsp70 promoter, *Carcinogenesis*, 36, 696-706 (DOI: 10.1093/carcin/bgv045).
  109. Xu R., Zhang Y., Ye X., Xue S., Shi J., Pan J., Chen Q. (2013), Inhibition effects and induction of apoptosis of flavonoids on the prostate cancer cell line PC-3 in vitro, *Food chem.*, 138, 48-53 (DOI: 10.1016/j.foodchem.2012.09.102).
  110. Balasubramanian S., Govindasamy S. (1996), Inhibitory effect of dietary flavonol quercetin on 7,12-dimethylbenz[a]anthracene-induced hamster buccal pouch carcinogenesis, *Carcinogenesis*, 17, 877-879 (DOI: 10.1093/carcin/17.4.877).
  111. Yang C.S., Yang G.Y., Landau J.M., Kim S., Liao J. (1998), Tea and tea polyphenols inhibit cell hyperproliferation, lung tumorigenesis, and tumor progression, *Exp. Lung Res.*, 24, 629-639).
  112. Yamagishi M., Natsume M., Osakabe N., Nakamura H., Furukawa F., Imazawa T., Nishikawa A., Hirose M. (2002), Effects of cacao liquor proanthocyanidins on PhIP-induced mutagenesis in vitro, and in vivo mammary and pancreatic tumorigenesis in female Sprague-Dawley rats, *Cancer Lett.*, 185, 123-130 (10.1016/S0304-3835(02)00276-8).
  113. Yamane T., Nakatani H., Kikuoka N., Matsumoto H., Iwata Y., Kitao Y., Oya K., Takahashi T. (1996), Inhibitory effects and toxicity of green tea polyphenols for gastrointestinal

carcinogenesis, *Cancer*, 77, 1662-1667 (DOI: 10.1002/(sici)1097-0142(19960415)77:8<1662::aid-cnrc36>3.0.co;2-w).

114. Gupta S., Hastak K., Ahmad N., Lewin J.S., Mukhtar H. (2001), Inhibition of prostate carcinogenesis in TRAMP mice by oral infusion of green tea polyphenols, *Proc. Natl. Acad. Sci. U S A*, 98, 10350-10355 (DOI: 10.1073/pnas.171326098).
115. Haddad A.Q., Venkateswaran V., Viswanathan L., Teahan S.J., Fleshner N.E., Klotz L.H. (2006), Novel antiproliferative flavonoids induce cell cycle arrest in human prostate cancer cell lines, *Prostate Cancer Prostatic Dis.*, 9, 68-76 (DOI: 10.1038/sj.pcan.4500845).
116. Lu J.-J., Bao J.-L., Chen X.-P., Huang M., Wang Y.-T. (2012), Alkaloids Isolated from Natural Herbs as the Anticancer Agents, *Evid. Based Complement. Alternat. Med.*, 2012, 12 (DOI: 10.1155/2012/485042).
117. Gulcin I. (2005), The antioxidant and radical scavenging activities of black pepper (*Piper nigrum*) seeds, *Int. J. Food Sci. Nutr.*, 56, 491-499 (DOI: 10.1080/09637480500450248).
118. Parmar V.S., Jain S.C., Bisht K.S., Jain R., Taneja P., Jha A., Tyagi O.D., Prasad A.K., Wengel J., Olsen C.E., Boll P.M. (1997), Phytochemistry of the genus *Piper*, *Phytochemistry*, 46, 597-673 (DOI: 10.1016/S0031-9422(97)00328-2).
119. Dong Y., Huihui Z., Li C. (2015), Piperine inhibit inflammation, alveolar bone loss and collagen fibers breakdown in a rat periodontitis model, *J. Periodont. Res.* 50, 758-765 (DOI: 10.1111/jre.12262).
120. Zutshi R.K., Singh R., Zutshi U., Johri R.K., Atal C.K. (1985), Influence of piperine on rifampicin blood levels in patients of pulmonary tuberculosis, *J. Assoc. Physicians India*, 33, 223-224.
121. Johnson J.J., Nihal M., Siddiqui I.A., Scarlett C.O., Bailey H.H., Mukhtar H., Ahmad N. (2011), Enhancing the bioavailability of resveratrol by combining it with piperine, *Mol. Nutr. Food Res.*, 55, 1169-1176 (DOI: 10.1002/mnfr.201100117).
122. Pradeep C.R., Kuttan G. (2004), Piperine is a potent inhibitor of nuclear factor-kappaB (NF-kappaB), c-Fos, CREB, ATF-2 and proinflammatory cytokine gene expression in B16F-10 melanoma cells, *Int. Immunopharmacol.*, 4, 1795-1803 (DOI: 10.1016/j.intimp.2004.08.005).
123. Yaffe P.B., Doucette C.D., Walsh M., Hoskin D.W. (2013), Piperine impairs cell cycle progression and causes reactive oxygen species-dependent apoptosis in rectal cancer cells, *Exp. Mol. Pathol.*, 94, 109-114 (DOI: 10.1016/j.yexmp.2012.10.008).

124. Kondo N., Takahashi A., Ono K., Ohnishi T. (2010), DNA Damage Induced by Alkylating Agents and Repair Pathways, *J. Nucleic Acids*, 2010, (DOI: 10.4061/2010/543531).
125. Kaplan D.J., Hurley L.H. (1981), Anthramycin binding to deoxyribonucleic acid-mitomycin C complexes. Evidence for drug-induced deoxyribonucleic acid conformational change and cooperativity in mitomycin C binding, *Biochemistry*, 20, 7572-7580 (DOI: 10.1021/bi00529a036).
126. Reedijk J. (2003), New clues for platinum antitumor chemistry: kinetically controlled metal binding to DNA, *Proc. Natl. Acad. Sci. U. S. A.*, 100, 3611-3616 (DOI: 10.1073/pnas.0737293100).
127. Paz M.M., Das A., Tomasz M. (1999), Mitomycin C linked to DNA minor groove binding agents: synthesis, reductive activation, DNA binding and cross-linking properties and in vitro antitumor activity, *Bioorg. Med. Chem.*, 7, 2713-2726 (DOI: 10.1016/S0968-0896(99)00223-0).
128. Bailly C., Laine W., Baldeyrou B., De Pauw-Gillet M.C., Colson P., Houssier C., Cimanga K., Van Miert S., Vlietinck A.J., Pieters L. (2000), DNA intercalation, topoisomerase II inhibition and cytotoxic activity of the plant alkaloid neocryptolepine, *Anticancer Drug Des.*, 15, 191-201.
129. Phillips D.R., Baguley B.C., Brownlee R.T., Cacioli P., Chandler C.J., Kyratzis I., Reiss J.A., Scourides P.A. (1990), The synthesis, stability and biological activity of bis-intercalating bis-daunomycin hydrazones, *Drug. Des. Deliv.*, 5, 203-219.
130. Neidle S. (2001), DNA minor-groove recognition by small molecules, *Nat. Prod. Rep.*, 18, 291-309 (DOI: 10.1039/A705982E).
131. Pullman A., Pullman B. (1981), Molecular electrostatic potential of the nucleic acids, *Q. Rev. Biophys.*, 14, 289-380 (DOI: 10.1017/S0033583500002341)
132. Dougherty D.A.M.P.O.C.S.,(2006) CA: Modern Physical Organic Chemistry. Sausalito, CA: University Science Books. (ISBN 1-891389-31-9.),
133. IUPAC, Compendium of Chemical Terminology, 2nd ed. (the "Gold Book") (1997)."hydrophobic interaction".(ISBN 0-9678550-9-8).
134. Lodish H B.A., Zipursky SL, et al. (2000), Molecular Cell Biology. 4th edition. New York: W. H. Freeman; 2000. Section 2.2, Noncovalent Bonds. , *New York: W. H. Freeman; 2000. Section 2.2, Noncovalent Bonds (ISBN-13: 978-0716737063).*



## Chapter 2

### Material, methods and instrumentation

---

---

#### 2.1 Material

Calf thymus (CT) DNA and oligonucleotide sequences forming G-quadruplex structures were purchased from Sigma Aldrich chemicals Ltd., USA. These sequences are:

Human telomeric DNA sequence (short):

tel7: d-5'-TTA GGG T-3'

Human telomeric DNA sequence (long):

tel22: d-5'-AGG GTT AGG GTT AGG GTT AGG G -3'

Human c-myc promoter DNA sequence:

Pu24T: d-5'-TGA GGG TGG TGA GGG TGG GGA AGG -3'

Human c-kit promoter DNA sequence:

ckit21: d-5'-CGG GCG GGC GCG AGG AGG GG -3'.

Other reagents used for buffer preparation like  $K_2HPO_4$ ,  $KH_2PO_4$ , KCl, NaCl,  $NaH_2PO_4$ ,  $Na_2HPO_4$ , Tris-HCl, NaOH, ethylene diamine tetra acetic acid (EDTA), 3-(trimethylsilyl) propionic-2, 2, 3, 3-d<sub>4</sub> acid sodium salt (TSP), 3-(4,5-dimethylthiazol-2-yl)-2, 5-diphenyltetrazolium bromide dye (MTT), dimethyl sulphoxide (DMSO), 4',6-diamidino-2-phenylindole (DAPI) and propidium iodide (PI), were of HPLC grade obtained from Sigma Aldrich chemicals Ltd., USA. Phenol: chloroform: isoamyl alcohol mixture (25:24:1 v/v) was obtained from Himedia. Agarose, acrylamide, bis-acrylamide and other reagents required for gel and buffer preparations were obtained from Sigma Aldrich chemicals Ltd., USA. Chemicals like Luteolin, Quercetin, Rutin, Genistein, Kaempferol, Puerarin, Hesperidin, Myricetin, Daidzein and Piperine were also purchased from Sigma-Aldrich Chemicals Ltd. Synthetic oligonucleotides and small molecule samples were used without further purification.

Human lung cancer cell lines (A549), Human prostate cancer cell lines (PC3), Human liver cancer cell line (HepG2), Human cervical cancer cell line (HeLa), Human breast cancer cell lines (MCF-7), Human embryonic kidney cell line (HEK) were purchased from National Centre for Cell Science (NCCS), Pune, India. Growth media like Dulbecco's modified Eagle's medium (DMEM), Ham's F12 medium, minimum essential media Eagle (MEM), fetal bovine serum (FBS), phosphate buffer saline (PBS), antibiotic solution were purchased

from Gibco, Life Technologies (Gaithersburg, MD, USA). DeadEnd fluorometric TUNEL system was obtained from Promega. FITC Annexin-V-Apoptosis Detection Kit I was purchased from BD Pharmingen. Cells-to-cDNAII Kit (Ambion) was purchased from Invitrogen. Autoclaved MilliQ water was used to make up the volume wherever required.

## 2.2 Preparation of samples

### 2.2.1 Sample preparation for UV-melting, steady state and time resolved fluorescence spectroscopy, circular dichroism studies and isothermal calorimetry

For quadruplex formation, oligomers were dissolved in phosphate buffer (10 mM ( $K^+$ ), pH 7.0 at 25 °C) with 50 mM KCl. The oligomers were annealed by heating at 90°C for 5 mins, followed by overnight incubation at room temperature to allow gradual cooling. All experiments related to calf thymus DNA were performed in the buffer solution containing 50 mM NaCl, 10 mM phosphate buffer, pH 7.0 at 25 °C. DNA concentrations were measured spectrophotometrically at their respective  $\lambda_{max}$  (Table 2.1). Solutions of small molecules were prepared by dissolving a known quantity of sample in DMSO and calculating its molarity. All the stock solutions were stored at appropriate temperatures.

### 2.2.2 Sample preparation for NMR studies

Solution of deoxyoligonucleotide, d-(T<sub>2</sub>AG<sub>3</sub>T)<sub>4</sub> (1.21 mM) was prepared by dissolving a known quantity of sample in 90% water and 10% D<sub>2</sub>O phosphate buffer (10 mM) of pH = 7.0 having 50 mM  $K^+$  salt and their concentrations were determined by absorbance measurements at 260 nm using the extinction coefficient ( $\epsilon$ ) value, 69800 L mol<sup>-1</sup> cm<sup>-1</sup> for d-(T<sub>2</sub>AG<sub>3</sub>T)<sub>4</sub>. To suppress paramagnetic impurities that may cause line broadening during NMR measurements, 0.1mM EDTA was added to buffer. In all NMR measurements, 1 $\mu$ L of 0.1 M solution of 3-(trimethylsilyl) propionic-2, 2, 3, 3-d<sub>4</sub> acid sodium salt (TSP) was added to the samples as an internal reference.

**(i) d-(T<sub>2</sub>AG<sub>3</sub>T)<sub>4</sub> and Quercetin complex:** A complex of d-(T<sub>2</sub>AG<sub>3</sub>T)<sub>4</sub> and Quercetin was prepared by titration. Total 41.40  $\mu$ L of 28.95 mM Quercetin was added in steps to 0.50 mL of 1.21 mM d-(T<sub>2</sub>AG<sub>3</sub>T)<sub>4</sub> sample during titration in order to make 2:1 complex of Quercetin: d-(T<sub>2</sub>AG<sub>3</sub>T)<sub>4</sub>. The concentration of Quercetin (D), d-(T<sub>2</sub>AG<sub>3</sub>T)<sub>4</sub> (N) and drug/nucleotide (D/N) ratio are shown in Table 2.2.

**(ii) Pu24T and Quercetin complex:** Similarly, for the formation of 2:1 complex

*Table 2.1. List of oligonucleotides with their molar extinction coefficient*

<b>DNA</b>	<b><math>\epsilon</math> Value (L mol<sup>-1</sup> cm<sup>-1</sup>)</b>
<b>CT - DNA</b>	<b>6600</b>
<b>(T<sub>2</sub>AG<sub>3</sub>T)<sub>4</sub></b>	<b>69800</b>
<b>Pu24T</b>	<b>0.2482</b>
<b>c-kit 21up</b>	<b>0.2056</b>
<b>tel22</b>	<b>0.2285</b>

*Table 2.2. Various concentration ratios (D/N) for the complex formed between Quercetin and d-(T<sub>2</sub>AG<sub>3</sub>T)<sub>4</sub>*

Concentration in (mM)		
Drug (D)	Nucleic Acid (N)	D/N
0.00	1.21	0.00
0.24	1.21	0.20
0.48	1.21	0.40
0.61	1.21	0.50
0.73	1.21	0.60
0.97	1.21	0.80
1.21	1.21	1.00
1.45	1.21	1.20
1.82	1.21	1.50
2.12	1.21	1.75
2.42	1.21	2.00

**Table 2.3. Various concentration ratios (D/N) for the complex formed between Quercetin and Pu24T DNA**

<b>Concentration in (mM)</b>		
<b>Drug (D)</b>	<b>Nucleic Acid (N)</b>	<b>D/N</b>
<b>0.76</b>	<b>3.84</b>	<b>0.20</b>
<b>1.53</b>	<b>3.84</b>	<b>0.40</b>
<b>1.91</b>	<b>3.84</b>	<b>0.50</b>
<b>2.29</b>	<b>3.84</b>	<b>0.60</b>
<b>3.06</b>	<b>3.84</b>	<b>0.80</b>
<b>3.82</b>	<b>3.84</b>	<b>1.00</b>
<b>4.59</b>	<b>3.84</b>	<b>1.20</b>
<b>5.35</b>	<b>3.84</b>	<b>1.40</b>
<b>5.74</b>	<b>3.84</b>	<b>1.50</b>
<b>6.12</b>	<b>3.84</b>	<b>1.60</b>
<b>6.88</b>	<b>3.84</b>	<b>1.80</b>
<b>7.65</b>	<b>3.84</b>	<b>2.00</b>

*Table 2.4. Various concentration ratios (D/N) for the complex formed between Piperine and Pu24T DNA*

<b>Concentration in (mM)</b>		
<b>Drug (D)</b>	<b>Nucleic Acid (N)</b>	<b>D/N</b>
<b>0.76</b>	<b>3.84</b>	<b>0.20</b>
<b>1.53</b>	<b>3.84</b>	<b>0.40</b>
<b>1.91</b>	<b>3.84</b>	<b>0.50</b>
<b>2.29</b>	<b>3.84</b>	<b>0.60</b>
<b>3.06</b>	<b>3.84</b>	<b>0.80</b>
<b>3.82</b>	<b>3.84</b>	<b>1.00</b>
<b>4.59</b>	<b>3.84</b>	<b>1.20</b>
<b>5.35</b>	<b>3.84</b>	<b>1.40</b>
<b>5.74</b>	<b>3.84</b>	<b>1.50</b>
<b>6.12</b>	<b>3.84</b>	<b>1.60</b>
<b>6.88</b>	<b>3.84</b>	<b>1.80</b>
<b>7.65</b>	<b>3.84</b>	<b>2.00</b>

of Quercetin: Pu24T, a total of 43.34  $\mu\text{L}$  of 478 mM Quercetin was added in steps to 0.50 mL of 3.82 mM Pu24T DNA solution and final concentration of ligands at D/N = 2.0 ratio was 7.7 mM. The concentration of Quercetin (D), Pu24T DNA (N) and drug/ nucleotide (D/N) ratio are shown in Table 2.3.

**(iii) Pu24T and Piperine complex:** In the same way, complex of Pu24T- G-quadruplex DNA and Piperine was prepared by titration. Total of 80.00  $\mu\text{L}$  of 478 mM Piperine was added in steps to 0.50 mL of 3.82 mM Pu24T DNA solution and final concentration of Piperine at D/N = 2.0 ratio was 7.65 mM. The concentration of Piperine (D), Pu24T DNA (N) and drug/ nucleotide (D/N) ratio are shown in Table 2.4. For NMR broadening experiments, a fixed concentration of ligand was prepared in 90% water and 10%  $\text{D}_2\text{O}$  phosphate buffer (20 mM) of pH = 7.0 having 50 mM  $\text{K}^+$  salt. TSP was used as NMR internal reference. G-quadruplex DNA was added to ligand solutions in steps up to D/N = 100:20 ratio and proton NMR spectra were collected at 298K at each titration step.

## 2.3 Methodology and instrumentation

### 2.3.1 Fluorescence spectroscopy

Fluorescence is a process in which a fluorophore absorbs light of a particular wavelength and re-emits it at longer wavelength. The emission of energy depends upon the chemical environment of the fluorophore. Thus, fluorescence spectroscopy gives significant information about both the excited state and relaxed state dynamics of fluorophore. As this process takes place at slower time scale, therefore, wide range of interactions and perturbations influence the spectrum<sup>[1-3]</sup> (Figure 2.1). Generally, nucleic acids have weak fluorescence. If a fluorescent probe binds at some specific site or it covalently attaches to DNA, then a variety of structural information can be obtained. Usually the probe is chosen in such a way that excited light should be absorbed by probe and not by the macromolecule, and thus, all information will be coming from the probe only. We have employed this principle in our study and observed the change in fluorescence intensity of ligands upon binding to DNA. We have performed fluorescence titration studies on Synergy H1 multi-mode microplate reader using 96-well plates at 25°C. The excitation and emission wavelengths for ligands were obtained by performing their absorption and fluorescence scan diluted in potassium phosphate buffer. The readings were taken at emission wavelength of 435 nm, 535 nm, 416 nm, 405 nm, 423 nm, 459 nm, 440 nm, 561 nm, 456 nm and 486 nm for Luteolin, Quercetin, Rutin Genistein, Kaempferol, Puerarin, Hesperidin, Myricetin, Daidzein and Piperine

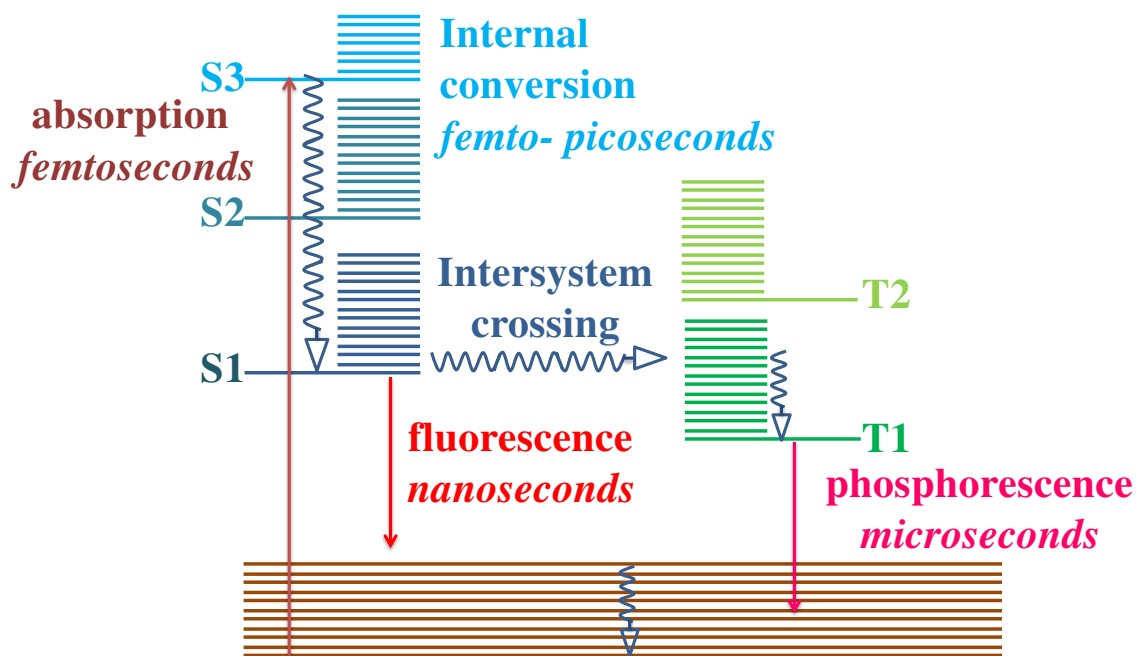


*Figure 2.1. Jablonski diagram showing the excitation of molecule and a time scale of photophysical processes for fluorophore.*

respectively, when excited at the wavelength of 380 nm, 375 nm, 360 nm, 269 nm, 373 nm, 305 nm, 390 nm, 369 nm, 305 nm and 341 nm. Each sample was tested in duplicates in 75  $\mu$ L reaction volumes with variable concentration of DNA ( $\mu$ M) that was serially diluted till saturation is reached; with the last well served as blank (no DNA). Data were analyzed using SigmaPlot 12.0 software (Systat Software, Chicago, USA) according to the following equation and vertical lines shows standard error:

$$f = \frac{B_{max1} \times abs(x)}{kd1 \times abs(x)} + \frac{B_{max2} \times abs(x)}{kd2 \times abs(x)} \quad (1)$$

$B_{max}$ = maximum number of binding sites.

$K_d$ = equilibrium binding constant.

### 2.3.2 Time Correlated Single-Photon Counting

In time resolved fluorescence spectroscopy, the fluorophore is excited by pulsed laser and its fluorescence is monitored as a function of time. It is employed to determine the lifetime of fluorophore and provides information about dynamic processes occurring on time scale as short as femtoseconds. Time resolved fluorescence decay was collected on a Time-Correlated Single-Photon Counting (TCSPC) spectrofluorometer (Horiba). It detects single photon of a pulsed laser signal and constructs decay curves from each time measurement of individual photon. This technique requires a start signal, a time halt and a stop signal. These two signals control the triggering, counting and timing of the measurement cycle. Signal generated from the laser driver was detected as start signal and the stop signal is pulse generated when the fluorescence photon arrived at detector. The arrival time of both of the signals are stored and the difference between the time of arrival of start and stop pulse is the time of detecting a single photon. The time is measured between the excitation pulse and the observed photon is stored in histogram as seen in Figure 2.2. This complete cycle is repeated several times in order to get good decay curve and as the sample is excited several times, thus this excited state population of fluorophore is high and its decay profile is observed. On repeating this cycle for several times, the accumulated photons, their arrival times and decay profiles are used to the construct fluorescence decay curve as seen in Figure.2.2. For our studies, we have used a fixed wavelength Nano LED as the excitation source (ex = 375 nm), and emission was detected at different wavelength. The fluorescence emission of ligand and its complex with DNA were counted with a micro channel plate photo multiplier tube (PMT)

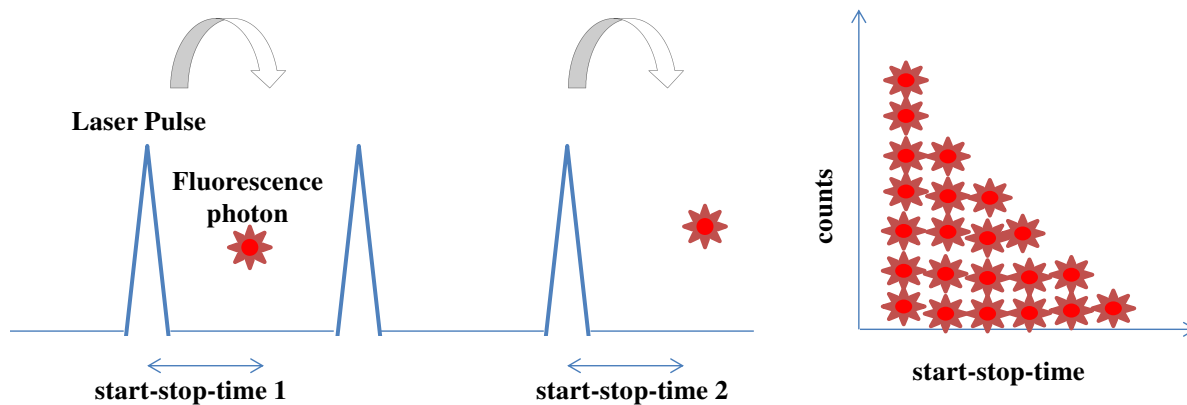


*Figure 2.2. Principle of TCSPC showing histogram for start and stop signals.*

after passing, through the monochromator and were further processed through a constant fraction discriminator (CFD), a time-to-amplitude converter (TAC) and a multi-channel analyser (MCA). The fluorescence decay was obtained and further analyzed using DAS software provided by FluoroLog-TCSPC instrument.

### 2.3.3 Circular Dichroism spectroscopy

Appreciating the sensitivity of Circular Dichroism (CD) spectroscopy for stereochemical variations, it has been employed as an important technique for studying conformational changes of biological macromolecules and perturbation occurred by external factors.<sup>[4]</sup> Every macromolecule gives a signature CD spectrum reflecting its conformation. Generally, all the possible conformations of G-quadruplex structure (parallel, antiparallel or mixed) could be determined from the observation of position and magnitude of CD bands. A positive band at 260 nm is signature of parallel conformation, whereas a negative band at 260 nm and positive band at 295 nm are indicative of an antiparallel conformation.<sup>[5]</sup> CD spectroscopy has also emerged as a technique to study interactions between G-quadruplex and ligands.<sup>[6]</sup> Generally small molecules are non-chiral in nature and in common norms, non-chiral molecules does not exhibit a CD signal in solution. When G-quadruplex structure is titrated with non-chiral molecule, the changes observed in UV region can be directly related to perturbations of G-quadruplex structure. Moreover, when this non-chiral ligand binds tightly to G-quadruplex structure (chiral molecule), an induced CD signal is observed in absorbance region of the bound compound.<sup>[7]</sup> A negative induced CD signal or very small positive signal is generated by intercalating compounds while groove binders generate a large positive induced CD signal upon titration of the compound into DNA.<sup>[8]</sup> In our study, we have performed CD titration experiment on J-815 Spectropolarimeter (JASCO) equipped with peltier junction temperature controller. A quartz cuvette with 0.2 cm path length was used to record the spectra of samples containing 20  $\mu$ M G-quadruplex DNA and titrating with increasing concentrations of ligands in 50 mM KCl containing phosphate buffer ( $K^+$ ) at pH 7.0. Spectra were recorded at 0.1 nm intervals from 200 nm to 600 nm with a 1 nm-slit width and averaged over three scans. Buffer CD spectra were subtracted from the CD spectra of DNA and the Drug-DNA complex.

### 2.3.4. Thermal melting experiments using absorption spectroscopy

Interaction between small molecules and nucleic acid could be demonstrated by

performing thermal melting experiment. The temperature at which 50% of nucleic acid retains in folded form and 50% in unfolded form is called as melting temperature ( $T_m$ ). Monitoring the changes in melting temperature of nucleic acid by absorption spectroscopy relies on the fact that nucleic acids show highest absorbance at 260 nm and value of absorbance increases when secondary structure is denatured. However for non-canonical secondary structures such as G-quadruplexes, a wavelength of 295 nm is used to monitor their denaturation.<sup>[9]</sup> It is observed that upon addition of ligand, the melting temperature of nucleic acid changes. Possibly the theory behind melting experiments suggest that the ligand with strongest binding affinity lead to the largest increase in  $T_m$ .<sup>[10]</sup> In our study, DNA denaturation experiments were carried out on a Perkin Elmer Lambda 35 spectrophotometer equipped with Peltier temperature programmer (PTP 6+6) and water Peltier system PCB-1500. Melting curves for DNA were collected at a heating rate of 1°C/min. in absence and presence of ligand upto 2:1 D/N ratio. The normalized absorbance changes at 295 nm vs temperature were plotted using Simga Plot and melting temperatures were determined.

### 2.3.5. Isothermal Titration Calorimetry

Isothermal titration calorimetry (ITC) is an impressive tool that provides thermodynamic information about drug-DNA interaction.<sup>[11-12]</sup> ITC is the only technique that will directly measure change in enthalpy ( $\Delta H^\circ$ ) and it also computes the binding affinities (k) as well as binding stoichiometry (n) for drug-DNA interactions. ITC experiment is performed on constant temperature thus; various thermodynamic parameters such as entropy change ( $\Delta S^\circ$ ) and free energy change ( $\Delta G^\circ$ ) could be computed from the thermodynamic expression:

$$\Delta G^\circ = - R T \ln K \quad (2)$$

where, R is the gas constant.

The change in entropy ( $\Delta S^\circ$ ) can be determined by:

$$\Delta S^\circ = (\Delta H^\circ - \Delta G^\circ) / T \quad (3)$$

The overall nature of forces governing the interaction could be further determined by dissecting the free energy component into enthalpic and entropic components.<sup>[13-14]</sup> In this method, a fixed concentration of one member of the complex is present in calorimeter's sample cell, and the second member is gradually and incrementally added to it. Generally, sample cell contains nucleic acid and small molecule ligand is filled in syringe. Usually, all interactions involve either the evolution or absorption of heat that led to change in enthalpy

of the system. Analyzing these thermodynamic parameters of the interaction will provide all the fundamental information driving this process. We have used MicroCal isothermal titration calorimeter iTC200 (Malvern) in our study. In calorimeter there are two cells one is reference cell and other is sample cell of ~ 300  $\mu\text{L}$  volume and kept in stable constant temperature bath to maintain the thermal equilibrium between them. The reference cell contains water or buffer solution and the sample cell is filled with macromolecule. The other reactant (small molecule) is filled in syringe (40  $\mu\text{L}$ ) and titrant is injected in steps by computer-controlled injections. Twisted shape of injection syringe provides a rapid but constant mixing of components. The change in heat of the system resulting due to interactions corresponds to the heat flow between the reaction vessel and the isothermal block. This is monitored as a function of time measured by thermoelectric device sensors that surround the vessel. The detected signals are further amplified and converted to a signal that corresponds to the heat change. In our experiments, ligand solution was added at each step to the sample cell containing fixed concentration of G-quadruplex DNA. The heat of dilution was also determined by injecting same concentration of ligand into the same buffer and subtracted from the binding isotherm prior to fit the curve. The obtained thermogram was best fitted with appropriate model for binding and thermodynamic parameters were also calculated using MicroCal Origin software.

### 2.3.6 NMR spectroscopy

Nuclear Magnetic Resonance (NMR) spectroscopy is a powerful tool that provides information about the structural, chemical and dynamics of small molecules as well as biomolecules.<sup>[15-16]</sup> The subatomic particles of many molecules spin on their axis and are electrically charged. When this electrically charged nucleus is placed in magnetic field, energy transfer takes place to higher energy level. Each energy level has a magnetic quantum number,  $m$ , characterizing  $Z$  component of spin,  $I$ . On interaction with magnetic field, nuclei with spin  $I > 1/2$  distributes themselves among  $2I + 1$  energy level with the separation by:

$$\Delta E = h g B_0 \quad (4)$$

A nucleus with spin  $1/2$  will have 2 possible orientations (Figure 2.3a). When these spins interact with a beam of electromagnetic radiation, some of spins aligned along and against the applied magnetic field  $B_0$ . While some of the spin do not align perfectly along  $B_0$  and give rise to a permanent torque and due to presence of angular momentum, the nuclei start to

precess (Figure 2.3b), with frequency of precession given by:

$$\omega_0 = gB_0 \quad (5)$$

where,  $g$  is proportionality constant,  $\omega_0$  is the Larmor frequency in radians/second and  $B_0$  is the magnitude of the applied magnetic field.

When the frequency of the beam is same as that of precessing spin then absorption of energy takes place, which causes the nuclei to flip from a lower energy state to a higher energy state by a process termed as resonance. All the electron(s) of an atom surrounds the proton and as electrons are charged particles, they move in response to the external magnetic field ( $B_0$ ) and generated a secondary field that opposes the applied field. This secondary field shields the nucleus from experiencing the applied field. In order to compensate this shielding,  $B_0$  must be increased. The magnetic field at the nucleus (the effective field) is therefore generally less than the applied field by a fraction  $\sigma$ .

$$\mathbf{B} = \mathbf{B}_0 (1 - \sigma) \quad (6)$$

The difference between applied magnetic field and experienced magnetic by nucleus is termed the nuclear shielding. Chemical shift is a function of the nucleus and its environment and is measured relative to a reference compound. For proton NMR, the reference is usually tetramethylsilane,  $\text{Si}(\text{CH}_3)_4$  (TMS). Chemical shift is expressed in parts per million (ppm) is given as:

$$\delta = 10^6 \times \frac{d_{ref} - d_{obs}}{d_{ref}} \quad (7)$$

where,  $d_{ref}$  is the position observed for a reference compound and  $d_{obs}$  is the position of the signal of interest.

Electronic shielding is one of the nuclear interactions contributing to the resonance frequency of nuclei. Interactions other than chemical shift are entirely independent of magnetic field strength. These interactions provide information on the structures and dynamics of biological molecules and are useful to conclude specific chemical shift value occurring due to the binding of the ligand. In sample, nuclei might experience the same chemical environment or

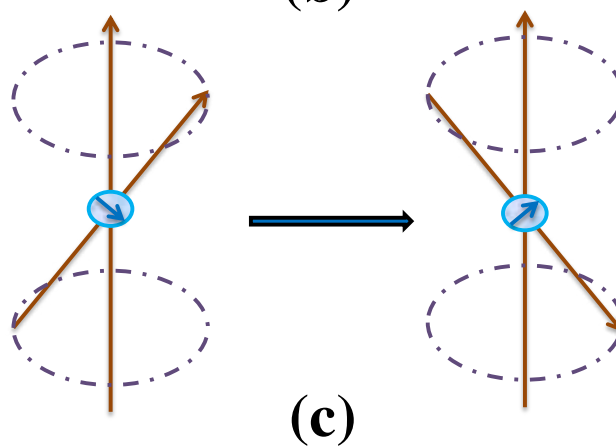
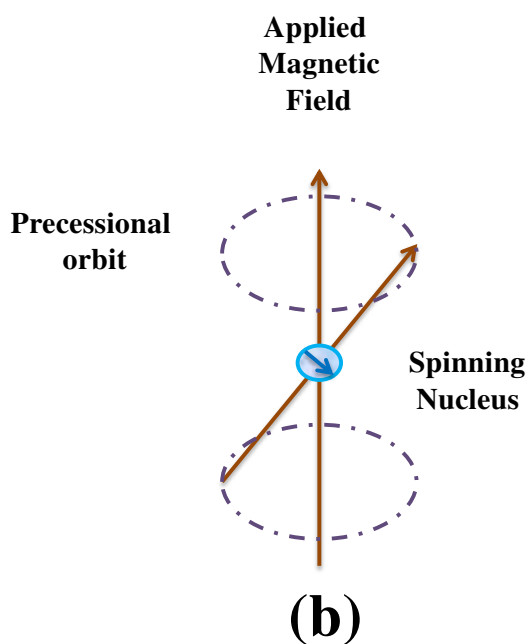
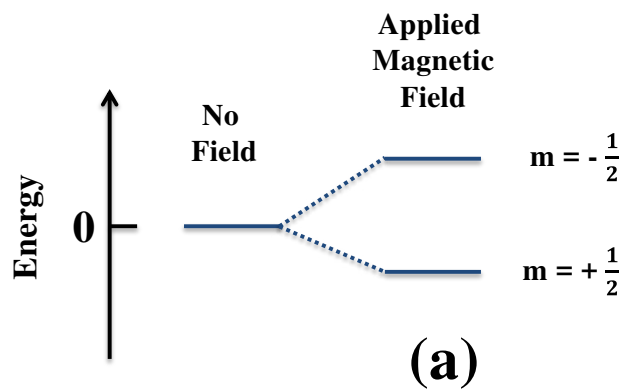


*Figure 2.3. (a) Energy levels for a nucleus with spin quantum number  $\frac{1}{2}$  (b) Precessional motion by the nucleus spinning on its axis in presence of the external magnetic field (c) Flipping of the magnetic moment on absorption of the radiations.*

different chemical environment. Those nuclei experiencing same chemical environment are strength. These interactions provide information on the structures and dynamics of biological molecules and are useful to conclude specific chemical shift value occurring due to the binding of the ligand. In sample, nuclei might experience the same chemical environment or different chemical environment. Those nuclei experiencing same chemical environment are called equivalent and other nuclei experiencing different environment are called nonequivalent. Being present in close vicinity to one another, neighboring nuclei influences the effective magnetic field of each other. This effect is prominent if coupling between non-equivalent nuclei is less other's than or equal to three bond lengths. This effect is called spin-spin coupling or J coupling and is expressed in Hertz (Hz). As charged electron behaves as magnet, thus magnetic dipoles in a sample can interact with each other in two ways: a. directly (through-space) or by direct dipolar interactions and b. indirectly via chemical bonds (through-bond) indirect dipolar interactions.<sup>[17-20]</sup> The direct dipolar coupling depends on the distance between the spins and gives rise to Nuclear Overhauser effect (NOE) that yields important distance information used for structure determination. While, indirect dipolar coupling (scalar coupling or J-coupling) leads to splitting of the resonances of two J-coupled nuclear dipoles. The separation of the lines is given by the scalar coupling constant J. The three-bond J-coupling constants (<sup>3</sup>J) depend on the torsion angles between the coupled spins; they yield important dihedral angle information for the structure calculation. This dependence is described by the semi-empirical Karplus equation<sup>[21]</sup>

$${}^3J = A \cos^2 \phi + B \cos \phi + C \quad (8)$$

where A, B and C where A, B and C depend on the types of coupled spins and  $\phi$  is the torsion angle between the coupled spins.

The magnetization in x-y plane does not remain for infinite time rather it is lost coherently. This process is called as Relaxation. When magnetization is recovered along the z-axis, the external magnetic field forces the spins to align with it and this process is known as T<sub>1</sub> relaxation or spin-lattice or longitudinal relaxation. This relaxation can be measured from the buildup of magnetization along the static applied magnetic field (conventionally the z-axis). The loss of coherence of the magnetization in the x-y plane is due to spins forgetting their orientation with respect to the bulk magnetization. This is known as T<sub>2</sub> relaxation or spin-spin

or transverse relaxation.  $T_2$  relaxation describes the decay of the excited magnetization perpendicular to the applied magnetic field and is responsible for the observed spectral line. The significance of these phenomena is utilized in the Nuclear Overhauser Effect (NOE), which can be used to determine inter-nuclear distances in a molecule.

### **2.3.6.1 Two-dimensional NMR techniques**

In one dimensional (1D) NMR experiment the data acquisition takes place right after the pulse sequence. However, in 2D-NMR experiment, there occur intermediate stages between acquisition and excitation stages. 2D pulse sequences consist of a preparation period (frequently a  $90^\circ$  pulse), an evolution period ( $t_1$ ) followed by a detection period ( $t_2$ ). The process of evolution continues for a period of time labeled  $t_1$  and data is acquired as follows: first the value of  $t_1$  is set close to zero and the first spectrum is acquired. The second time,  $t_1$  is increased by  $\Delta t$  and another spectrum is acquired. A series of FIDs are recorded with incrementing value of  $t_1$  in regular manner until sufficient data is acquired for 2D fourier transformation. Fourier transformation of  $t_1$  time domain gives a 2D spectrum revealing the frequencies of the modulation that were occurring during the  $t_1$  evolution period while fourier transformation of  $t_2$  time domain provides a set of spectra as a function of  $t_1$  step size. The spectrum is usually represented as a topographic map where one of the axes is  $f_1$  that is the spectrum in the  $t_1$  dimension and the second axis is that which is acquired after the evolution and mixing stages (similar to 1D acquisition). The basic 2D NMR experiment consists of a pulse sequence that excites the nuclei with two pulses or groups of pulses then receiving the free induction decay (fid). In a 2D-NMR experiment, magnetization transfer is measured and can be used to probe specific NMR interactions selectively Sometimes this occurs through bonds to the same type of nucleus such as in COSY, TOCSY or to another type of nucleus such as in HSQC and HMBC or through space such as in NOESY and ROESY.

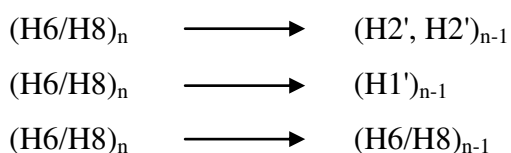
#### **2.3.6.1.1 Nuclear Overhauser Effect Spectroscopy**

NOESY is one of the main techniques of 2D NMR techniques. Nuclear Overhauser effect or NOE is a relaxation parameter which has been used as the key tool for determining three-dimensional molecular structure. Interactions between two dipole moments take place when two nuclei are in sufficiently close spatial proximity to each other. The nuclear dipole-dipole coupling thus leads to the NOE as well as  $T_1$  relaxation. 2D NOE pulse sequence that

starts with a  $90^\circ$  pulse followed by an evolution time  $t_1$ , then  $90^\circ$  pulse transmits some of the magnetization to the Z-axis and during the following mixing period, the non-equilibrium Z component will exchange magnetization through relaxation (dipole-dipole mechanism). This exchange of magnetization is known as Nuclear Overhauser Effect (NOE). After some time (shorter than the relaxation time  $T_1$ ), the transverse magnetization is restored and detected. If relaxation exchange (or chemical exchange) has taken place during the mixing time, cross peaks will be observed in the spectra. The intensities of the cross-peaks in the spectrum depend on the distance between the interacting nuclei; it is this relationship that provides structural information. With current high field instruments, it is possible to detect cross-peaks from protons up to 5-6 Å.

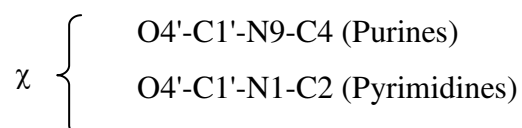
### 2.3.6.1.2 Determination of three-dimensional structure

In order to determine 3D structure of DNA, the first step is resonance assignment. In NMR, protons are categorized into following categories; exchangeable NH and NH<sub>2</sub> protons of the bases, non-exchangeable base protons between 7-15 ppm, non-exchangeable sugar protons between 2-6.5 ppm, and methyl protons of thymine between 0.5-2 ppm. First of all, coupled spins are determined by J correlated spectra, then these identified spin systems are assigned to particular nucleotides belonging to the sequence of nucleic acid used in study. J correlated spin networks were originated from the sugar protons H1', H2', H2'', H3', H4', H5' and H5'' and various cross peaks were observed in the 2D spectra. J-correlation between these protons was used in identification of spin system within individual nucleotide units. For example, H1' proton of sugar shows a cross peak with H2', H2'' protons, H2' and H2'' protons are further coupled to H3' proton and so on. Secondly, sequential assignment was carried out using NOESY spectrum. Every nucleotide of DNA is associated with different chemical shift and a convenient strategy for sequential assignment employed is:



where, n stands for nth residue in 5'-3' oligonucleotide sequence.

Nucleotides have two major conformations depending upon torsional angle designated as syn and anti-conformation.<sup>[22-23]</sup>



The relative magnitudes of the intra-nucleotide and inter-nucleotide (H8/H6)-H1' and (H8/H6)-(H2', H2'') cross peaks in NOESY spectra at different mixing times can be used to establish the domains of glycosidic dihedral angles of individual nucleotide unit.<sup>[22]</sup> The conformation of sugar could be determined by observing the intensity patterns of cross peak at various mixing time. The expected intensity patterns of cross peaks for different glycosidic dihedral angles will vary as mentioned. In syn-conformation there will be a strong NOE between base H8/H6 and H1' protons while the NOEs from base to H2' and H2'' protons will be relatively weak and will have different intensities. In the anti-conformation, the NOE from base H8/H6 to H2' is stronger than the NOE from base H8/H6 to H2''. Also, for right handed structures the H2'' proton shows a stronger NOE to the base proton of the next nucleotide. Nuclear Overhauser Effect is utilized for determination of 3D structural features and stereochemistry of nucleic acids. NOE cross peaks provides cross-relaxation rate between protons i and j that is related to the distance between them in the following way:

$$s_{ij} = \langle d_{ij}^{-6} \rangle f(t_{ij}) \quad (9)$$

Where,  $\langle d_{ij}^{-6} \rangle$  denotes an ensemble average of molecular structures interconverting in thermal equilibrium,  $f(t_{ij})$  is a function of correlation time  $t_{ij}$  for the vector connecting the two spins. As per equation, initially the intensity of the cross peak varies linearly with mixing time, and this condition is referred to as “linear regime”, however, at higher mixing times, due to multi-spin relaxation, linear regime no more exists. Inter-proton distances can be estimated by measuring the intensities of cross peaks in the “linear regime”. Further, for computing inter-proton distances, values of correlation time  $\tau_c$  were taken into account. If protons i, j, k, l have similar of correlation time  $\tau_c$  and if  $r_{ij}$  is a known distance, then the unknown distance  $r_{kl}$  can be calculated by comparing the intensities  $I_{ij}$  and  $I_{kl}$  in a single spectrum.

$$\frac{I_{ij}}{I_{kl}} = \frac{r_{kl}^6}{r_{ij}^6} \quad (10)$$

In this case, it is very important to choose the value of known distance. Gronenborn<sup>[24]</sup> suggested that  $r(\text{CH5-CH6})$  and  $r(\text{H2'-H2''})$  have different effective correlation times and can be used as reference. Cytidine H5-H6 distance of 2.45 Å can be used as reference for all NOEs except NOEs involving CH<sub>3</sub> protons and sugar H2'-H2'' protons for which thymidine

(H6-CH3) distance of 2.5 Å can be used. SPARKY was used to visualise the spectra and calculate 1H-1H NOE distances. These distances were used to restrain the RNA duplex for restrained Molecular Dynamic simulation studies.

### 2.3.7 Restrained molecular dynamics and simulated annealing

One of the primary tools for theoretical study of biological molecules is through molecular dynamics simulations (MD). This method computes the time dependent behavior of a molecular system and provides detailed information on conformational changes of nucleic acids. NMR spectra provide the solution structure of nucleic acids, it needs to be translated into the structural features and compiled into a usable form for structure determination that are demonstrated as structural restraints. Restraints are applied to a structure calculation as an additive component of the overall energy of the system and to achieve<sup>[24]</sup> the lowest energy state that would be the most likely conformation of the molecule. While employing restraints, it is important to have knowledge force field<sup>[25]</sup>, energy of all possible types defining atom-atom interactions like covalent, Van der Waals, electrostatic etc. Simulating annealing is one of the best tools that aim to find the global energy minimum with an equitable amount of computational power.<sup>[26]</sup> NOESY-derived distance restraints are used to determine the structure obtained from solution NMR of nucleic acid. The peak volumes are inversely correlated to inter-proton distance by  $r^6$ , where  $r$  is the inter-proton distance. By employing this relationship, the volumes of all assigned NOESY peaks were taken and used to calculate into distance restraints. The distance restraints was computed by using the program SPARKY.<sup>[27]</sup> The calibrated distances were calculated and compared to H5-H6 (cytosine base) distance of 2.45 Å. A set of NOESY volumes recorded at various mixing times were converted to distances and the obtained sets of distance restraints for each proton-proton pair were averaged and combined into final NOESY-derived restraints. The peaks with smaller volume have high uncertainty due to lower signal-to-noise ratio thus longer NOE-derived distances have a greater uncertainty than shorter distances. Therefore, when calculating the structure, the NOE-derived distances were not force to adhere strictly to the exact calculated NOE distance; instead, these distances were allowed to deviate away from the calculated NOE distances in a distance-dependent manner to fall within a range of values. These distances were categorized into five groups in a qualitative manner, in which the distances were approximately 1.8–2.5 Å for those NOEs which have intensely strong peaks (ss), 2.5–3.0 Å for those NOEs which have strong peaks (s), 3.0–3.5 Å

for those NOEs which have medium intensity (m), 3.5–4.0 Å for those NOEs which have weak intensity (w) and 4.0–5.0 Å for long distance NOEs (vw).

### **2.3.8. Docking studies and molecular modelling simulation**

Molecular docking is a useful tool not only for development and designing of new drugs but also for predicting the drug DNA interactions. There are many ways by which small molecules could interact with various conformations of DNA and at different sites. We have used Autodock 4.0<sup>[28]</sup> in our study for performing docking experiment, in which docking is done by pre-calculating energy grids created around the site of interest. In our study we have created grid in such a way that it covers complete G-quadruplex DNA structure so as to rule out the biasing for site prediction. Exploration of grid space and evaluations of energy for ligand position with respect to target was performed by utilizing Lamarckian Genetic Algorithm (LGA).<sup>[29]</sup> This algorithm searches the various possible orientations and conformations of complete ligand (without its fragmentation) relative to the energy grids for the specific number of energy evaluations.<sup>[29]</sup> The scoring function for Autodock is partially empirically that incorporates Amber type force field for ligand and target.<sup>[29-30]</sup> Autodock evaluates pairwise interactions based on Vander Waals radii of the atoms to determine the free energy of binding and returns the lowest energy docked conformation as the best docked pose.<sup>[31]</sup>

Molecular modelling simulation studies involve simulating the drug-DNA complex by computational algorithms. These simulations can provide precise details for the motion of individual particle in space as a function of time. These minute information are often required to address various queries related to interaction.<sup>[31]</sup> Combined with simulated annealing, dynamics are also employed to determine the refine structures obtained from other experiments and sampling the configuration in space. Initially, simulations were performed for less than 10 ps but now-a-days they are as long as 100 ns and some studies have reported in microseconds also.<sup>[31]</sup> MD simulation studies could be employed on larger systems for longer times to observe greater conformational changes and to monitor various precise parameters that might not be accessible from experimental data.

### **2.3.9 Polymerase Chain Reaction stop assay**

Polymerase Chain Reaction (PCR) is an *in vitro* replication process utilizing two oligonucleotide primers that hybridize to opposite strands flanking the region of

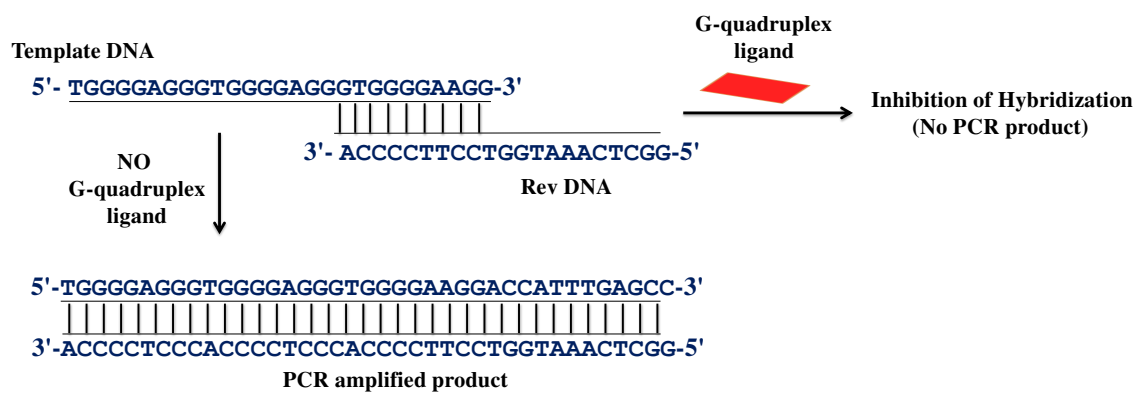


*Figure 2.4. Principle of PCR stop assay.*

interest in the target DNA.<sup>[32]</sup> PCR concept was given by Kary Mullis in 1983 and today it has become a common and vital technique in biological research.<sup>[33]</sup> PCR consists of 20 -40 cycles at variable temperature, in which each cycle consisting of three steps: DNA denaturation, primer annealing and primer extension; and subsequently next cycle begins thus in this way it amplifies the target DNA.<sup>[34]</sup> PCR stop assay is used to evaluate the efficiency of ligands to stabilize G-quadruplex structure. In this assay, two oligonucleotide sequences were used, one is target DNA forming G-quadruplex structure and other is its complimentary sequence.<sup>[35]</sup> This assay works on the principle (Figure 2.4) that if ligand binds and stabilizes G-quadruplex structure formed by target DNA, then it will prevent the hybridization of complementary sequence. *Taq polymerase* enzyme will not be able to recognize this G-quadruplex structure and thus the process of DNA amplification is inhibited. This inhibition could be manifested in reduction of intensity of the amplified product observed on agarose gel electrophoresis.<sup>[36]</sup> For our study we have performed PCR stop assay by employing modified protocol of previous study<sup>[35]</sup> using a test oligonucleotide c-myc Pu24T: d-(5'-TGA GGG TGG TGA GGG TGG GGA AGG-3') and a complementary oligonucleotide (Rev Pu24T): d-(5'-TTC TCG TCC TTC CC CA-3'). Assay reactions were performed in a final volume of 25  $\mu$ L reaction mixture containing 10 mM Tris buffer, 50 mM KCl, 10.0 pmol of each oligonucleotide, 2.5 units of *Taq polymerase* and varied concentration of ligands. Reaction mixtures were incubated in Mastercycler Nexus Gradient (Eppendorf) with the following cycling conditions: 94°C for 2 min, followed by 30 cycles of 94°C for 30 s, 58°C for 30 s, and 72°C for 30 s. Amplified products were resolved on a 3% agarose gel in 1X TBE and stained with ethidium bromide (EtBr). Gel Image was analyzed on ImageQuant LAS 4000 (GE Healthcare).

### 2.3.10 Gel mobility shift assay

One of the methods for detecting the interaction of drug with DNA is gel mobility shift assay. It is based on the fact that during electrophoresis, drug-DNA complex will migrate much slower than free DNA. Reaction mixture consists of 1X potassium phosphate buffer, a fixed concentration of G-quadruplex DNA, increasing concentrations of ligand and ddH<sub>2</sub>O to make final reaction volume of 10  $\mu$ L and incubated for 30 mins at room temperature. The products were resolved on 20% native polyacrylamide gel [29:1 acrylamide/bis(acrylamide)] prepared by polymerizing acrylamide in 1X TBE containing phosphate buffer (10 mM (K<sup>+</sup>), 50 mM KCl). Gel was visualized by staining with EtBr and

analyzed on ImageQuant LAS 4000 (GE Healthcare).

### 2.3.11 Cytotoxicity test with MTT

Cell-based assays are used to determine the effect of ligands on cell proliferation or to understand their cytotoxic effects. 3-(4, 5-dimethylthiazol-2-yl)-2, 5- tetrazolium bromide (MTT) assay is one of the quantitative colorimetric assays used for determination of mammalian cell survival and proliferation. This assay is based on the principle (Figure 2.5) of reduction of MTT from a pale yellow tetrazolium salt to a dark purple formazan product by mitochondrial succinate dehydrogenase when incubated with metabolically active cells that is live cells.<sup>[37-39]</sup> MTT enters the cells and reaches to mitochondria, where it is reduced to an insoluble, dark purple formazan product. These formazans were solubilized with an organic solvent (e.g. isopropanol or dimethyl sulfoxide), and quantified using a plate reader by taking absorbance at 570 nm. In our study, we have performed MTT assay to determine the cytotoxicity of ligands against cancer cells lines that is HepG2 cells, HeLa cells, PC3 cells, MCF-7 cells, A549 cells and also normal human fibroblast HEK cells. For performing MTT assay,  $5.0 \times 10^3$  cells/well were seeded in a 96-well flat-bottomed microplate (Corning) and allowed to grow in complete growth medium. Serial dilutions of compounds were added to each well with solvent as control. The microplate was incubated at 37 °C, 5% CO<sub>2</sub>, in a humidified incubator (Thermofischer) for 24 or 72 h. After incubation, 10 μL of MTT (5 mg/mL in PBS) was added to each well and further incubated for additional 4 h at 37°C to allow intracellular reduction of the soluble yellow MTT to insoluble purple formazan crystals. These crystals were dissolved by adding 100 μL of DMSO and absorbance was read at 570 nm using a microplate reader (Synergy H1 multi-mode microplate reader). Concentration of ligands causing 50% reduction of cell viability, i.e. inhibitory concentration (IC<sub>50</sub> value), was determined by the using formula:

$$\% \textit{inhibition} = \frac{\textit{Control abs} - \textit{Sample abs}}{\textit{Control abs}} \times 100 \quad (11)$$

### 2.3.12 Semi-quantitative RT PCR analysis

Reverse transcription-polymerase chain reaction (RT-PCR) has been emerged as standard tool for performing gene expression studies.<sup>[40-41]</sup> In this method, total RNA is

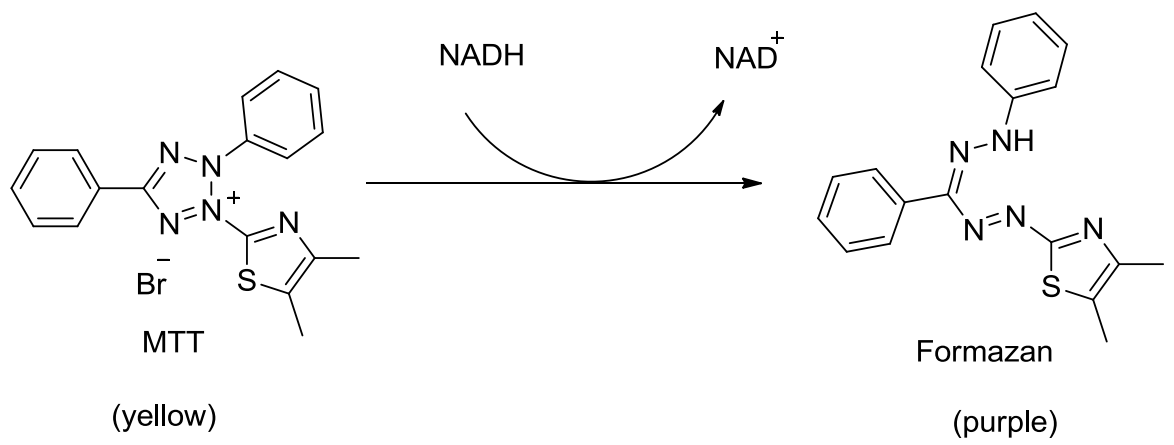


*Figure 2.5. Principle of MTT assay*

copied by a process of reverse transcription (RT) to produce single stranded, complimentary DNA (cDNA). Generally, cDNA is more stable than RNA in terms of degradation. This cDNA is further amplified by PCR and quantified to determine the relative abundance of expressed genes or to confirm gene expression (mRNA) profile of target genes. Semi-quantitative real-time RT-PCR involves the following individual steps: preparation of RNA, first strand DNA synthesis (cDNA production), amplification of cDNA, data analysis. In our study, cells were treated with variable concentration of ligands and after incubating them for 24 or 48 h, total RNA was prepared from treated and control cells followed by cDNA synthesis using Cells-to-cDNA II Kit (Ambion) according to the manufacturer's protocol. Reverse transcriptase reaction was performed on Mastercycler Nexus Gradient (Eppendorf). The thermal cycling condition was programmed as 45 min at 45°C, 10 min at 95 °C for one cycle. Semi – quantitative PCR was performed using gene specific primers with the following sequences:

c - MYC (forward): 5'-CTT CTC TCC GTC CTC GGA TTC T-3';

c - MYC (reverse): 5'-GAA GGT GAT CCA GAC TCT GAC CTT-3';

β - actin (forward): 5'- GAG CTA CGA GCT GCC TGA C-3';

β - actin (reverse): 5'-AGC ACT GTG TTG GCG TAC AG-3'.

### **2.3.13 DNA fragmentation, TUNEL assay, morphological evaluation and FACS analysis of apoptosis.**

Flow cytometry is a laser and fluidics based method used for analyzing various parameters of single cells in suspension. These parameters could be cell size, its complexity, as well as expression of various molecules by using fluorochrome-conjugated dyes and antibodies. Cells in suspension are allowed to enter the capillary system of the cytometer within a liquid sheath stream. Single cells are focused to pass the laser beam that excites the fluorescence of interest. Fluorescence intensities obtained from several thousand cells are then processed to multi-dimensional histograms. Usually, 10,000 or more cells (events) are analyzed simultaneously in a single plot. In our study, flow cytometry was used to detect apoptosis by utilizing the externalization of phosphatidylserine found in apoptotic cells. Briefly, from culture plates, the cells were washed with PBS, trypsinized and centrifuged for 3 min at 6000x g. The cell suspension concentration was adjusted to approximately  $1 \times 10^6$  cells/ mL and 0.5 mL of cell suspension were transferred to 1.5 mL centrifuge tube. 100 μL of cold 1X binding buffer was added to the cell suspension followed by addition of 1.25 μL

of Annexin V-FITC into the sample and incubated for 15 min. at room temperature in the dark. The samples were centrifuged at 1000x g for 5 min. at room temperature and media was removed. The cells were suspended in 0.5 mL cold 1X binding buffer and 10  $\mu$ L of propidium iodide was added to cell suspension. The samples were placed on ice away from light. FACS data was collected using BD FACS Aria III Cell-Sorting System (BD, Bioscience) and analysis was done with FACS Diva software (Becton Dickinson, USA). For morphological evaluation of apoptosis bright field images were taken of untreated and treated cells. Following cell counting, to assess cell viability, above described experimental cells were stained with DAPI for nuclear morphological analysis. DNA fragmentation was observed in treated cells using agarose gel electrophoresis and TUNEL staining. DNA was isolated from treated cells using phenol-chloroform method and TUNEL staining was performed as per manufacturer's instructions.

## 2.4 References

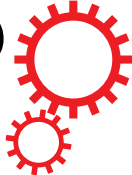
1. Chen Y., Periasamy A. (2004), Characterization of two-photon excitation fluorescence lifetime imaging microscopy for protein localization, *Microsc. Res. Tech.*, 63, 72-80 (DOI: 10.1002/jemt.10430).
2. Berezin M.Y., Achilefu S. (2010), Fluorescence Lifetime Measurements and Biological Imaging, *Chem. Rev.*, 110, 2641-2684 (DOI: 10.1021/cr900343z).
3. Lakowicz J.R. in Springer Science+Business Media, New York, (ISBN 978-0-387-46312-4). (2006).
4. Fasman G.D. (1996), Circular Dichroism and the Conformational Analysis of Biomolecules, *Springer Science+Business Media New York* (ISBN 978-0-306-45142-3).
5. Burge S., Parkinson G.N., Hazel P., Todd A.K., Neidle S. (2006), Quadruplex DNA: sequence, topology and structure, *Nucleic Acids Res.*, 34, 5402-5415 (DOI: 10.1093/nar/gkl655).
6. Randazzo A., Spada G.P., da Silva M.W. (2013), Circular dichroism of quadruplex structures, *Top Curr. Chem.*, 330, 67-86 (DOI: 10.1007/128\_2012\_331).
7. Jaumot J., Gargallo R. (2012), Experimental methods for studying the interactions between G-quadruplex structures and ligands, *Curr. Pharm. Des.*, 18, 1900-1916 (DOI: 10.2174/138161212799958486).
8. Garbett N.C., Ragazzon P.A., Chaires J.B. (2007), Circular dichroism to determine binding

- mode and affinity of ligand-DNA interactions, *Nat. Protoc.*, 2, 3166-3172 (DOI: 10.1038/nprot.2007.475).
9. Mergny J.-L., Phan A.-T., Lacroix L. (1998), Following G-quartet formation by UV-spectroscopy, *FEBS Lett.*, 435, 74-78 (DOI: 10.1016/S0014-5793(98)01043-6).
  10. Guedin A., Lacroix L., Mergny J.L. (2010), Thermal melting studies of ligand DNA interactions, *Methods Mol. Biol.*, 613, 25-35 (DOI: 10.1007/978-1-60327-418-0\_2).
  11. Doyle M.L. (1997), Characterization of binding interactions by isothermal titration calorimetry, *Curr. Opin. Biotechnol.*, 8, 31-35 (DOI: 10.1016/S0958-1669(97)80154-1).
  12. Ababou A., Ladbury J.E. (2006), Survey of the year 2004: literature on applications of isothermal titration calorimetry, *J. Mol. Recognit.*, 19, 79-89 (DOI: 10.1002/jmr.750).
  13. Pierce M.M., Raman C.S., Nall B.T. (1999), Isothermal titration calorimetry of protein-protein interactions, *Methods*, 19, 213-221 (DOI: 10.1006/meth.1999.0852).
  14. Haq I., Ladbury J. (2000), Drug-DNA recognition: energetics and implications for design, *J. Mol. Recognit.*, 13, 188-197 (DOI: 10.1002/1099-1352(200007/08)13:4<188::aid-jmr503>3.0.co;2-1).
  15. K W. (1991), NMR of proteins and nucleic acids, 320, (ISBN: 978-0-471-82893-8).
  16. Simpson P.J. (2015), Nuclear Magnetic Resonance: The Royal Society of Chemistry, 44, 44 348-384 (ISBN: 978-1-78262-052-5).
  17. Aue W.P., Bartholdi E., Ernst R.R. (1976), Two-dimensional spectroscopy. Application to nuclear magnetic resonance, *J. Chem. Phys.*, 64, 2229-2246 (DOI: 10.1063/1.432450).
  18. Braunschweiler L., Ernst R.R. (1983), Coherence transfer by isotropic mixing: Application to proton correlation spectroscopy, *Journal of Magnetic Resonance (1969)*, 53, 521-528 (DOI: 10.1016/0022-2364(83)90226-3).
  19. Ernst R.R., Anderson W.A. (1966), Application of Fourier Transform Spectroscopy to Magnetic Resonance, *Rev. Sci. Instrum.*, 37, 93-102 (DOI: 10.1063/1.1719961).
  20. Ernst R. R. B.G., Wokaun, A. (1987), Principles of nuclear magnetic resonance in one and two dimensions, *Oxford University Press, New York, USA (ISBN-10: 0198556470)*.
  21. Karplus M. (1963), Vicinal Proton Coupling in Nuclear Magnetic Resonance, *J. Am. Chem. Soc.*, 85, 2870-2871 (DOI: 10.1021/ja00901a059).
  22. Hosur R.V., Ravikumar M., Chary K.V.R., Sheth A., Govil G., Zu-Kun T., Miles H.T. (1986), Solution structure of d-GAATTCGAATTC by 2D NMR: A new approach to determination of sugar geometries in DNA segments, *FEBS Lett.*, 205, 71-76 (DOI: 10.1016/0014-5793(86)80868-7).

23. Sundaralingam M. (1969), Stereochemistry of nucleic acids and their constituents. IV. Allowed and preferred conformations of nucleosides, nucleoside mono-, di-, tri-, tetraphosphates, nucleic acids and polynucleotides, *Biopolymers*, 7, 821-860 (DOI: 10.1002/bip.1969.360070602).
24. Clore G.M., Gronenborn A.M., Brunger A.T., Karplus M. (1985), Solution conformation of a heptadecapeptide comprising the DNA binding helix F of the cyclic AMP receptor protein of *Escherichia coli*. Combined use of <sup>1</sup>H nuclear magnetic resonance and restrained molecular dynamics, *J. Mol. Biol.*, 186, 435-455 (DOI: 10.1016/0022-2836(85)90116-0).
25. Pérez S., Imberty A., Engelsen S.B., Gruza J., Mazeau K., Jimenez-Barbero J., Poveda A., Espinosa J.-F., van Eyck B.P., Johnson G., French A.D., Kouwijzer M.L.C.E., Grootenuis P.D.J., Bernardi A., Raimondi L., Senderowitz H., Durier V., Vergoten G., Rasmussen K. (1998), A comparison and chemometric analysis of several molecular mechanics force fields and parameter sets applied to carbohydrates, *Carbohydr. Res.*, 314, 141-155 (DOI: 10.1016/S0008-6215(98)00305-X).
26. Kirkpatrick S. (1984), Optimization by simulated annealing: Quantitative studies, *J. Stat. Phys.*, 34, 975-986 (DOI: 10.1007/bf01009452).
27. Kneller T.D.G.a.D.G. SPARKY 3, *University of California, San Francisco*.
28. Morris G.M., Huey R., Lindstrom W., Sanner M.F., Belew R.K., Goodsell D.S., Olson A.J. (2009), AutoDock4 and AutoDockTools4: Automated docking with selective receptor flexibility, *J. Comput. Chem.*, 30, 2785-2791 (DOI: 10.1002/jcc.21256).
29. Morris G.M., Goodsell D.S., Halliday R.S., Huey R., Hart W.E., Belew R.K., Olson A.J. (1998), Automated docking using a Lamarckian genetic algorithm and an empirical binding free energy function, *J. Comput. Chem.*, 19, 1639-1662 (DOI:10.1002/(SICI)1096-987X(19981115)19:14<1639::AID-JCC10>3.0.CO;2-B).
30. Huey R., Morris G.M., Olson A.J., Goodsell D.S. (2007), A semiempirical free energy force field with charge-based desolvation, *J. Comput. Chem.*, 28, 1145-1152 (DOI: 10.1002/jcc.20634).
31. Moitessier N., Englebienne P., Lee D., Lawandi J., Corbeil C.R. (2008), Towards the development of universal, fast and highly accurate docking/scoring methods: a long way to go, *Br. J. Pharmacol.*, 153 Suppl 1, S7-26 (DOI: 10.1038/sj.bjp.0707515).
32. Erlich H.A. (1989), Polymerase chain reaction, *J. Clin. Immunol.*, 9, 437-447 (DOI: 10.1007/bf00918012).

33. Saiki R.K., Gelfand D.H., Stoffel S., Scharf S.J., Higuchi R., Horn G.T., Mullis K.B., Erlich H.A. (1988), Primer-directed enzymatic amplification of DNA with a thermostable DNA polymerase, *Science*, 239, 487-491 (DOI: 10.1126/science.2448875).
34. Rychlik W., Spencer W.J., Rhoads R.E. (1990), Optimization of the annealing temperature for DNA amplification in vitro, *Nucleic Acids Res.*, 18, 6409-6412.
35. Lemarteleur T., Gomez D., Paterski R., Mandine E., Mailliet P., Riou J.F. (2004), Stabilization of the c-myc gene promoter quadruplex by specific ligands' inhibitors of telomerase, *Biochem. Biophys. Res. Commun.*, 323, 802-808 (DOI: 10.1016/j.bbrc.2004.08.150).
36. Ou T.M., Lu Y.J., Zhang C., Huang Z.S., Wang X.D., Tan J.H., Chen Y., Ma D.L., Wong K.Y., Tang J.C., Chan A.S., Gu L.Q. (2007), Stabilization of G-quadruplex DNA and down-regulation of oncogene c-myc by quindoline derivatives, *J. Med. Chem.*, 50, 1465-1474 (DOI: 10.1021/jm0610088).
37. Mosmann T. (1983), Rapid colorimetric assay for cellular growth and survival: application to proliferation and cytotoxicity assays, *J. Immunol. Methods*, 65, 55-63 (DOI: 10.1016/0022-1759(83)90303-4).
38. Berridge M.V., Herst P.M., Tan A.S. (2005), Tetrazolium dyes as tools in cell biology: new insights into their cellular reduction, *Biotechnol. Annu. Rev.*, 11, 127-152 (DOI: 10.1016/s1387-2656(05)11004-7).
39. Berridge M.V., Tan A.S. (1993), Characterization of the cellular reduction of 3-(4,5-dimethylthiazol-2-yl)-2,5-diphenyltetrazolium bromide (MTT): subcellular localization, substrate dependence, and involvement of mitochondrial electron transport in MTT reduction, *Arch. Biochem. Biophys.*, 303, 474-482 (DOI: 10.1006/abbi.1993.1311).
40. Freeman W.M., Walker S.J., Vrana K.E. (1999), Quantitative RT-PCR: pitfalls and potential, *Biotechniques*, 26, 112-122, 124-115.
41. Freeman W.M., Vrana S.L., Vrana K.E. (1996), Use of elevated reverse transcription reaction temperatures in RT-PCR, *Biotechniques*, 20, 782-783.

# SCIENTIFIC REPORTS



OPEN

## Structural Insight into the interaction of Flavonoids with Human Telomeric Sequence

Arpita Tawani &amp; Amit Kumar

Received: 18 June 2015  
Accepted: 03 November 2015  
Published: 02 December 2015

Flavonoids are a group of naturally available compounds that are an attractive source for drug discovery. Their potential to act as anti-tumourigenic and anti-proliferative agents has been reported previously but is not yet fully understood. Targeting human telomeric G-quadruplex DNA could be one of the mechanisms by which these flavonoids exert anticancer activity. We have performed detailed biophysical studies for the interaction of four representative flavonoids, Luteolin, Quercetin, Rutin and Genistein, with the human telomeric G-quadruplex sequence tetramolecular d-(T<sub>2</sub>AG<sub>3</sub>T) (Tel7). In addition, we used NMR spectroscopy to derive the first model for the complex formed between Quercetin and G-quadruplex sequence. The model showed that Quercetin stabilises the G-quadruplex structure and does not open the G-tetrad. It interacts with the telomeric sequence through  $\pi$ -stacking at two sites: between T1pT2 and between G6pT7. Based on our findings, we suggest that Quercetin could be a potent candidate for targeting the telomere and thus, act as a potent anti-cancer agent.

The importance of human telomeric ends having the sequence d-(TTAGGG)<sub>n</sub> is evident in somatic cells in which telomeres reach a critical limit (Hayflick limit), leading to the shortening of chromosomes and apoptosis<sup>1,2</sup>. In 80–85% of tumours, the aberrant cell proliferation and immortalisation is due to over-expression of a ribonucleozyme called telomerase, which maintains the length of telomeres by adding hexanucleotide repeats to the 3' ends<sup>3–5</sup>. Telomerase utilises this end as primer for its reverse transcriptase (hTERT) activity, using its own hRNA component as a template for DNA synthesis<sup>6,7</sup>. Recent studies revealed that the G-quadruplex inhibits this enzymatic activity by dissociating the primer from the RNA template<sup>8,9</sup>. Therefore, the replication process of cancer cells via elongation of telomeric ends could be interrupted by stabilisation of the G-quadruplex, suggesting this mechanism as a potent cancer target for therapeutics<sup>8</sup>. Thus, the significance of the telomeric G-quadruplex in cancer treatment drives the exploration of small molecules that induce the formation of G-quadruplexes or that stabilise these structures<sup>10,11</sup>.

For the last decade, considerable research has been focused on exploiting small molecules<sup>12</sup> with extended planar aromatic moieties, allowing them to intercalate into G-quadruplexes and form a stable conformation, but the major limitation to using these molecules is cytotoxicity and other side effects. Low molecular weight ligands with a lower level of systemic toxicity and high selectivity for the G-quadruplex could be effective telomerase inhibitors that induce the formation or stabilisation of the G-quadruplex<sup>13–16</sup>. Considering this, many groups have investigated the interaction of the G-quadruplex with naturally available small molecules such as berberine<sup>17</sup>, sanguinarine<sup>18</sup>, and others<sup>19–21</sup>, which usually offer relatively less toxicity and fewer side effects than the synthetic molecules. Most of these compounds stabilise the G-tetrad by  $\pi$ -stacking due to the presence of extended aromatic rings<sup>22</sup>. Among these, flavonoids are one of the important naturally available small molecules in our daily diets and have been considered for use as potential drug candidates for anticancer therapy<sup>23</sup>. The common dietary flavonoids Luteolin, Quercetin, Rutin and Genistein have received significant attention for their protective as well as potentially destructive anti-tumour, anti-cancer and anti-oxidant activities<sup>23–28</sup>. Various

Centre for Biosciences and Biomedical Engineering, Indian Institute of Technology Indore, Indore, Madhya Pradesh, India. Correspondence and requests for materials should be addressed to A.K. (email: amitk@iiti.ac.in)

## Chapter 3

# Structural Insight into the interaction of Flavonoids with Human Telomeric Sequence

---

---

### 3.1 Introduction

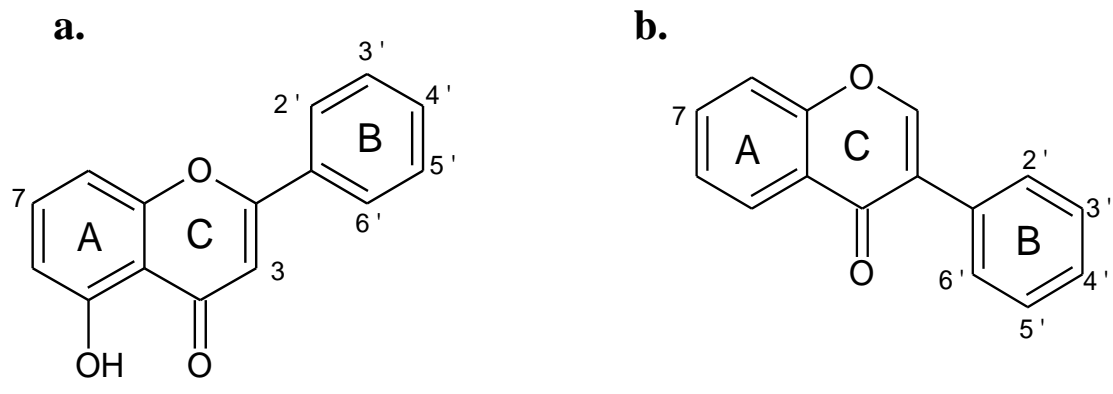
The importance of human telomeric ends having repetitive sequence d-(TTAGGG)<sub>n</sub> is evident in somatic cells. Telomeres plays important role in maintaining the genome integrity by protecting its degradation and deadly recombination events like end-to-end fusion, chromosomal translocations and rearrangements.<sup>[1]</sup> With every round of cell cycle, telomeres get shortened due to end replication problem. Once the length of telomeres reaches a critical limit (Hayflick limit), cell stops dividing and finally lead to apoptosis.<sup>[2-3]</sup> On contrary, in cancer cells there occurs aberrant cell proliferation. In 80-85% of tumors, this aberrant cell proliferation and immortalization is due to overexpression of telomerase enzyme that maintains the length of telomeres by adding hexanucleotide repeats 3' ends of telomeric DNA.<sup>[4-6]</sup> Telomerase utilizes this end as primer for its reverse transcriptase (hTERT) activity, using its own hRNA component as a template for DNA synthesis.<sup>[7-8]</sup> Recent studies revealed that telomeric DNA sequence d- (TTAGGG)<sub>n</sub> forming G-quadruplex structure could inhibit telomerase activity by dissociating the primer from RNA template.<sup>[9-10]</sup> Therefore, the replication process in cancer cells via elongation of telomeric ends could be interrupted by stabilization of G-quadruplex structure, suggesting this mechanism as a potent target for cancer therapeutics.<sup>[9]</sup> Thus, the significance of telomeric G-quadruplex structure in cancer treatment drives the exploration of small molecules that induce the formation of G-quadruplexes or that stabilize these structures.<sup>[11-12]</sup> G-quadruplex structures are secondary structure of DNA formed in G-rich sequences. Square planar arrangement of four guanine nucleotides forms basic unit of G-quadruplex structure i.e. G-quartets or G-tetrads. They are stabilized by Hoogsteen hydrogen bonding in addition to canonical Watson-Crick hydrogen bonding. When two or more G-quartets units stack onto each other, it forms G-quadruplex structure.

For the last decade, considerable research has been focused on exploiting the stabilization potential of small molecules <sup>[13]</sup> containing extended planar aromatic moieties. The ring system allows them to intercalate in G-quartets and stabilizes the G-quadruplex conformation. As majority of these small molecules are of synthetic origin, therefore, the main limitation in using them is cytotoxicity to normal cells and other side effects. Low

molecular weight ligands with a lesser systemic toxicity and high selectivity for G-quadruplex structure could act as potent telomerase inhibitors. They can inhibit the telomerase activity either by inducing the formation of G-quadruplex structure or stabilizes them.<sup>[14-17]</sup> Considering this, many groups have investigated the interaction of G-quadruplex DNA with naturally available small molecules such as berberine,<sup>[18]</sup> sanguinarine,<sup>[19]</sup> and others,<sup>[20-22]</sup> which usually offer relatively less toxicity and fewer side effects than the synthetic molecules. Most of these compounds stabilize the G-tetrad by  $\pi$ -stacking due to the presence of extended aromatic rings.<sup>[23]</sup> Among these, flavonoids are one of the important group of naturally available small molecules in our daily diets that have been considered as a potential drug candidates for anticancer therapy.<sup>[24]</sup> The common dietary flavonoids Luteolin, Quercetin, Rutin and Genistein have received significant attention for their protective as well as potentially destructive effects like anti-tumour, anti-cancer and anti-oxidant activities.<sup>[24-29]</sup> Various mechanisms have been proposed for such activities of these flavonoids for example the inhibition of phosphatidylinositol 3-kinase, phosphorylase kinase and DNA topoisomerases activities.<sup>[30-31]</sup> Furthermore, flavonoids have been also reported to exert their anti-cancer effects at different stages of cancer development and inhibit cellular proliferation, induce cellular cytotoxicity by modulating mitogenic and apoptotic signaling pathways, and affect cell-cycle regulation.<sup>[32]</sup> The anti-proliferative and cytotoxic effects of these flavonoids on different cancer cell lines have also been well studied that showed Quercetin exhibited the lowest EC<sub>50</sub>.<sup>[33-34]</sup>

Despite many studies on the anti-tumor, anti-proliferative and anti-apoptotic activities of these flavonoids, the major cellular target of their action remains elusive. Moreover, it has been known that ligands with planar aromatic regions intercalate effectively into the G-quadruplex structure and stabilize it.<sup>[35]</sup> The flavonoid skeleton contains a planar chromophore with an additional carboxyl group for protonation. As mentioned earlier, the presence of aromatic planar moiety helps in effective binding of ligands to G-quadruplex structure via  $\pi$ - $\pi$  interactions;<sup>[36-37]</sup> therefore, flavonoids could possibly be a choice of molecules that could stacks on G-tetrads and stabilizes its structure.

Previous studies suggest that among the major known flavonoids, the interaction of these flavonoids with nucleic acid (calf thymus) was in the order of Quercetin > Kaempferol > Delphinidin, with  $K_{\text{que}} = 7.25 \times 10^4 \text{ M}^{-1}$ .<sup>[38]</sup> Furthermore, studies on interactions of flavonoids with triplexes and tetraplexes showed that Quercetin interacts favorably with tetraplexes with a  $K_{\text{ass}}$  value of  $\sim 10^3 \text{ M}^{-1}$  for human telomeric sequences.<sup>[39]</sup> Their interaction



**Luteolin:** 3' = OH, 4' = OH, 5' = H, 3 = H, 7 = OH      **Genistein:** 5 = OH, 7 = OH, 4 = OH, 8 = H  
**Quercetin:** 3' = OH, 4' = OH, 5' = H, 3 = OH, 7 = OH  
**Rutin:** 3' = OH, 4' = OH, 5' = H, 3 = Rutinose, 7 = OH

*Figure 3.1. Chemical structure of flavonoids (a) Luteolin, Quercetin, Rutin (b) Genistein.*

with various forms of DNA and their reported anticancer activity prompted us to investigate its mode of interaction with human telomeric G-quadruplex DNA sequence. In 2006, Sun *et al.* has reported the interaction of Quercetin with monomeric and dimeric G-quadruplexes by utilizing spectroscopic studies. Their results suggested that Quercetin acts as groove binder for the monomeric conformation, whereas it binds to the dimeric conformation via end-stacking mode.<sup>[40]</sup>

Nevertheless, extensive research has been done for the interaction of flavonoids with nucleic acids,<sup>[38-39]</sup> but no structural studies assessing their interaction with human telomeric G-quadruplex sequence has been reported in the literature to date. In this chapter, we have studied the interaction of four different flavonoids, Luteolin, Quercetin, Rutin and Genistein (Figure 3.1) with human telomeric DNA sequence d(T<sub>2</sub>AG<sub>3</sub>T)<sub>4</sub> forming G-quadruplex structure Tel7. NMR studies along with other biophysical techniques, such as Circular Dichroism (CD), steady-state and time-resolved fluorescence spectroscopies, were employed to investigate the binding mode of these flavonoids to Tel7 G-quadruplex DNA. Furthermore, this study aimed to achieve a structural basis for the interaction and stabilization of the intermolecular parallel G-quadruplex DNA by flavonoids.

## **3.2 Results and Discussion**

### **3.2.1 Fluorescence spectroscopic studies**

#### **3.2.1.1 Steady state fluorescence studies**

Fluorescence spectroscopy is one of the major techniques that has been widely used in research as an analytical tool.<sup>[41]</sup> In this technique, higher frequency of light is absorbed and emitted back from an electronically excited state.<sup>[42]</sup> It could be employed to investigate the changes in the physicochemical properties of ligands occurs due to presence of DNA.<sup>[43-44]</sup> We have utilized this principle to understand the changes occur in fluorescence of flavonoids upon binding with DNA. It will provide us indication about their interaction and formation of drug-DNA complex. The fluorescence emission of all four flavonoids was examined at their emission maximum wavelength in their unbound form. Flavonoids have very weak fluorescence emission likely due to the torsional motion of the phenyl and c-pyrone rings.<sup>[45]</sup> These flavonoids have an emission spectrum with a  $\lambda_{\text{max}}$  centered around 435 nm for Luteolin, 535 nm for Quercetin, 416 nm for Rutin and 405 nm for Genistein, when excited at 380 nm, 375 nm, 360 nm and 269 nm respectively. Upon addition of Tel7 G-quadruplex DNA to flavonoid solution, changes in fluorescent intensity were observed that might occur by limiting the torsional motion of the phenyl and c-pyrone rings.

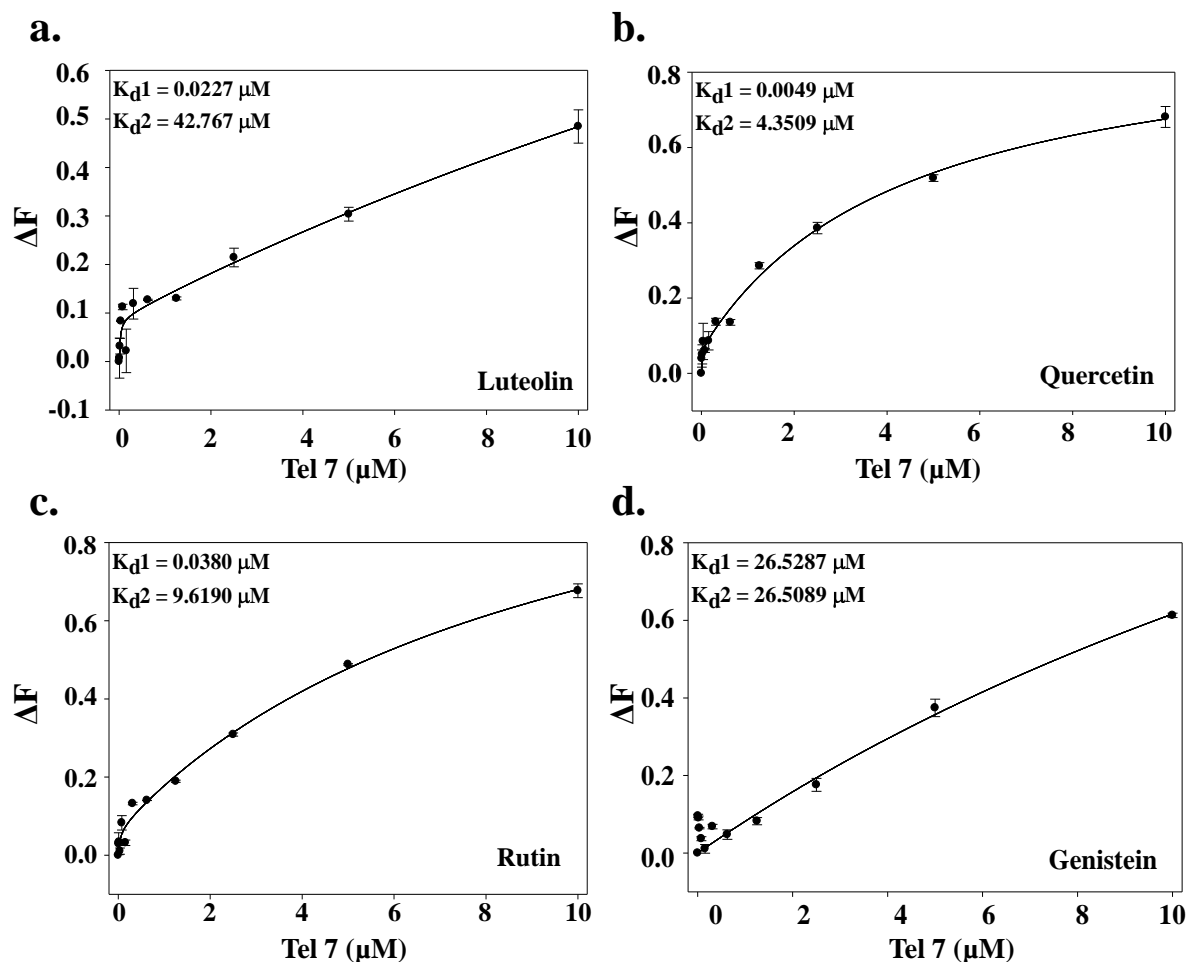


*Figure 3.2. Fluorescence titration curve of flavonoids as a function of Tel7 G-quadruplex DNA concentration (a) Luteolin (b) Quercetin (c) Rutin (d) Genistein. Solid lines represent fit according to the ligand binding two site saturation. Value of Binding constant(s) ( $K_d$ ) are indicated at the top left side of the plot. The normalized data was plotted for Genistein, as it shows quenching.*

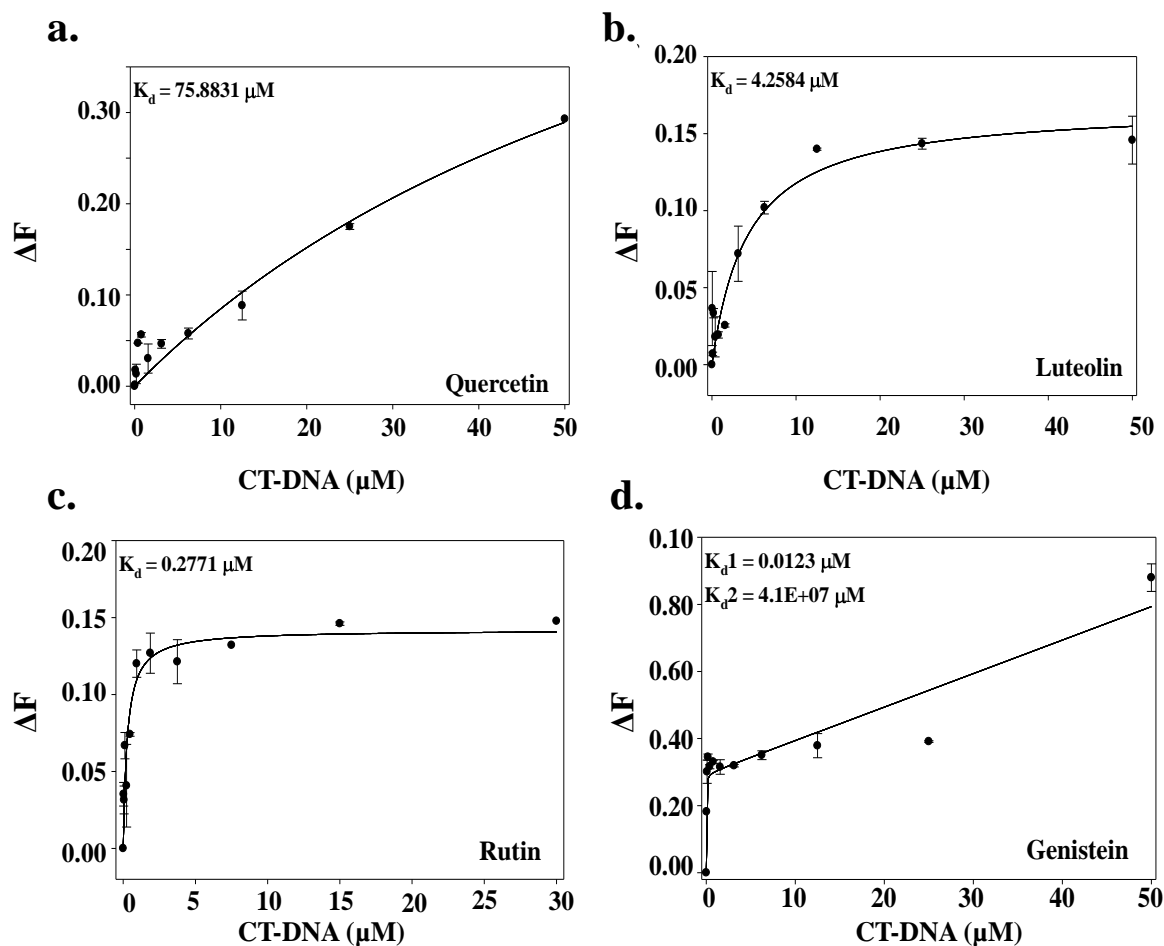


**Figure 3.3.** Fluorescence titration curve of flavonoids as a function of CT-DNA concentration (a) Luteolin (b) Quercetin (c) Rutin (d) Genistein. Solid lines represent fit according to the ligand binding two site saturation. Value of Binding constant(s) ( $K_d$ ) are indicated at the top left side of the plot. The normalized data was plotted for Genistein, as it shows quenching.

**Table 3.1. Binding constant ( $K_d$ (M)) values of flavonoids with G-quadruplex DNA in comparison to CT-DNA**

Flavonoids	Tel7 G-quadruplex DNA		CT-DNA	
	$K_d1$ (M)	$K_d2$ (M)	$K_d1$ (M)	$K_d2$ (M)
<b>Luteolin</b>	$2.30 \times 10^{-8}$	$4.28 \times 10^{-5}$	$2.65 \times 10^{-5}$	--
<b>Quercetin</b>	$4.90 \times 10^{-9}$	$4.35 \times 10^{-6}$	$4.26 \times 10^{-6}$	--
<b>Rutin</b>	$3.80 \times 10^{-8}$	$9.63 \times 10^{-6}$	$7.59 \times 10^{-5}$	--
<b>Genistein</b>	$2.65 \times 10^{-5}$	$2.65 \times 10^{-5}$	$2.77 \times 10^{-7}$	<b>41.00</b>

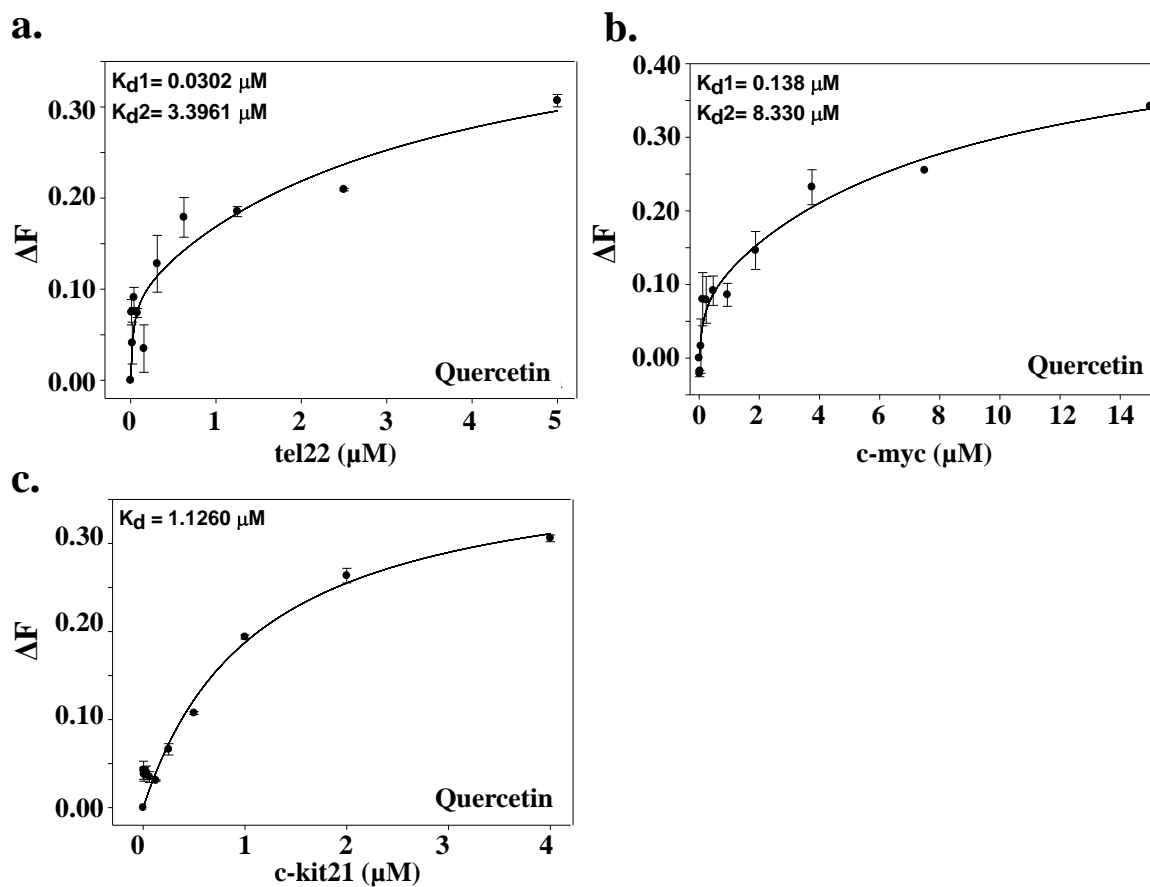


*Figure 3.4. Fluorescence titration curve of Quercetin as a function of various G-quadruplex DNA concentration (a) tel22 DNA (b) c-myc DNA (c) c-kit21 DNA. Solid lines represent fit according to the ligand binding two site saturation. Value of Binding constant(s) ( $K_d$ ) are indicated at the top left side of the plot.*

*Table 3.2. Binding constant ( $K_d$ (M)) values of Quercetin with various G-quadruplex forming DNA sequences*

G-quadruplex DNA	Quercetin	
	$K_d1$ (M)	$K_d2$ (M)
tel22	$3.02 \times 10^{-8}$	$3.40 \times 10^{-6}$
c-myc	$1.38 \times 10^{-7}$	$8.33 \times 10^{-6}$
c-kit21	$1.13 \times 10^{-6}$	--

An enhancement in fluorescence intensity of Luteolin, Quercetin and Rutin was observed, while quenching was observed for Genistein. These observed spectral changes depicted the binding of flavonoids to Tel7 G-quadruplex DNA and generated G-quadruplex-flavonoid complex. The plot of  $\Delta F$  (change in the fluorescence intensity) against G-quadruplex DNA concentration was fitted with ligand binding two site saturation model (Figure 3.2); and the computed binding constant values ( $K_d$ ) (Table 3.1). These values suggested that Quercetin has higher affinity for Tel7 G-quadruplex DNA as compared to the other flavonoids. It is important for G-quadruplex binders to be specific for G-quadruplex topology. Therefore, to know the specificity of flavonoids towards G-quadruplex structures, we have performed fluorescence titration experiment of flavonoids with duplex DNA (CT-DNA) (Figure 3.3) We have observed the same trend for change in fluorescence intensity of flavonoids with addition of CT-DNA, that is, enhancement was observed for Luteolin, Quercetin and Rutin, while quenching was observed for Genistein. Binding constant values of these flavonoids with CT-DNA were lower as compared to Tel7 G-quadruplex DNA. Amongst which Quercetin shows ~1000 fold higher affinity for Tel7 G-quadruplex DNA (Table 3.2). This depicted the higher specificity of Quercetin for G-quadruplex structure over duplex DNA.

Further, for this study we have chosen small sequence of human telomeric DNA forming G-quadruplex DNA, that is d-(T<sub>2</sub>AG<sub>3</sub>T)<sub>4</sub>. In order to understand the binding behaviour of Quercetin with other biologically relevant G-quadruplex DNA, we have also performed the fluorescence titration experiment of Quercetin with tel22, c-myc and c-kit G-quadruplex DNA. Tel22 DNA sequence is 22 mer human telomeric DNA sequence that forms G-quadruplex structure. c-myc and c-kit21 DNA sequences are present at promoter regions of c-myc and c-kit proto-oncogenes and forms G-quadruplex structure. All these G-quadruplex forming regions are involved in progression of cancer growth. The binding constant values ( $K_d$ ) of these flavonoids (Table 3.2) obtained from this experiment suggested that Quercetin binds to G-quadruplex DNA sequences (Figure 3.3). The mode of binding as observed are slightly different and that could be due to the difference topologies of G-quadruplex structures formed by different G-rich DNA.<sup>[46]</sup> These results suggested the high specificity and affinity of Quercetin for various G-quadruplex forming DNA sequences viz. tel7, tel22, c-myc and c-kit21 DNA as compared to duplex DNA. Further to reveal the binding more of flavonoids to Tel & G-quadruplex DNA, we have performed life time decay measurements as mentioned in next sub-section.

### 3.2.1.2 Time resolved fluorescence studies

In order to get insights about the binding mode of flavonoids to Tel7 DNA forming G-quadruplex structure, we have measured time-resolved fluorescence spectra that provide detailed information of environment around a fluorophore. In aqueous solution, the changes in the photo-physical process of an excited fluorescent probe can be inferred via time-resolved fluorescence decay studies. As the fluorescence life time of excited state fluorophore is very sensitive to its structure and dynamics, thus, this study provides insight into how DNA structure influences the fluorescence decay profiles of these flavonoids. Time resolved fluorescence decays were obtained by Time-Correlated Single-Photon Counting (TSCPC) method on the spectrofluorimeter (Horiba). The life time decay profiles were measured for free flavonoids and their complex with Tel7 G-quadruplex DNA sequence. On performing global analysis for each set of fluorescence decays, we have found that complexity of the model is well calculated with tri exponential decay function that fits well in terms of statistical quality having global  $\chi^2$  value  $\sim 1.3$  for flavonoids and their complexes with Tel7 DNA. These low global values for  $\chi^2$  indicate that tri exponential decay function is an admirable statistical description of both the systems.<sup>[47]</sup> It could be attributed to presence of three different conformations in the solution that were likely due to the rotation of a single bond between benzopyran rings to phenyl rings of flavonoids. Thus, the decay profiles of free flavonoids have three lifetimes ( $\tau_1$ ,  $\tau_2$  and  $\tau_3$ ) and three amplitudes ( $\beta_1$ ,  $\beta_2$  and  $\beta_3$ ) and their values are mentioned in Table 3.3. Figure 3.5 displayed the fluorescence decay profile of flavonoids in their free form and complexed with Tel7 G-quadruplex DNA at D/N = 2.0. It was observed that fluorescence decay lifetime of the free flavonoids was lesser as compared to that of G-quadruplex-flavonoid complex (Figure 3.5). Quercetin – Tel7 DNA complex at D/N = 2.0 ratio also gives best fit with tri - exponential decay profile that attributed the requirement of three life time components to give a satisfactory fit. This indicated the existence of three binding states of flavonoids wherein these molecules experiences diverse environment that might raise due to various interactions and thus displays different quenching rate. From TSCPC data analysis, it has been found that Genistein have lower decay rate (in range of ps) with highest amplitude value when complexed with Tel7 DNA. This may indicate the existence of single binding pattern of Genistein in which the major population of complex contributed to generate decay profile. But, unlikely to Genistein, other flavonoids followed the trend of shorter and longer lifetimes for free and complexed flavonoids, respectively, along with slight changes in amplitudes. This stipulated the presence of a different pattern of complex formation, credited to the binding of flavonoids to Tel7 DNA at

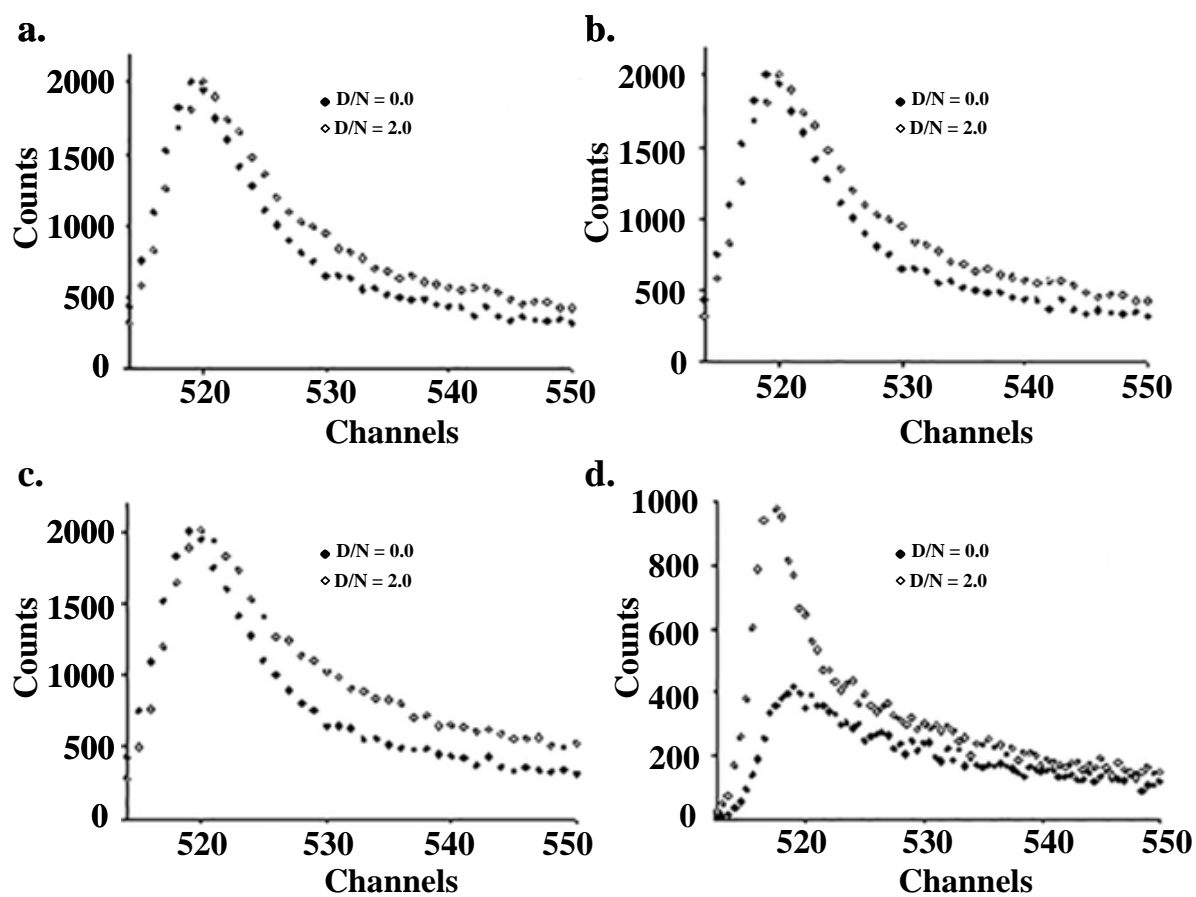


Figure 3.5. Fluorescence lifetime decay curve of flavonoids and their complex with Tel7 G-quadruplex DNA at  $D/N = 2.0$  for (a) Luteolin (b) Quercetin (c) Rutin (d) Genistein.

*Table 3.3. Life time fluorescence decay parameters for flavonoids and their D/N = 2:1 complex with Tel7 G-quadruplex DNA at 298 K*

Flavonoids	Uncomplexed Flavonoids						
	Life Time Decay (ns)			Amplitude			$\chi^2$
	$\tau_1$	$\tau_2$	$\tau_3$	$\beta_1$	$\beta_2$	$\beta_3$	
<b>Luteolin</b>	<b>3.20</b>	<b>1.40</b>	<b>7.50</b>	<b>64.40</b>	<b>19.50</b>	<b>16.10</b>	<b>1.36</b>
<b>Quercetin</b>	<b>0.03</b>	<b>2.40</b>	<b>9.30</b>	<b>79.50</b>	<b>7.90</b>	<b>12.50</b>	<b>1.34</b>
<b>Rutin</b>	<b>1.40</b>	<b>2.70</b>	<b>7.50</b>	<b>81.40</b>	<b>9.70</b>	<b>8.90</b>	<b>1.21</b>
<b>Genistein</b>	<b>5.60</b>	<b>21.90</b>	<b>0.50</b>	<b>59.50</b>	<b>29.00</b>	<b>11.50</b>	<b>1.44</b>
Flavonoids	Flavonoids and Tel7 complex						
	Life Time Decay (ns)			Amplitude			$\chi^2$
	$\tau_1$	$\tau_2$	$\tau_3$	$\beta_1$	$\beta_2$	$\beta_3$	
<b>Luteolin</b>	<b>4.50</b>	<b>14.80</b>	<b>0.16</b>	<b>43.40</b>	<b>21.00</b>	<b>35.60</b>	<b>1.32</b>
<b>Quercetin</b>	<b>3.80</b>	<b>13.10</b>	<b>0.12</b>	<b>34.10</b>	<b>18.00</b>	<b>47.80</b>	<b>1.20</b>
<b>Rutin</b>	<b>4.90</b>	<b>12.80</b>	<b>0.54</b>	<b>64.50</b>	<b>19.30</b>	<b>16.20</b>	<b>1.14</b>
<b>Genistein</b>	<b>5.90</b>	<b>38.30</b>	<b>0.007</b>	<b>0.00</b>	<b>0.00</b>	<b>100.00</b>	<b>1.16</b>

more than one site. The binding mode of ligand to DNA could be obtained by analyzing fluorescence lifetime decay profile using TCSPC studies. Usually, planar molecules with an extended aromatic core interact with G-quadruplex structure via two modes: either via intercalation or via end-stacking and external or groove binding. The lifetimes in the end-stacking mode are larger than those in the external binding.<sup>[48]</sup> Additionally, previous reports showed that Quercetin interacts with G-quadruplexes by end-stacking and outside binding.<sup>[40]</sup> Thus, the significant changes observed in the values of both the decay components and the amplitudes of the flavonoids upon binding to Tel7 DNA at D/N = 2:1 ratio clearly indicate the intercalation of flavonoids with Tel7 DNA and formation of drug-DNA complex. Further, the binding of these flavonoids and its effect on stability of G-quadruple structure were ascertained by other biophysical methods like circular dichroism as described in next section.

### **3.2.2 Circular Dichroism spectroscopy**

Circular dichroism CD spectroscopy is often the ideal technique to recognize the conformation of macromolecules like proteins and nucleic acids. Small molecules like Luteolin, Quercetin, Rutin and Genistein are optically inactive and hence do not have any CD spectrum. The interaction of these flavonoids to human telomeric G-quadruplex DNA sequence Tel7 was monitored in ultraviolet region. Tel7 DNA sequence is known to form a parallel G-quadruplex structure in K<sup>+</sup> solution,<sup>[49]</sup> which is evident by a positive peak at 260 nm and a trough at 240 nm, as exhibited in the CD spectra for Tel7 sequence (Figure 3.6). CD spectra of Tel7 DNA were slightly changed after the addition of flavonoids at twice the concentration of G-quadruplex sequence. But, global conformation of G-quadruplex DNA remained same. This change in CD spectra of DNA due to complexation of flavonoids is clearly depicted in Figure 3.6 and suggested that binding of flavonoids does not induce any distortion in G-quadruplex topology of telomeric DNA Tel7. It could also be corroborated that binding of flavonoids may stabilize G-quadruplex structure formed by human telomeric DNA sequence. Thus, it is interesting to know which protons of Quercetin participate in the binding to Tel7 G-quadruplex DNA, we have performed one dimensional proton NMR spectroscopy as mentioned in next section.

### **3.2.3 Nuclear Magnetic Resonance spectroscopy**

#### **3.2.3.1 One dimensional proton NMR studies**

Nuclear magnetic resonance (NMR) spectroscopy is an essential tool to study Drug-DNA interactions. It allows the determination of atomic resolution structures and provides

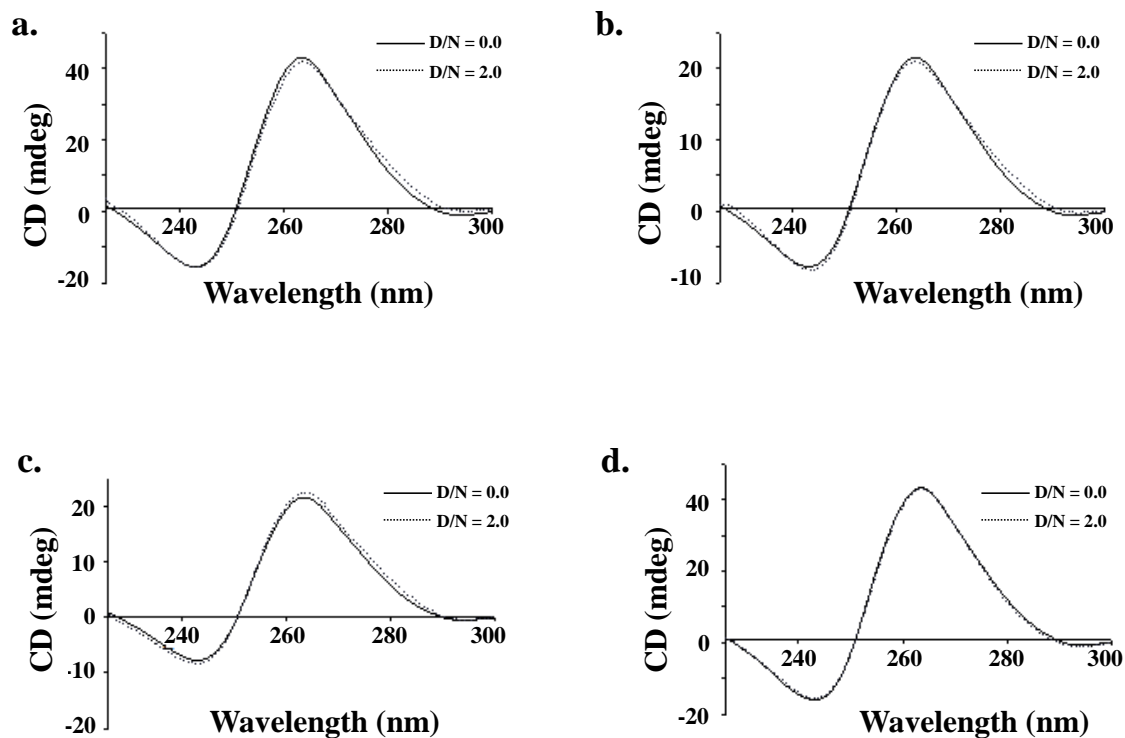


**Figure 3.6.** Circular Dichroism titration spectrum for free DNA (straight line) and in the presence of (a) Luteolin (b) Quercetin (c) Rutin (d) Genistein (dotted line); at  $D/N = 2.0$  ratio.

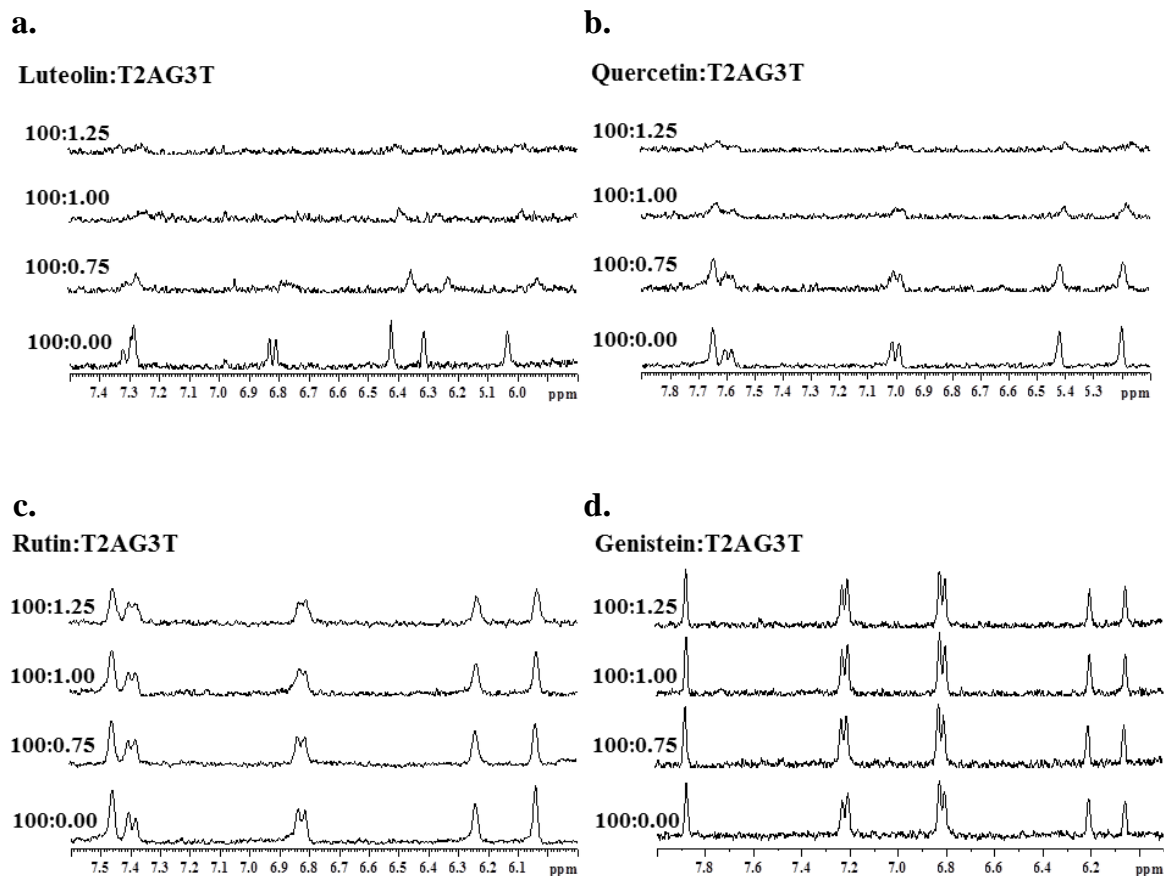


**Figure 3.7.** One dimensional proton NMR spectra of 200  $\mu\text{M}$  flavonoids and their titration with increasing concentration of Tel7 DNA (a) Luteolin (b) Quercetin (c) Rutin (d) Genistein.

insights into the intermolecular interactions, dynamics as well as stability. To know the involvement of flavonoids protons in binding to Tel7 G-quadruplex DNA, we have performed one-dimensional proton NMR titration studies. We have collected  $^1\text{H}$  NMR spectra of all flavonoids and monitored it by titrating Tel7 G-quadruplex DNA to them. The changes in the shape of flavonoid resonances were observed with successive addition of DNA to flavonoid solution (Figure 3.7). At D/N ratio of 100:1, the broadening of the Quercetin and Luteolin proton were seen, while Rutin and Genistein protons showed no changes even at higher concentration of DNA. These broadening of signals were accompanied by their disappearance at D/N ratio of 100:1.25 for Luteolin and 100:3 for Quercetin. This suggested the involvement of these protons in the binding of flavonoids to Tel7 G-quadruplex DNA. Our results from other biophysical experiments performed in this study suggested that Quercetin showed the highest affinity for Tel7 G-quadruplex DNA amongst all four flavonoids used in this study. Therefore, we have performed the detailed NMR studies with Quercetin in order to understand the structural basis of its interaction with Tel7 G-quadruplex DNA.

#### **3.2.3.1.1 Assessment of G-quadruplex structure formation**

For this purpose, we have performed NMR titration experiments of human telomeric DNA Tel7 forming G-quadruplex structure with the gradual addition of Quercetin. The structural conformation of G-quadruplex DNA formed by human telomeric sequence Tel7 in  $\text{K}^+$  solution was monitored by proton NMR. We have observed three well-resolved resonances in the imino region (10 - 12 ppm) of  $^1\text{H}$ -NMR and the presence of clear peaks in this region is evident of unique feature of higher ordered DNA structures such as G-quadruplexes. The assignment of nucleotide protons has been carried out by following the strategies adopted for standard B - DNA structures that is, sequential NOEs (base H8/H6)<sub>n</sub> - sugar (H1')<sub>n-1</sub>, (base H8/H6)<sub>n</sub> - sugar(H2'')<sub>n-1</sub>, (base H8/H6)<sub>n</sub> - sugar(H2')<sub>n-1</sub>; expected NOEs due to several short intra nucleotide distances<sup>[50]</sup> as well as NMR data of uncomplexed d-(TTAGGGT)<sub>4</sub>.<sup>[51]</sup> The present oligonucleotide Tel7 exists as G-quadruplex structure that can be evident from sequential connectivities between the base protons of G4-G5-G6 (Figure 3.11) as well as adjacent guanine imino protons in the sequence, G4NH-G5NH and G5NH-G6NH. The position of each and every resonance was thus ascertained and unambiguous assignment of was performed on the basis of a previously reported strategy.<sup>[49]</sup>

#### **3.2.3.1.2 One –Dimensional proton NMR titration studies**

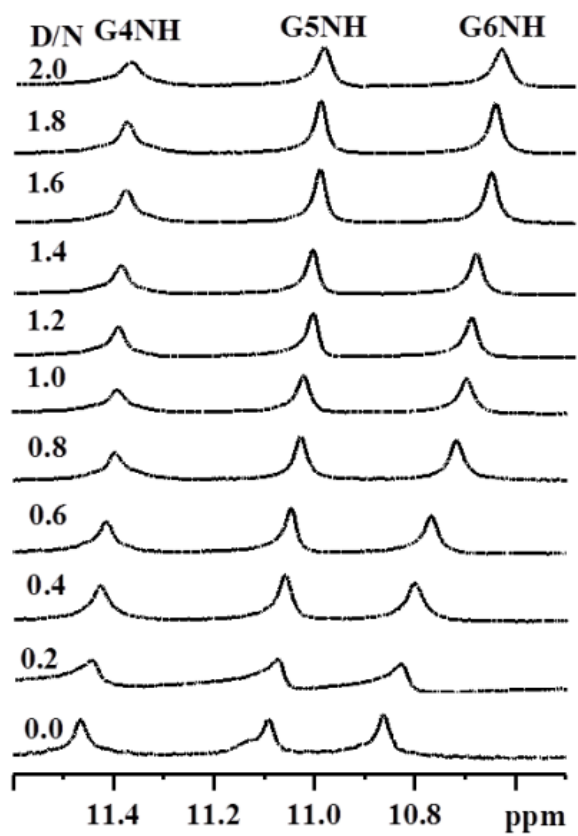


*Figure 3.8. NMR spectra for Quercetin and Tel7 DNA complex monitored by imino region as a function of ligand/DNA ratio at 298 K.*

In the  $^1\text{H}$ -NMR spectra of unbound G-quadruplex DNA, 11.45, 11.10 and 10.86 ppm mark the resonances for G4NH, G5NH, and G6NH, respectively (Figure 3.7a, D/N = 0.0). Most likely due to solvent exchange, peaks for the thymine imino protons were not observed. We have performed NMR titration experiments to characterize the interaction of Quercetin with Tel7 DNA sequence. As Quercetin was gradually titrated into Tel7 G- quadruplex DNA solution, remarkable changes in chemical shifts were observed in imino (Figure 3.8) as well as other regions of the proton NMR spectrum (Figure 3.9a). The significant broadening of spectral lines uniformly at higher ratios indicated the binding of Quercetin to Tel7 DNA. In imino region, G6NH, G5NH, G4NH resonances of d-(T<sub>2</sub>AG<sub>3</sub>T)<sub>4</sub> were upfield shifted upon the addition of Quercetin (Figure 3.8). At D/N = 2.0, G6NH resonance showed the largest change in chemical shift value of ~ 0.20 ppm (Figure 3.8). These upfield shifts for the imino resonances are in line with previously reported results<sup>[40]</sup> and could be due to its  $\pi$ -electronic cloud<sup>[52]</sup> suggesting the stacking of Quercetin below the G6-tetrad. Further, these resonances were broadened remarkably with increasing D/N ratio and upon reaching D/N = 2.0, G4NH showed significant broadening that starts from D/N = 1.0 (Figure 3.8). As thymine imino protons were not observed even at D/N =2.0, it indicated that binding of Quercetin does not induces T-tetrad formation.

In base as well as H1' region of proton NMR, we have also observed considerable changes in shape and chemical shifts of resonances with incremental addition of Quercetin to Tel7 G-quadruplex DNA solution. T1H6, T2H6 and T7H6 resonances were observed to be shifted downfield (Figure 3.9a). A significant broadening was observed in T1H6 resonance after D/N ratio 1.0 while Guanine base protons shows upfield shift up to 0.16 ppm and rest other base protons showed downfield shift maximum up to 0.11 for T7H6 at D/N = 1.0. Further, a ~ 0.04 ppm upfield shift was observed for T1H1' and ~ 0.05 ppm for G4H1' protons at D/N =1.0. The downfield shift of 0.07 ppm was observed in T7H1'. Furthermore, T1H1' and G4H1' showed maximum upfield shift than other protons while only T7H1' showed the downfield shift and G5H1', G6H1' protons were least affected. Similarly, A3H2 started broaden after D/N ratio 0.50. Thus, the remarkable broadening and change in chemical shifts of the G4, T7, G6, A3, T1, and T2 protons suggested that the binding site of Quercetin on d-(T<sub>2</sub>AG<sub>3</sub>T)<sub>4</sub> was most likely close to the T1/T2/A3 or G6/T7 base step.

### 3.2.3.1.3 Temperature dependent one –dimensional proton NMR studies

The binding of Quercetin to Tel7 G-quadruplex DNA was also assessed using temperature-dependent NMR studies.  $^1\text{H}$  NMR spectra of the Quercetin – d (T<sub>2</sub>AG<sub>3</sub>T)<sub>4</sub> DNA

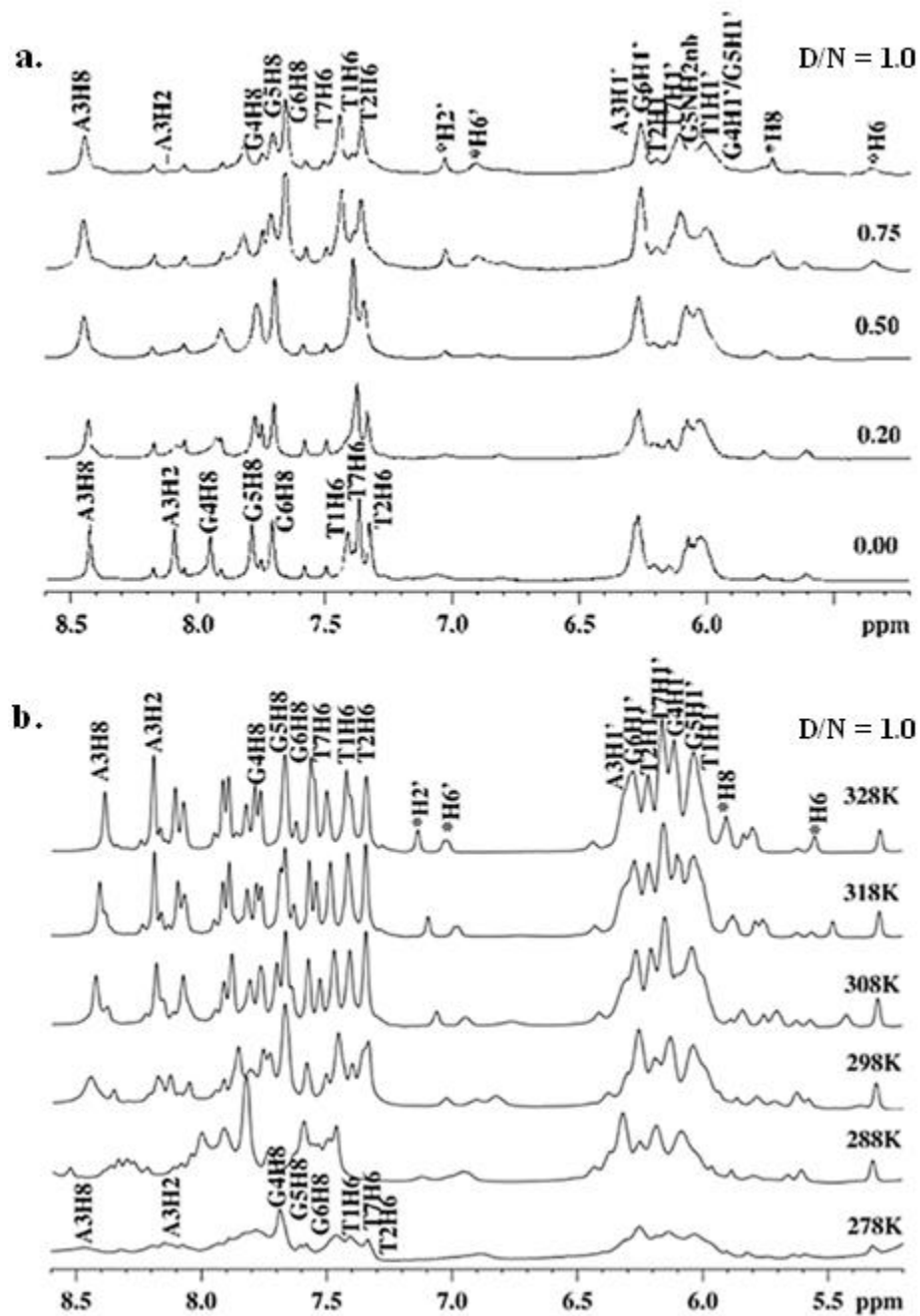
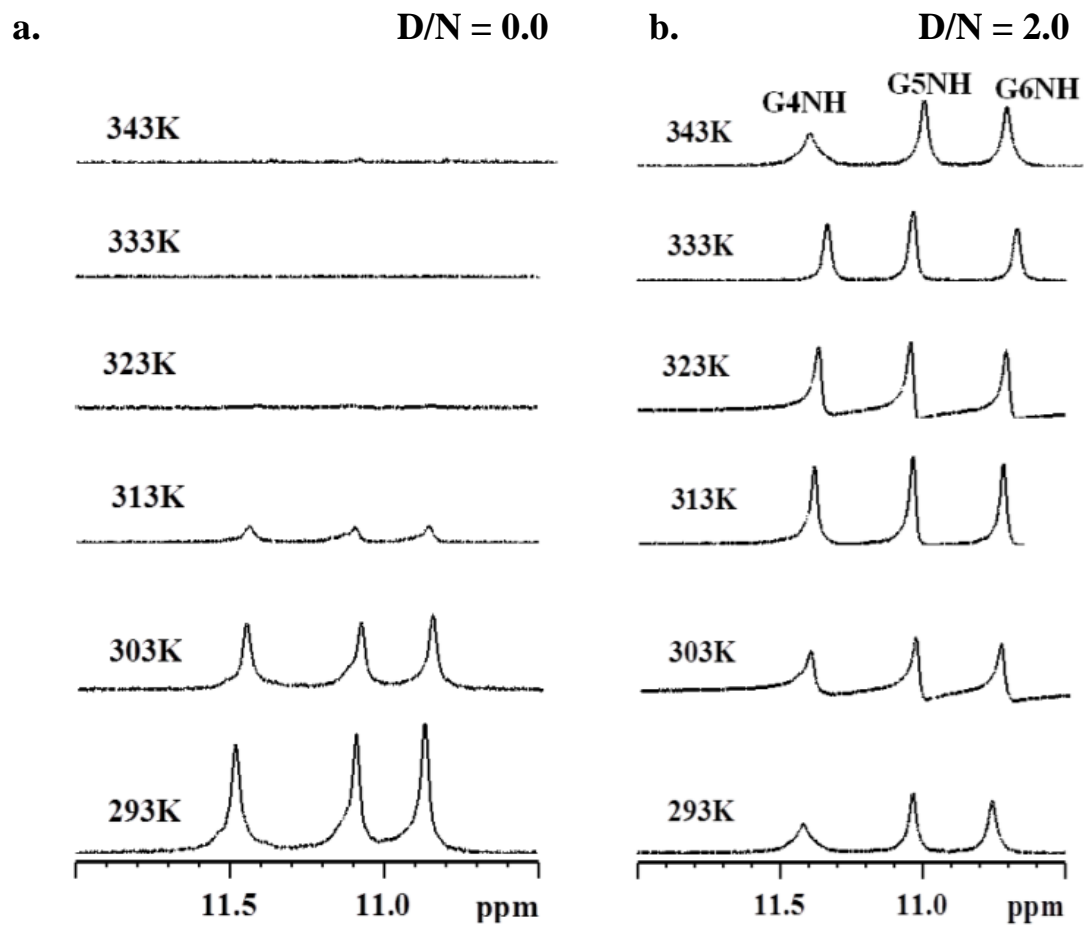


Figure 3.9. One dimensional proton NMR spectra for Quercetin and Tel7 DNA complex monitored by base proton and H1' region as a function of (a) increasing concentration of Quercetin upto D/N = 1.0 ratio at 298 K (b) temperature at D/N = 1.0 ratio. Proton resonances from Quercetin are marked with asterisk.



*Figure 3.10. NMR spectra for Quercetin and Tel7 DNA complex monitored by imino region as a function at temperature at (a)  $D/N = 0.0$  (b)  $D/N = 2.0$  ratio.*

complex at  $D/N=1.0$ , was observed for the temperature range of 278 to 343 K (Figure 3.9b and 3.10). This experiment would help to resolve the overlapping resonance peaks. It was observed that chemical shift of G-quadruplex DNA sequence varied with temperature and these changes due to titrimetric and temperature dependent studies showed that Quercetin binds to Tel7 DNA. Moreover, Quercetin proton resonances in Quercetin – Tel7 complex were shift downfield with the increase in temperature (Figure 3.9b). The shift in Quercetin protons on binding are expected to be maximum at low  $D/N$  ratio as at this situation maximum amount of drug is present in the bound state. At 298K in  $D/N = 1.0$  population, the H2' and H6' protons of Quercetin benzopyrone ring showed an upfield shift 0.74 and 0.68 ppm and phenyl ring protons H6 and H8 showed upfield shift of 0.89 and 0.73 ppm substantially with respect to their chemical shift positions at  $D/N = 0.0$  (Figure 3.9a). Further the changes in chemical shift are almost similar in all these drug protons which indicate that these protons experience the similar kind of environment during complexation with DNA. This substantial upfield shift of  $\sim 0.8$  ppm in H6, H8, H2' and H6' of Quercetin, respectively on binding is indicative of stacking of Quercetin aromatic chromophore with base pair of DNA. Anticancer drugs like camptothecin and topotecan that act as DNA binders via stacking at the terminal end of oligonucleotides, also displayed a chemical shift variation of  $\sim 0.50$  ppm for several oligonucleotides.<sup>[53]</sup> Moreover, at  $D/N = 1.0$ , with the increase in temperature, the resonances of Quercetin H6, H8, H2' and H6' protons become sharp and clearly visible, which were otherwise slightly broader at low temperature. Thus, the participation of Quercetin H6, H8, H2' and H6' protons in binding was corroborated by the clear visibility of these protons at high temperature, which occurred due to the weakening of the drug- DNA interactions and results in destacking of nucleotides. This stacking interaction can also be supported by temperature dependent studies in which a significant change in chemical shift with temperature for Quercetin protons was observed. These protons were shifted downfield by  $\sim 0.2$  ppm with increase in temperature clearly indicating destacking of Quercetin chromophore from the Quercetin-DNA complex (Figure 3.9b).

Furthermore, the rise in temperature causes the breaking of hydrogen bond in G-quartet structure, which results in the disappearance of imino proton signals. At  $D/N = 0.0$ , the imino proton resonances start disappearing at 313 K and were completely lost at 323 K. However, at  $D/N = 2.0$ , these imino proton resonances can be seen upto 343 K. These results clearly show that binding of Quercetin stabilizes the G-quadruplex structure (Figure 3.10). However, the change in chemical shift is not a sufficient indicator of the interaction; instead the observed intermolecular short contacts are a direct proof of the structure of a specific

drug–DNA complex. For this evaluation, NOESY experiment has been performed as mentioned in next sub-section.

### 3.2.3.2 Two dimensional NMR spectroscopy

The 2D NOESY spectra of Quercetin – Tel7 DNA complex was collected at various mixing times and at three different temperatures (288 K, 298 K and 318 K) for D/N= 0.25, 0.50, 0.75, 1.00, 1.5 and 2.00 ratios. NOEs for intranucleotide connectivities, sequential connectivities, as well as inter nucleotide connectivities were observed and their cross peak intensities were estimated qualitatively as strong intense (ss), strong (s) medium (m) weakly (w) and very weakly (vw) for distances of about 1.8 - 2.5, 2.5 - 3.0, 3.0 - 3.5, 3.5 - 4.0, and 4.0 - 5.0 Å respectively. At D/N = 0.0, NOEs between adjacent guanine imino protons in the d-(T<sub>2</sub>AG<sub>3</sub>T)<sub>4</sub> sequence that is G<sub>4</sub>NH–G<sub>5</sub>NH and G<sub>5</sub>NH–G<sub>6</sub>NH, are evident in Figure 3.12a. These guanine imino protons show NOEs with their own base protons and also to their 5'-flanking base protons in the A<sub>3</sub>–G<sub>4</sub>–G<sub>5</sub>–G<sub>6</sub> part of the d-(T<sub>2</sub>AG<sub>3</sub>T)<sub>4</sub> quadruplex structure (Figure 3.12a). The G<sub>6</sub>NH at 10.9 ppm exhibits NOEs to the base protons of G<sub>6</sub>H<sub>8</sub> and G<sub>5</sub>H<sub>8</sub>, and the 11.2 ppm imino proton of the G<sub>5</sub> exhibits NOEs with the base protons of G<sub>5</sub>H<sub>8</sub> and G<sub>4</sub>H<sub>8</sub>. Importantly, we also observe NOEs from the base protons A<sub>3</sub>H<sub>8</sub> and A<sub>3</sub>H<sub>2</sub> to the imino proton of G<sub>4</sub> at 11.67 ppm. These NOEs showed inter-strand interactions between guanine residues that are involved in formation of G-tetrad. Thus, in the unbound form Tel7 G-quadruplex DNA displayed strong NOEs accounted by intra-nucleotide connectivity and sequential connectivity that denoted a well-established stacking interaction between DNA base pairs. Upon addition of Quercetin to Tel7 DNA, this stacking interaction is slightly perturbed as evident by disappearance of G<sub>4</sub>NH–A<sub>3</sub>H<sub>2</sub> NOE cross peak (Figure 3.12b). Interestingly, there was emergence of one new NOE for G<sub>5</sub>NH–G<sub>6</sub>H<sub>8</sub>. The loss of the cross peak at 11.67 ppm for G<sub>4</sub>NH with A<sub>3</sub>H<sub>2</sub> (Figure 3.12a) and the emergence of a new cross peak for G<sub>5</sub>NH and G<sub>6</sub>H<sub>8</sub> suggested the binding of two Quercetin molecules, one near the A<sub>3</sub> residue and other near the G<sub>6</sub> residue. Similarly, the emergence of new sets of cross peak at 318 K was observed in the imino region of the NOESY spectra (Figure 3.11). But, upon comparing with Tel7 -NH resonance at this temperature, no other set of peak were observed. This may account for the bound and free –NH peak which can also be seen in NOESY in Quercetin- Tel7 DNA complex (Figure 3.11b). Moreover, it was also observed that there is loss of sequential connectivity between T<sub>1</sub>H<sub>1</sub>'–T<sub>2</sub>H<sub>6</sub> in the drug-DNA complex (Figure 3.13). In addition, a total of 24 drug-DNA intermolecular NOEs were identified in the 2:1 complex (Table 3.4). By far the majority of NOEs involves the base and sugar protons of

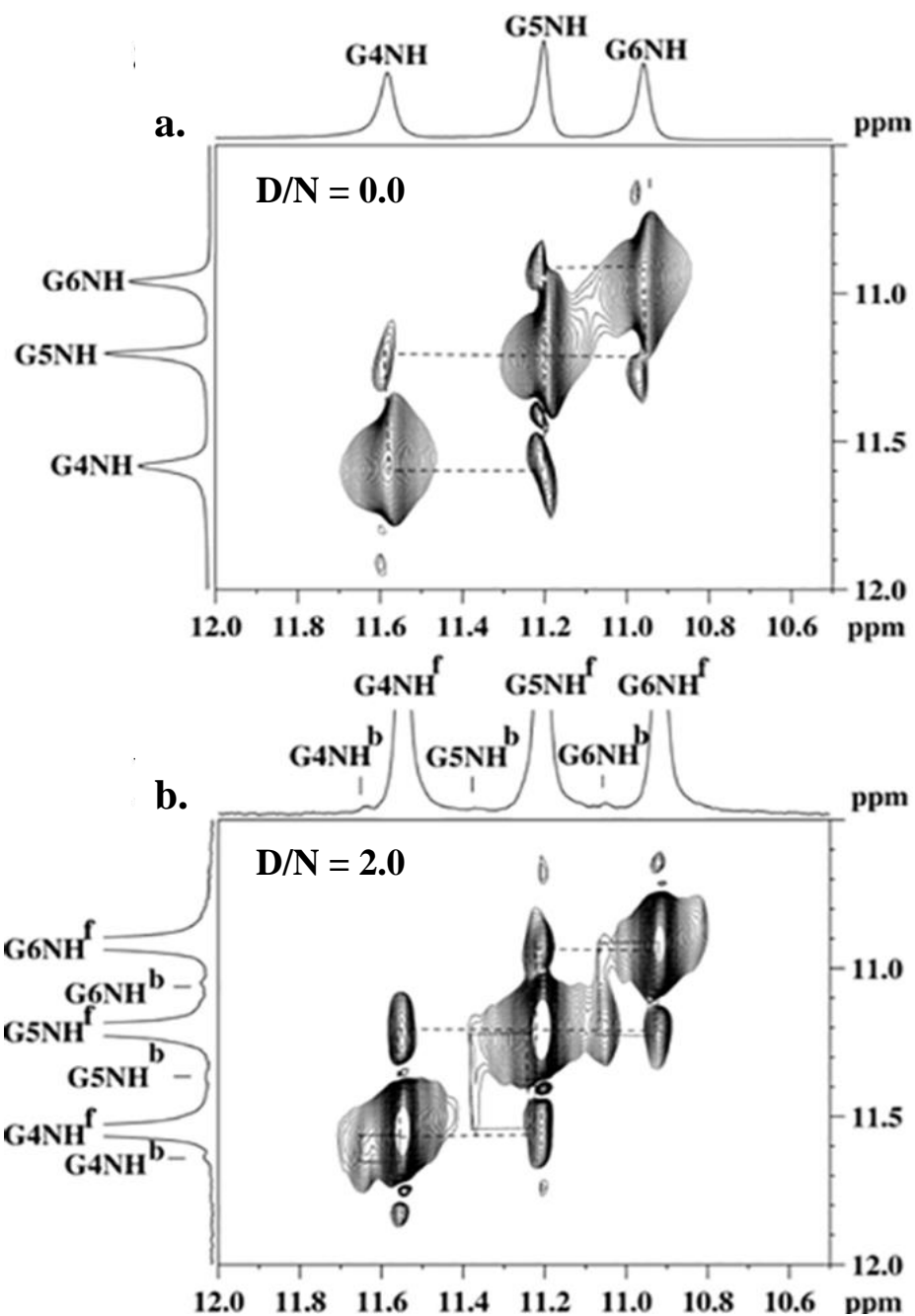
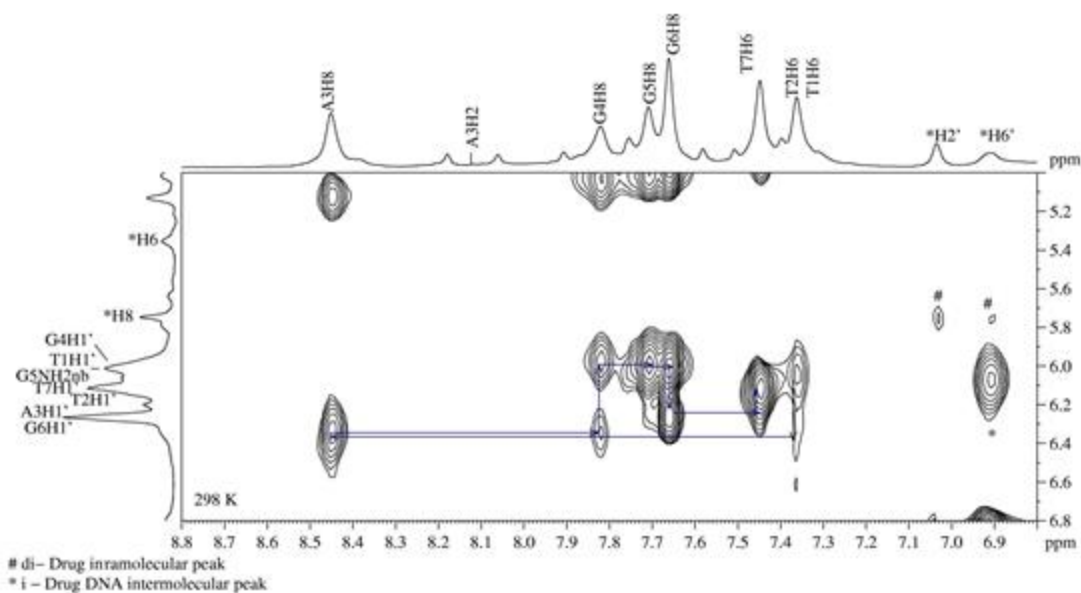
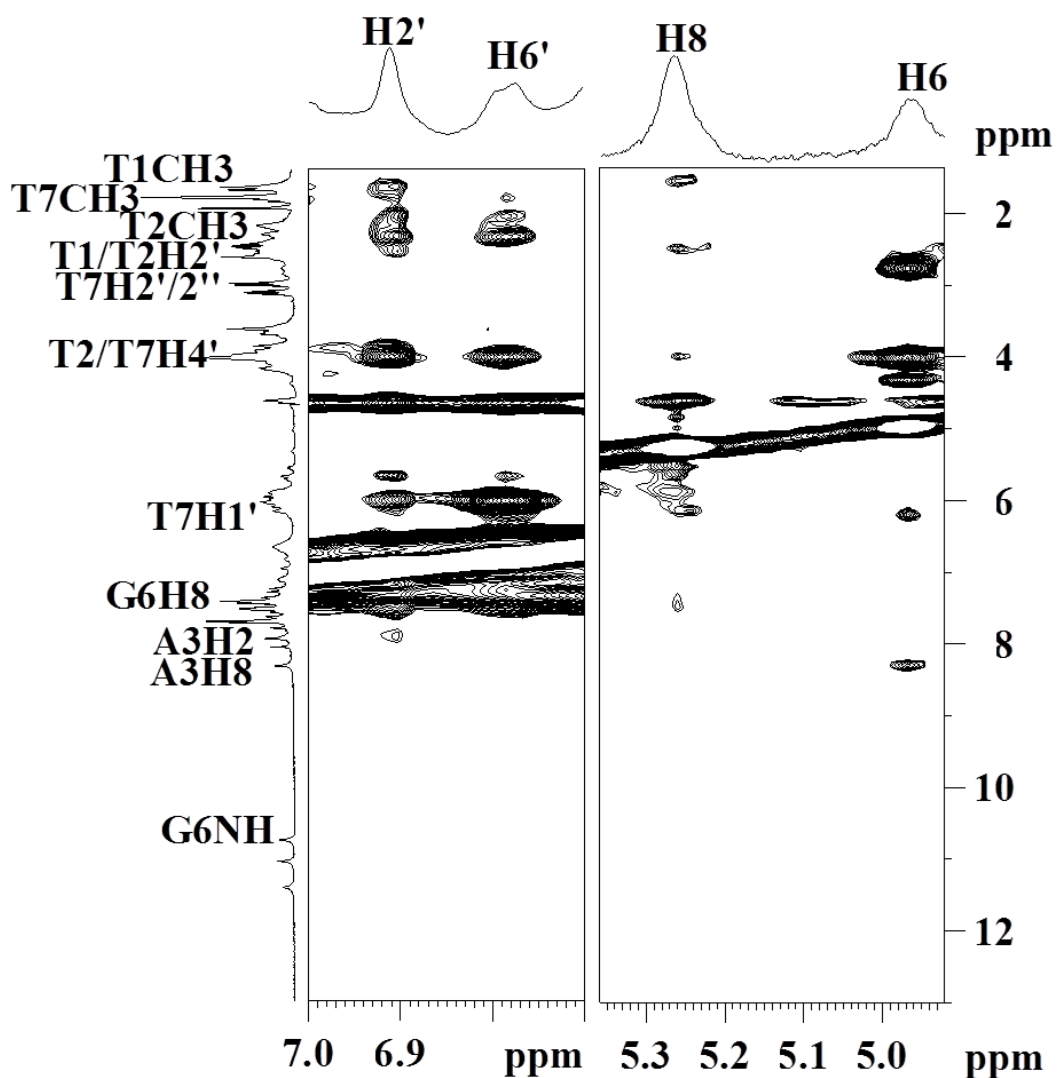


Figure 3.11. Portion of 200ms NOESY spectrum of Quercetin - Tel7 DNA complex showing (a) NH-NH NOEs between adjacent G-tetrads at 298 K at D/N = 1.0 (b) Free and bound NH signals due to Drug-DNA complex formation at 318 K at D/N = 1.0 ratio.





**Figure 3.13.** Expansion of NOESY spectrum of Tel7 DNA complexed with Quercetin showing loss of sequential connectivity between T1H1'-T2H6 in drug-DNA complex at  $D/N = 1.0$  ratio.



*Figure 3.14. Portion of 200ms NOESY spectrum of Quercetin – Tel7 DNA complex at D/N = 2.0 ratio showing intramolecular cross peak within Quercetin and intermolecular cross peaks of Quercetin H2', H6', H8, H6 with Tel7 G-quadruplex DNA.*

**Table 3.4. Relative intensity of intermolecular NOE connectivity between Tel7 DNA and Quercetin in the complex at D/N=2.0 from NOESY spectra at 298K**

<b>S.No.</b>	<b>Sequence Connectivity</b>	<b>NOE Intensity</b>	<b>Distances obtained by rMD (Å) (2MS6)</b>
1.	T7H1'-H2'	w	3.80
2.	T7H1'-H6'	ss	2.10
3.	G6H8-H2'	s	2.80
4.	T7H6-H2'	s	2.80
5.	T7H6-H6'	vw	4.50
6.	G6H1-H2'	vw	4.50
7.	G6H1-H6'	ss	2.10
8.	G6H2'1-H8	vw	4.50
9.	G6H2'1-H6	vw	4.50
10.	T7H4'-H8	ss	2.10
11.	G6H3'-H8	ss	2.10
12.	G6H3'-H6	ss	2.10
13.	G6H1-H8	vw	4.50
14.	A3H2-H6	vw	4.50
15.	T1H6-H8	s	2.80
16.	T1H1'-H8	s	2.80
17.	T2H1'-H6	s	2.80
18.	T2H1'-H8	s	2.80
19.	T1H2'2-H8	ss	2.80
20.	T1H2'1-H8	s	2.80
21.	T1H2'1-H2'	s	2.80
22.	T1H2'1-H6'	s	2.80
23.	T1H2'2-H2'	s	2.80
24.	T1H2'2-H6'	s	2.80

T1pT2 and G6pT7 (Figure 3.14). In contrast, no NOE to G4 and G5 were identified that excludes any possibility of Quercetin molecules end-stacking at the A3-G4 or G4-G5 step. Also, the loss of sequential connectivity between T1H1'-T2H6 in the drug-DNA complex might occurred due to the end-stacking of the Quercetin chromophore at these base steps (Figure 3.13). A number of NOEs to T7 show that the drug inserts also at the G6-T7 step. Majority of NOEs came from Quercetin H2', H6', H8 and H6 protons to T1, T2 and T7 of DNA base and sugar protons position the edges of the benzopyran ring of ligand in between the base. Other NOE cross-peaks between Quercetin and protons of A3 and G6 are evident in the portion of the NOESY spectrum shown in Figure 3.14. Thus, Quercetin molecule also orients itself in such a way that it achieved better interaction with the T1/T2 or the G6/T7 base step in the end-stacking mode, with the H6, H8, H2' and H6' protons involved in the binding. The loss of the G4NH and A3H2 cross peak and the emergence of new NOEs supported the binding of two molecules of Quercetin to the d-(T<sub>2</sub>AG<sub>3</sub>T)<sub>4</sub> G-quadruplex DNA near the T1/T2 or G6/T7 base step, which was also observed in the <sup>1</sup>H NMR spectra as stated above. Briefly, all of the results indicate the binding of Quercetin to two sites on d-(T<sub>2</sub>AG<sub>3</sub>T)<sub>4</sub> at T1pT2 and G6pT7 steps via the end stacking mode (Figure 3.15a). A detailed analysis of the unbound quadruplex showed clear evidence from guanine imino and adenine base proton NOE data that both guanine and adenine nucleotides form hydrogen-bonded tetrads. NOEs from adenine H2 are consistent with intermolecular A-tetrad formation and stabilizing stacking interactions with the adjacent G-tetrad of G4.<sup>[51]</sup> This is evident from strong NOEs of G4 imino to A3H2 and H8. However, because of the significant line-broadening effects of the Quercetin on A3H2, analogous NOEs to those described above could not be identified to confirm the integrity of a hydrogen bonded A-tetrad. NOEs between A3 and G4, which were relatively strong for the unbound quadruplex, are weaker, reflecting the structural distortions caused by drug end-stacking at the T1pT2 step. We investigate further the stability of the complex and its contribution to drug binding in restrained molecular dynamic simulations.

### 3.2.3.3 Restrained molecular dynamics studies

Restrained Molecular Dynamics (rMD) permits the system to undergo conformational and momentum change. This provides different parts of the phase space accessible to the molecule that can be explored and stable conformations could be identified by energy minimization. Therefore, to gain a better understanding of Quercetin-Tel7 DNA interaction, restrained molecular dynamics (rMD) simulation was performed using Discovery Studio

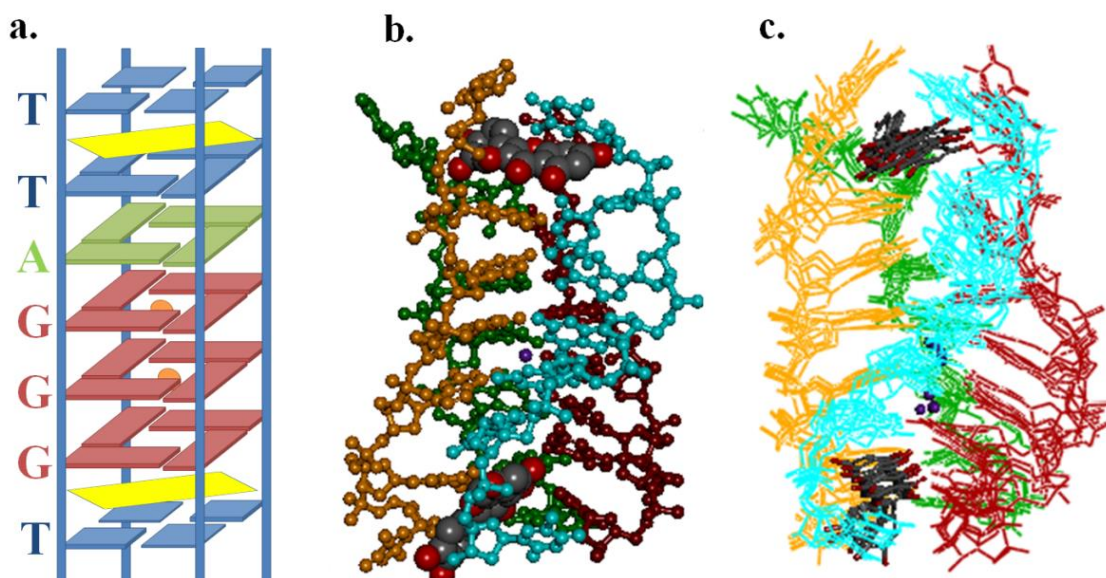


**Figure 3.15.** *Quercetin and Tel7 DNA complex at  $D/N = 2.0$  ratio. (a) Schematic representation showing Quercetin (yellow) stacking at the T1pT2 and G6pT7 steps. Potassium ions (orange) are bound at the GpG steps (PDB Code: 2MS6) (b) Energy minimised model of Quercetin and Tel7 DNA complex showing Quercetin end-stacks at the T1pT2 and G6pT7 steps. The four strands of Tel7 DNA are shown in red, green, cyan and magenta color (c) Ensemble of five lowest energy structures after restrained molecular dynamics (rMD) simulation showing the position of Quercetin at the T1pT2 (top) and G6pT7 steps (bottom) of Tel7 G-quadruplex DNA. The four strands of Tel7 DNA are shown in red, green, cyan and orange color.*

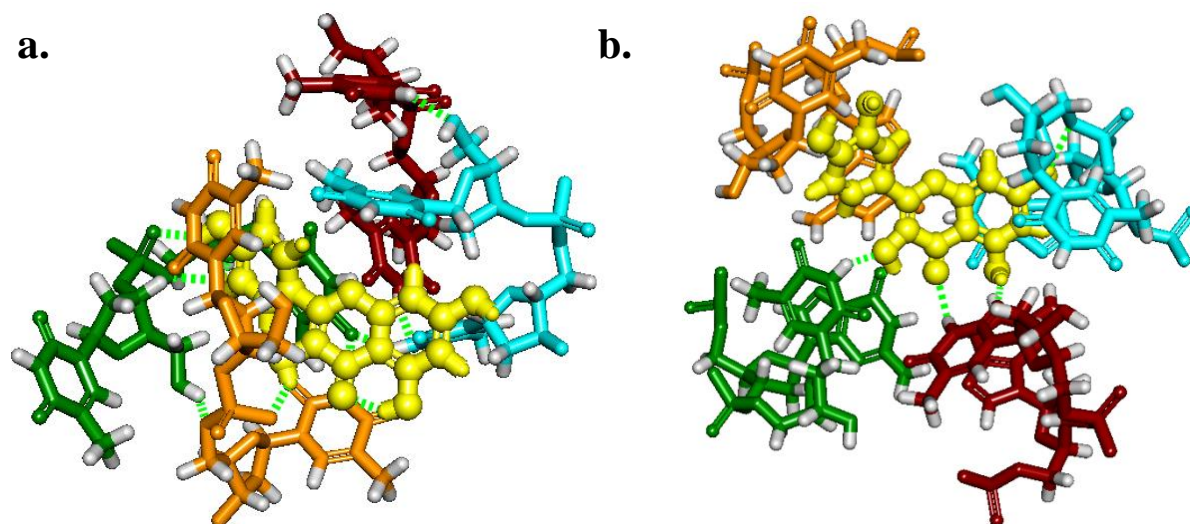


*Figure 3.16. Interaction of Quercetin at (a) T1/T2 (b) G6/T7 base steps of Tel7 G-quadruplex DNA. Green dots represent the hydrogen bonds.*

*Table 3.5. NMR statistics for complex formed between Quercetin and Tel7G-quadruplex DNA*

<b>NMR distance</b>	<b>Nucleic acid/ligand</b>
<b>Distance restraints</b>	
<b>Total NOE</b>	<b>712</b>
<b>Intra-residue</b>	<b>336</b>
<b>Inter-residue</b>	<b>96</b>
<b>NOE- derived distance restraints</b>	<b>24</b>
<b>Hydrogen bonds</b>	<b>54</b>
<b>Average pair wise R.M.S.D.(Å)</b>	
<b>All DNA heavy</b>	<b>2.44</b>
<b>DNA binding site (T1/T2)</b>	<b>2.46</b>
<b>DNA binding site (G6/T7)</b>	<b>2.49</b>
<b>All nucleotides</b>	<b>2.36</b>

*Table 3.6. Energy terms (kcal mol<sup>-1</sup>) for initial structure and final rMD structure*

<b>Structure</b>	<b>Potential energy (kcal mol<sup>-1</sup>)</b>	<b>Van der Waals Energy (kcal mol<sup>-1</sup>)</b>	<b>Electrostatic Energy (kcal mol<sup>-1</sup>)</b>
<b>Initial</b>	<b>31204815.569</b>	<b>191.19652</b>	<b>-5659.55869</b>
<b>Final</b>	<b>-10256.458</b>	<b>-39.53001</b>	<b>-5596.76652</b>

Client 3.5 (Accelrys, San Diego, CA). Quercetin was docked at the T1-T2 step and the G6-T7 step in an orientation that satisfied all of the observed intermolecular and intramolecular NOE restraints. The cross peak intensities were used in a qualitative manner, in which the distances were approximately 1.8 - 2.5, 2.5 - 3.0, 3.0 - 3.5, 3.5 - 4.0, and 4.0 - 5.0 Å for strong intense (ss), strong (s) medium (m) and weak (w) and very weak intense (vw) peaks, respectively (Table 3.4). After the production runs of 1 ns, the lowest potential energy model showed that complex was stabilized via  $\pi$ - $\pi$  stacking and hydrogen bonding. The final structure obtained after rMD is shown in Figure 3.16b having potential energy of -10256.458 kcal/mol (Table 3.5). Ensembles of five conformations with the lowest potential energy were superimposed (Figure 3.16c). Table 3.5 and 3.6 indicates an assessment of refined structures in terms of energetics including restraint violations energies and root mean square derivative of energy w.r.t atomic coordinates. This simulation results showed that one of the Quercetin molecules stacks below the G6 tetrad and the other end-stacks at the T1-T2 step and G6-T7 steps (Figure 3.16a), which complies with the previous conclusions obtained from the other biophysical experiments performed. The results favored the distances obtained from the NOE experiment and show that Quercetin binds to d-(T<sub>2</sub>AG<sub>3</sub>T)<sub>4</sub> between the T1pT2 and G6pT7 position of the G-quadruplex (Table 3.3).

### 3.3 Conclusion

It is well known fact that flavonoids have potent anti-cancer activity that is likely involved in their cellular binding targets. The human telomeric G-quadruplex DNA d-(T<sub>2</sub>AG<sub>3</sub>T)<sub>4</sub> sequence could be one of the binding targets of flavonoids to exert their anti-cancer activity. Thus, the examination of the binding of flavonoids to human telomeric DNA is important. In this chapter, various biophysical experiments were performed to gain insight about the interaction of flavonoids with human telomeric G-quadruplex DNA structure formed by d-(T<sub>2</sub>AG<sub>3</sub>T)<sub>4</sub> sequence (Tel7). We have reported the interaction of four flavonoids namely, Luteolin, Quercetin, Rutin and Genistein with the human telomeric G-quadruplex structure formed by Tel7 DNA sequence and the stabilization of this structure.

The binding properties of flavonoids with the G-quadruplex structure have been characterized via CD spectroscopy, fluorescence titration studies. The mode of binding was deduced according to analysis of their lifetime decay profiles. Quercetin was found to bind most effectively according to the binding studies performed. The NMR melting experiment showed that the binding of Quercetin to the d-(T<sub>2</sub>AG<sub>3</sub>T)<sub>4</sub> sequence stabilizes the G-quadruplex structure. Generally, G-quadruplex ligands have an extended aromatic plane.

Quercetin provides the same molecular frame for  $\pi$ - $\pi$  stacking and might stabilize the G-quadruplex structure by the strong  $\pi$ - $\pi$  stacking between guanine tetrads and the Quercetin chromophore. Proton chemical shift was also observed through titration and it was found that one more set of  $-NH$  protons appeared with increasing concentration of Quercetin. It is suggested that the signals were in slow exchange regime and the observed resonance was considered to be of free and bound proton. It was proved by titrimetric analysis of  $^1H$  chemical shift and temperature dependence studies at D/N 2.0 that the central aromatic chromophore of the Quercetin was involved in the interaction with d-(TTAGGGT)<sub>4</sub>. The loss of inter-nucleotide NOEs was also not observed for the core G-tetrad. Additionally, the existence of intra-nucleotide sequential connectivity along with the appearance of new NOEs in the NOESY spectra prove that the G-tetrad is intact and does not open to provide access to Quercetin. This result is also supported by our CD experiment in which we observed no changes when Quercetin and other flavonoids were bound to DNA, even at D/N = 2:1 ratio. These results suggest that Quercetin binding involves T1pT2, T2pA3 and G6pT7 bases. Thus, a better understanding of the interaction between Quercetin and d-(T<sub>2</sub>AG<sub>3</sub>T)<sub>4</sub> was deduced from the resolved model. This interaction occurs via  $\pi$ - $\pi$  stacking in D/N = 2:1 ratio and Quercetin end-stakes at the T1pT2 and G6pT7 steps. Our investigation highlights the structural aspects of the binding of flavonoids to G-quadruplexes formed by the human telomeric DNA sequence and also revealed the potential of flavonoids as useful candidates for anti-cancer therapeutics by regulating the telomeric G-quadruplex structure. The coordinates of the NMR model of the Quercetin and d-(T<sub>2</sub>AG<sub>3</sub>T)<sub>4</sub> complex have been deposited in the PDB as 2MS6.

### **3.4 Material and methods**

#### **3.4.1 Reagents**

Luteolin, Quercetin, Rutin and Genistein were purchased from Sigma Aldrich Chemicals Ltd. These flavonoids were used without further purification. The solvents, including deuterium oxide, dimethyl sulphoxide (DMSO) and other reagents used for buffer preparation such as NaCl, KCl, NaH<sub>2</sub>PO<sub>4</sub>, Na<sub>2</sub>HPO<sub>4</sub>, KH<sub>2</sub>PO<sub>4</sub> and K<sub>2</sub>HPO<sub>4</sub> (HPLC Grade) were also purchased from Sigma Aldrich Chemicals Ltd. The stock solutions of flavonoids were prepared by dissolving them in DMSO, and they were stored at the appropriate storage temperature. The concentration of the solutions was determined spectrophotometrically at the  $\lambda_{max}$  of 380 nm ( $\epsilon = 14,920 \text{ M}^{-1}\text{cm}^{-1}$ ), 368 nm ( $\epsilon = 19,700 \text{ M}^{-1}\text{cm}^{-1}$ ), 349 nm ( $\epsilon = 20,417 \text{ M}^{-1}\text{cm}^{-1}$ ).

$^1\text{cm}^{-1}$ ) and 260 nm ( $\epsilon = 37,260 \text{ M}^{-1}\text{cm}^{-1}$ ) for Quercetin, Rutin, Luteolin and Genistein, respectively.

Calf thymus DNA (CT-DNA) and other DNA oligomers i.e.

Tel7: d-(5'-TTA GGG T-3'),

tel22:d-(5'-AGG GTT AGG GTT AGG GTT AGG G -3'),

c-myc: d-(5'-TGA GGG TGG TGA GGG TGG GGA AGG -3'),

ckit21:d-(5'- CGG GCG GGC GCG AGG GAG GGG -3') were purchased from Sigma Aldrich Chemicals Ltd. ct-DNA solution was prepared in the sodium phosphate buffer and its concentration was measured spectrophotometrically using a molar absorptivity of  $6600 \text{ M}^{-1} \text{ cm}^{-1}$  (260 nm).

For quadruplex formation, 100  $\mu\text{M}$  of oligomers were dissolved in phosphate buffer ( $\text{K}^+$ ) (10 mM, pH 7.0) with 100 mM KCl. The oligomer was annealed by heating at  $90^\circ\text{C}$  for 5 mins, followed by overnight incubation at room temperature to allow gradual cooling.

### 3.4.2 Fluorescence titrations

The fluorescence titration experiment was performed on Synergy<sup>TM</sup> H1 multi-mode microplate reader using 96-well microplates from corning. The volume of 75  $\mu\text{L}$  for each sample was tested in duplicates at  $25^\circ\text{C}$ . The G-quadruplex DNA at a final concentration of 10  $\mu\text{M}$  was serially diluted; with the last well serve as blank (no DNA). The CT-DNA at a final concentration of 50  $\mu\text{M}$  for Luteolin, Quercetin and Genistein, while 30  $\mu\text{M}$  for Rutin was serially diluted; with the last well serve as blank (no DNA). The readings were taken at emission wavelength of 435 nm, 535 nm, 416 nm and 405 nm for Luteolin, Quercetin, Rutin and Genistein respectively, when excited at the excitation wavelength of 380 nm, 375 nm, and 360nm and 269 nm. Data were analyzed using SigmaPlot 12.0 software (Systat Software, Chicago, USA) according to:

$$f = \frac{B_{\max 1} \times \text{abs}(x)}{k_{d1} \times \text{abs}(x)} + \frac{B_{\max 2} \times \text{abs}(x)}{k_{d2} \times \text{abs}(x)} \quad (1)$$

$B_{\max}$ = maximum number of binding sites.

$K_d$ = equilibrium binding constant.

### 3.4.3 Circular Dichroism

The Circular Dichroism (CD) experiment was performed on a J-815 Spectropolarimeter(JASCO). A constant temperature of 298 K was maintained during the

entire experiment with the help of a Peltier junction temperature controller. To avoid water condensation on the outside of the cuvette, a constant stream of dry nitrogen gas was flushed into the cuvette-holding chamber. A quartz cuvette with a 0.2 cm path length was used to record the spectra of samples containing 20  $\mu$ M G-quadruplex and increasing concentrations of flavonoids in 100 mM KCl, 10 mM phosphate buffer ( $K^+$ ) at pH 7.0. Spectra were recorded at 0.1 nm intervals from 200 nm to 350 nm with a 1 nm-slit width and averaged over three scans. Buffer CD spectra were subtracted from the CD spectra of DNA and the Drug-DNA complex.

#### **3.4.4 Time-resolved fluorescence measurements**

The time-correlated single-photon counting (TCSPC) method was used to perform the lifetime measurement study. Time resolved fluorescence decays were collected on a Time-Correlated Single-Photon Counting (TCSPC) Spectrofluorometer (Horiba). A fixed wavelength Nano LED was used as the excitation source ( $k_{ex} = 470$  nm), and emission was detected at a different wavelength. The fluorescence emission of the flavonoids and their complexes with G-quadruplex DNA were counted with a micro channel plate photo multiplier tube after passing through the monochromator and were further processed through a constant fraction discriminator (CFD), a time-to-amplitude converter (TAC) and a multi-channel analyser (MCA). The fluorescence decay was obtained and further analysed using DAS software, provided by FluoroLog-TCSPC instruments.

#### **3.4.5 Nuclear Magnetic Resonance**

NMR experiments were conducted on a high-resolution AVANCE III 400 and 500 MHz BioSpin International AG, Switzerland equipped with a 5 mm broad band inverse probe able to deliver z-field gradients. NMR data were processed, integrated and analysed on Topspin (1.3 version) software. NMR samples were referenced with 3 - (trimethylsilyl) propionic-2, 2, 3, 3- $d_4$  acid sodium salt (TSP). The drug-DNA complex was formed by titrating tel7 with successive additions of the drug. All of the titration studies were performed in  $H_2O + D_2O$  solvent at a 9:1 ratio. The 64K data points were recorded for 1D proton NMR spectra with 64-128 numbers of scan at 298K and a digital resolution of 0.15 - 0.3 Hz / point. To attain the best signal to noise ratio, the receiver gain was optimised at each instance. Two-dimensional proton nuclear overhauser enhancement spectroscopy (NOESY) <sup>[54]</sup> experiments were performed at a temperature range of 298 K with 20 ppm spectral width. Spectra were recorded at variable mixing times ( $t_m$ ) of 350 ms, 300 ms and 200 ms with 256 free induction

decays along the  $t_1$  dimension and 2048 complex data points in the  $t_2$  dimension. A digital resolution of 1.495 Hz/point in the  $t_1$  dimension was obtained in 48-64 scans with a relaxation decay of 2.0 secs. The titration studies for D/N= 0.00 , 0.20 upto 2.00 complex were performed at 100, 200 and 300 ms mixing time. SPARKY was used to visualise the spectra and calculate  $^1\text{H}$ - $^1\text{H}$  NOE distances, which were used to restrain Quercetin- tel7 G-quadruplex DNA for restrained molecular dynamic simulation studies.

### 3.4.6 Restrained molecular dynamics studies

The structure of G-quadruplex tel7(PDB code: 1NP9) <sup>[49]</sup> was taken as the starting model for the rMD studies. The required replacements, addition of residues and the G-quadruplex-Quercetin complex were built in Discovery studio 3.5 (Accelrys Inc., USA). For maintaining the structure of the quadruplex, the two internal  $\text{K}^+$  ions were placed between three quartets. The ligand was docked manually between the T1-T2 and G6-T7 steps with orientations obtained from NOE experimental data. A set of NOE distances was introduced as restraints with a force constant of  $-30 \text{ kcal/mol/ \AA}^2$ . The drug-quadruplex system was typed in charmMforcefield<sup>[55]</sup> followed by solvation using an explicit solvent model. A periodic TIP3P <sup>[56]</sup> orthorhombic water box extending to a distance of  $10 \text{ \AA}$  surrounds the complex and contained 679 water molecules. Subsequently, the complex was minimised by 500 steps each of Steepest Descent and Conjugate Gradient algorithms with an RMS gradient of 0.1 and 0.0001, respectively. To obtain the conformations with the lowest potential energy, the quadruplex-ligand complex was subjected to simulated annealing restrained molecular dynamics with the whole set of NOE restraints. Standard dynamic cascade runs were performed on the complex in which the system was heated to 300 K and allowed to equilibrate under constant pressure for 1 ps. The production was done for 1ns in an NPT ensemble where the Hoover constant temperature method specifies the thermal mass with time step of 1 fs. Long range electrostatics were treated with the Particle Mesh Ewald (PME) method <sup>[57]</sup>, and a  $14 \text{ \AA}$  cut-off radius counted the non-bonded distances. The equation of motion was numerically integrated using the LepfrogVerlet integrator. To constrain the motion of H-bonds, the SHAKE algorithm <sup>[58]</sup> was applied during the whole simulation runs. The coordinates of iterations were saved every 10 steps. The trajectory analysis was performed using Discovery studio client 3.5.

### 3.5 References

1. Blackburn E.H. (1994), Telomeres: no end in sight, *Cell*, 77, 621-623 (DOI:

- 10.1016/0092-8674(94)90046-9).
2. Hayflick L., Moorhead P.S. (1961), The serial cultivation of human diploid cell strains, *Exp. Cell. Res.*, 25, 585-621 (DOI: 10.1016/0014-4827(61)90192-6).
  3. Harley C.B., Futcher A.B., Greider C.W. (1990), Telomeres shorten during ageing of human fibroblasts, *Nature*, 345, 458-460 (DOI: 10.1038/345458a0).
  4. Stewart S.A., Weinberg R.A. (2006), Telomeres: cancer to human aging, *Annu. Rev. Cell Dev. Biol.*, 22, 531-557 (DOI: 10.1146/annurev.cellbio.22.010305.104518).
  5. Kim N.W., Piatyszek M.A., Prowse K.R., Harley C.B., West M.D., Ho P.L., Coviello G.M., Wright W.E., Weinrich S.L., Shay J.W. (1994), Specific association of human telomerase activity with immortal cells and cancer, *Science*, 266, 2011-2015 (DOI: 10.1126/science.7605428).
  6. Greider C.W. (1996), Telomere length regulation, *Annu. Rev. Biochem.*, 65, 337-365 (DOI: 10.1146/annurev.bi.65.070196.002005).
  7. Nakamura T. M., Morin G. B., Chapman K. B., Weinrich S. L., Andrews W. H., Lingner J., Harley C. B., Cech T. R. (1997), Telomerase catalytic subunit homologs from fission yeast and human, *Science*, 277, 955-959 (DOI: 10.1126/science.277.5328.955).
  8. Feng J., Funk W. D., Wang S.S., Weinrich S.L., Avilion A.A., Chiu C.P., Adams R.R., Chang E., Allsopp R.C., Yu J., et al. (1995), The RNA component of human telomerase, *Science*, 269, 1236-1241).
  9. Zahler A.M., Williamson J.R., Cech T.R., Prescott D.M. (1991), Inhibition of telomerase by G-quartet DNA structures, *Nature*, 350, 718-720 (DOI: 10.1038/350718a0).
  10. Fletcher T.M., Sun D., Salazar M., Hurley L.H. (1998), Effect of DNA secondary structure on human telomerase activity, *Biochemistry*, 37, 5536-5541 (DOI: 10.1021/bi972681p).
  11. De Cian A., Lacroix L., Douarre C., Temime-Smaali N., Trentesaux C., Riou J.F., Mergny J.L. (2008), Targeting telomeres and telomerase, *Biochimie.*, 90, 131-155 (DOI: 10.1016/j.biochi.2007.07.011).
  12. Ou T.M., Lu Y.J., Tan J.H., Huang Z.S., Wong K.Y., Gu L.Q. (2008), G-quadruplexes: targets in anticancer drug design, *ChemMedChem*, 3, 690-713 (DOI: 10.1002/cmdc.200700300).
  13. Ferreira R., Artali R., Benoit A., Gargallo R., Eritja R., Ferguson D.M., Sham Y.Y., Mazzini S. (2013), Structure and stability of human telomeric G-quadruplex with preclinical 9-amino acridines, *PLoS One*, 8, e57701 (DOI: 10.1371/journal.pone.0057701).

14. Mergny J.L., Mailliet P., Lavelle F., Riou J.F., Laoui A., Helene C. (1999), The development of telomerase inhibitors: the G-quartet approach, *Anticancer Drug Des.*, 14, 327-339.
15. Perry P.J., Jenkins T.C. (1999), Recent advances in the development of telomerase inhibitors for the treatment of cancer, *Expert. Opin. Investig. Drugs*, 8, 1981-2008 (DOI: 10.1517/13543784.8.12.1981).
16. Raymond E., Soria J.C., Izbicka E., Boussin F., Hurley L., Von Hoff D.D. (2000), DNA G-quadruplexes, telomere-specific proteins and telomere-associated enzymes as potential targets for new anticancer drugs, *Invest. New. Drugs*, 18, 123-137 (DOI: 10.1023/A:1006373812586).
17. Neidle S., Parkinson G. (2002), Telomere maintenance as a target for anticancer drug discovery, *Nat. Rev. Drug Discov.*, 1, 383-393 (DOI: 10.1038/nrd793).
18. Franceschin M., Rossetti L., D'Ambrosio A., Schirripa S., Bianco A., Ortaggi G., Savino M., Schultes C., Neidle S. (2006), Natural and synthetic G-quadruplex interactive berberine derivatives, *Bioorg. Med. Chem. Lett.*, 16, 1707-1711 (DOI: 10.1016/j.bmcl.2005.12.001).
19. Bessi I., Bazzicalupi C., Richter C., Jonker H.R., Saxena K., Sissi C., Chioccioli M., Bianco S., Bilia A.R., Schwalbe H., Gratteri P. (2012), Spectroscopic, molecular modeling, and NMR-spectroscopic investigation of the binding mode of the natural alkaloids berberine and sanguinarine to human telomeric G-quadruplex DNA, *ACS Chem. Biol.*, 7, 1109-1119 (DOI: 10.1021/cb300096g).
20. Maiti M., Kumar G.S. (2010), Polymorphic nucleic Acid binding of bioactive isoquinoline alkaloids and their role in cancer, *J. Nucleic Acids*, 2010, (DOI: 10.4061/2010/593408).
21. Bhadra K., Kumar G.S. (2011), Interaction of berberine, palmatine, coralyne, and sanguinarine to quadruplex DNA: a comparative spectroscopic and calorimetric study, *Biochim. Biophys. Acta*, 1810, 485-496 (DOI: 10.1016/j.bbagen.2011.01.011).
22. Liu Y., Zheng B., Xu X., Yuan G. (2010), Probing the binding affinity of small-molecule natural products to the G-quadruplex in C-myc oncogene by electrospray ionization mass spectrometry, *Rapid. Commun. Mass Spectrom.*, 24, 3072-3075 (DOI: 10.1002/rcm.4730).
23. Fedoroff O.Y., Salazar M., Han H., Chemeris V.V., Kerwin S.M., Hurley L.H. (1998), NMR-Based model of a telomerase-inhibiting compound bound to G-quadruplex DNA, *Biochemistry*, 37, 12367-12374 (DOI: 10.1021/bi981330n).

24. Carini J.P., Klamt F., Bassani V.L. (2014), Flavonoids from *Achyrocline satureioides*: promising biomolecules for anticancer therapy, *RSC Adv.*, 4, 3131-3144 (DOI: 10.1039/c3ra43627f).
25. Bjeldanes L.F., Chang G.W. (1977), Mutagenic activity of quercetin and related compounds, *Science*, 197, 577-578 (DOI: 10.1126/science.327550).
26. Rueff J., Laires A., Borba H., Chaveca T., Gomes M.I., Halpern M. (1986), Genetic toxicology of flavonoids: the role of metabolic conditions in the induction of reverse mutation, SOS functions and sister-chromatid exchanges, *Mutagenesis.*, 1, 179-183 (DOI: 10.1093/mutage/1.3.179).
27. Kessler M., Ubeaud G., Jung L. (2003), Anti- and pro-oxidant activity of rutin and quercetin derivatives, *J. Pharm. Pharmacol.*, 55, 131-142 (DOI: 10.1211/002235702559).
28. Chowdhury A.R., Sharma S., Mandal S., Goswami A., Mukhopadhyay S., Majumder H.K. (2002), Luteolin, an emerging anti-cancer flavonoid, poisons eukaryotic DNA topoisomerase I, *Biochem. J.*, 366, 653-661 (DOI: 10.1042/BJ20020098).
29. Bhatia N., Agarwal R. (2001), Detrimental effect of cancer preventive phytochemicals silymarin, genistein and epigallocatechin 3-gallate on epigenetic events in human prostate carcinoma DU145 cells, *Prostate*, 46, 98-107 (DOI: 10.1002/1097-0045(20010201)46:2<98::AID-PROS1013>3.0.CO;2-K).
30. Sengupta B., Sengupta P.K. (2002), The interaction of quercetin with human serum albumin: a fluorescence spectroscopic study, *Biochem. Biophys. Res. Commun.*, 299, 400-403 (DOI: 10.1016/S0006-291X(02)02667-0).
31. Snyder R.D., Gillies P.J. (2003), Reduction of genistein clastogenicity in Chinese hamster V79 cells by daidzein and other flavonoids, *Food Chem Toxicol*, 41, 1291-1298 (DOI: 10.1016/S0278-6915(03)00117-0).
32. Ren W., Qiao Z., Wang H., Zhu L., Zhang L. (2003), Flavonoids: promising anticancer agents, *Med. Res. Rev.*, 23, 519-534 (DOI: 10.1002/med.10033).
33. Kuntz S., Wenzel U., Daniel H. (1999), Comparative analysis of the effects of flavonoids on proliferation, cytotoxicity, and apoptosis in human colon cancer cell lines, *Eur. J. Nutr.*, 38, 133-142 (DOI: 10.1007/s003940050054).
34. Zhang Q., Zhao X.H., Wang Z.J. (2008), Flavones and flavonols exert cytotoxic effects on a human oesophageal adenocarcinoma cell line (OE33) by causing G2/M arrest and inducing apoptosis, *Food Chem. Toxicol.*, 46, 2042-2053 (DOI: 10.1016/j.fct.2008.01.049).

35. Saretzki G. (2003), Telomerase inhibition as cancer therapy, *Cancer Lett.*, 194, 209-219 (DOI: 10.1016/S0304-3835(02)00708-5).
36. Solimani R., Bayon F., Domini I., Pifferi P.G., Todesco P.E., Marconi G., Samori B. (1995), Flavonoid-DNA Interaction Studied with Flow Linear Dichroism Technique, *J. Agric. Food Chem.*, 43, 876-882 (DOI: 10.1021/jf00052a006).
37. Solimani R. (1996), Quercetin and DNA in solution: analysis of the dynamics of their interaction with a linear dichroism study, *Int. J. Biol. Macromol.*, 18, 287-295 (DOI: 10.1016/0141-8130(95)01089-0).
38. Kanakis C.D., Tarantilis P.A., Polissiou M.G., Diamantoglou S., Tajmir-Riahi H.A. (2007), An overview of DNA and RNA bindings to antioxidant flavonoids, *Cell Biochem. Biophys.*, 49, 29-36 (DOI: 10.1007/s12013-007-0037-2).
39. Ragazzon P.A., Bradshaw T., Matthews C., Iley J., Missailidis S. (2009), The characterisation of flavone-DNA isoform interactions as a basis for anticancer drug development, *Anticancer Res.*, 29, 2273-2283.
40. Sun H., Tang Y., Xiang J., Xu G., Zhang Y., Zhang H., Xu L. (2006), Spectroscopic studies of the interaction between quercetin and G-quadruplex DNA, *Bioorg. Med. Chem. Lett.*, 16, 3586-3589 (DOI: 10.1016/j.bmcl.2006.03.087).
41. Joo C., Balci H., Ishitsuka Y., Buranachai C., Ha T. (2008), Advances in single-molecule fluorescence methods for molecular biology, *Annu. Rev. Biochem.*, 77, 51-76 (DOI: 10.1146/annurev.biochem.77.070606.101543).
42. Croney J.C., Jameson D.M., Learmonth R.P. (2001), Fluorescence spectroscopy in biochemistry: teaching basic principles with visual demonstrations, *Biochem. Mol. Biol. Educ.*, 29, 60-65 (DOI: 10.1111/j.1539-3429.2001.tb00071.x).
43. Zhao D., Li J., Yang T., He Z. (2014), "Turn off-on" fluorescent sensor for platinum drugs-DNA interactions based on quantum dots, *Biosens. Bioelectron.*, 52, 29-35 (DOI: 10.1016/j.bios.2013.08.031).
44. Temerk Y., Ibrahim M., Ibrahim H., Kotb M. (2016), Interactions of an anticancer drug lomustine with single and double stranded DNA at physiological conditions analyzed by electrochemical and spectroscopic methods, *J. Electroanal. Chem.*, 769, 62-71 (DOI: 10.1016/j.jelechem.2016.03.020).
45. Woolfe G.J., Thistlethwaite P.J. (1981), Direct observation of excited state intramolecular proton transfer kinetics in 3-hydroxyflavone, *J. Am. Chem. Soc.*, 103, 6916-6923 (DOI: 10.1021/ja00413a026).

46. Ambrus A., Chen D., Dai J., Bialis T., Jones R.A., Yang D. (2006), Human telomeric sequence forms a hybrid-type intramolecular G-quadruplex structure with mixed parallel/antiparallel strands in potassium solution, *Nucleic Acids Res.*, 34, 2723-2735 (DOI: 10.1093/nar/gkl348).
47. Byrne C.D., de Mello A.J. (1998), Photophysics of ethidium bromide complexed to ct-DNA: a maximum entropy study, *Biophys. Chem.*, 70, 173-184 (DOI: 10.1016/S0301-4622(97)00091-4).
48. Wei C., Wang J., Zhang M. (2010), Spectroscopic study on the binding of porphyrins to (G(4)T(4)G(4))<sub>4</sub> parallel G-quadruplex, *Biophys. Chem.*, 148, 51-55 (DOI: 10.1016/j.bpc.2010.02.009).
49. Gavathiotis E., Searle M.S. (2003), Structure of the parallel-stranded DNA quadruplex d(TTAGGGT)<sub>4</sub> containing the human telomeric repeat: evidence for A-tetrad formation from NMR and molecular dynamics simulations, *Org. Biomol. Chem.*, 1, 1650-1656 (DOI: 10.1039/B300845M).
50. Wuthrich K. (1986), NMR of Proteins and Nucleic Acids, *Wiley*, ISBN: 978-0-471-82893-8.
51. Gavathiotis E., Searle M.S. (2003), Structure of the parallel-stranded DNA quadruplex d(TTAGGGT)<sub>4</sub> containing the human telomeric repeat: evidence for A-tetrad formation from NMR and molecular dynamics simulations, *Org. Biomol. Chem.*, 1, 1650-1656 (DOI: 10.1039/B300845M).
52. Simonsson T., Pecinka P., Kubista M. (1998), DNA tetraplex formation in the control region of c-myc, *Nucleic Acids Res.*, 26, 1167-1172.
53. Mazzini S., Bellucci M.C., Dallavalle S., Fraternali F., Mondelli R. (2004), Mode of binding of camptothecins to double helix oligonucleotides, *Org. Biomol. Chem.*, 2, 505-513 (DOI: 10.1039/B312780J).
54. Jeener J., Meier B.H., Bachmann P., Ernst R.R. (1979), Investigation of exchange processes by two-dimensional NMR spectroscopy, *J. Chem. Phys.*, 71, 4546-4553 (DOI: 10.1063/1.438208).
55. Brooks B.R., Brooks C.L., 3rd, Mackerell A.D., Jr., Nilsson L., Petrella R.J., Roux B., Won Y., Archontis G., Bartels C., Boresch S., Caflisch A., Caves L., Cui Q., Dinner A.R., Feig M., Fischer S., Gao J., Hodoscek M., Im W., Kuczera K., Lazaridis T., Ma J., Ovchinnikov V., Paci E., Pastor R.W., Post C.B., Pu J.Z., Schaefer M., Tidor B., Venable R.M., Woodcock H.L., Wu X., Yang W., York D.M., Karplus M. (2009), CHARMM: the

- biomolecular simulation program, *J. Comput. Chem.*, 30, 1545-1614 (DOI: 10.1002/jcc.21287).
56. Jorgensen W.L., Chandrasekhar J., Madura J.D., Impey R.W., Klein M.L. (1983), Comparison of simple potential functions for simulating liquid water, *J. Chem. Phys.*, 79, 926-935 (DOI: 10.1063/1.445869).
57. Darden T., York D., Pedersen L. (1993), Particle mesh Ewald: An  $N \cdot \log(N)$  method for Ewald sums in large systems, *J. Chem. Phys.*, 98, 10089-10092 (DOI: 10.1063/1.464397).
58. Ryckaert J.-P., Ciccotti G., Berendsen H.J.C. (1977), Numerical integration of the cartesian equations of motion of a system with constraints: molecular dynamics of n-alkanes, *J. Comp. Phys.*, 23, 327-341 (DOI: 10.1016/0021-9991(77)90098-5).

# SCIENTIFIC REPORTS



OPEN

## Structural insight for the recognition of G-quadruplex structure at human c-myc promoter sequence by flavonoid Quercetin

Arpita Tawani, Subodh Kumar Mishra & Amit Kumar 

Small molecule ligands that could stabilize G-quadruplex structure formed at the promoter region of human c-myc oncogene will regulate its expression in cancer cells. Flavonoids, a group of naturally available small molecule, have been known for their various promising effects on human health. In present study, we have performed detailed biophysical studies for the interaction of human c-myc G-quadruplex DNA with nine representative flavonoids: Luteolin, Quercetin, Rutin, Genistein, Kaempferol, Puerarin, Hesperidin, Myricetin and Daidzein. We found by using fluorescence titration that Quercetin interacts with c-myc G-quadruplex DNA sequence Pu24T with highest affinity. This interaction was further explored by using NMR spectroscopy and we have derived the first solution structure for the complex formed between Quercetin and biologically significant c-myc promoter DNA sequence forming G-quadruplex structure. In present solution structure, Quercetin stacks at 5' and 3' G-tetrads of Pu24T G-quadruplex structure and stabilize it via  $\pi$ - $\pi$  stacking interactions. Furthermore, *in vitro* studies on HeLa cells suggested that Quercetin induces apoptosis-mediated cell death and down-regulated c-myc gene expression. This study emphasizes the potential of flavonoids as a promising candidate for targeting c-myc promoter region and thus, could act as a potential anti-cancer agent.

G-quadruplexes are well-known secondary structures of DNA. These are non-canonical DNA structures formed by square planar arrangement of G-quartets that is stabilized by Hoogsteen hydrogen bonding<sup>1</sup>. In the human genome, many guanine rich sequences have potential to form G-quadruplex structures. Some of these regions are telomere<sup>2</sup>, regulatory regions of oncogenes such as KRAS<sup>3</sup>, c-myc<sup>4</sup>. These proto-oncogenes were found to be over expressed in 80% of cancers such as breast cancer, cervical cancer, lung cancer, etc. The promoter region of c-myc gene is composed of seven nuclease-hypersensitive elements (NHEs), of which, NHE III1 controls 80–90% transcription of c-myc gene. This 27 nucleotide sequence (5'-TGGGGAGGGTGGGGAGGGTGGGGAAGG-3') is purine rich sequence that is also called as Pu27, has potential to form G-quadruplex structure. It is evident from one of the studies in which suppression of MYC expression was observed when Burkitt lymphoma cell lines was treated with TMPyP4, by formation of stable G-quadruplex structure. This stabilized G-quadruplex structure act as silencer element and thereby reduces the expression of c-myc gene<sup>5</sup>. Thus, the G-quadruplex structure in this region plays an important role as transcriptional regulator<sup>5</sup>.

Over the past decades, the exploration of small molecules that induces the formation of G-quadruplex structures or stabilizes them could be a potent anti-cancer agent and may act by down-regulating the oncogene expression<sup>6</sup>. Nature is an ample source for chemically diverse scaffolds of molecules. These naturally occurring small molecules are less toxic than the synthetic molecules and have better bio-availability<sup>7</sup>. Owing to the larger molecular diversity of natural compounds, research have already been initiated since long back to explore these compounds for targeting c-myc G-quadruplex structure and investigated their interaction<sup>8</sup> like quindoline derivative SYUIQ-5<sup>9</sup>, 9-N-substituted berberine derivatives<sup>10</sup>, etc. Most of these compounds have planar aromatic ring system that stabilizes the G-tetrad by  $\pi$ - $\pi$  stacking<sup>11</sup>. One of the major groups of naturally occurring molecules is flavonoids, that are readily available in our daily diets and have been considered as nontoxic drug candidates for anticancer therapy<sup>12</sup>. The common dietary flavonoids, Luteolin, Quercetin, Rutin, Genistein, Kaempferol,

Centre for Biosciences and Biomedical Engineering, Indian Institute of Technology, Indore, Indore, 453552, Madhya Pradesh, India. Correspondence and requests for materials should be addressed to A.K. (email: [amitk@iiti.ac.in](mailto:amitk@iiti.ac.in))

## Chapter 4

# Structural insight for the recognition of G-quadruplex structure at human c-myc promoter sequence by flavonoid Quercetin

---

### 4.1 Introduction

G-quadruplex structures are higher-ordered DNA structures formed by G-rich sequences. These structures are built around hydrogen as well as Hoogsteen bonded<sup>[1]</sup> guanine bases and stabilized by the presence of monovalent cations. Their location in human genome is not only limited to eukaryotic telomeres,<sup>[2]</sup> rather they have also found in non-telomere regions e.g. in nuclease-hypersensitive promoter regions,<sup>[3-4]</sup> regulatory regions of oncogenes such as KRAS,<sup>[5]</sup> etc. These proto-oncogenes were found to be over expressed in 80% of cancers such as breast cancer, cervical cancer, lung cancer, etc. The promoter region of c-myc gene is composed of seven nuclease-hypersensitive elements (NHEs), of which, NHE III<sub>1</sub> controls 80–90% transcription of c-myc gene. This 27 nucleotide sequence (5'-TGGGGAGGGTGGGGAGGGTGGGGAAGG-3') is purine rich sequence that is also called as Pu27, has potential to form G-quadruplex structure. Previous studies suggested that the formation of stable G-quadruplex structure in this region could suppress the expression of MYC gene in Burkitt lymphoma cell lines upon treatment with TMPyP4. This stabilized G-quadruplex structure act as silencer element and thereby reduces the expression of c-myc gene.<sup>[6]</sup> Thus, the G-quadruplex structure in this region plays an important role as transcriptional regulator.<sup>[6]</sup> Over the past decades, the exploration of small molecules that induces the formation of G-quadruplex structures or stabilizes them could be a potent anti-cancer agent and may act by down-regulating the oncogene expression.<sup>[7]</sup> Nature is an ample source for chemically diverse scaffolds of molecules. Appreciating the properties of naturally occurring small molecules for being less toxic than the synthetic molecules and having better bio-availability,<sup>[8]</sup> research have already been initiated since long back to explore these compounds for targeting c-myc G-quadruplex structure and investigated their interaction<sup>[9]</sup> like quindoline derivative SYUIQ-5,<sup>[10]</sup> 9-N-substituted berberine derivatives,<sup>[11]</sup> etc. Most of these compounds have planar aromatic ring system that stabilizes the G-tetrad by  $\pi$ - $\pi$  stacking.<sup>[12]</sup> One of the major groups of naturally occurring molecules is flavonoids, that are readily available in our daily diets and have been considered as nontoxic drug candidates for anticancer therapy.<sup>[13]</sup> The common dietary flavonoids, Luteolin, Quercetin, Rutin, Genistein, Kaempferol, Puerarin, Hesperidin, Myricetin and Daidzein, have

received significant attention for their anti-angiogenesis, anti-proliferative and anti-metastatic effects.<sup>[14]</sup> Recently, in 2013, a study was performed to investigate the interactions of c-myc G-quadruplex structure with a series of pyridinium side chains containing flavone derivatives. They have showed that these compounds have stronger affinity for c-myc G-quadruplex DNA over other quadruplexes and duplex DNA.<sup>[15]</sup>

Albeit many studies for these effects of flavonoids, their main target for action and its mechanism still remains to be explored. Thorough structural information for mode of interaction of these flavonoids with DNA is requisite for a better understanding of the molecular basis for their therapeutic activities. In previous chapter we have demonstrated the interaction of Quercetin with small sequence of telomeric DNA that is TTAGGGT,<sup>[16]</sup> and, in order to get better insights about interaction of flavonoids with other G-quadruplex DNA structures, we have extended our studies with biologically significant DNA sequence in c-myc promoter region forming G-quadruplex structure. To the best of our knowledge, there is no structure available for flavonoids complexed with c-myc G-quadruplex DNA till date.

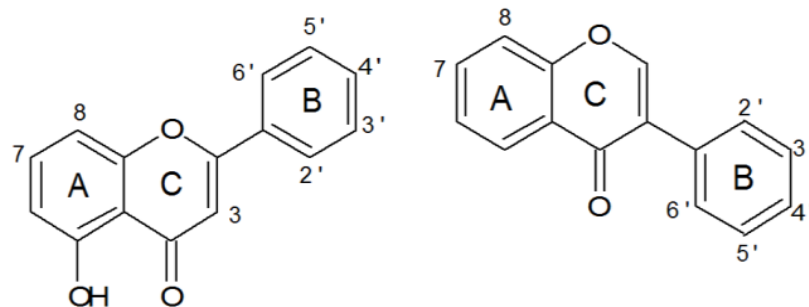
In this chapter, we have chosen 24 nucleotide c-myc promoter G-quadruplex sequence Pu24T (5'-TGAGGGTGGTGAGGGTGGGGAAGG-3') comprising of central guanine tracks of c-myc and focused on its interaction with nine representative flavonoids Luteolin, Quercetin, Rutin, Genistein, Kaempferol, Hesperidin, Daidzein, Myricetin and Puerarin (Figure 1).

NMR studies along with other biophysical techniques, such as circular dichroism (CD), steady-state and time-resolved fluorescence spectroscopy, Isothermal titration calorimetry (ITC) were employed to investigate the binding mode of flavonoids with G-quadruplex structure formed in the human c-myc promoter region. Further, this study is centralized to get a structural basis of interaction and stabilization of intramolecular parallel G-quadruplex DNA Pu24T with lead molecule obtained in this study, Quercetin<sup>[17]</sup>. Furthermore, in vitro studies were also employed to understand the cytotoxic effects of Quercetin and its subcellular localization showing its potential to down-regulate c-myc expression in human cervical carcinoma cells (HeLa cell lines).

## **4.2 Results and Discussion**

### **4.2.1 Steady state fluorescence spectroscopic studies**

Since the last several decades, fluorescence techniques have been applied to study the interaction behavior of drug with DNA. We have also employed fluorescence titration experiments to understand the interaction and binding affinities of flavonoids with c-myc G-



**Quercetin:** 3' = OH, 4' = OH, 5' = H, 3 = OH, 7 = OH

**Rutin:** 3' = OH, 4' = OH, 5' = H, 3 = Rutinose, 7 = OH

**Luteolin :** 3' = OH, 4' = OH, 5' = H, 3 = H, 7 = OH

**Kaempferol:** 3' = H, 4' = OH, 5' = H, 3 = H, 7 = OH

**Hesperidin:** 3' = OH, 4' = OCH<sub>3</sub>, 5' = H, 3 = H, 7 = O-Sugar

**Myricetin :** 3' = OH, 4' = OH, 5' = OH, 3 = OH, 7 = OH

**Genistein :** 5 = OH, 7 = OH, 4 = OH, 8 = H

**Daidezein:** 7 = OH, 4' = OH, 8 = H

**Puerarin :** 4' = OH, 8 = C-gluconoside

*Figure 4.1. Chemical structure of flavonoids showing flavones, flavonols, flavanones (left side) and isoflavanols (Right side). Ring A-benzoyl system, Ring B- cinnamoyl system.*

quadruplex DNA Pu24T. Fluorescence emission of all nine flavonoids was examined at the emission maximum in their unbound form. Flavonoids have very weak fluorescence emission likely due to the torsional motion of the phenyl and c-pyrone rings.<sup>[18]</sup> The readings were taken at emission wavelength of 435 nm, 535 nm, 416 nm, 405 nm, 423 nm, 459 nm, 440 nm, 561 nm and 456 nm for Luteolin, Quercetin, Rutin, Genistein, Kaempferol, Puerarin, Hesperidin, Myricetin and Daidzein respectively, when excited at the wavelength of 380 nm, 375 nm, 360 nm, 269 nm, 373 nm, 305 nm, 390 nm, 369 nm and 305 nm. As Genistein has excitation wavelength near to 260 nm, we have not performed this assay with Genistein. On addition of Pu24T DNA, changes in fluorescent intensity were observed that might occur by limiting the torsional motion of phenyl and c-pyrone rings. An increase in fluorescence intensity of flavonoids was observed that suggested binding of these flavonoids to Pu24T DNA and generated G-quadruplex-flavonoid complex. We have computed the binding constant values ( $K_d$ ) (Table 4.1) by fitting the plot of  $\Delta F$  (change in the fluorescence intensity) against G-quadruplex DNA concentration with ligand binding two site saturation model (Figure 4.2). It was observed that Quercetin shows higher affinity as compared to other flavonoids used in this study. Further, G-quadruplex binders should have specificity for quadruplex topology over duplex DNA. Thus, the specificity of flavonoids was also monitored by performing fluorescence titration experiment with duplex DNA (calf thymus (CT) DNA) (Figure 4.3). An enhancement in fluorescence intensity was observed for all flavonoids upon binding with CT-DNA. But, the binding constant values of these flavonoids with CT-DNA were lower as compared to Pu24T G-quadruplex DNA, in which Quercetin showed ~300 fold higher affinity Pu24T DNA as compared to duplex CT-DNA (Table 4.2). This result suggested the high affinity and specificity of Quercetin for Pu24T G-quadruplex DNA over duplex DNA. This observed higher affinity of Quercetin amongst other flavonoids could be due to differences in the chemical structure of flavonoids. Although all of these flavonoids have similar ring structure consisting of a heterocyclic pyrane ring (C) that links two benzene rings (A and B),<sup>[19]</sup> the difference in pattern of substitution of the C ring along with the presence of functional groups on A and B rings causes the difference in their activity.<sup>[20-22]</sup> As in isoflavones, the B ring is attached at C3 (carbon-3) of C ring while in flavones this B ring is attached to the C2 of C ring. Moreover, the presence of hydroxyl groups enhances the DNA binding activity.<sup>[23]</sup> Further, the presence of bulky sugar rings such as in Rutin, Hesperidin, Puerarin might hinders their intercalation and binding of these flavonoids to G-quadruplex DNA.<sup>[22]</sup> Luteolin and Kaempferol lacks the hydroxyl group at 3' of B ring while Quercetin has this hydroxyl group that might leads to the better activity of

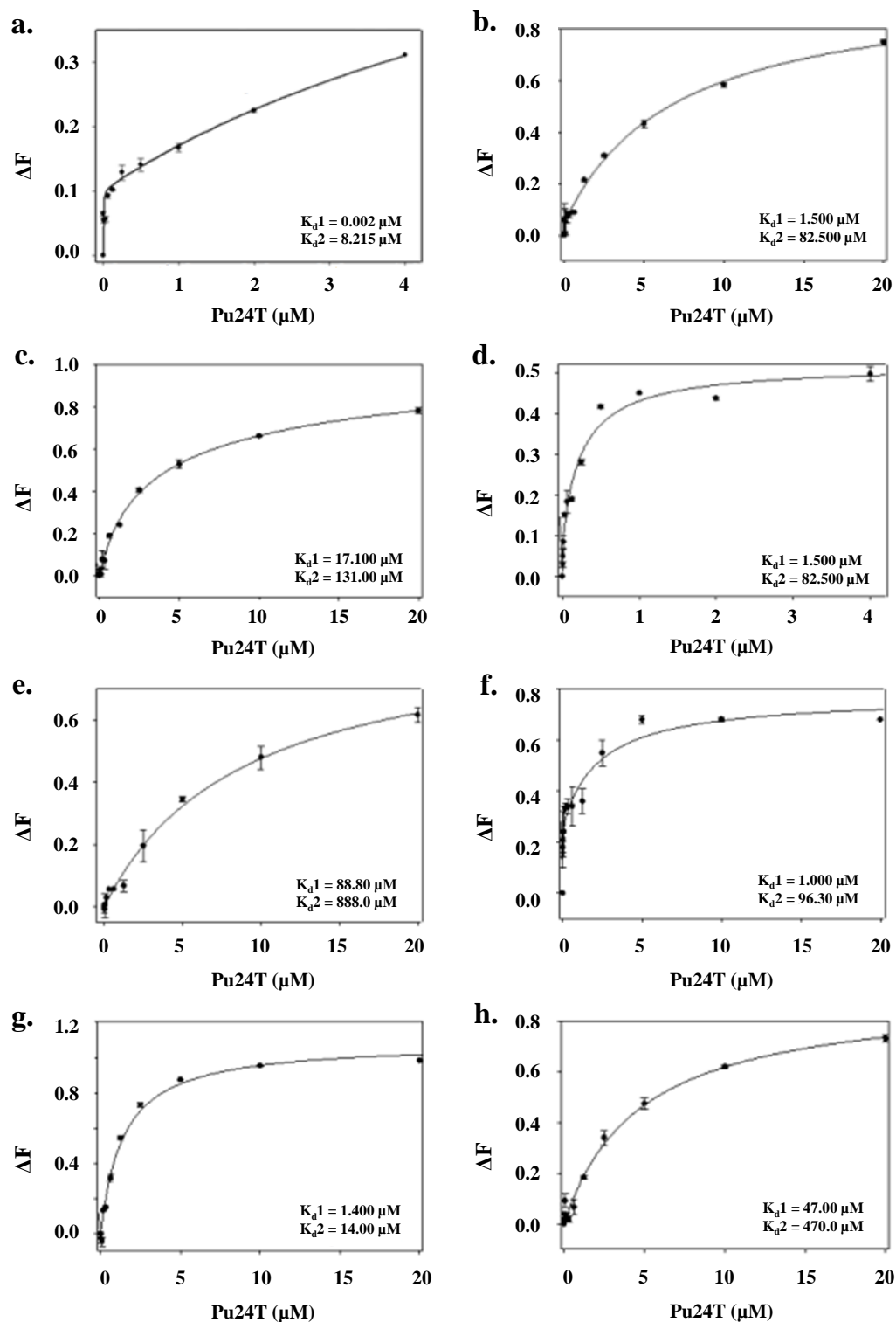


**Figure 4.2.** Fluorescence titration curve of flavonoids as a function of Pu24T G-quadruplex DNA concentration (a) Quercetin (b) Luteolin (c) Rutin (d) Kaempferol (e) Puerarin (f) Hesperidin (g) Myricetin (h) Daidzein. Solid lines represent best fit according to the ligand binding two site saturation. Values of binding constant(s) ( $K_d$ ) are indicated at the bottom right side of the plot.

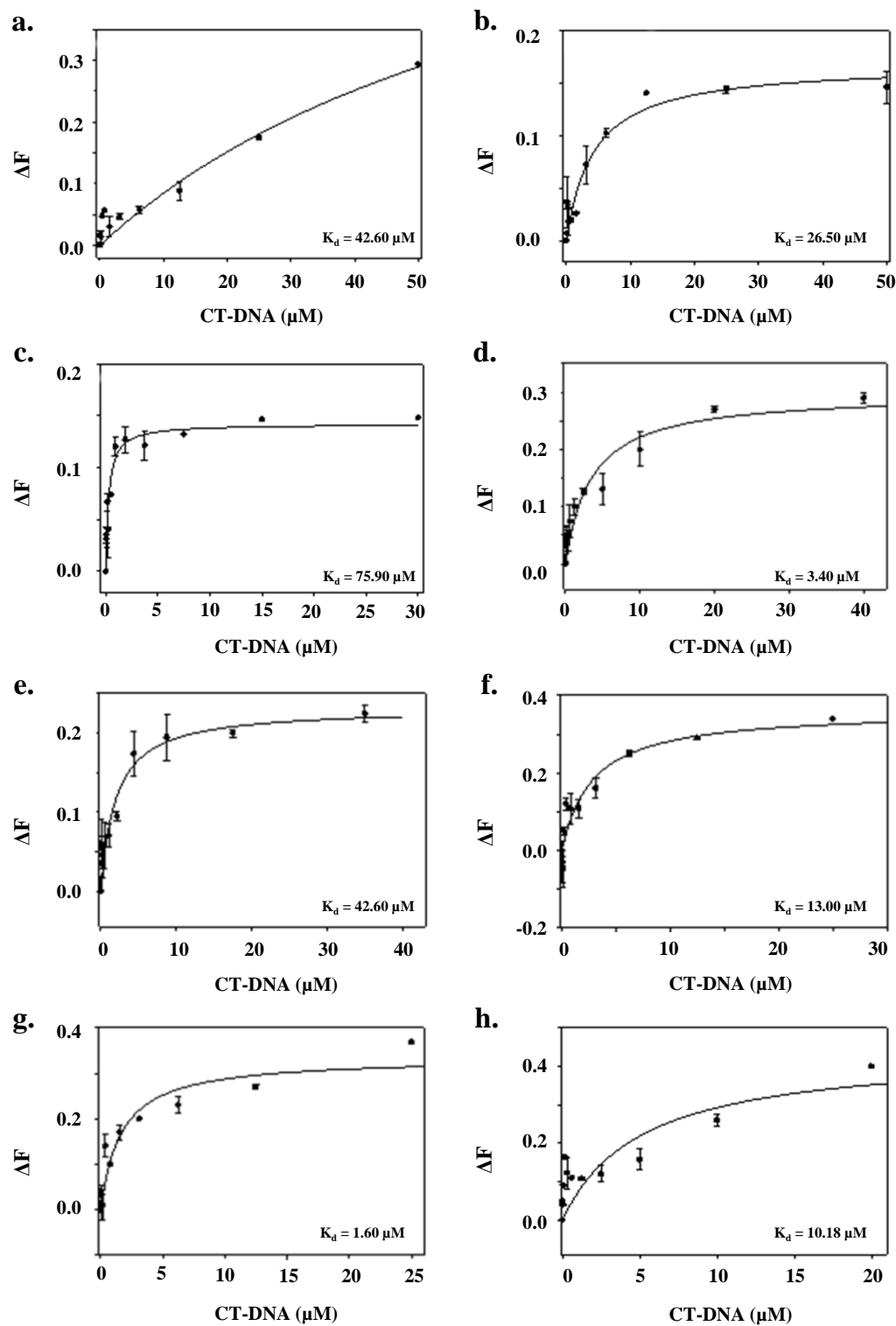


**Figure 4.3.** Fluorescence titration curve of flavonoids as a function of CT-DNA concentration (a) Quercetin (b) Luteolin (c) Rutin (d) Kaempferol (e) Puerarin (f) Hesperidin (g) Myricetin (h) Daidzein. Solid lines represent best fit according to the ligand binding two site saturation. Values of binding constant(s) ( $K_d$ ) are indicated at the bottom right side of the plot.

**Table 4.1. Binding constant ( $K_d$ (M)) values of flavonoids with G-quadruplex DNA in comparison to CT-DNA**

Flavonoids	Pu24T DNA		CT-DNA
	$K_d1$ (M)	$K_d2$ (M)	$K_d$ (M)
Quercetin	$1.38 \times 10^{-7}$	$8.21 \times 10^{-6}$	$4.26 \times 10^{-5}$
Luteolin	$1.50 \times 10^{-6}$	$8.25 \times 10^{-5}$	$2.65 \times 10^{-5}$
Rutin	$1.71 \times 10^{-5}$	$13.11 \times 10^{-4}$	$7.59 \times 10^{-5}$
Kaempferol	$1.30 \times 10^{-6}$	$2.69 \times 10^{-5}$	$3.40 \times 10^{-6}$
Puerarin	$8.88 \times 10^{-5}$	$8.88 \times 10^{-4}$	$4.26 \times 10^{-5}$
Hesperidin	$1.00 \times 10^{-6}$	$9.63 \times 10^{-5}$	$1.30 \times 10^{-5}$
Myricetin	$1.40 \times 10^{-6}$	$1.40 \times 10^{-5}$	$1.60 \times 10^{-6}$
Daidzein	$4.70 \times 10^{-5}$	$4.70 \times 10^{-4}$	$10.18 \times 10^{-6}$

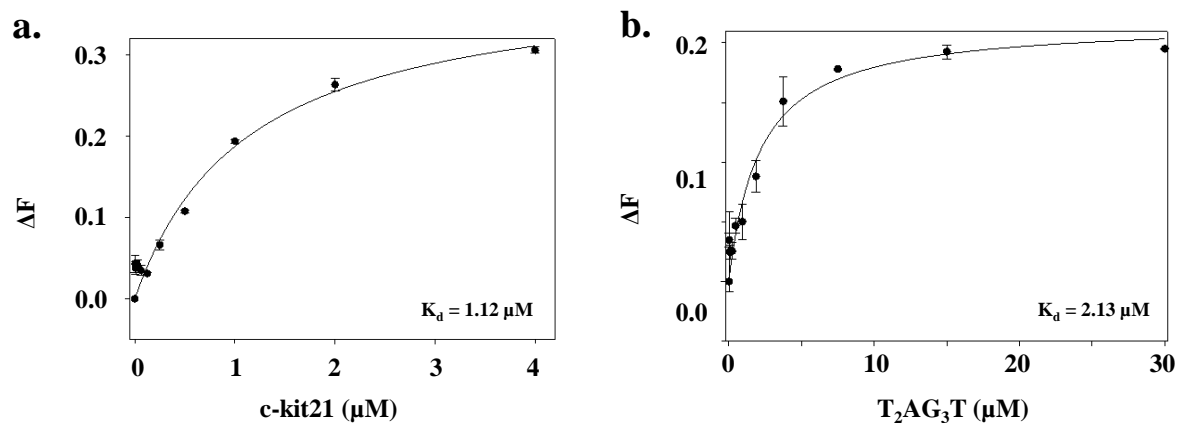


*Figure 4.4. Fluorescence titration curve of Quercetin as a function of various G-quadruplex DNA concentration (a) c-kit21 DNA (b) T<sub>2</sub>AG<sub>3</sub>T DNA (in presence of Na<sup>+</sup> ions forming anti-parallel structure). Solid lines represent best fit according to the ligand binding two site saturation. Values of binding constant(s) ( $K_d$ ) are indicated at the bottom right side of the plot.*

**Table 4.2. Binding constant ( $K_d$ (M)) values of Quercetin with various G-quadruplex DNA**

<b>G-quadruplex DNA</b>	<b><math>K_d1</math>(M)</b>	<b><math>K_d2</math> (M)</b>
<b>Pu24T- <i>c-myc</i> DNA</b>	<b><math>1.38 \times 10^{-7}</math></b>	<b><math>8.21 \times 10^{-6}</math></b>
<b>ckit 21upDNA</b>	<b><math>1.12 \times 10^{-6}</math></b>	<b>--</b>
<b>T2AG3T (forming antiparallel G-quadruplex structure)</b>	<b><math>2.13 \times 10^{-6}</math></b>	<b>--</b>

Quercetin as compared to other flavonoids. Furthermore, to understand the specificity of Quercetin for c-myc promoter region over other promoter regions forming G- quadruplex structure in human genome, we have also performed this experiment with c-kit G-quadruplex DNA. c-kit21 DNA sequence is present at promoter regions of c-kit proto-oncogenes and forms G-quadruplex structure. It is involved in progression of cancer growth. The binding constant values of Quercetin (Table 4.2 and Figure 4.4) suggested ~10 fold poor affinity than that of c-myc promoter DNA and could suggest the specificity of Quercetin for c-myc promoter region over other promoter regions. Moreover, the preferential binding of Quercetin for parallel and anti-parallel G-quartets was also assessed by performing fluorescence titration experiment with d- (T<sub>2</sub>AG<sub>3</sub>T)<sub>4</sub> human telomeric DNA sequence in 70 mM Na<sup>+</sup> ions containing buffer. In the presence of 70mM Na<sup>+</sup> ions, (T<sub>2</sub>AG<sub>3</sub>T)<sub>4</sub> forms anti-parallel G-quadruplex structure.<sup>[24]</sup> A ~15 fold weaker affinity was observed (Table 4.2 and Figure 4.4) for anti-parallel G-quadruplex topology as compared to Pu24T c-myc DNA forming parallel topology that suggested the preference of Quercetin for parallel G-quadruplex structures over anti-parallel G-quadruplex structure.

Now, in order to have a better understanding of thermodynamics of the reaction between the flavonoids and DNA, it is important to determine the contributions of enthalpy and entropy of the reaction. For this we have performed isothermal titration calorimetry (ITC) studies as mentioned in next section.

#### **4.2.2 Isothermal Titration Calorimetry studies**

Owing to the sensitivity and reliability of ITC, it has become an important technique for direct measurements of thermodynamic parameters of interactions. It provides various parameters such as change in Gibb's free energy  $\Delta G$ , entropy change ( $\Delta S$ ), enthalpy change ( $\Delta H$ ), etc. Most importantly, it also provides information about number of binding sites (N) and binding constant values in terms of  $k_a$ . Figure 4.5 shows integrated heat data for the titration of all flavonoids with Pu24T G-quadruplex DNA along with the binding constant as well as binding sites (N) were mentioned in Table 4.3. Amongst all the available binding models, two binding modes involving "two independent sites" model provides the best fitting with relatively good  $\chi^2$  values. It has been observed that all flavonoids have a higher affinity quadruplex site,  $K_1$  than binding to the lower affinity site,  $K_2$ , (with few exceptions). The higher binding affinity values for the stronger binding site are in accordance with the fluorescence titration data. The total stoichiometries of interaction for the binding were found

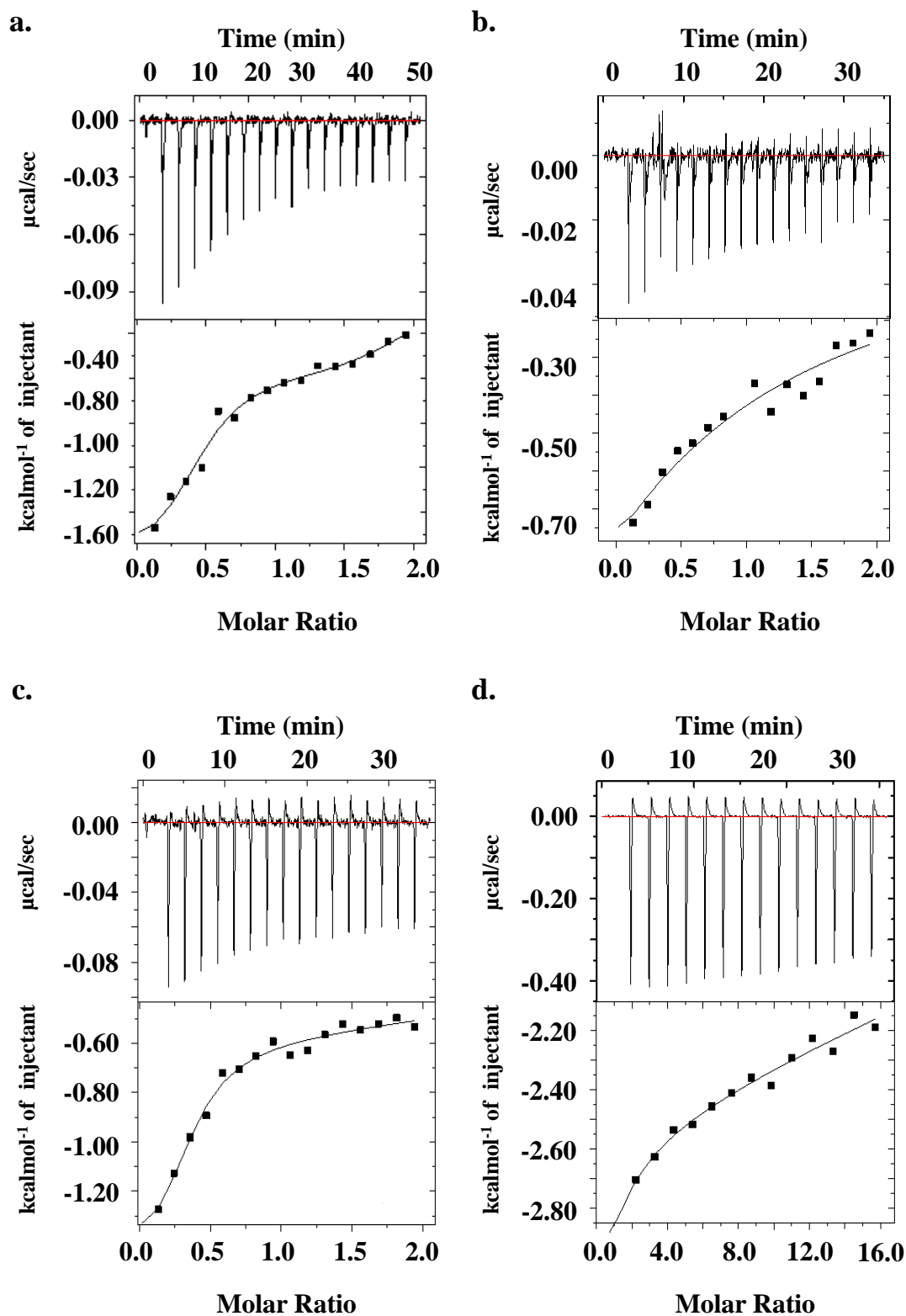


*Figure 4.5. (a-d) Isothermal Titration Calorimetry data (points) for various flavonoids binding to Pu24T G-quadruplex DNA at 25°C (a) Quercetin (b) Luteolin (c) Rutin (d) Kaempferol. Solid line represents the fitted data results from two site binding mode.*

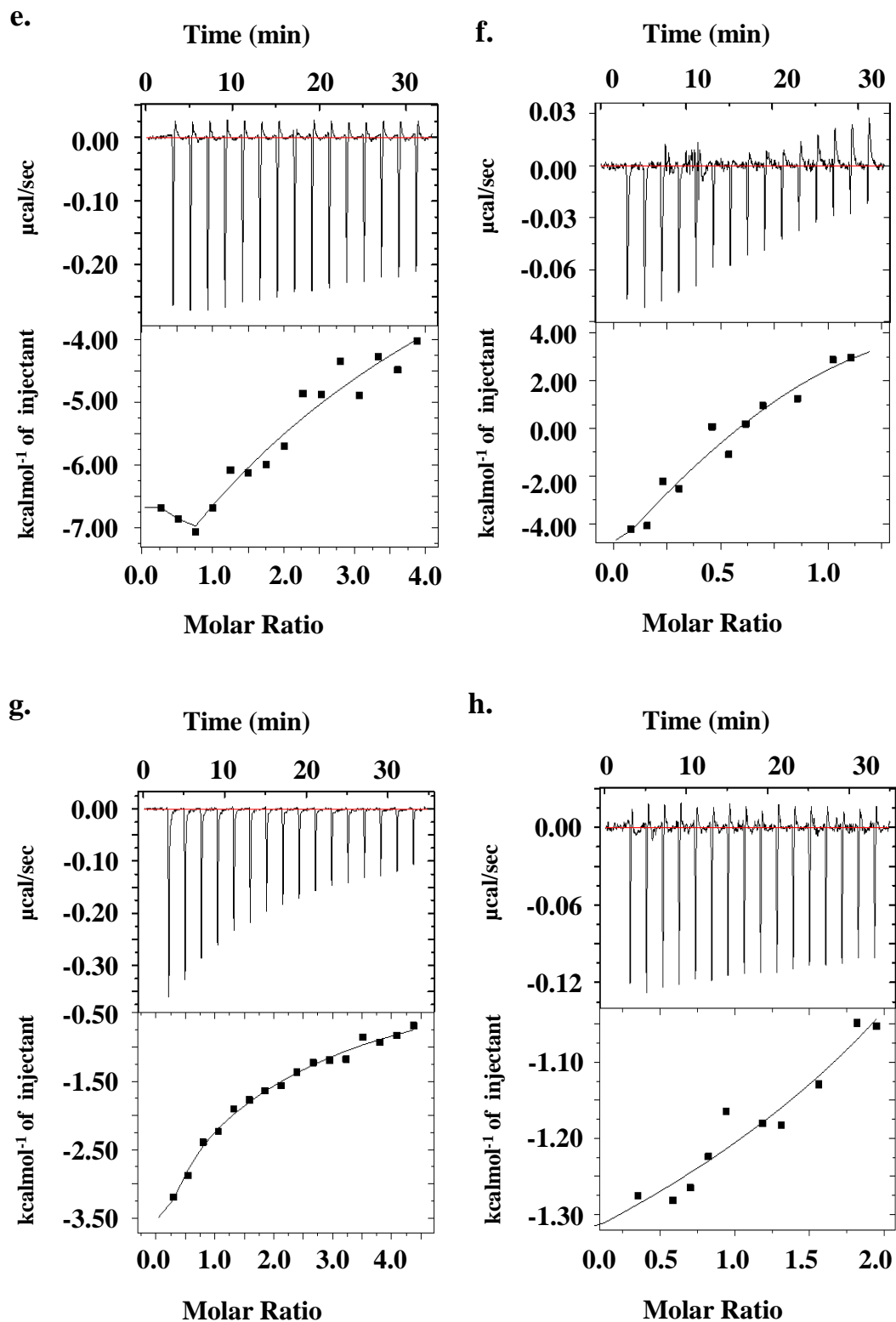


*Figure 4.5.(e-h) Isothermal Titration Calorimetry data (points) for various flavonoids binding to Pu24T G-quadruplex DNA at 25°C (e) Puerarin (f) Hesperidin (g) Myricetin (h) Daidzein. Solid line represents the fitted data results from two site binding mode.*

*Table 4.3. Values of binding constant and number of binding sites for the interaction flavonoids with Pu24T DNA as obtained from ITC experiment*

<b>Flavonoids</b>	<b>N<sub>1</sub> (Sites)</b>	<b>N<sub>2</sub> (Sites)</b>	<b>K<sub>1</sub> (M<sup>-1</sup>)</b>	<b>K<sub>2</sub> (M<sup>-1</sup>)</b>
<b>Quercetin</b>	<b>0.41 ± 0.05</b>	<b>1.54 ± 0.14</b>	<b>1.57×10<sup>7</sup> ± 2.14</b>	<b>8.50×10<sup>5</sup> ± 1.54</b>
<b>Luteolin</b>	<b>0.49 ± 0.78</b>	<b>0.90 ± 6.55</b>	<b>1.32×10<sup>5</sup> ± 3.76</b>	<b>1.70×10<sup>-5</sup> ± 2.93</b>
<b>Rutin</b>	<b>0.32 ± 0.34</b>	<b>34.80 ± 3.27</b>	<b>7.23×10<sup>5</sup> ± 8.60</b>	<b>6.50×10<sup>2</sup> ± 8.43</b>
<b>Kaempferol</b>	<b>1.15 ± 2.45</b>	<b>0.24 ± 160</b>	<b>2.09×10<sup>0</sup> ± 4.40</b>	<b>1.34×10<sup>5</sup> ± 3.81</b>
<b>Puerarin</b>	<b>0.22 ± 50.4</b>	<b>0.43 ± 0.191</b>	<b>1.10×10<sup>4</sup> ± 7.75</b>	<b>4.48×10<sup>17</sup> ± 2.81</b>
<b>Hesperidin</b>	<b>2.18 ± 4.74</b>	<b>0.20 ± 2.84</b>	<b>7.35×10<sup>5</sup> ± 1.06</b>	<b>6.04×10<sup>5</sup> ± 4.07</b>
<b>Myricetin</b>	<b>0.34 ± 0.285</b>	<b>2.05 ± 0.00</b>	<b>1.65×10<sup>5</sup> ± 1.2</b>	<b>1.58×10<sup>4</sup> ± 4.60</b>
<b>Daidzein</b>	<b>1.39 ± 9.57</b>	<b>2.28±1.07</b>	<b>3.34×10<sup>5</sup> ± 1.50</b>	<b>2.93×10<sup>5</sup> ± 1.01</b>

*Table 4.4. Detailed thermodynamic and energetics data for the interaction Quercetin with Pu24T DNA as obtained from ITC experiment*

<b>Parameters</b>	<b>Values</b>
<b>N<sub>1</sub> (Sites)</b>	<b>0.415 ± 0.05</b>
<b>K<sub>1</sub> (M<sup>-1</sup>)</b>	<b>1.57 × 10<sup>7</sup> ± 2.14</b>
<b>ΔH<sub>1</sub> (kcal/mol)</b>	<b>-1.86 ± 284</b>
<b>ΔS<sub>1</sub> (cal/mol/deg)</b>	<b>26.7</b>
<b>N<sub>2</sub> (Sites)</b>	<b>1.54 ± 0.14</b>
<b>K<sub>2</sub> (M<sup>-1</sup>)</b>	<b>8.50 × 10<sup>5</sup> ± 1.54</b>
<b>ΔH<sub>2</sub> (kcal/mol)</b>	<b>-0.59 ± 179</b>
<b>ΔS<sub>2</sub> (cal/mol/deg)</b>	<b>25.1</b>

to be ~2 for all the flavonoids except Rutin. As already mentioned, the difference in binding behavior of binding of these flavonoids may attribute to the difference in the substitution pattern on basic moiety of their chemical structures. The ITC thermogram of all flavonoids exhibited a two binding site for Pu24T DNA and displayed exothermic process. As we have obtained Quercetin as a lead molecule from our fluorescence titration data, similar trend is observed in ITC data. Therefore, we have explored the detailed thermodynamic parameters of interaction of Quercetin with Pu24T DNA (Table 4.4). ITC data for Quercetin and Pu24T DNA showed exothermic peaks that implies the end-stacking of Quercetin due to increased  $\pi$ - $\pi$  stacking interaction with bases of Pu24T G-quadruplex DNA. Also, the primary binding constant value 0.064  $\mu$ M fairly shows strong interaction of Quercetin with DNA and complimented the binding constant obtained in fluorescence titration data.

Since, Quercetin showed highest affinity for Pu24T amongst all the flavonoids used in this study, thus we proceeded further with Quercetin as a lead molecule and explore its detailed binding to Pu24T G-quadruplex DNA. For this purpose, we have first evaluated the binding mode of Quercetin to Pu24T DNA as mentioned in next section.

#### **4.2.3 Time resolved fluorescence studies**

The time-correlated single-photon counting (TCSPC) method was used to perform the fluorescence lifetime decay measurements that allowed us to determine the mode of binding of Quercetin to Pu24T G-quadruplex DNA. The fluorescence life time measurement is one of the useful techniques that delved the environment of fluorophore in excited state and is sentient to its interaction with DNA structure. The life time decay profiles were measured for free Quercetin and its complex with Pu24T DNA sequence. The tri exponential decay component provides best fit for fluorescence decay of Quercetin with  $\chi^2$  value ~1.96. This suggested that tri exponential decay function is an estimable statistical description and could be attributed to presence of three different conformations in the solution. As mentioned in previous chapter that this may be likely due to the rotation of a single bond between benzopyran rings to phenyl rings of Quercetin. Thus, the decay profile of unbounded Quercetin has three lifetimes ( $\tau_1$ ,  $\tau_2$  and  $\tau_3$ ) and three amplitudes ( $\beta_1$ ,  $\beta_2$ , and  $\beta_3$ ) (Table 4.5), with an average lifetime of 1.02 ps. Figure 4.6 displayed the fluorescence decay profile of Quercetin in its free form and complexed with Pu24T G-quadruplex DNA at Drug/Nucleic acid (D/N) ratio = 2.0. On addition of Pu24T in 2:1 molar ratio of the D/N, the average lifetime of complex increased by ~25 times (Table 4.5). The complex of Quercetin – Pu24T

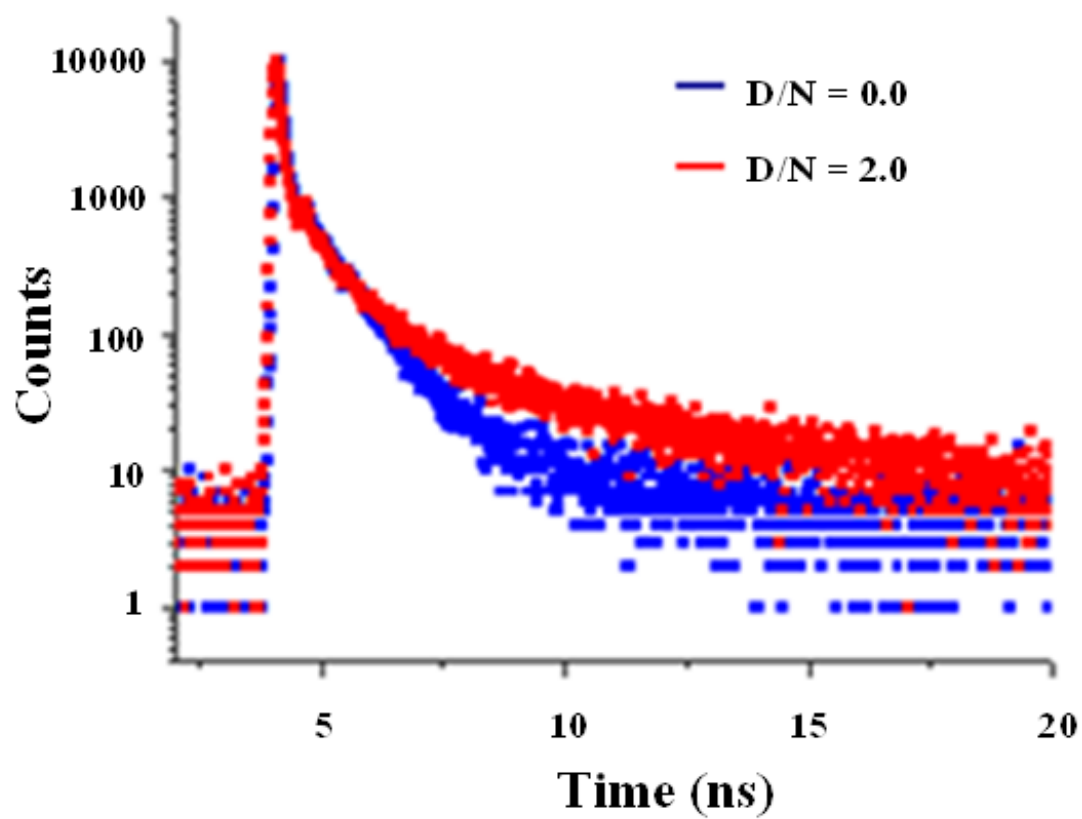


*Figure 4.6. Fluorescence life time decay curve of 40.0  $\mu$ M free Quercetin (Blue) and its complex with Pu24T DNA at D/N ratio = 2.0 (Red). D= Quercetin; N= Pu24T.*

**Table 4.5. Life time fluorescence decay parameters for Quercetin and its D/N = 2:1 complex with Pu24T DNA at 298 K**

D/N = 0.0								
DNA	Life Time Decay (ns)			Amplitude			Chi Square	Average life time (ps)
	$\tau_1$	$\tau_2$	$\tau_3$	$\beta_1$	$\beta_2$	$\beta_3$		
	5.23	62.95	7.36 $\times 10^{-2}$	-3.39 $\times 10^{-2}$	9.15 $\times 10^{-3}$	8.06 $\times 10^5$	1.96	1.02
D/N = 2.0								
DNA	Life Time Decay (ns)			Amplitude			Chi Square	Average life time (ps)
	$\tau_1$	$\tau_2$	$\tau_3$	$\beta_1$	$\beta_2$	$\beta_3$		
Pu24T	59.10	277.44	1.27	7.05 $\times 10^{-3}$	8.40 $\times 10^{-4}$	1.14	2.38	25.42

at D/N = 2.0 ratio also gives best fit with tri - exponential decay profile that attributed the requirement of three life time components to give a satisfactory fit. The life time decay data attributed to the binding of Quercetin to Pu24T c-myc DNA at more than one site. In general, molecules with planar scaffold interact with G-quadruplex structure via end-stacking mode and external or groove binding mode. The lifetime property of both the binding modes is different with larger lifetime in the end-stacking mode.<sup>[25]</sup> Likely to previous study,<sup>[16]</sup> the significant changes observed in the values of both the decay components and amplitudes of Quercetin on binding with Pu24T at 2:1 D/N ratio, specifies the interaction of flavonoids to Pu24T and the formation of the complex via end-stacking.<sup>[26]</sup>

Further, the effect of binding of Quercetin to the stability of G-quadruplex structure was ascertained by other biophysical methods like circular dichroism (CD) as described in next section.

#### **4.2.4 Circular Dichroism studies**

CD spectroscopy is provides information about the conformation of macromolecules and could be used to determine the changes occurs in due to addition of ligands. Quercetin is an optically inactive and hence do not have any circular dichroism (CD) spectrum. Its interaction with Pu24T G-quadruplex DNA was monitored in ultraviolet region. In K<sup>+</sup> solution, Pu24T DNA sequence forms a parallel G-quadruplex as evident by presence of positive peak at 260 nm and a negative peak at 240 nm that represent the parallel quadruplex topology<sup>[27]</sup> (Figure 4.7). Upon addition of Quercetin at twice the concentration of G-quadruplex sequence that is at D/N = 2.0, the global conformation of G-quadruplex DNA remained same. Slight changes in negative peak suggested that Quercetin binds to Pu24T DNA but there was the preservation of folded G-quadruplex structure. It could be concluded that Quercetin imparts stability of G-quadruplex structure upon binding<sup>[28]</sup> and Quercetin does not induces any distortion in G-quadruplex topology of Pu24T DNA sequence. Thus, now it is interesting to know which protons of Quercetin participates in the binding to Pu24T G-quadruplex DNA, we have performed one dimensional proton NMR spectroscopy as mentioned in next section.

#### **4.2.5 Nuclear Magnetic Resonance studies**

##### **4.2.5.1 One dimensional proton NMR studies**

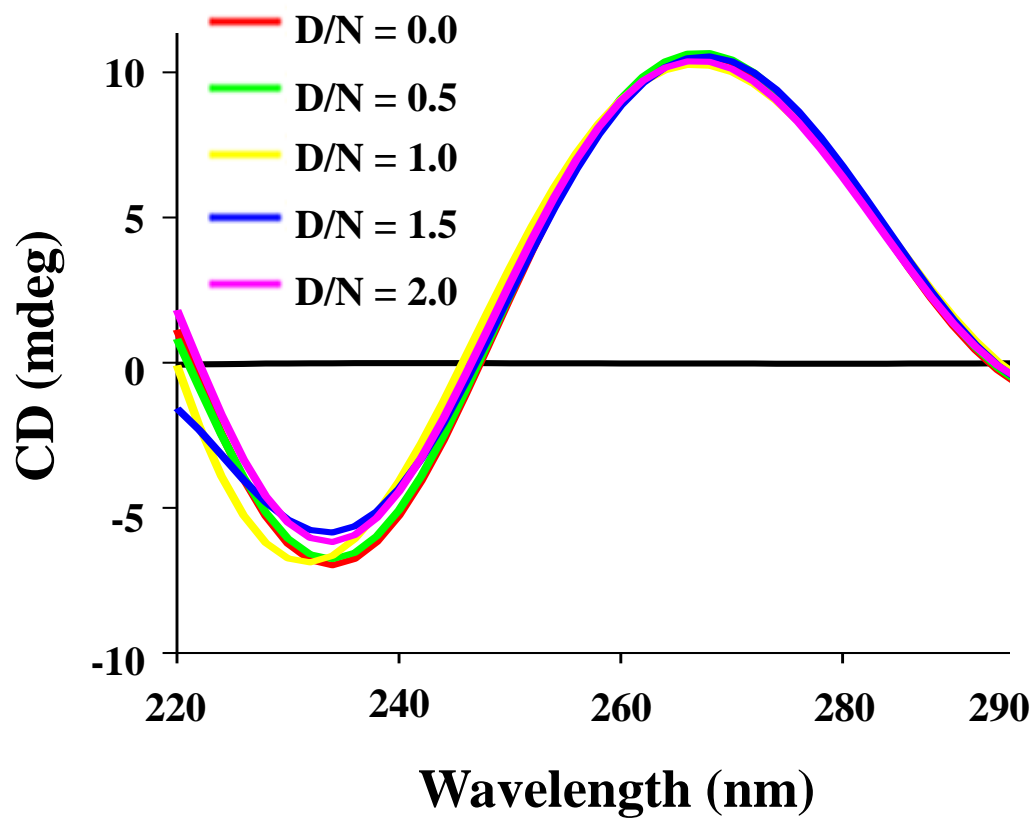


*Figure 4.7. Circular Dichroism titration spectrum for free Pu24T (Red) and in the presence of Quercetin as a function of Quercetin concentration at D/N ratio = 0.5 to D/N ratio = 2.0. D= Quercetin; N= Pu24T.*

Solution NMR spectroscopy plays a significant role in understanding the G-quadruplex structure, its dynamics and interactions with ligands. It could also be used to monitor interaction of ligand with DNA sequence as well as to elucidate the structure of Drug - DNA complex. Firstly, in order to determine the involvement of Quercetin protons in its interaction with Pu24T G-quadruplex DNA, we have performed one dimensional (1D) proton NMR titration experiment by gradual addition of Pu24T DNA into Quercetin solution. With the successive addition of Pu24T DNA, the resonances of Quercetin protons get broadened and finally disappeared at 100: 1 D/N ratio (Figure 4.8). This result suggested the involvement of protons in binding of Quercetin with Pu24T DNA. Further, to understand the structural basis of this interaction, we have performed detailed NMR studies of Drug-DNA formed by Quercetin and Pu24T DNA sequence forming G-quadruplex structure; as mentioned in next sub-section.

#### **4.2.5.1.1 Assessment of G-quadruplex structure formation**

Structural conformation of G-quadruplex DNA formed by c-myc promoter sequence Pu24T in  $K^+$  solution was monitored by proton NMR. We have observed thirteen well-resolved resonances in the imino region (10 - 12 ppm) of  $^1H$ -NMR spectra (Figure 4.9). Their occurrence illustrated the formation of well-defined G-quadruplex structure.<sup>[29]</sup> The assignment of nucleotide protons has been carried out by following the strategies adopted for standard B - DNA structures that is, sequential NOEs (base H8/H6)<sub>n</sub> - sugar (H1')<sub>n-1</sub>, (base H8/H6)<sub>n</sub> - sugar(H2'')<sub>n-1</sub>, (base H8/H6)<sub>n</sub> - sugar(H2')<sub>n-1</sub>; expected NOEs due to several short intra nucleotide distances<sup>[30]</sup> as well as NMR data of uncomplexed Pu24I,<sup>[29]</sup> Pu24T.<sup>[31]</sup> The present oligonucleotide Pu24T exists as G-quadruplex structure that can be evident from sequential connectivities between adjacent guanine imino protons in the sequence. The position of each and every resonance was thus ascertained and unambiguous assignment of was performed on the basis of a previously reported strategy.<sup>[32]</sup> Pu24T DNA sequence forms intramolecular parallel stranded G-quadruplex structure that has a unique fold-back configuration for G24. In this structure, the G20–A21–A22–G23 forms a diagonal loop that concerted G24 into the core of G-quadruplex structure. The G-tetrad layers were bridged via formation of double-chain-reversal loops by T7, T16, and T10–G11–A12 connecting G6 to G8, G15 to G17 and G9 to G13, respectively.<sup>[33]</sup>

#### **4.2.5.1.2 One - Dimensional proton NMR titration studies**

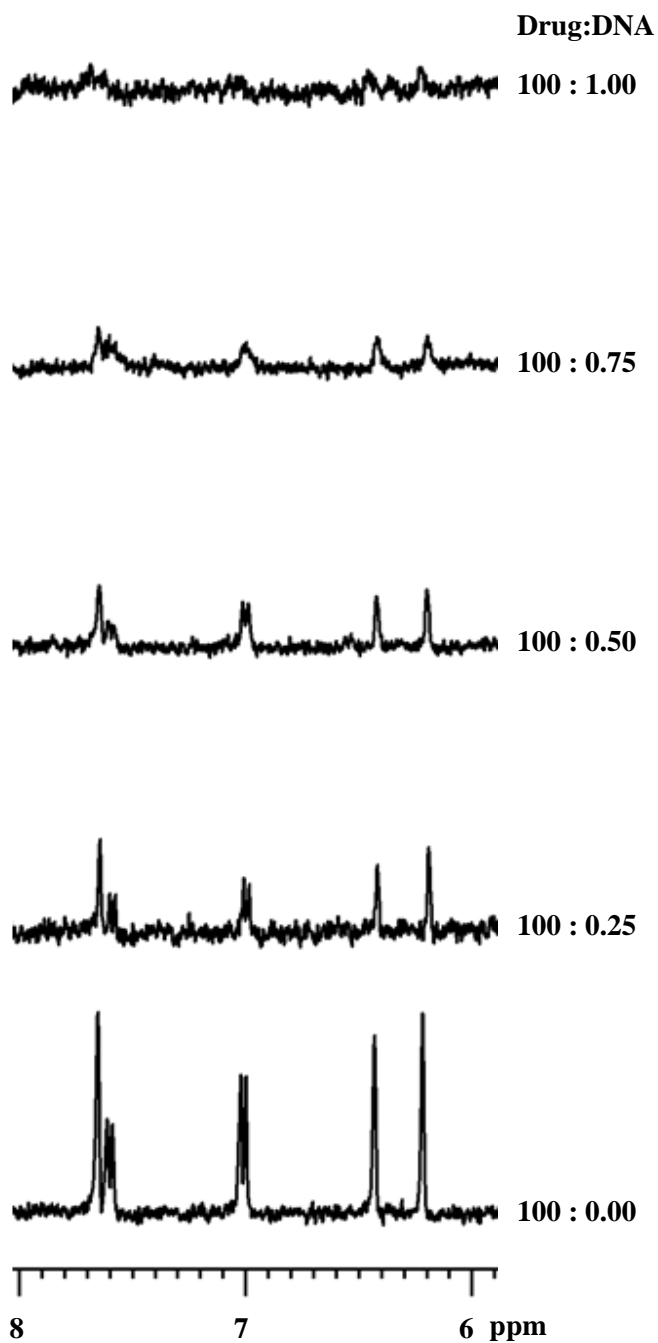


*Figure 4.8. One dimensional proton NMR spectra of 200  $\mu$ M Quercetin and its titration with increasing concentration of Pu24T DNA from D: N = 100: 0 to 100:1.*

The unbounded Pu24T DNA sequence displayed thirteen resonances in 10.5 ppm - 12.0 ppm region of  $^1\text{H}$ -NMR spectra, accounted for guanine imino proton resonances (Figure 4.9, D/N = 0.0). To characterize the interaction of Quercetin with Pu24T DNA sequence, we have performed 1D proton NMR titration experiment. For the ease of analysis, the positions of the bases in this oligomer are designated as follows: d-(T<sup>1</sup><sub>p</sub> G<sup>2</sup><sub>p</sub> A<sup>3</sup><sub>p</sub> G<sup>4</sup><sub>p</sub> G<sup>5</sup><sub>p</sub> G<sup>6</sup><sub>p</sub> T<sup>7</sup><sub>p</sub> G<sup>8</sup><sub>p</sub> G<sup>9</sup><sub>p</sub> T<sup>10</sup><sub>p</sub> G<sup>11</sup><sub>p</sub> A<sup>12</sup><sub>p</sub> G<sup>13</sup><sub>p</sub> G<sup>14</sup><sub>p</sub> G<sup>15</sup><sub>p</sub> T<sup>16</sup><sub>p</sub> G<sup>17</sup><sub>p</sub> G<sup>18</sup><sub>p</sub> G<sup>19</sup><sub>p</sub> G<sup>20</sup><sub>p</sub> A<sup>21</sup><sub>p</sub> A<sup>22</sup><sub>p</sub> G<sup>23</sup><sub>p</sub> G<sup>24</sup><sub>p</sub>). With the incremental addition of Quercetin to Pu24T G- quadruplex DNA solution, significant changes in chemical shift as well as in shape of resonances were observed. These changes could be seen in imino (Figure 4.9) as well as base region of the proton NMR spectrum (Figure 4.10). Broadening of DNA proton resonances in linear fashion with increase in D/N ratios indicated the binding of Quercetin to Pu24T DNA. These changes started from D/N = 0.4 ratio and became prominent at D/N = 1.0 ratio and significantly clear at D/N = 2.0 ratio, thereby suggested the formation of Quercetin-Pu24T DNA complex. In the imino region of  $^1\text{H}$ -NMR spectra upto D/N = 2.0 (Figure 4.9), G4NH and G13NH resonances showed the largest upfield shift of ~ 0.18 ppm and ~ 0.07 ppm was observed for G18NH, while G17NH was shifted downfield by ~ 0.10 ppm. These guanines were found to form upper i.e. 5' G- tetrad of Pu24T G-quadruplex DNA. Thus, it could be inferred that Quercetin binds near to 5' G- tetrad of Pu24T DNA. Moreover, an upfield shift of 0.08 ppm was also observed for G24NH resonance along with 0.04 ppm upfield shift in G19NH and G6NH resonances of Pu24T DNA. Additionally, G20 imino proton was also significantly broadened and it gradually disappeared at D/N = 2.0. These shifts of imino resonances could be due to  $\pi$ -electronic cloud,<sup>[34]</sup> and as G24, G6, G19 forms bottom i.e. 3' G- tetrad and G20 base is located near to this G-tetrad, it could be inferred that Quercetin also binds near to 3' G- tetrad of Pu24T G-quadruplex DNA.

In addition to imino region, perturbations of resonances were also seen in nitrogenous base H8/H6 region of  $^1\text{H}$ -NMR spectra (Figure 4.10a). Likewise in imino region, these changes were majorly observed for those bases that form upper and lower G-tetrad. For instance, with the incremental addition of Quercetin to Pu24T DNA solution, G4H8 proton resonance showed downfield shift of ~ 0.17 ppm. Further, there were 0.04 ppm upfield shift of resonances of G6H8, G17H8 protons while G13H8 and G20H8 protons shifted upfield by ~ 0.03 ppm. As depicted in Figure 4.10a, from D/N = 1.0, the G2H8 resonance begin to shift downfield that become prominent at D/N = 2.0 with a change of ~ 0.07 ppm. Also, the resonance of G24H8 proton shifted downfield with 0.01 ppm and became distinct with the addition of Quercetin that was initially merged at D/N = 0.0. Altogether, from the above

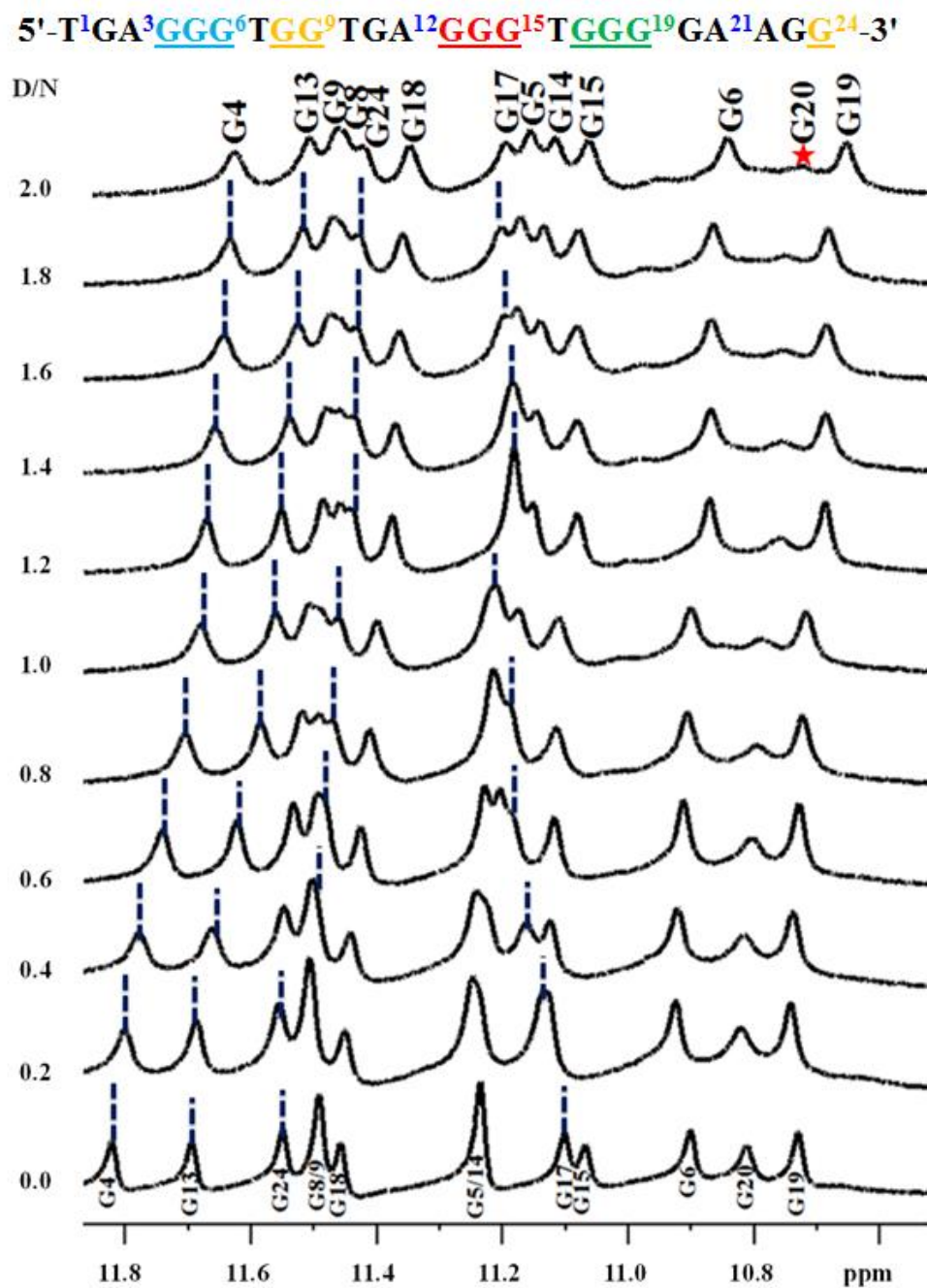


*Figure 4.9. One dimensional proton spectra for Quercetin - Pu24T complex monitored by imino region as a function of D/N ratio at 298 K (Changes in the chemical shift for G4, G13, G24, G17 were followed by blue dotted lines from D/N = 0.0 to D/N = 2.0 and broadening of G20 was marked as asterisk).*



results it could be clearly seen that perturbations in the proton resonances were observed for the guanine bases that form 5' and 3' G-tetrad thus corroborates the binding of Quercetin at two sites on Pu24T DNA near to these tetrads. Besides, the negligible changes in imino resonances of residues forming the middle G-tetrad indicate that Quercetin does not bind in between the G-quadruplex structure and does not cause the distortion of its structure. This is in good agreement with our CD titration data that also confirms the stability of G-quadruplex structure upon addition of Quercetin. Moreover, as depicted in Figure 4.10b, the Quercetin H6' (LH6') and H8 (LH8) proton resonates at  $\sim 6.9$  ppm and  $\sim 8.63$  ppm respectively, and in this region, no proton signals of free DNA were observed, therefore, it allowed us to easily monitored by 1D NMR and helps to provide the interpretation of NOE correlation in 2D NOESY spectra.

Furthermore, the splitting of Quercetin protons was not observed due to a rapid exchange process. Also as seen from our TSCPC studies the relaxation takes places in pico seconds (ps). The changes in the chemical environment of ligand (Quercetin) took places in very this short period of time. As the time scale for NMR experiments is in milli seconds that might make it unable to capture the changes in the range of NMR time scale. However, due to overlapping with DNA proton resonances, other protons of Quercetin might not be observed that were found to be involved in the interaction as shown in Figure 4.8. The proton chemical shifts and individual assignments of Quercetin- Pu24T complex at D/N = 2.0 resonances are reported in table 4.6.

Along with this observed changes in the chemical shift of DNA resonances upon interaction with Quercetin, it is requisite to explore intermolecular short contacts that could provide a direct hint of the structure of a specific drug - DNA complex. Thus, we have performed NOESY experiment as mentioned in next sub-section.

#### **4.2.5.2 Two dimensional proton NMR studies**

NOESY spectra were collected at various mixing time for Quercetin-Pu24T complex at different D/N ratios, that is, 0.0, 0.6, 1.0 and 2.0. The unbounded form of Pu24T displayed strong NOEs contributed by intra-nucleotide and sequential connectivities of imino protons (Figure 4.11). The cross peak intensities for intra-nucleotide connectivities and sequential connectivities were estimated qualitatively as strong intense (ss), strong (s) medium (m) weakly (w) and very weakly (vw) for distances of about 1.8 - 2.5, 2.5 - 3.0, 3.0 - 3.5, 3.5 - 4.0, and 4.0 - 5.0 Å respectively. At D/N = 0.0, NOEs between adjacent guanine imino protons in Pu24T DNA sequence, that is G4NH-G5NH, G5NH-G6NH, G8NH-G9NH,

G13NH–G14NH, G14NH–G15NH, G17NH–G18NH, G18NH–G19NH are evident in Figure 4.11. These NOEs showed intramolecular interactions between guanine residues that are involved in formation of G-tetrads. Thus, in the unbound form Pu24T G-quadruplex DNA displayed strong NOEs accounted for well-established stacking interaction between DNA base pairs and formation of well-defined G-quadruplex structure. Upon addition of Quercetin to DNA solution, this sequential connectivity was found to be intact which substantiates that no disruption occurs in the stacking interactions of G-quadruplex structure (Figure 4.11). Remarkably, at D/N = 2.0, thirteen intermolecular NOEs were observed for Quercetin LH8 and LH6' protons with the Pu24T protons (Figure 4.12) and these intermolecular NOEs can be correlated with Pu24T bases that forms both of its terminal G-tetrads, including G6, G17, G19, G15 (Figure 4.12). This compliments the observation made from 1D NMR experiment and suggested the probable binding site of Quercetin near to both of terminal G-tetrads. Additionally, we have also observed a strong NOE peak for G23H8 and Quercetin LH8 proton (Figure 4.12). This G23 nucleotide is located below the bottom G-tetrad, so, the observed NOE ruled out the chances of binding Quercetin in between the middle G-tetrad and thus confirms the binding of Quercetin below the bottom G-tetrad. Also as depicted in Figure 4.1, the intensities of NOE cross peaks of drug DNA complex were changed as compared to free DNA that might occurred due to broadening of resonances upon binding of Quercetin. In contrast to above changes, no significant changes and NOE - peaks were observed for guanines forming middle G-tetrad of Pu24T G-quadruplex DNA.

Moreover, Pu24T G-quadruplex DNA structure has well-defined capping structures at both terminals. As mentioned above, at 5'- end, it has TGA flanking strand; T10–G11–A12 connecting G9 to G13. The G-tetrad layers were bridged via formation of double-chain-reversal loops by T7 that connects G6 to G8, T16 connecting G15 to G17, and G20–A21–A22–G23 forms a diagonal loop that concerted G24 into the core of G-quadruplex structure. And from NOESY experiment, it could be interpreted that two molecules of Quercetin end-stack at each of the terminal tetrads, therefore, it is obvious to know whether these interactions were disrupted in the complex or not. In one dimensional proton spectra of Pu24T DNA, we have seen that the resonances of G2H8 and A3H8 protons were seen as individual peak at D/N = 2.0 and they were also present as same at D/N = 0.0. Further, we didn't observe any loss of cross peak between them in NOESY spectra at D/N = 2.0 (Figure 4.11). Likewise for G20 and G23 H8 protons, their resonances were observed at D/N = 2.0, but due to overlapping of peaks we couldn't found proper sequential connectivities for A21 and A22 bases. In case of G11 and A12, their H8 proton resonances were merged at D/N

**Table 4.6. Proton chemical shift table for Pu24T-c-myc DNA and Quercetin complex at D/N = 2.0**

	<b>NH/H1</b>	<b>H8/H6</b>	<b>H1'</b>	<b>H2'</b>	<b>H2''</b>	<b>H3'</b>	<b>H71/72/73</b>
<b>T1</b>							
<b>G2</b>		<b>8.057</b>					
<b>A3</b>		<b>7.684</b>	<b>6.471</b>	<b>2.894</b>	<b>2.817</b>		
<b>G4</b>	<b>11.758</b>	<b>8.014</b>					
<b>G5</b>	<b>11.206</b>	<b>7.957</b>	<b>5.861</b>				
<b>G6</b>	<b>10.920</b>	<b>7.894</b>	<b>5.761</b>	<b>2.481</b>	<b>2.641</b>	<b>4.048</b>	
<b>T7</b>		<b>7.915</b>	<b>5.508</b>				
<b>G8</b>	<b>11.510</b>	<b>7.718</b>	<b>6.328</b>				
<b>G9</b>	<b>11.529</b>	<b>7.212</b>	<b>5.891</b>	<b>2.534</b>	<b>2.077</b>	<b>4.540</b>	
<b>T10</b>		<b>7.392</b>					<b>1.837</b>
<b>G11</b>	<b>11.529</b>	<b>7.502</b>	<b>5.463</b>	<b>2.660</b>	<b>2.307</b>	<b>4.167</b>	
<b>A12</b>		<b>7.555</b>	<b>6.150</b>	<b>2.627</b>	<b>2.875</b>	<b>4.240</b>	
<b>G13</b>	<b>11.675</b>	<b>7.93</b>	<b>6.549</b>	<b>2.708</b>	<b>2.523</b>	<b>4.044</b>	
<b>G14</b>	<b>11.212</b>	<b>7.760</b>	<b>5.887</b>	<b>2.536</b>	<b>2.002</b>	<b>4.538</b>	
<b>G15</b>	<b>11.161</b>	<b>7.232</b>	<b>5.946</b>				
<b>T16</b>							
<b>G17</b>	<b>11.133</b>	<b>7.861</b>	<b>5.704</b>				
<b>G18</b>	<b>11.422</b>	<b>7.646</b>	<b>5.955</b>	<b>2.395</b>	<b>2.716</b>	<b>4.178</b>	
<b>G19</b>	<b>10.731</b>	<b>7.464</b>	<b>5.596</b>				
<b>G20</b>	<b>10.852</b>	<b>7.182</b>	<b>5.786</b>				
<b>A21</b>		<b>8.122</b>	<b>6.381</b>				
<b>A22</b>		<b>8.151</b>	<b>6.205</b>	<b>2.345</b>	<b>2.522</b>	<b>3.542</b>	
<b>G23</b>		<b>7.539</b>	<b>5.712</b>				
<b>G24</b>	<b>11.506</b>	<b>7.561</b>	<b>5.930</b>				

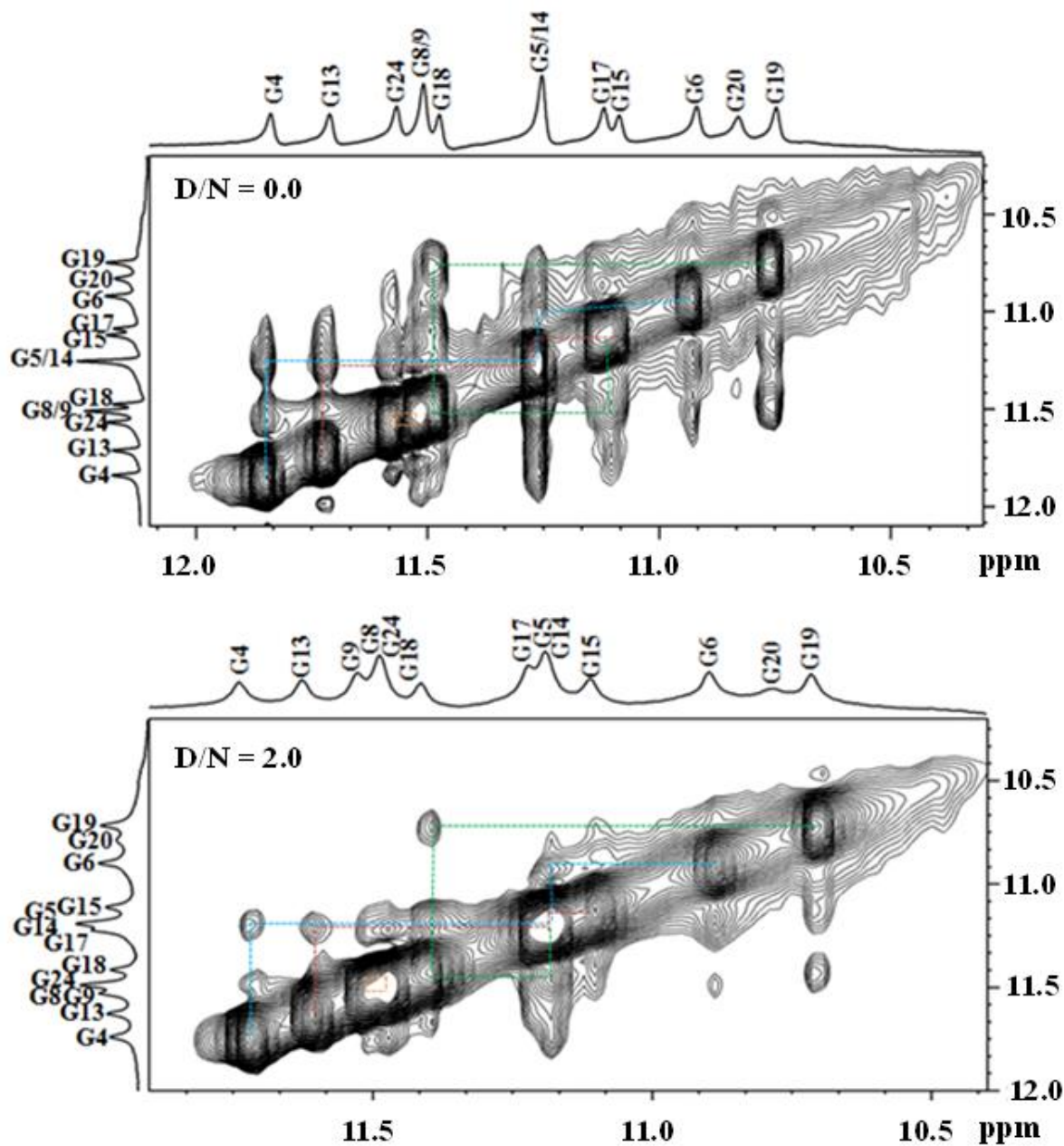


Figure 4.11. Portion of NOESY spectrum of Quercetin - Pu24T complex showing NH-NH NOEs between adjacent G-tetrads at 298 K at D/N ratio = 0.0 (top) and 2.0 (bottom). (Dash lines show the sequential connectivity).

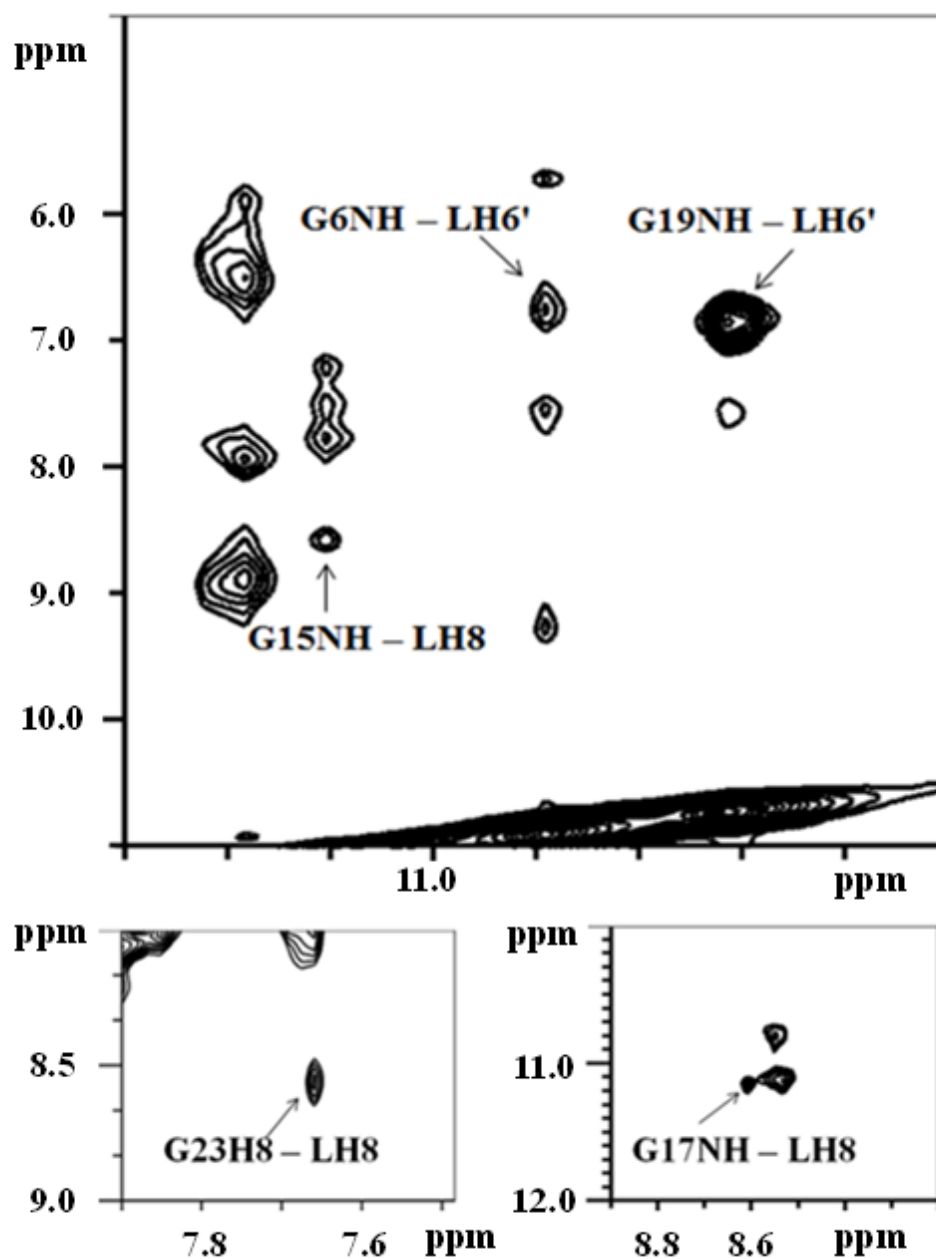


Figure 4.12. NOE cross peaks of Quercetin - Pu24T complex at D/N = 2.0. Various regions of NOESY spectrum showing intermolecular cross-peaks between Quercetin and Pu24T DNA.

**Table 4.7. Relative intensity of intermolecular NOE connectivity between Pu24T and Quercetin in complex at D/N=2.0 from NOESY spectra at 298K**

<b>S.No.</b>	<b>NOE restraints</b>	<b>Input Range</b>	<b>Input Distance</b>	<b>Output Distance (2N6C)</b>
<b>1</b>	<b>A22:H8-Que:H8</b>	<b>m/w</b>	<b>3.5</b>	<b>4.8</b>
<b>2</b>	<b>G13:H8-Que:H8</b>	<b>m</b>	<b>4.9</b>	<b>5.3</b>
<b>3</b>	<b>G19:H8-Que:H8</b>	<b>s</b>	<b>4.3</b>	<b>5.4</b>
<b>4</b>	<b>G23:H8-Que:H8</b>	<b>ss</b>	<b>2.1</b>	<b>3.3</b>
<b>5</b>	<b>G2:H8-Que:H8</b>	<b>m</b>	<b>3.1</b>	<b>3.8</b>
<b>6</b>	<b>G6:H8-Que:H8</b>	<b>m</b>	<b>4.2</b>	<b>5.1</b>
<b>7</b>	<b>G17:NH-Que:H8</b>	<b>ss</b>	<b>2.8</b>	<b>3.5</b>
<b>8</b>	<b>G15:NH-Que:H8</b>	<b>s</b>	<b>3.0</b>	<b>3.6</b>
<b>9</b>	<b>G19:NH-Que:H6'</b>	<b>m</b>	<b>4.8</b>	<b>5.1</b>
<b>10</b>	<b>G13:H1'-Que:H6'</b>	<b>m</b>	<b>3.4</b>	<b>4.1</b>
<b>11</b>	<b>G24:H1'-Que:H6'</b>	<b>m</b>	<b>3.3</b>	<b>4.1</b>
<b>12</b>	<b>G6NH-Que:H6'</b>	<b>s</b>	<b>2.8</b>	<b>3.2</b>
<b>13</b>	<b>G4:H8-Que:H6'</b>	<b>m</b>	<b>3.1</b>	<b>3.7</b>

= 0.0, however, these resonances were found as individual peaks at D/N = 2.0. These observations could suggest that the loop interactions were not significantly disrupted in the complex formation.

Thus, the observation of major number of NOEs to upper and bottom G-tetrad of Pu24T G-quadruplex DNA with Quercetin H6' (LH6') and H8 (LH8) protons suggested the position the edges of the benzopyran ring of ligand in between the base. It could be estimated that Quercetin molecule also orients itself in such a way that it achieved better interaction at both the terminal G-tetrads of Pu24T DNA. Concisely, all of the results indicate the binding of Quercetin to two sites on Pu24T by end-stacking above and below the terminal G-tetrads via the end stacking mode. Therefore, we further investigated the formation of Quercetin – Pu24T complex by performing restrained molecular dynamic simulations as mentioned in next section.

#### **4.2.5.3 Restrained molecular dynamics Studies**

Restrained molecular dynamic simulation is an approach in which NMR chemical shifts are incorporated as restraints in a way similar to that obtained in standard NMR structure calculations and the system is subjected to simulate. It will provide the energetic contribution of the complex formation and give a better understanding of the structure of this complex. Therefore, with the observed intermolecular NOEs, we have calculated the structure of Pu24T G-quadruplex DNA complexed with Quercetin at D/N = 2.0 via performing restrained molecular dynamics simulation on Discovery Studio Client 3.5 (Accelrys, San Diego, CA). Quercetin was placed above the 5' G-tetrad and below the 3' G-tetrad in an orientation that satisfied all of the NOE restraints. As previously mentioned, the cross peak intensities were used in a qualitative manner, in which the distances were approximately 1.8 - 2.5, 2.5 - 3.0, 3.0 - 3.5, 3.5 - 4.0, and 4.0 - 5.0 Å for strong intense (ss), strong (s) medium (m) and weak (w) and very weak intense (vw) peaks, respectively (Table 4.7). After the production runs of 100 ns, the lowest energy model (Figure 4.13a) has potential energy of -18685.50 kcal/mol (Table 4.8). An ensemble of ten conformations with the lowest potential energy were superimposed (Figure 4.13b) and assessment of refined structure in terms of its energetic parameters was mentioned in table 4.9. The distances obtained from rMD simulation results favored the experimental NOE distances (Table 4.7). The rMD simulation of Quercetin-Pu24T DNA complex showed that both the Quercetin molecules displayed dynamic behavior over the run of 100 ns but they remained bound to their respective G-

*Table 4.8. Energy terms (kcal mol<sup>-1</sup>) for starting structure and final rMD structure*

<b>Structure</b>	<b>Potential energy (kcal mol<sup>-1</sup>)</b>	<b>Van der Waals Energy (kcal mol<sup>-1</sup>)</b>	<b>Electrostatic Energy (kcal mol<sup>-1</sup>)</b>
<b>Initial</b>	4.46 × 10 <sup>11</sup>	1664.30	-15813.47
<b>Final</b>	-18685.50	-14891.95	-14908.78

*Table 4.9. Statistics of the solution structure of Quercetin- Pu24T complex*

<b>NMR distance</b>	<b>Nucleic acid/ligand</b>
<b>Distance restraints</b>	
Total NOE	428
Intra-residue	317
Inter-residue	98
NOE- derived distance restraints	13
Hydrogen bonds	154
<b>Structural Statistics</b>	
<b>Violations (mean and SD)</b>	
Number (> 0.2 Å)	0.0
Maximum violations (Å)	0.158 ± 0.026
Distance constraints (Å)	0.044 ± 0.019
Dihedral angle constraints (°)	0.090 ± 0.10
<b>Average pairwise r.m.s.d.** (Å)</b>	
All nucleotides	0.9976 ± 0.11
All heavy atoms	0.5964 ± 0.16

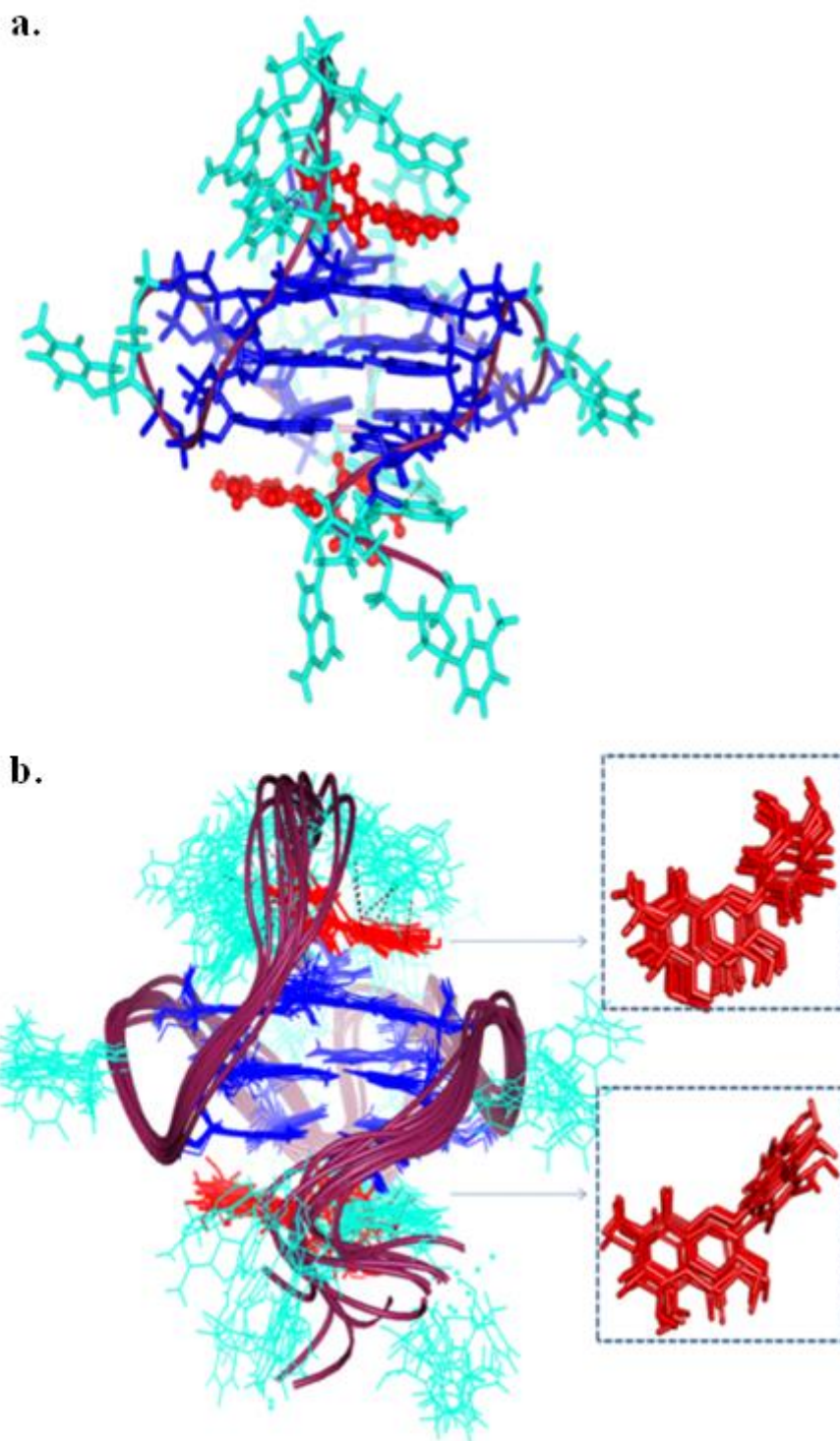


**Figure 4.13. (a-b) Quercetin and Pu24T complex at  $D/N = 2.0$  (a) Lowest potential energy model of the complex after rMD simulation. Black dashes showing hydrogen bond formed between Quercetin (red) and Pu24T DNA. All the three G-tetrads are shown in blue and rest nucleotides are shown in cyan color, DNA backbone is shown in worm-representation. (b) Ensemble of ten lowest energy structures after restrained molecular dynamics simulation (PDB Code: 2N6C)**

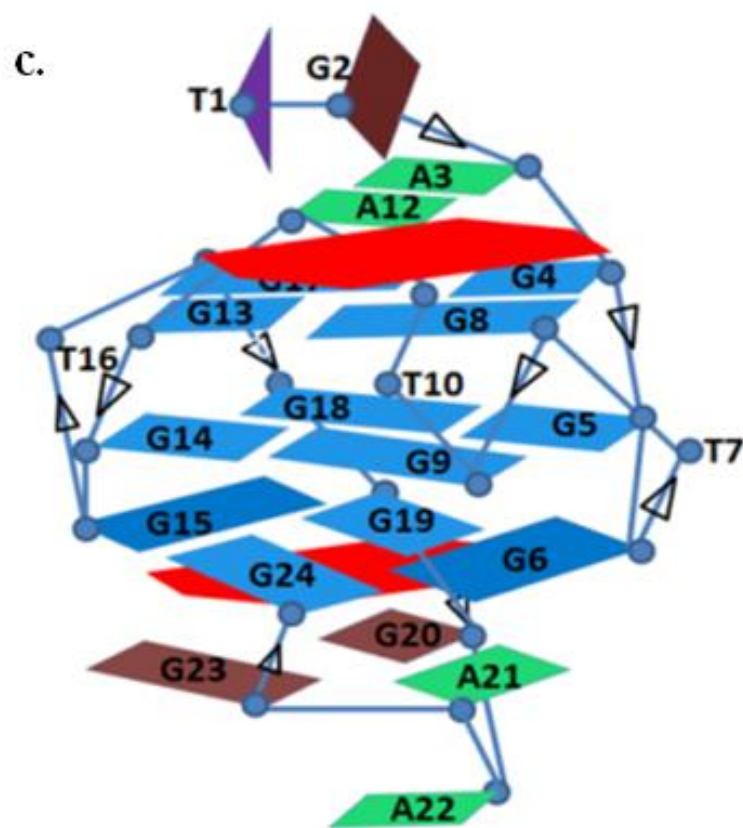


*Figure 4.13. (c) Schematic representation showing Quercetin (red) stacking at 5' G-tetrad and the 3' G-tetrad of Pu24T G-quadruplex DNA.*

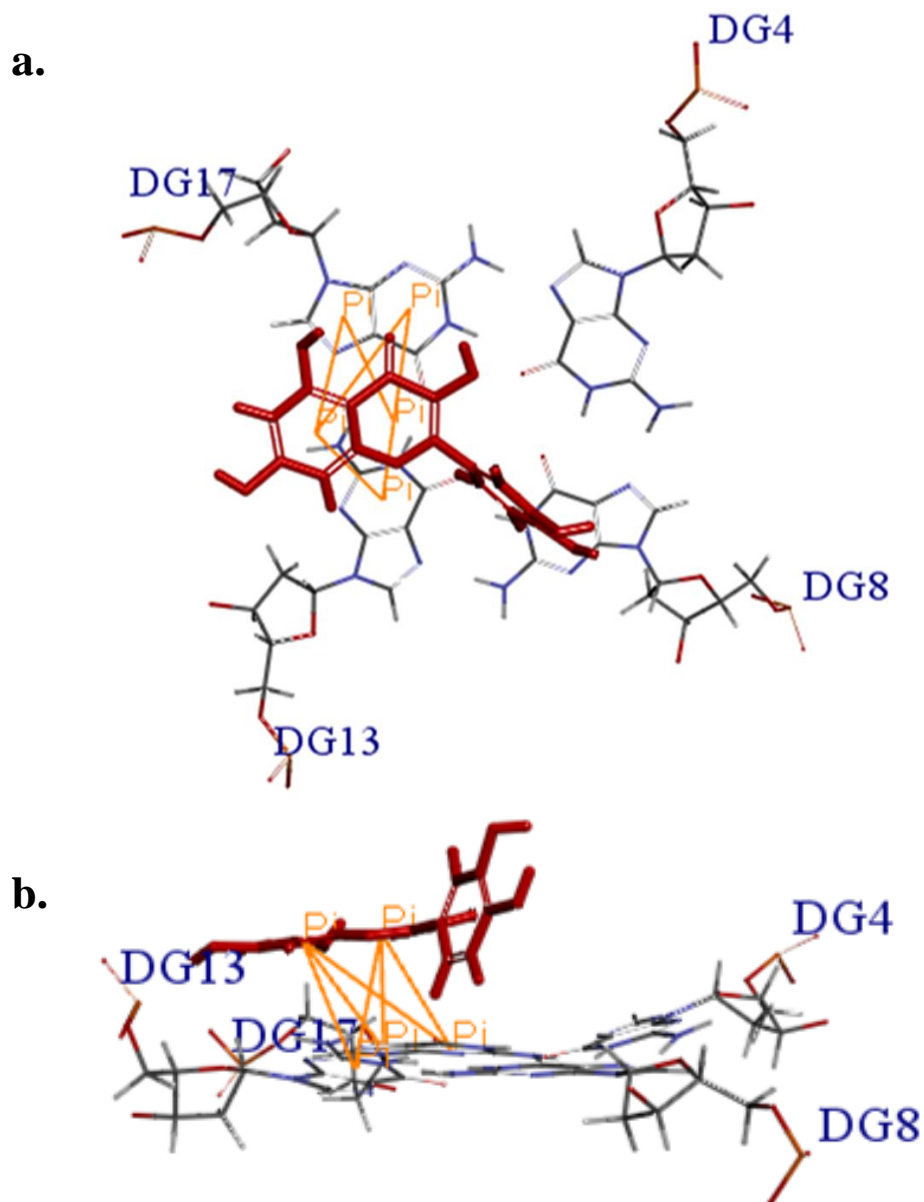


*Figure 4.14. Quercetin interacting with Pu24T G-quadruplex DNA via  $\pi$ - $\pi$  stacking interaction with 5' G-tetrad (a) top view (b) side view(Orange coloured lines showing  $\pi$  bonds).*

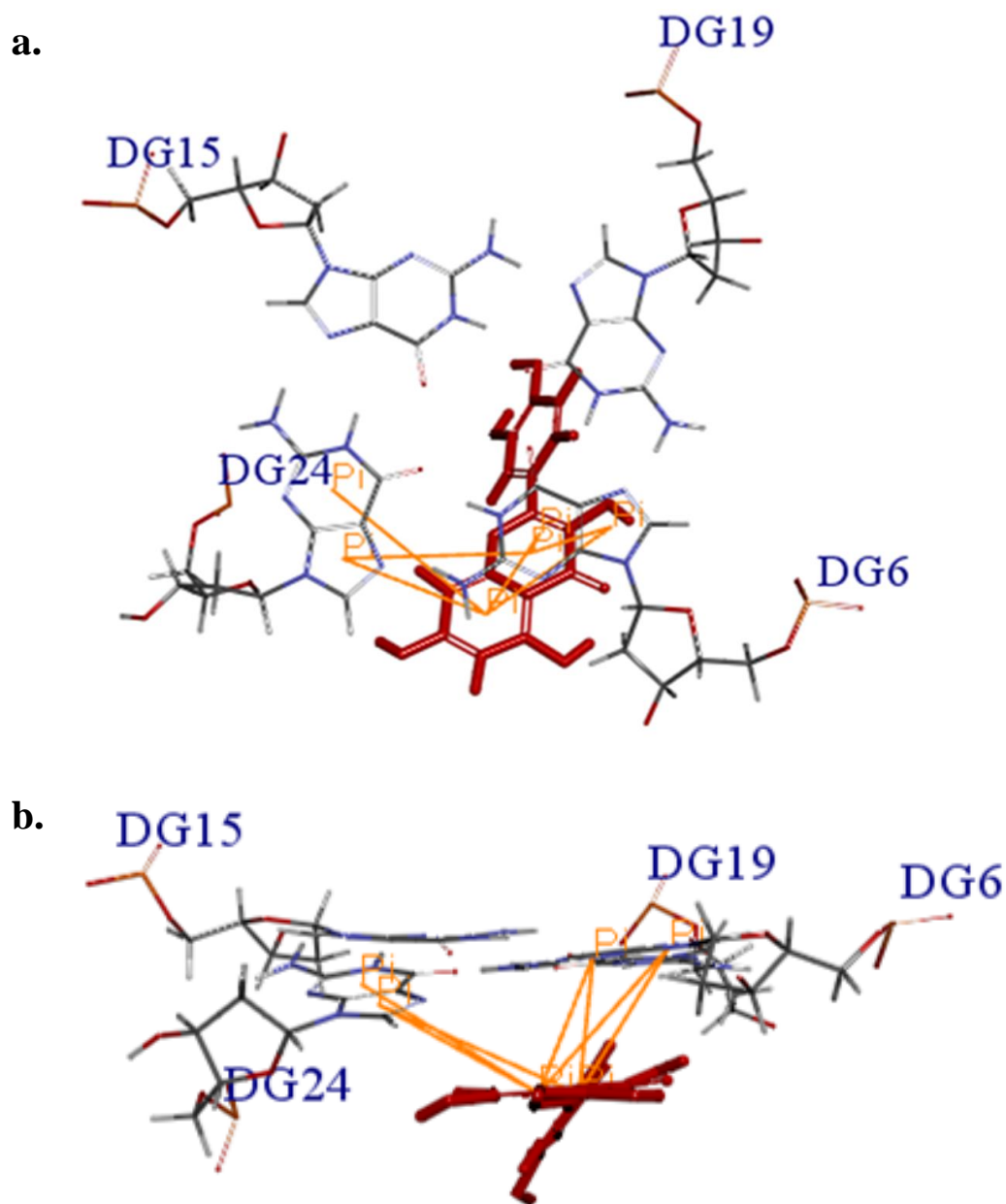


*Figure 4.15. Quercetin interacting with Pu24T G-quadruplex DNA via  $\pi$ - $\pi$  stacking interaction with 3' G-tetrad (a) top view (b) side view (Orange coloured lines showing  $\pi$  bonds).*

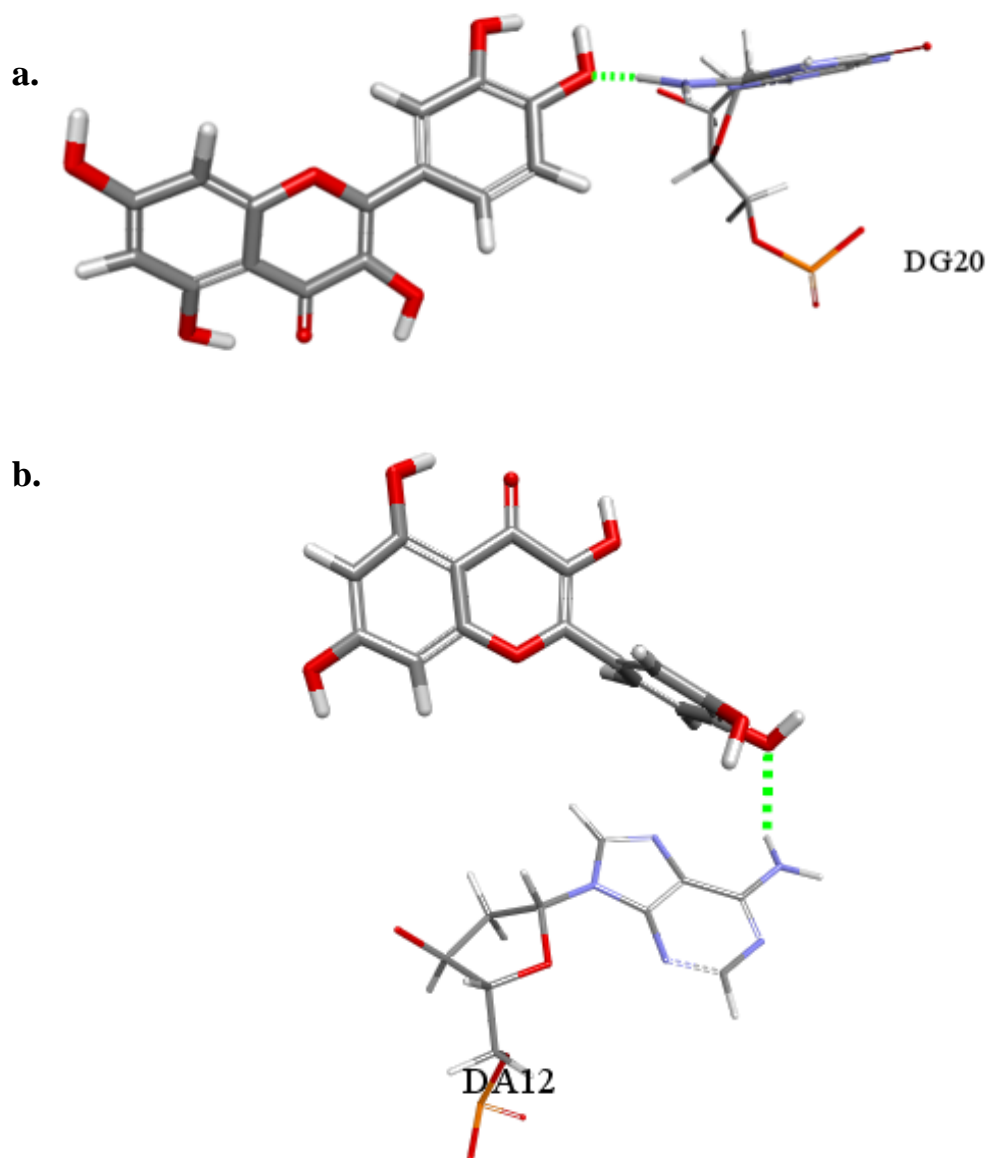


*Figure 4.16. Quercetin interacting with Pu24T G-quadruplex DNA by formation of hydrogen bonds with (a) G-20 (b) A12 (Green coloured dashed lines showing hydrogen bonds).*

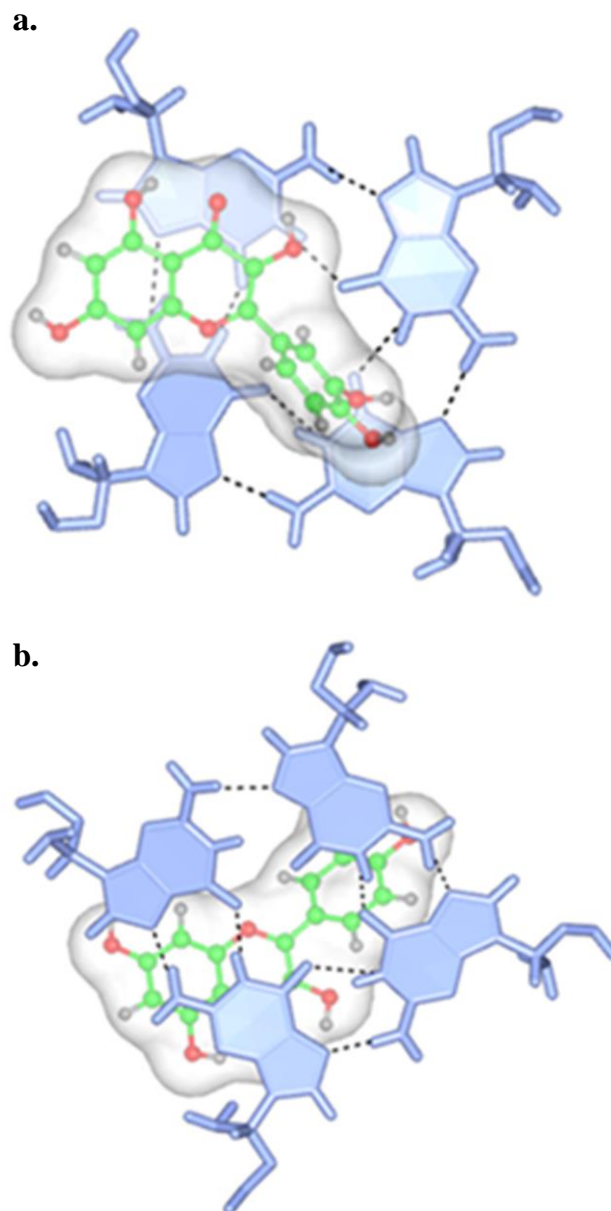


*Figure 4.17. Quercetin interacting with Pu24T c-myc G-quadruplex DNA by stacking (a) above the top G-tetrad (b) below the bottom G-tetrad.*

tetrads. This simulation also revealed that Quercetin stacks over G-tetrad with its A ring and C ring parallel and in between G17 and G13 at 5' end while G24 and G6 at 3' end via  $\pi - \pi$  stacking interactions (Figure 4.14, 4.15, 4.16). Also, the oxygen atom of 4'OH of Quercetin forms hydrogen bond with A12 and G20 bases at 5' end and 3' G-tetrads respectively (Figure 4.16). This is in agreement with the changes observed in resonances for these bases in the imino and base region of 1D NMR spectra. Thus, it may be inferred that observed the strong binding affinity of Quercetin with Pu24T could be due to the aromatic planar shape of Quercetin that enables it to easily end- stacks at G-tetrads of Pu24T G-quadruplex DNA and stabilize its structure (Figure 4.13c, 4.17).

After this part of work, we have explored the cytotoxic effects of Quercetin on human cervical carcinoma (HeLa) cancer cells and in vitro stabilization of c-myc G-quadruplex DNA by Quercetin as mentioned in next section.

## **4.2.4 Assessment of biological activity of Quercetin**

### **4.2.4.1 Evaluation of cytotoxicity and mechanism of action**

We have performed MTT assay to determine the cytotoxicity of Quercetin in HeLa cells (Figure 4.18a), that shows its potential to inhibit cell growth with an  $IC_{50}$  value of 4.0  $\mu$ M. This is in agreement with previous study that shows Quercetin inhibits survival of HeLa cell with  $EC_{50} = 7.3 \mu$ M.<sup>[35]</sup> Moreover, cytotoxicity of Quercetin was also examined on normal cell line (HEK) by employing MTT assay (Figure 4.18b). Our results suggested that Quercetin shows much weaker cytotoxic effect on HEK cell with over thirty-fold higher  $IC_{50}$  value of  $\sim 0.12$  mM as compared to HeLa cell. One of the major hallmarks of cancer is the interruption in the apoptotic pathway<sup>[36]</sup> and anti-cancer agents induces apoptosis to overcome this interruption. In congruence with previous reports,<sup>[37-38]</sup> we have also observed that Quercetin induces apoptosis in HeLa cells in a dose-dependent as well as in a time-dependent manner. It also shows typical apoptotic morphological changes in the cell nucleus like membrane blebbing and condensation of chromatin (Figure 4.18 c-d). As previous studies demonstrated that cellular uptake of Quercetin occurs via various ways for example, in nerve cell line (SH-SY5Y), it was uptaken by mitochondria<sup>[39]</sup>, while in intestinal cell line (Caco-2), Quercetin glucoside was transported via sodium-dependent glucose transporter SGLT1.<sup>[40]</sup> In hepatocytes, it was passively diffused in cells and gets accumulated in cytoplasm as well as in nucleus; however, it was detected in cytoplasm for short time and finally get accumulated in nucleus.<sup>[41-42]</sup> Owing to these studies, we have also determined the

localization of Quercetin inside cell nucleus. It was examined by utilizing its auto fluorescence property and confirmed by co-localization with DAPI. As DAPI is known to bind nucleus thus, upon colocalization it could be inferred that Quercetin also goes inside cell nucleus (Figure 4.19). Further to substantiate the effect of Quercetin on transcriptional regulation of c-myc gene, we have performed semi – quantitative reverse transcriptase PCR as mentioned in next sub- section.

#### **4.2.4.2 Semi quantitative reverse transcriptase PCR**

Reverse Transcription-Polymerase Chain Reaction (RT-PCR) is a technique of choice for monitoring the level of gene expression between control and treated cells. We have employed semi - quantitative RT-PCR to understand the effect of Quercetin on regulation of c-myc gene. This enabled us to semi-quantitate the expression of c-myc gene relative to a constitutively expressed housekeeping gene,  $\beta$ -actin. A significant reduction in the level of c-myc mRNA in a dose-dependent manner (Figure 4.20a) was observed and as it is clearly seen that  $\beta$ -actin mRNA is expressed likewise in both the control as well as in treated cells, thus, the reduction of mRNA level could be specific to c-myc gene. Moreover, to confirm this reduction of c-myc gene expression is due to the stabilization of G-quadruplex structure, we have performed PCR stop assay as mentioned in next sub section.

#### **4.2.4.3 PCR stop assay**

*Taq* Polymerase requires single stranded DNA in order to amplify the template DNA sequence. However, its activity could be hindered due to presence of secondary structure in template DNA. These secondary structures may be formed by G-rich sequences that folds into intramolecular G-quadruplex topology. Small molecules that could stabilize these G-quadruplex structures could lead to arrest of DNA synthesis process. In our study, we have employed this fact and validated the stabilization of G-quadruplex structure by binding of Quercetin. Pu24T DNA sequence was incubated with increasing concentration of Quercetin and PCR is performed. With increase in Quercetin concentration, a significant decrease in the intensity of PCR products was observed. This result indicates that Quercetin stabilizes c-myc G-quadruplex DNA and thus blocks *Taq* Polymerase activity to amplify DNA (Figure 4.20b). Furthermore, to confirm the stabilizing effect of binding of Quercetin on regulation of translational activity of c-myc gene we have performed luciferase activity assay as mentioned in next sub- section.

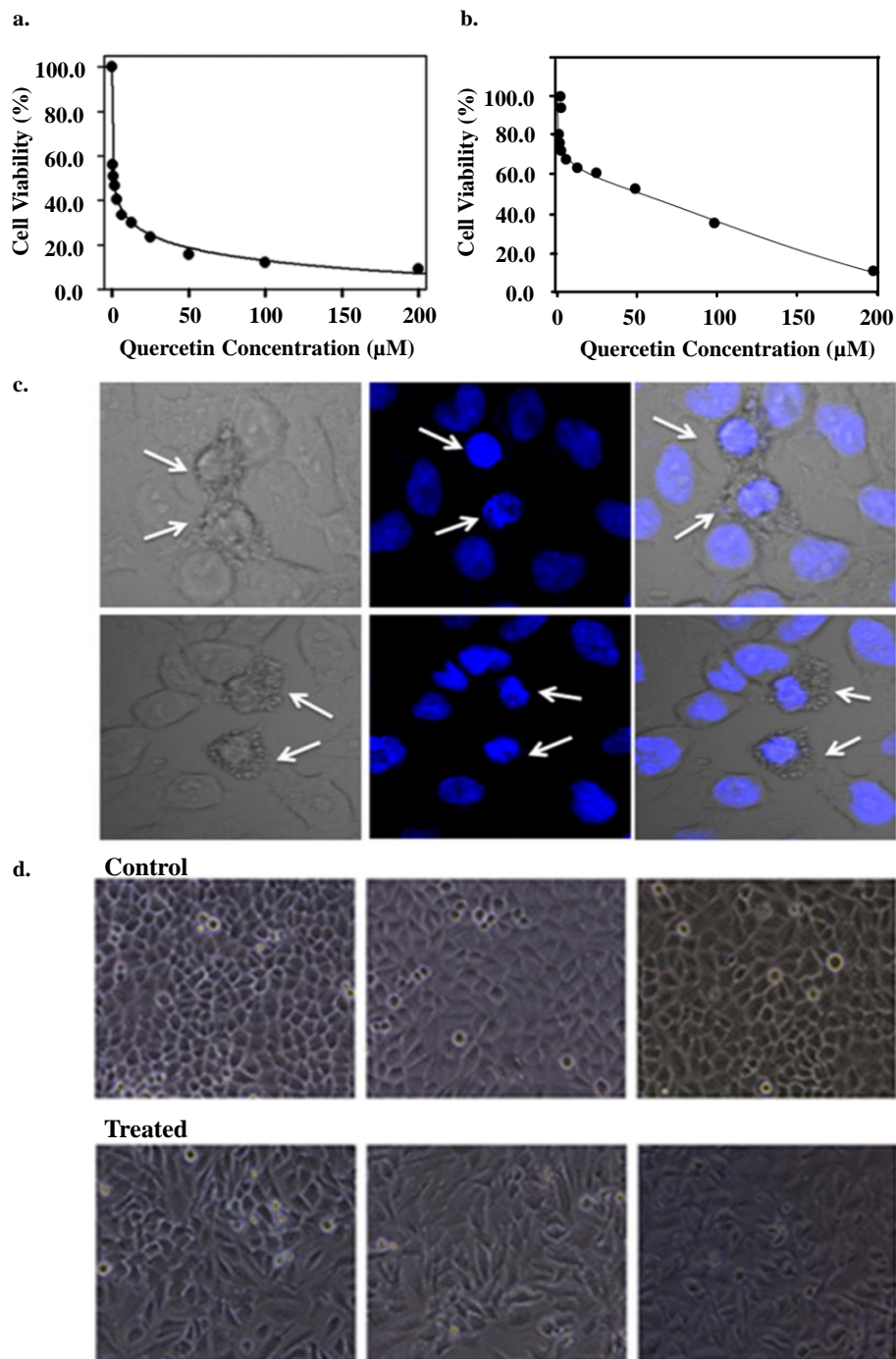
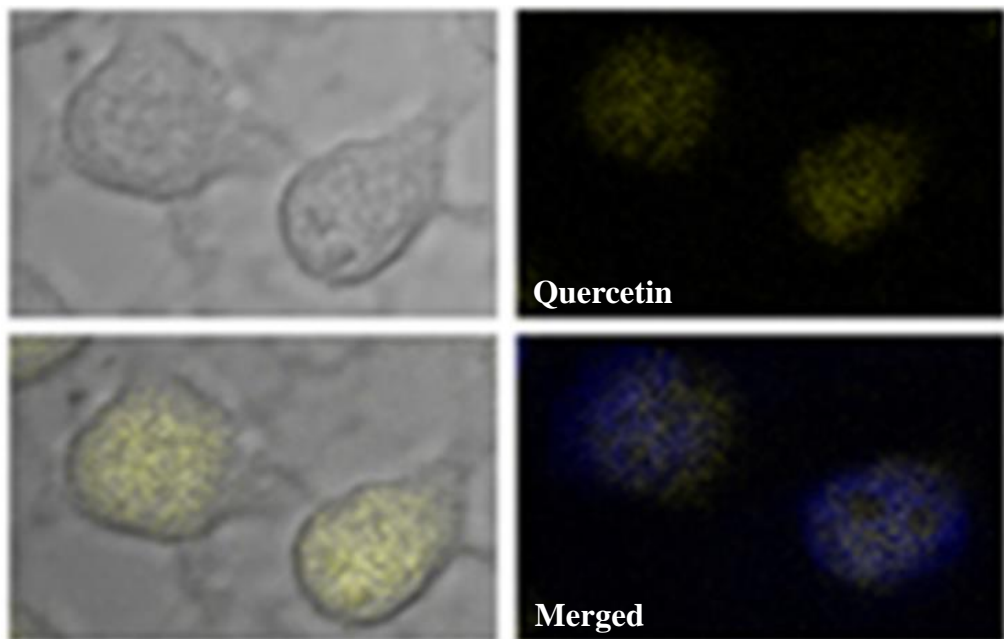


**Figure 4.18.** Cell viability was measured by MTT assay after 48 h (a) HeLa cells (b) HEK cells (c) Morphological changes observed under confocal microscope for Quercetin (100  $\mu\text{M}$  for 4 hr) treated HeLa cells followed by DAPI staining (Arrow indicates the apoptotic cells) (d) Morphological changes in Quercetin treated HeLa cells as compared to control cells monitored under phase contrast microscope.

**a. Treated**



**b. Control**

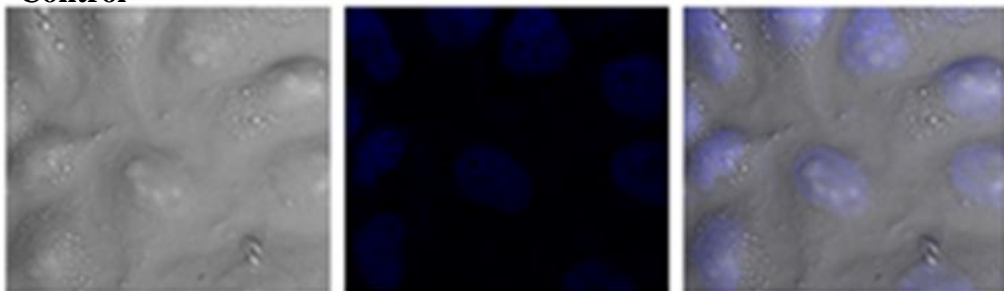


*Figure 4.19. Confocal images of control HeLa cells stained with DAPI for monitoring colocalization of Quercetin inside nucleus of the cell detected by its autofluorescence (a) Quercetin treated cells (b) Control cells.*

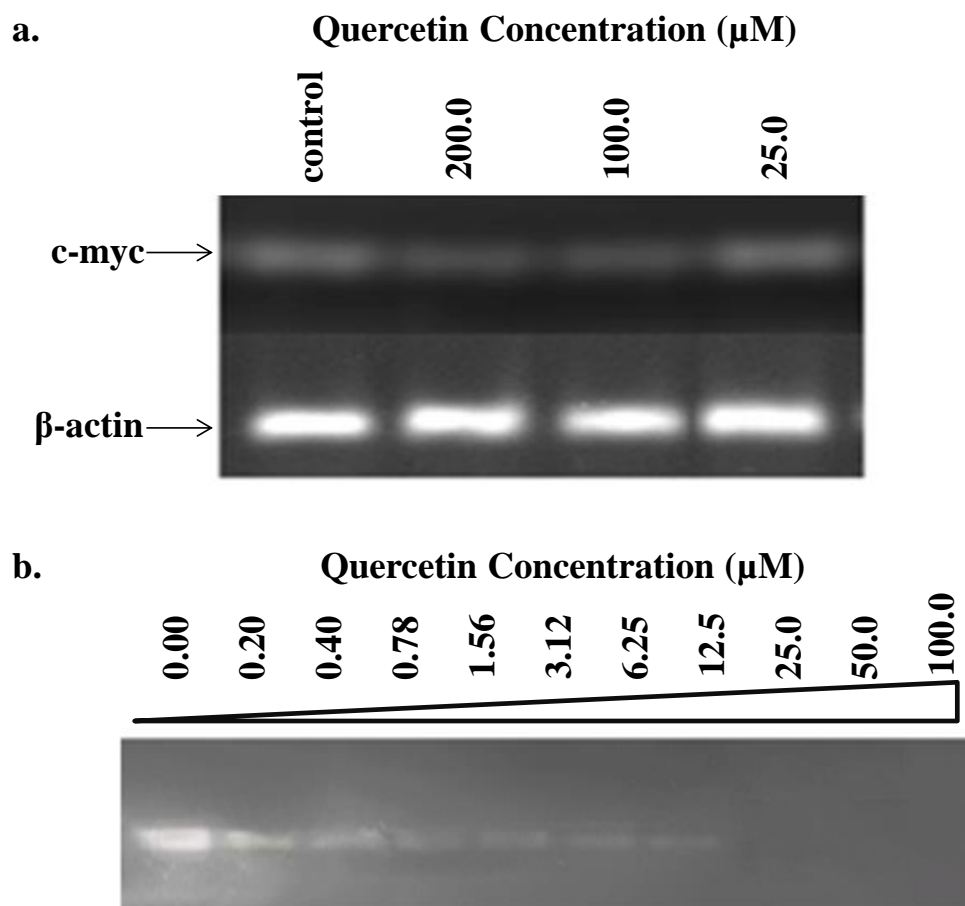


*Figure 4.20. (a) Representative semi-quantitative RT-PCR analysis.  $\beta$ -actin was used as internal control (b) Polymerase stop assay for determination of the effect of Quercetin on stabilization of Pu24T G-quadruplex DNA with increasing concentrations of Quercetin as shown.*

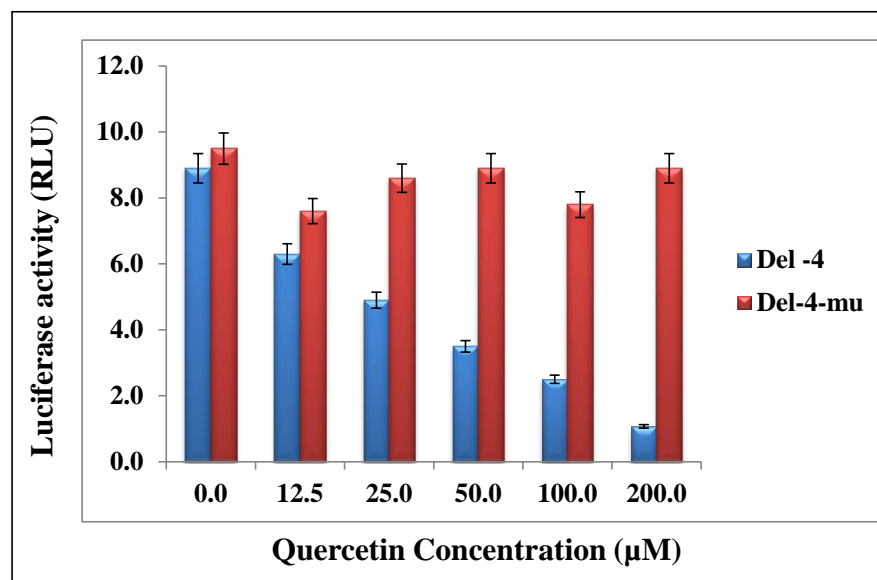


*Figure 4.21. Luciferase activity assay for monitoring the effect of Quercetin on c-MYC promoter activity.*

#### 4.2.4.4 Luciferase assay

We have performed Luciferase activity assay by transfecting Del - 4 (wt) and Del - 4 - mu plasmids into HeLa cells. ("Del - 4" plasmid that contains 850 bp of c-MYC promoter sequences in P1 and P2 in a luciferase reporter cassette and its variant "Del-4-mu" has specific base substitutions due to which, it is very unlikely that it forms G-quadruplex structure (gift from Dr. Shantanu Chowdhury). Reduction in luciferase activity was observed in dose dependent manner for wild promoter construct, however, , at the same concentrations, no trend in the change of luciferase activity was seen in cells transfected with plasmid containing mutant promoter. These results thus suggested that Quercetin inhibits the activity of c-MYC promoter by interacting and stabilizing G-quadruplex DNA structure (Figure 4.20).

#### 4.3 Conclusions

As it is well evident that flavonoids are beneficial to human health as they exhibit various activities including anti-cancer activity. In previous chapter, we have shown that flavonoids bind to G-quadruplex structure formed by human telomeric DNA sequence; therefore, in continuation of it, in this chapter, we have examined the interaction of nine flavonoids with biologically relevant G-quadruplex DNA structure formed at promoter region of human c-myc gene (Pu24T). We have probed the interaction of flavonoids with the Pu24T DNA sequence forming G-quadruplex structure via fluorescence titration studies. Amongst all flavonoids used in this study, Quercetin was found to bind most effectively as it has highest binding affinity as well as specificity for Pu24T DNA sequence forming parallel G-quadruplex structure over other duplex and G- quadruplex structures. Further, thermodynamic and lifetime decay profiles of interaction of Quercetin with Pu24T DNA were used to deduce the thermodynamic parameters and mode of binding. Circular dichroism studies suggested that binding of Quercetin to Pu24T DNA sequence does not hampers G-quadruplex topology. Further, 1D and 2D proton NMR experiments were carried out to deduce the structure formed by Quercetin - Pu24T G quadruplex DNA. We believe that this is the first report for solution structure of Quercetin - c-myc G-quadruplex complex in which Quercetin stacks at 5' and 3' G-tetrads of Pu24T G-quadruplex DNA structure and stabilize it via  $\pi$ - $\pi$  stacking. Further, the biological activity of Quercetin was assessed in HeLa cells that showed its subcellular localization in nucleus. It inhibits the cell growth by inducing apoptosis and down-regulates c-myc gene expression in cancer cell. Furthermore, the

stabilization of G-quadruplex structure upon binding of Quercetin was validated by PCR stop assay that shows the inhibition of *Taq Polymerase* activity. Our study provides favorable evidences for the interaction of Quercetin with c-myc G-quadruplex DNA and its stabilization upon binding; and revealed the potential of flavonoid, Quercetin, as suitable candidate for anti-cancer therapeutics by down regulating the c-myc gene expression.

#### **4.4 Material and methods**

##### **4.4.1 Reagents and cell lines**

Luteolin, Quercetin, Rutin, Genistein, Kaempferol, Puerarin, Hesperidin, Myricetin, Daidzein were purchased from Sigma Aldrich Chemicals Ltd. These flavonoids were used without further purification. The solvents such as deuterium oxide, dimethyl sulphoxide (DMSO) and other reagents used for buffer preparation such as NaCl, KCl, NaH<sub>2</sub>PO<sub>4</sub>, Na<sub>2</sub>HPO<sub>4</sub>, KH<sub>2</sub>PO<sub>4</sub> and K<sub>2</sub>HPO<sub>4</sub> (HPLC Grade) were also purchased from Sigma Aldrich Chemicals Ltd. The stock solutions of flavonoids were prepared by dissolving them in DMSO and stored at the appropriate storage temperature. Calf thymus DNA (CT-DNA) as well as other oligonucleotide sequences such as

Pu24T-c-myc DNA (d-5'-TGAGGGTGGTGGAGGGTGGGGAAGG-3'),  
c-kit21up: (d-5' - CGGGCGGGCGCGAGGGAGGGG - 3') and

Tel7 (d-5'-T2AG3T-3') were purchased from Sigma Aldrich Chemicals Ltd. CT-DNA solution was prepared in the sodium phosphate buffer and its concentration was measured spectrophotometrically. For quadruplex formation, 100 µM of oligomers was dissolved in phosphate buffer (10 mM (K<sup>+</sup>), pH 7.0) with 100 mM KCl. For anti-parallel quadruplex formation, 100 µM of Tel7 oligomers were dissolved in buffer containing 70mM Na<sup>+</sup> ions. The oligomer was annealed by heating at 90°C for 5 mins, followed by overnight incubation at room temperature to allow gradual cooling. All the biophysical experiments were performed in the above mentioned buffer otherwise stated separately.

Human cervical carcinoma (HeLa) cell lines, Human embryonic kidney cell lines (HEK) were purchased from National Centre for Cell Science (NCCS), Pune, India. Growth media Minimum Essential Medium (MEM), Fetal bovine serum (FBS), Phosphate buffer saline (PBS), Antibiotic solution were purchased from Gibco. Cells-to-cDNA™ II Kit (Ambion) was purchased from Invitrogen. DAPI and other reagents for PCR reaction like primers, dNTPs, Taq Polymerase was also obtained from Sigma Aldrich Chemicals Ltd.

##### **4.4.2 Fluorescence titrations**

The fluorescence titration experiment was performed on Synergy™ H1 multi-mode microplate reader using 96-well microplates at 25°C. The excitation and emission wavelengths for flavonoids were obtained by performing their absorption and fluorescence scan diluted in potassium phosphate buffer. The readings were taken at emission wavelength of 435 nm, 535 nm, 416 nm, 405 nm, 423nm, 459 nm, 440 nm, 561 nm and 456 nm for Luteolin, Quercetin, RutinGenistein, Kaempferol, Puerarin, Hesperidin, Myricetin and Daidzein respectively, when excited at the wavelength of 380 nm, 375 nm, 360 nm, 269 nm, 373 nm, 305 nm, 390 nm, 369 nm and 305 nm. Each sample was tested in duplicates in 75 µL reaction volume at 25°C. The G-quadruplex DNA at a final concentration of 20 µM (4 µM for Kaempferol) was serially diluted; with the last well serve as blank (no DNA). A varied final concentration of CT-DNA (25-50 µM) was serially diluted; with the last well serve as blank (no DNA). Data were analyzed using SigmaPlot 12.0 software (Systat Software, Chicago, USA) according to the following equation and vertical lines shows standard error:

$$f = \frac{B_{max1} \times abs(x)}{kd1 \times abs(x)} + \frac{B_{max2} \times abs(x)}{kd2 \times abs(x)} \quad (1)$$

$B_{max}$  = maximum number of binding sites.

$K_d$  = equilibrium binding constant.

#### 4.4.3 Isothermal titration calorimetry experiment

The Isothermal titration calorimetry (ITC) measurements were performed at a constant temperature of 25°C using a MicroCal™ isothermal titration calorimeter iTC200 (Malvern). 2.30 µL of Quercetin was added at each step to the sample cell containing 25 µM G-quadruplex DNA. The heats of dilution were also determined by injecting same concentration of Quercetin into the same buffer. These heats of dilution were subtracted from the binding isotherm prior to fit the curve. The obtained thermogram was fitted with ‘two set of sites’ model and other thermodynamic parameters were also calculated using MicroCal Origin software.

#### 4.4.4 Time-resolved fluorescence measurements

Time resolved fluorescence decays were collected on a Time-Correlated Single-Photon Counting (TCSPC) Spectrofluorometer (Horiba). A fixed wavelength Nano LED was used as the excitation source (ex = 375 nm), and emission was detected at a different wavelength. The fluorescence emission of Quercetin and its complex with G-quadruplex

DNA were counted with a micro channel plate photo multiplier tube after passing through the monochromator and were further processed through a constant fraction discriminator (CFD), a time-to-amplitude converter (TAC) and a multi-channel analyser (MCA). The fluorescence decay was obtained and further analysed using DAS software, provided by FluoroLog-TCSPC instruments.

#### **4.4.5 Circular Dichroism**

The Circular Dichroism (CD) experiment was performed on a J-815 Spectropolarimeter (JASCO) equipped with peltier junction temperature controller. A quartz cuvette with 0.2 cm path length was used to record the spectra of samples containing 20  $\mu$ M G-quadruplex and increasing concentrations of flavonoids in 100 mM KCl, 10 mM phosphate buffer (K<sup>+</sup>) at pH 7.0. Spectra were recorded at 0.1 nm intervals from 200 nm to 350 nm with a 1 nm-slit width and averaged over three scans. Buffer CD spectra were subtracted from the CD spectra of DNA and the Drug-DNA complex.

#### **4.4.6 Nuclear Magnetic Resonance**

NMR experiments were conducted on AVANCE 500 MHz BioSpin International AG, Switzerland equipped with a 5 mm broad band inverse probe. NMR data were processed, integrated and analysed on Topspin (1.3 version) software. NMR samples were referenced with 3 - (Trimethylsilyl) propionic-2, 2, 3, 3-d<sub>4</sub> acid sodium salt (TSP). NMR studies were performed in H<sub>2</sub>O / D<sub>2</sub>O solvent at 9:1 ratio. Two-dimensional proton nuclear overhauser enhancement spectroscopy (NOESY)<sup>[43]</sup> experiments were performed at a temperature range of 298 K with 20 ppm spectral width. Spectra were recorded at variable mixing times ( $t_m$ ) of 400 ms, 350 ms and 300 ms. SPARKY was used to visualize the spectra and calculate 1H-1H NOE distances, which were used to restrain Quercetin-Pu24T- G-quadruplex DNA for restrained molecular dynamic simulation studies.

#### **4.4.7 Restrained molecular dynamics studies**

The structure of G-quadruplex Pu24T (PDB code: 2MGN<sup>[31]</sup>) was taken as the starting model and the required replacements, addition of residues were performed on Discovery studio 3.5 (Accelrys Inc., USA). G-quadruplex- the Quercetin complex was built by placing ligand above the 5' G-tetrad and below the 3' G-tetrad with orientations obtained from NOE experimental data. A set of NOE distances was introduced as restraints with a force constant of -10 kcal/mol/Å<sup>2</sup>. The drug-quadruplex system was typed in charmmforcefield<sup>[44]</sup> and

solvated with periodic TIP3P<sup>[45]</sup> orthorhombic water box containing 1720 water molecules. After minimization of complex, the conformations with the lowest potential energy were obtained by subjecting the quadruplex-ligand complex to simulated annealing restrained molecular dynamics with the whole set of NOE restraints. Standard dynamic cascade runs were performed on the complex in which the system was heated to 700 K followed by equilibration under constant pressure for 1ps. The production was done at 300 K for 100 ns in an NPT ensemble and long range electrostatics were treated with the Particle Mesh Ewald (PME) method<sup>[46]</sup> with a 14 Å cut-off radius counted the non-bonded distances. To constrain the motion of H-bonds, the SHAKE algorithm<sup>[47]</sup> was applied during the whole simulation runs.

#### 4.4.8 PCR stop assay

The assay was performed by employing modified protocol of previous study<sup>[48]</sup> using a test oligonucleotide c-myc Pu24T: d-(5'-TGAGGGTGGTGAGGGTGGGGAAGG-3') and a complementary oligonucleotide (RevPu24T): d-(5'-TTCTCGTCCTTCCCCA-3'). Assay reactions were performed in a final volume of 25 µL reaction mixture containing 10mM Tris buffer, 50 mM KCl, 10.0 pmol of each oligonucleotide, 2.5 units of Taq polymerase and the varied concentration of Quercetin from 0.00 µM to 100.00 µM. Reaction mixtures were incubated in Mastercycler Nexus Gradient (Eppendorf) with the following cycling conditions: 94 °C for 2 min, followed by 30 cycles of 94 °C for 30 s, 58 °C for 30 s, and 72 °C for 30 s. Amplified products were resolved on a 3% agarose gel in 1X TBE and stained with EtBr. Gel Image was analyzed on ImageQuant LAS 4000 (GE Healthcare).

#### 4.4.9 MTT assay

The cytotoxic effects of Quercetin was evaluated by performing MTT (3-(4, 5-dimethylthiazol-2-yl)-2, 5 diphenyltetrazolium bromide dye) assay. HeLa cells ( $5.0 \times 10^3$  cells/well) were seeded in a 96-well culture plate in triplicate and allowed to grow in MEM complete medium. Cells were treated with different concentrations (200 µM to 0.2 µM) of Quercetin with DMSO in control sample for 48 h at 37°C, 5% CO<sub>2</sub>. After incubation, 10 µL of MTT (5 mg/mL in PBS) was added to each well and incubated for additional four hours at 37°C to allow intracellular reduction of the soluble yellow MTT to insoluble purple formazan crystals. These crystals were dissolved by adding 100 µL of DMSO and absorbance was read at 570 nm using a microplatereader (Synergy™ H1 multi-mode microplate reader).

Concentration of Quercetin causing 50% reduction of cell viability was inhibitory concentration (IC<sub>50</sub> value), was determined by the using formula:

$$\% \textit{inhibition} = \frac{\textit{Control abs} - \textit{Sample abs}}{\textit{Control abs}} \times 100 \quad (2)$$

#### 4.4.10 Confocal microscopy for localization of Quercetin in cells

HeLa cells were grown on glass cover slip treated with 100 µM Quercetin for 4 h. Cells were fixed with 10% formalin and cover slip was mounted on glass slide. Simultaneously, one of the set of cells was processed for DAPI staining for 20 mins at room temperature in dark. Afterwards, the auto fluorescence of Quercetin in HeLa cells was monitored under confocal laser scanning microscope (Olympus 1x83, Japan) and data were analysed using Olympus Fluoview 4.2a software. Control cells were treated with DMSO and they do not exhibit auto-fluorescence, therefore they were not shown here. At least 10 fields per slide and three independent sets were examined.

#### 4.4.11 Semi-quantitative RT PCR analysis

HeLa cells were grown in T-25 tissue culture flask and incubated with various concentrations (200.0, 100.0, 50.0 and 25.0 µM) of Quercetin for 24h at 37 °C in humidified 5% CO<sub>2</sub> incubator. Total RNA was prepared from treated and control cells and cDNA was prepared using Cells-to-cDNA™ II Kit (Ambion) according to the manufacturer's protocol. Reverse transcriptase reaction was performed on Mastercycler Nexus Gradient (Eppendorf). The thermal cycling condition was programmed as 45 min at 45°C, 10 min at 95 °C for one single cycle. Semi – quantitative PCR was performed using gene specific primers with the following sequences: c-MYC (forward): 5'-CTTCTCTCCGTCCTCGGATTCT-3'; c-MYC (reverse): 5'-GAAGGTGATCCAGACTCTGACCTT-3'; β-actin (forward): 5'-GAGCTACGAGCTGCCTGAC-3'; β - actin (reverse): 5'-AGCACTGTGTTGGCGTACAG-3'.

#### 4.5 References

1. Sen D., Gilbert W. (1988), Formation of parallel four-stranded complexes by guanine-rich motifs in DNA and its implications for meiosis, *Nature*, 334, 364-366 (DOI: 10.1038/334364a0).

2. Wang Y., Patel D.J. (1993), Solution structure of the human telomeric repeat d[AG3(T2AG3)3] G-tetraplex, *Structure*, 1, 263-282 (DOI: 10.1016/0969-2126(93)90015-9).
3. Burge S., Parkinson G.N., Hazel P., Todd A.K., Neidle S. (2006), Quadruplex DNA: sequence, topology and structure, *Nucleic Acids Res.*, 34, 5402-5415 (DOI: 10.1093/nar/gkl655).
4. Yang D., Hurley L.H. (2006), Structure of the biologically relevant G-quadruplex in the c-MYC promoter, *Nucleosides Nucleotides Nucleic Acids*, 25, 951-968 (DOI: 10.1080/15257770600809913).
5. Cogoi S., Xodo L.E. (2006), G-quadruplex formation within the promoter of the KRAS proto-oncogene and its effect on transcription, *Nucleic Acids Res.*, 34, 2536-2549 (DOI: 10.1093/nar/gkl286).
6. Siddiqui-Jain A., Grand C.L., Bearss D.J., Hurley L.H. (2002), Direct evidence for a G-quadruplex in a promoter region and its targeting with a small molecule to repress c-MYC transcription, *Proc. Natl. Acad. Sci. U. S. A.*, 99, 11593-11598 (DOI: 10.1073/pnas.182256799).
7. Nasiri H.R., Bell N.M., McLuckie K.I., Husby J., Abell C., Neidle S., Balasubramanian S. (2014), Targeting a c-MYC G-quadruplex DNA with a fragment library, *Chem. Commun. (Camb)*, 50, 1704-1707 (DOI: 10.1039/c3cc48390h).
8. Neidle S., Thurston D.E. (2005), Chemical approaches to the discovery and development of cancer therapies, *Nat. Rev. Cancer*, 5, 285-296 (DOI: 10.1038/nrc1587).
9. Efferth T., Li P.C., Konkimalla V.S., Kaina B. (2007), From traditional Chinese medicine to rational cancer therapy, *Trends. Mol. Med.*, 13, 353-361 (DOI: 10.1016/j.molmed.2007.07.001).
10. Liu J.N., Deng R., Guo J.F., Zhou J.M., Feng G.K., Huang Z.S., Gu L.Q., Zeng Y.X., Zhu X.F. (2007), Inhibition of myc promoter and telomerase activity and induction of delayed apoptosis by SYUIQ-5, a novel G-quadruplex interactive agent in leukemia cells, *Leukemia*, 21, 1300-1302 (DOI: 10.1038/sj.leu.2404652).
11. Ma Y., Ou T.M., Hou J.Q., Lu Y.J., Tan J.H., Gu L.Q., Huang Z.S. (2008), 9-N-Substituted berberine derivatives: stabilization of G-quadruplex DNA and down-regulation of oncogene c-myc, *Bioorg. Med. Chem.*, 16, 7582-7591 (DOI: 10.1016/j.bmc.2008.07.029).
12. Fedoroff O.Y., Salazar M., Han H., Chemeris V.V., Kerwin S.M., Hurley L.H. (1998), NMR-Based model of a telomerase-inhibiting compound bound to G-quadruplex DNA, *Biochemistry*, 37, 12367-12374 (DOI: 10.1021/bi981330n).

13. Carini J.P., Klamt F., Bassani V.L. (2014), Flavonoids from *Achyrocline satureioides*: promising biomolecules for anticancer therapy, *RSC Adv.*, 4, 3131 (DOI: 10.1039/c3ra43627f).
14. Kuntz S., Wenzel U., Daniel H. (1999), Comparative analysis of the effects of flavonoids on proliferation, cytotoxicity, and apoptosis in human colon cancer cell lines, *Eur. J. Nutr.*, 38, 133-142 (DOI: 10.1007/s003940050054).
15. Yang H., Zhong H.J., Leung K.H., Chan D.S., Ma V.P., Fu W.C., Nanjunda R., Wilson W.D., Ma D.L., Leung C.H. (2013), Structure-based design of flavone derivatives as c-myc oncogene down-regulators, *Eur. J. Pharm. Sci.*, 48, 130-141 (DOI: 10.1016/j.ejps.2012.10.010).
16. Tawani A., Kumar A. (2015), Structural Insight into the interaction of Flavonoids with Human Telomeric Sequence, *Sci. Rep.*, 5, 17574 (DOI: 10.1038/srep17574).
17. Burda S., Oleszek W. (2001), Antioxidant and antiradical activities of flavonoids, *J. Agric. Food Chem.*, 49, 2774-2779 (DOI: 10.1021/jf001413m).
18. Woolfe G.J., Thistlethwaite P.J. (1981), Direct observation of excited state intramolecular proton transfer kinetics in 3-hydroxyflavone, *J. Am. Chem. Soc.*, 103, 6916-6923 (DOI: 10.1021/ja00413a026).
19. Kumar S., Pandey A.K. (2013), Chemistry and Biological Activities of Flavonoids: An Overview, *Scientific World J.*, 2013, 16 (DOI: 10.1155/2013/162750).
20. Rice-Evans C.A., Miller N.J., Bolwell P.G., Bramley P.M., Pridham J.B. (1995), The relative antioxidant activities of plant-derived polyphenolic flavonoids, *Free Radic. Res.*, 22, 375-383 (DOI: 10.3109/10715769509145649).
21. Sroka Z. (2005), Antioxidative and antiradical properties of plant phenolics, *Z. Naturforsch. C.*, 60, 833-843 (DOI: 10.1515/znc-2005-11-1204).
22. Wang Z., Cui M., Song F., Lu L., Liu Z., Liu S. (2008), Evaluation of Flavonoids Binding to DNA Duplexes by Electrospray Ionization Mass Spectrometry, *J. Am. Soc. Mass Spectrom.*, 19, 914-922 (DOI: 10.1016/j.jasms.2008.04.018).
23. Ragazzon P.A., Iley J., Missailidis S. (2009), Structure-activity studies of the binding of the flavonoid scaffold to DNA, *Anticancer Res.*, 29, 2285-2293.
24. Balagurumoorthy P., Brahmachari S.K. (1994), Structure and stability of human telomeric sequence, *J. Biol. Chem.*, 269, 21858-21869).
25. Wei C., Wang J., Zhang M. (2010), Spectroscopic study on the binding of porphyrins to (G(4)T(4)G(4))<sub>4</sub> parallel G-quadruplex, *Biophys. Chem.*, 148, 51-55 (DOI: 10.1016/j.bpc.2010.02.009).

26. Tysoe S.A., Morgan R.J., Baker A.D., Streckas T.C. (1993), Spectroscopic investigation of differential binding modes of .DELTA.- and .LAMBDA.-Ru(bpy)<sub>2</sub>(ppz)<sub>2</sub><sup>+</sup> with calf thymus DNA, *J. Phys. Chem.*, 97, 1707-1711 (DOI: 10.1021/j100110a038).
27. Kypr J., Kejnovská I., Renčíuk D., Vorlíčková M. (2009), Circular dichroism and conformational polymorphism of DNA, *Nucleic Acids Res.*, 37, 1713-1725 (DOI: 10.1093/nar/gkp026).
28. Ranjan N., Andreasen K.F., Kumar S., Hyde-Volpe D., Arya D.P. (2010), Aminoglycoside binding to *Oxytricha nova* telomeric DNA, *Biochemistry*, 49, 9891-9903 (DOI: 10.1021/bi101517e).
29. Phan A.T., Kuryavyi V., Gaw H.Y., Patel D.J. (2005), Small-molecule interaction with a five-guanine-tract G-quadruplex structure from the human MYC promoter, *Nat. Chem. Biol.*, 1, 167-173 (DOI: 10.1038/nchembio723).
30. Wuthrich K. (1986), NMR of Proteins and Nucleic Acids, *Wiley*, (ISBN: 978-0-471-82893-8).
31. Chung W.J., Heddi B., Hamon F., Teulade-Fichou M.P., Phan A.T. (2014), Solution structure of a G-quadruplex bound to the bisquinolinium compound Phen-DC(3), *Angew. Chem. Int. Ed. Engl.*, 53, 999-1002 (DOI: 10.1002/anie.201308063).
32. Gavathiotis E., Searle M.S. (2003), Structure of the parallel-stranded DNA quadruplex d(TTAGGGT)<sub>4</sub> containing the human telomeric repeat: evidence for A-tetrad formation from NMR and molecular dynamics simulations, *Org. Biomol. Chem.*, 1, 1650-1656 (DOI: 10.1039/B300845M).
33. Ma D.L., Chan D.S., Fu W.C., He H.Z., Yang H., Yan S.C., Leung C.H. (2012), Discovery of a natural product-like c-myc G-quadruplex DNA groove-binder by molecular docking, *PLoS One*, 7, e43278 (DOI: 10.1371/journal.pone.0043278).
34. Simonsson T., Pecinka P., Kubista M. (1998), DNA tetraplex formation in the control region of c-myc, *Nucleic Acids Res.*, 26, 1167-1172.
35. Durgo K., Vukovic L., Rusak G., Osmak M., Colic J.F. (2009), Cytotoxic and apoptotic effect of structurally similar flavonoids on parental and drug-resistant cells of a human cervical carcinoma, *Food. Technol. Biotechnol.*, 47, 356-363.
36. Hanahan D., Weinberg R.A. (2000), The hallmarks of cancer, *Cell*, 100, 57-70 (DOI: 10.1016/S0092-8674(00)81683-9)
37. Zhang W., Zhang F. (2009), Effects of quercetin on proliferation, apoptosis, adhesion and migration, and invasion of HeLa cells, *Eur. J. Gynaecol. Oncol.*, 30, 60-64.

38. Wang Y., Zhang W., Lv Q., Zhang J., Zhu D. (2016), The critical role of quercetin in autophagy and apoptosis in HeLa cells, *Tumor Biol.*, 37, 925-929 (DOI: 10.1007/s13277-015-3890-4).
39. Bandaruk Y., Mukai R., Terao J. (2014), Cellular uptake of quercetin and luteolin and their effects on monoamine oxidase-A in human neuroblastoma SH-SY5Y cells, *Toxicol. Rep.*, 1, 639-649 (DOI: 10.1016/j.toxrep.2014.08.016).
40. Walgren R.A., Lin J.T., Kinne R.K., Walle T. (2000), Cellular uptake of dietary flavonoid quercetin 4'-beta-glucoside by sodium-dependent glucose transporter SGLT1, *J. Pharmacol. Exp. Ther.*, 294, 837-843.
41. Mukai R., Shirai Y., Saito N., Yoshida K.-i., Ashida H. (2009), Subcellular localization of flavonol aglycone in hepatocytes visualized by confocal laser scanning fluorescence microscope, *Cytotechnology*, 59, 177-182 (DOI: 10.1007/s10616-009-9206-z).
42. Gonzales G.B., Van Camp J., Vissenaekens H., Raes K., Smagghe G., Grootaert C. (2015), Review on the Use of Cell Cultures to Study Metabolism, Transport, and Accumulation of Flavonoids: From Mono-Cultures to Co-Culture Systems, *Compr. Rev. Food. Sci. Food Saf.*, 14, 741-754 (DOI: 10.1111/1541-4337.12158).
43. Jeener J., Meier B.H., Bachmann P., Ernst R.R. (1979), Investigation of exchange processes by two-dimensional NMR spectroscopy, *J. Chem. Phys.*, 71, 4546-4553 (DOI: 10.1063/1.438208).
44. Brooks B.R., Brooks C.L., 3rd, Mackerell A.D., Jr., Nilsson L., Petrella R.J., Roux B., Won Y., Archontis G., Bartels C., Boresch S., Caflisch A., Caves L., Cui Q., Dinner A.R., Feig M., Fischer S., Gao J., Hodoscek M., Im W., Kuczera K., Lazaridis T., Ma J., Ovchinnikov V., Paci E., Pastor R.W., Post C.B., Pu J.Z., Schaefer M., Tidor B., Venable R.M., Woodcock H.L., Wu X., Yang W., York D.M., Karplus M. (2009), CHARMM: the biomolecular simulation program, *J. Comput. Chem.*, 30, 1545-1614 (DOI: 10.1002/jcc.21287).
45. Jorgensen W.L., Chandrasekhar J., Madura J.D., Impey R.W., Klein M.L. (1983), Comparison of simple potential functions for simulating liquid water, *J. Chem. Phys.*, 79, 926-935 (DOI: 10.1063/1.445869).
46. Darden T., York D., Pedersen L. (1993), Particle mesh Ewald: An N·log(N) method for Ewald sums in large systems, *J. Chem. Phys.*, 98, 10089-10092 (DOI: 10.1063/1.464397).

47. Ryckaert J.-P., Ciccotti G., Berendsen H.J.C. (1977), Numerical integration of the cartesian equations of motion of a system with constraints: molecular dynamics of n-alkanes, *J. Comput. Phys.*, 23, 327-341 (DOI: 10.1016/0021-9991(77)90098-5).
48. Lemarteleur T., Gomez D., Paterski R., Mandine E., Mailliet P., Riou J.-F. (2004), Stabilization of the c-myc gene promoter quadruplex by specific ligands' inhibitors of telomerase, *Biochem. Biophys. Res. Commun.*, 323, 802-808 (DOI: 10.1016/j.bbrc.2004.08.150).

# SCIENTIFIC REPORTS



OPEN

## Evidences for Piperine inhibiting cancer by targeting human G-quadruplex DNA sequences

Arpita Tawani<sup>1</sup>, Ayeman Amanullah<sup>2</sup>, Amit Mishra<sup>2</sup> & Amit Kumar<sup>1</sup>

Received: 02 September 2016

Accepted: 21 November 2016

Published: 20 December 2016

Piperine, a naturally occurring alkaloid, is well known as anti-oxidant, anti-mutagenic, anti-tumor and anti-proliferative agent. Piperine exerts such pharmacological activities by binding or interacting with various cellular targets. Recently, the first report for Piperine interaction with duplex DNA has been published last year but its interaction with G-quadruplex structures has not been studied yet. Herein, we report for the first time the interaction of Piperine with various DNA G-quadruplex structures. Comprehensive biophysical techniques were employed to determine the basis of interaction for the complex formed between Piperine and G-quadruplex DNA sequences. Piperine showed specificity for G-quadruplex DNA over double stranded DNA, with highest affinity for G-quadruplex structure formed at c-myc promoter region. Further, *in-vitro* studies show that Piperine causes apoptosis-mediated cell death that further emphasizes the potential of this natural product, Piperine, as a promising candidate for targeting G-quadruplex structure and thus, acts as a potent anti-cancer agent.

G-quadruplex DNA structures are classified as non-canonical DNA structures that were formed by square planar arrangement of G-quartets. Apart from Watson-crick hydrogen bonding, these G-quartets are stabilized by Hoogsteen hydrogen bonding<sup>1</sup>. This non-canonical form of DNA was formed by guanine-rich sequences and is widespread in human genome. Approximately, 300,000 sequences have ability to form G-quadruplex structures<sup>2</sup> and majority of them includes telomeres<sup>3</sup>, regulatory regions of oncogenes such as c-kit, c-myc<sup>4</sup>, and hence makes these regions as a potent pharmacological targets for anti-tumor or anti-cancer therapeutics. Telomeric DNA contains repetitive DNA sequence (TTAGGG)<sub>n</sub> forming G-quadruplex structures; this structures inhibits telomerase activity that is required to maintain telomeres<sup>5</sup>. As in 85% of cancers, the activity of this enzyme has been found to be elevated, thus, inhibition of its activity could be an striking approach in the advancement of anticancer drugs development<sup>6</sup>. Another impressive target is G-quadruplex structure formed at promoter region of c-myc gene. This c-myc proto-oncogene regulates approximately 15% of all gene expression and controls various processes of cell-cycle regulation such as apoptosis, growth and proliferation. Its overexpression has been found to be associated with sustained tumor progression. The promoter region of c-myc gene is composed of seven nuclease-hypersensitive elements (NHEs), of which, NHE III<sub>1</sub>, located at -142 to -115 base pairs upstream of the P1 promoter, controls 80–90% transcription of c-myc gene<sup>7,8</sup>. This 27 nucleotide sequence (5'-TGGGGAGGGTGGGGAGGGTGGGGAAGG-3') is purine rich sequence which is also called as Pu27, has potential to form G-quadruplex structure<sup>9,10</sup>. It has been known that this NHE III<sub>1</sub> element could form transcriptionally active and silenced forms (single stranded and duplex DNA respectively). The transcriptional silencing of this promoter is believed to be achieved by the formation of G-quadruplex DNA structures. This was also evident from one of the studies in which suppression of MYC expression was observed when Burkitt lymphoma cell lines was treated with TMPyP4 aids in the formation of stable G-quadruplex structure<sup>11</sup>. Ligands have been reported to interfere with transcription of c-myc gene by stabilizing G-quadruplex structure<sup>11–14</sup>.

Moreover in last few years various ligands with synthetic and natural origin have been reported that binds to various human G-quadruplex DNA like telomeric DNA<sup>15</sup>, promoter region of c-myc DNA<sup>16</sup>. One of such naturally available small molecule is Piperine. It is a chief alkaloid from black pepper (*Piper nigrum* L.) and from the times of Ayurveda, this phytochemical is known for its various pharmacological and physiological properties<sup>17</sup>. These activities include antifungal, antimicrobial<sup>18</sup>, antidepressant<sup>19</sup>, antipyretic<sup>20</sup>, anti-oxidant<sup>21</sup>, anti-inflammatory, anti-apoptotic<sup>22</sup>, etc. It has also been reported that Piperine enhances the bioavailability of

<sup>1</sup>Centre for Biosciences and Biomedical Engineering, Indian Institute of Technology Indore, Indore, Madhya Pradesh, 453552, India. <sup>2</sup>Cellular and Molecular Neurobiology Unit, Indian Institute of Technology Jodhpur, Rajasthan, 342011, India. Correspondence and requests for materials should be addressed to A.K. (email: amitk@iiti.ac.in)

## Chapter 5

# Evidences for Piperine inhibiting cancer by targeting human G-quadruplex DNA sequences

---

---

### 5.1 Introduction

A square planar arrangement of four guanine nucleotides held together by Watson-Crick hydrogen bonding as well as Hoogsteen hydrogen bonding forms G-tetrads.<sup>[1]</sup> Stacking of two or more G-tetrads on each other forms non-canonical secondary structure of DNA known as G-quadruplex structure. It is formed by guanine-rich sequences and is widespread in human genome.<sup>[2]</sup> Majority of these sequences are located at regions like telomeres,<sup>[3]</sup> oncogenic promoter region,<sup>[4]</sup> immunoglobulin switch regions<sup>[5]</sup> etc. Telomeric DNA contains repetitive DNA sequence (TTAGGG)<sub>n</sub> forming G-quadruplex structures that inhibits activity of telomerase enzyme. Telomerase enzyme maintains the length of telomeres,<sup>[6]</sup> and its activity has been found to be elevated in 85% of cancers. Thus, inhibition of its activity could be an striking approach in the advancement of anticancer drugs development.<sup>[7]</sup>

Apart from telomeres, G-quadruplex structures are also formed at promoter region of human proto-oncogene like *c-MYC*, *c-KIT*, *k-RAS*, *BCL-2*, *VEGF*, etc.<sup>[8-11]</sup> The *c-myc* proto-oncogene regulates approximately 15% of all gene expression and controls various processes of cell-cycle regulation such as apoptosis, growth and proliferation. Its overexpression has been found to be associated with sustained tumor progression. Promoter region of *c-myc* gene is composed of seven nuclease-hypersensitive elements (NHEs), of which, NHE III<sub>1</sub>, located at -142 to -115 base pairs upstream of the P1 promoter, controls 80–90% transcription of *c-myc* gene.<sup>[12-13]</sup> This 27 nucleotide sequence (5'-TGGGGAGGGTGGGGAGGGTGGGGAAGG-3') is purine rich sequence which is also called as Pu27, has potential to form G-quadruplex structure.<sup>[14-15]</sup> This NHE III<sub>1</sub> element could form transcriptionally active and silenced forms (single stranded and duplex DNA respectively) and its silencing is believed to be achieved by formation of G-quadruplex structure. Ligands have been reported to interfere with transcription of *c-myc* gene by stabilizing G-quadruplex structure.<sup>[16-18]</sup> It was also evident from one the studies in which suppression of MYC expression was observed when Burkitt lymphoma cell lines was treated with TMPyP4 that aids in the formation of stable G-quadruplex structure.<sup>[8]</sup> Another oncogenic promoter sequence that also forms G-quadruplex structure is *c-kit* oncogene. It codes for a tyrosine kinase receptor and is crucial for communicating the extracellular

signals. It codes for a tyrosine kinase receptor and is crucial for communicating the extracellular signals. Activation of KIT stimulates differentiation, proliferation, and migration<sup>[19]</sup>, but, its overexpression results in uncontrolled cell proliferation and lead to tumor formation notably gastrointestinal tumours.<sup>[20]</sup> A 21- nucleotide long sequence present at upstream of the transcription initiation site is required for core promoter activity.<sup>[9]</sup> This site contains G-rich strand that is capable of forming G-quadruplex structures.<sup>[9]</sup> This location of quadruplex sequence in the promoter region of *c-kit* makes it an impressive target for the regulation of *c-kit* at the transcriptional level.

Moreover in last few years various ligands with synthetic and natural origin have been reported that binds to various human G-quadruplex DNA like telomeric DNA,<sup>[21]</sup> promoter region of c-myc DNA,<sup>[22]</sup> c-kit DNA.<sup>[23]</sup> Nature is a prodigious source of small molecules with therapeutic activities and low toxicity. One of such naturally available small molecule is Piperine. It is a chief alkaloid from black pepper (*Piper nigrum* L.) and from the times of Ayurveda, this phytochemical is known for its various pharmacological and physiological properties.<sup>[24]</sup> It also exerts antifungal, antimicrobial,<sup>[25]</sup> antidepressant,<sup>[26]</sup> antipyretic,<sup>[27]</sup> anti-oxidant,<sup>[28]</sup> anti-inflammatory, anti-apoptotic,<sup>[29]</sup> activities. Moreover, it also enhances the bioavailability of other phytochemicals<sup>[30]</sup> and drugs, for example, rifampicin,<sup>[31]</sup> resveratrol,<sup>[32]</sup> etc. This naturally available non-toxic molecule has been used for the treatment of leukemia, malaria<sup>[33]</sup> as well leishmaniasis.<sup>[34]</sup> Piperine also inhibits Akt phosphorylation<sup>[35]</sup> and suppresses angiogenesis as well as it exerts anti-cancer effect by inhibiting CREB, NF- $\kappa$ B, c-Fos activities.<sup>[36]</sup> The beneficial effect of Piperine towards human health makes it a suitable candidate for targeting macromolecules inside cells. Despite of these studies, the molecular mechanism for action of Piperine with biologically significant macromolecules is not fully studied yet. In literature, only few reports are available for the interaction of Piperine with proteins such as bovine  $\beta$ -lactoglobulin,<sup>[37]</sup> chicken  $\alpha$ 1-acid glycoprotein<sup>[38]</sup> and human serum albumin.<sup>[39]</sup> However, DNA is often a potential target for antibiotic, anti-fungal, anti-viral, anti-tumor and anti-cancer drugs.

Very recently, Haris *et. al.* has reported the interaction of Piperine with duplex DNA.<sup>[40]</sup> This study revealed the molecular mechanism of interaction of Piperine with calf thymus DNA and showed that Piperine binds in minor groove of DNA. Howbeit in anti-cancer drug discovery domain, structure specific targeting of drugs helps in improving drug specificity and affinity for particular target. Structures formed by G-quadruplex DNA are potent targets for anti-cancer drug discovery.<sup>[41]</sup> Small molecule ligands with high specificity and affinity for G-quadruplex structures could be used as potent therapeutics for targeting

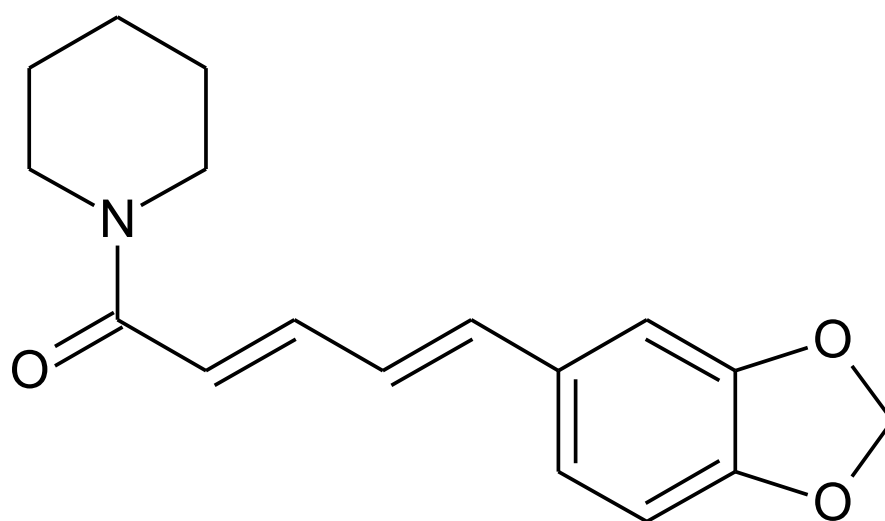


*Figure 5.1. Chemical structure of Piperine.*

cancer by regulating the gene expression. Generally, molecules with planar and aromatic ring system provide scaffolds that assist in binding and stabilization of G-quadruplex structure by  $\pi$ - $\pi$  stacking.<sup>[42]</sup> Piperine has aromatic ring and its planar structure that could provide a framework for end-stacking or  $\pi$ - $\pi$  stacking with G-quadruplex structure. Further credence has been lent to the strategy to explore Piperine because there were no reports available for its interaction with any of DNA sequences forming G-quadruplex structures.

Here in this chapter, we have chosen three biologically significant DNA sequences forming G-quadruplex structure in human genome as mentioned below:

telomeric DNA : tel22 : (d-5'-AGGGTTAGGGTTAGGGTTAGGG-3'),

c-kit promoter region : ckit21up (d-5'-CGGGCGGGCGCGAGGGAGGGG-3')

c-myc promoter region : Pu24T (5'-TGAGGGTGGTGGAGGGTGGGGAAGG-3').

We have studied the interaction of above-mentioned G-quadruplex forming DNA sequences with Piperine (Figure 5.1). In order to understand this interaction, various biophysical techniques were employed such as circular dichroism (CD), DNA melting studies, steady-state, time-resolved fluorescence and proton NMR spectroscopy. Further, computational analysis for the dynamics of Piperine-Pu24T DNA interaction were also performed by using docking and molecular dynamics (MD) simulation methods. Furthermore, *in vitro* studies were employed to understand the cytotoxic effects of Piperine on various cancer cell lines. The mechanism of its action was explored on human lung carcinoma (A549) cell lines and established its potential to down-regulate c-myc gene expression cancer cells.

## 5.2 Results and Discussion

### 5.2.1 Fluorescence spectroscopic studies

#### 5.2.1.1 Steady state fluorescence studies

Fluorescence spectroscopy provides significant information about change in local environment of fluorophore, therefore, it could be used to probe the interactions. We first investigated the binding of Piperine to DNA by employing fluorescence titration experiment. This interaction was monitored at the emission maximum of unbound form of Piperine. It has emission maximum at a wavelength of 486 nm when excited at 341 nm. With incremental addition of G-quadruplex DNA to Piperine solution, significant increase in fluorescence intensity was observed. This indicated the binding of Piperine to DNA and the formation of Piperine - G-quadruplex DNA complex. The plot of change in fluorescence intensity versus concentration of G-quadruplex DNA was found to be hyperbolic, indicating the formation of a saturable complex (Figure 5.2). The binding curve was fitted with two site saturation model

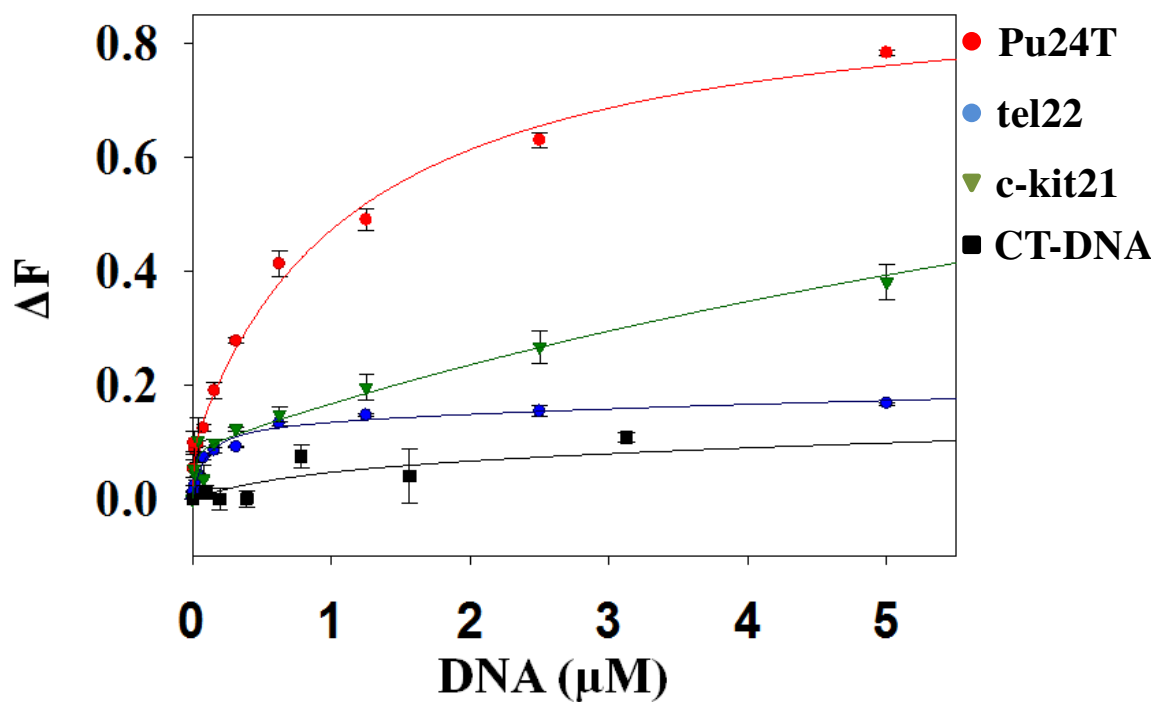


*Figure 5.2. Fluorescence titration curve of Piperine as a function of various DNA concentration; Red: Pu24T; Blue: tel22; Green: c-kit21; Black: CT-DNA. Solid lines represent fit according to the ligand binding two site saturation.*

**Table 5.1. Binding constant ( $K_d$ (M)) values of Piperine with DNA**

DNA	Binding Constant	
	$K_d1$ (M)	$K_d2$ (M)
Pu24T	$2.50 \times 10^{-9}$	$1.14 \times 10^{-6}$
Tel22	$8.75 \times 10^{-8}$	$14.8 \times 10^{-6}$
c-kit21	$1.12 \times 10^{-8}$	$12.73 \times 10^{-6}$
CT-DNA	$24.12 \times 10^{-6}$	--

of ligand binding that computes the values of binding constant ( $k_{d1}$  and  $k_{d2}$ ) for two different affinities of Piperine for G-quadruplex DNA (Table 5.1). These values show that binding affinity of Piperine was found maximum when bound to Pu24T DNA as compared to other G-quadruplex structures. Further, a  $\sim 10^4$  fold higher affinity of Piperine was observed for G-quadruplex structures as compared to that of duplex DNA i.e. calf thymus DNA (CT-DNA). This result propounded that apart from high affinity for Pu24T, Piperine showed high specificity towards G-quadruplex structure as compared to duplex DNA with  $\sim 10^4$  fold higher affinity for G-quadruplex structures.

#### 5.2.1.2 Time-resolved fluorescence studies

The excited state of a fluorophore is sensitive to the changes in its structure and dynamics. This will be helpful in providing information about interaction behavior drug-DNA complex. In order to explore the environment of fluorophore in its excited state, we have measured the fluorescence lifetime decay profile of Piperine in absence and presence of various DNA sequences forming G-quadruplex structure. Time resolved fluorescence decays were collected by Time-Correlated Single-Photon Counting (TSCPC) method on the spectrofluorimeter (Horiba). The life time decay profile was measured for free Piperine and its complex with DNA sequences. Global analysis for each set of fluorescence decays provides the best fit by tri-exponential decay function. This best fit in terms of statistical quality having global  $\chi^2$  value  $\sim 1.5$  for Piperine and its complex with DNA sequences. Piperine is a heterocyclic compound containing methylenedioxyphenyl (MDP) ring, a basic piperidine moiety attached by a carbonylamide linkage to side chain containing conjugated double bonds.<sup>[43]</sup> Each of these moieties might contribute to decay profile of Piperine and thus, in principle, it has more than one conformer in solution because of rotational sites. Thus, the decay profile of uncomplexed Piperine exhibits three lifetimes ( $\tau_1$ ,  $\tau_2$  and  $\tau_3$ ) and three relative amplitudes ( $\beta_1$ ,  $\beta_2$ , and  $\beta_3$ ); and their values are mentioned in Table 5.2. Figure 5.3 displayed the fluorescence decay profile of Piperine in its free form and complexed with various DNA sequences upto  $D/N = 2.0$ . From TSCPC data analysis, it has been with addition of DNA, the average life time of Piperine has increased (Table 5.2). This might occur due to changes in the environment of Piperine fluorophore due to formation drug-DNA complex. As clearly evident from data this increment is highest for Pu24T DNA with  $\sim 19$  folds higher at  $D/N = 2.0$ . The life time decay data attributed to the binding of Piperine to Pu24T c-myc DNA at more than one site. Usually, molecules with planar scaffold interact with G-quadruplex structure via end- stacking mode and external groove binding mode. In

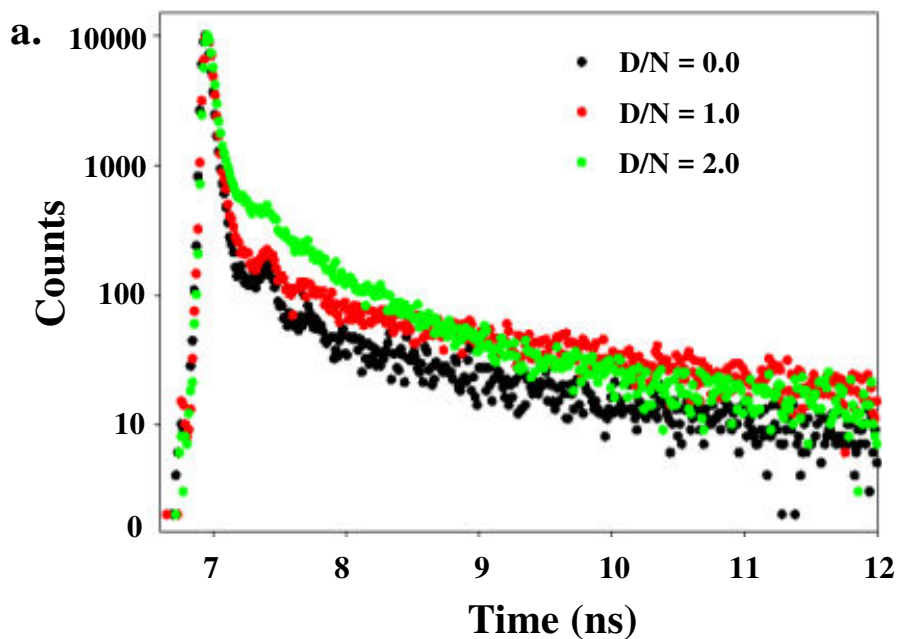


*Figure 5.3(a) Fluorescence life time decay curve of 40.0  $\mu$ M Piperine (Black) and its complex with Pu24T G-quadruplex DNA at D/N ratio = 1.0 (Red) and D/N ratio = 2.0 (Green).*

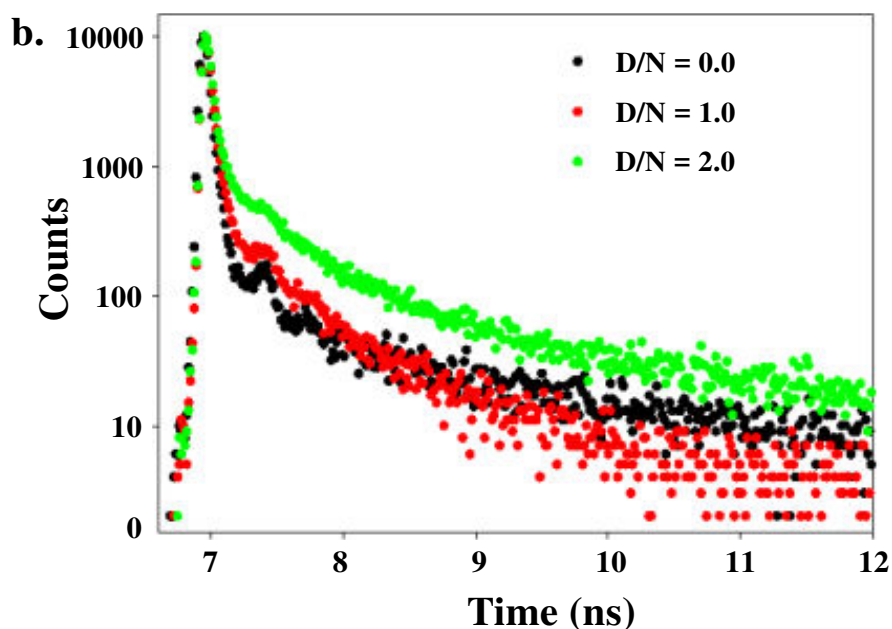


*Figure 5.3(b) Fluorescence life time decay curve of 40.0  $\mu$ M Piperine (Black) and its complex with tel22 G-quadruplex DNA at D/N ratio = 1.0 (Red) and D/N ratio = 2.0 (Green).*

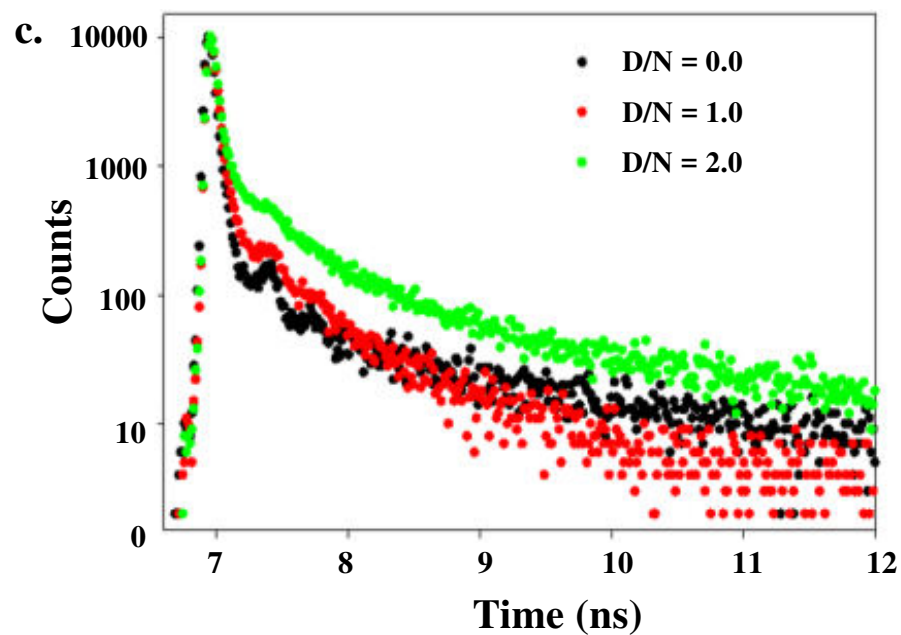


*Figure 5.3(c) Fluorescence life time decay curve of 40.0  $\mu$ M Piperine (Black) and its complex with ckit21 G-quadruplex DNA at D/N ratio = 1.0 (Red) and D/N ratio = 2.0 (Green).*

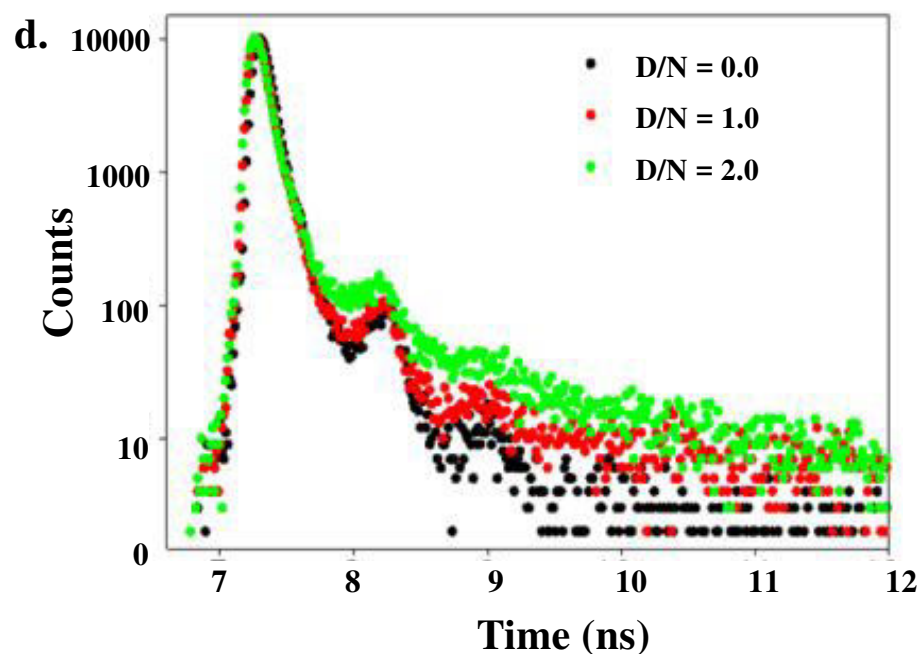


*Figure 5.3(d) Fluorescence life time decay curve of 40.0  $\mu$ M Piperine (Black) and its complex with CT-DNA at D/N ratio = 1.0 (Red) and D/N ratio = 2.0 (Green).*

**Table 5.2. Life time fluorescence decay parameters for Piperine and its complex with various DNA at D/N = 2:1 collected at 298K**

D/N = 0.0								
DNA	Life Time Decay (ns)			Amplitude			Chi Square	Average life time (ns)
	$\tau_1$	$\tau_2$	$\tau_3$	$\beta_1$	$\beta_2$	$\beta_3$	$\chi^2$	
	0.48	3.37	0.02	18.34	3.65	78.01	1.93	1.60
D/N = 1.0								
DNA	Life Time Decay (ns)			Amplitude			Chi Square	Average life time (ns)
	$\tau_1$	$\tau_2$	$\tau_3$	$\beta_1$	$\beta_2$	$\beta_3$	$\chi^2$	
Pu24T	0.68	4.37	0.06	15.63	4.59	95.41	1.66	8.00
tel22	0.50	2.00	0.03	16.58	3.96	79.46	1.93	5.80
ckit21	0.61	3.78	0.02	19.56	4.19	76.25	1.61	7.62
CT	0.56	3.58	0.05	18.63	4.67	76.70	1.10	3.06
D/N = 2.0								
DNA	Life Time Decay (ns)			Amplitude			Chi Square	Average life time (ns)
	$\tau_1$	$\tau_2$	$\tau_3$	$\beta_1$	$\beta_2$	$\beta_3$	$\chi^2$	
Pu24T	2.15	4.17	0.26	17.23	7.65	75.12	1.54	33.3
tel22	0.68	0.75	0.25	15.75	6.65	77.60	1.75	20.20
ckit21	1.29	0.74	0.20	17.92	5.45	76.63	1.38	25.08
CT	0.64	3.60	0.09	15.36	3.98	80.66	2.86	3.73

In both the modes, the lifetime property varies with larger lifetime in the end-stacking mode.<sup>[44]</sup> Likely to previous study,<sup>[21]</sup> the significant changes observed in life time decay profile of Piperine complexed with Pu24T at D/N = 2:1 corroborates that this interaction is mediated via end-stacking mode.<sup>[45]</sup> However, no significant change in the decay profile of Piperine was observed for when it bound to CT-DNA (Figure 5.3d).

Further, the binding of Piperine was ascertained by other biophysical methods like UV- melting experiment as described in next section.

### 5.2.2 UV -Thermal denaturation studies

Thermal denaturation of DNA forming G-quadruplex structures provides distinctive changes in UV absorbance spectra. The thermal denaturation profile of G-quadruplex DNA in the presence of ligand provides details about the conformational changes in terms of its stability upon addition of ligand. Thus, to explicit this stability of G-quadruplex structure on binding of Piperine, we have performed thermal melting studies of DNA in absence and presence of Piperine. The melting curves were recorded at a wavelength of 295 nm for all the three G-quadruplex DNA sequences upto D/N = 2.0 ratio (Figure 5.4). A plot of absorbance versus temperature can provide information on the thermal stability of complex formation. At D/N = 0.0, the melting curve of DNA sequences showed a reverse “S” shape at 295 nm with melting temperature ( $T_m$ ) of 75.0 °C<sup>[46]</sup>, 60.0°C<sup>[47]</sup> and 66.6°C<sup>[48]</sup> for Pu24T, tel22 and ckit21 DNA respectively (Table 5.3), indicating the formation of G-quadruplex structure. After addition of Piperine, it has been observed that  $T_m$  of the Pu24T DNA increased to 78.0°C and 79.0°C at D/N = 1.0 and 2.0 respectively. However, not much significant results were observed for tel22 and ckit-21 DNA. It is well known that a better stabilization of quadruplex structure could be an indication from increased melting temperature after addition of ligand.<sup>[49]</sup> Thus, our data implies that Piperine stabilizes Pu24T G-quadruplex DNA structure. Also, it has been reported that regulation of c-myc gene is closely related to the stabilization of quadruplex structure formed at its promoter region.<sup>[8]</sup> Therefore, Piperine might exert its anti-cancer activity by stabilizing G-quadruplex structure and regulates its expression in cancer cells. However, the differences in  $\Delta T_m$  for all the three G-quadruplex DNA may originate from the different DNA-binding affinity of Piperine and also reflected its sequence specific binding property.

Further, the stability of G-quadruplex topology upon binding of Piperine is evaluated by Circular Dichroism (CD) method as described in next section.

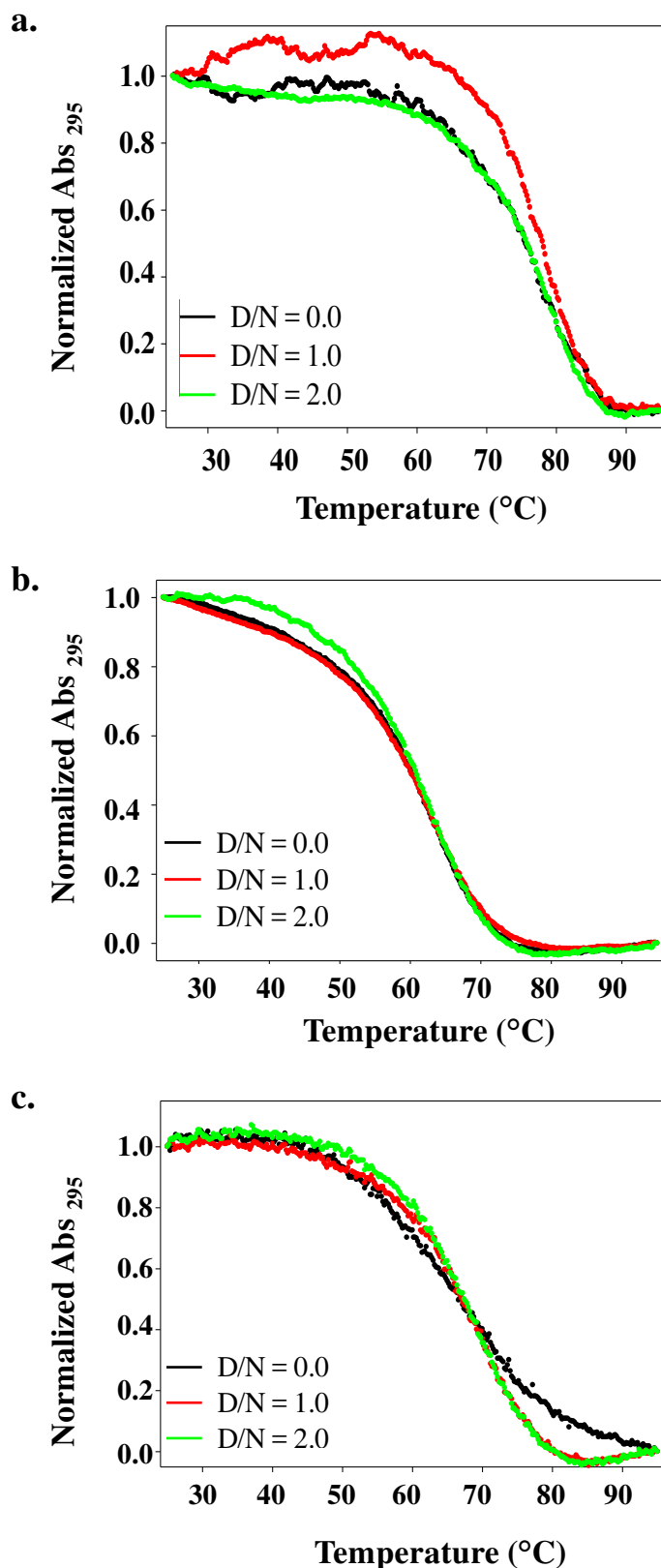


*Figure 5.4. UV- thermal denaturation profile of (a) Pu24T G-quadruplex DNA (b) tel22 G-quadruplex DNA (c) c-kit21 G-quadruplex DNA in the absence (black) and presence of Piperine upto D/N = 2.0.*

**Table 5.3. Values of melting temperature of G-quadruplex DNA in absence and presence of Piperine**

<b>DNA</b>	<b>Melting Temperature (°C)</b>		
	<b>D/N = 0.0</b>	<b>D/N = 1.0</b>	<b>D/N = 2.0</b>
<b>Pu24T</b>	<b>75.0</b>	<b>78.0</b>	<b>79.0</b>
<b>Tel22</b>	<b>60.0</b>	<b>61.0</b>	<b>62.0</b>
<b>c-kit21</b>	<b>66.6</b>	<b>67.2</b>	<b>67.4</b>

### 5.2.3 Circular Dichroism studies

Circular dichroism technique provides information about the changes in the secondary structure of DNA. CD spectra of all the three G-quadruplex forming DNA sequences used in this study were portrayed in Figure 5.5. The uncomplexed Pu24T and c-kit21 DNA displayed a positive peak around 260-265 nm and a negative peak at 240 nm (Figure 5.5a, c), that are signature peaks for parallel G-quadruplex DNA topology.<sup>[50]</sup> While, a positive band at 280 nm with a hump at 255 nm and a negative peak at 240 nm is a characteristic of (3+1) hybrid topology of G-quadruplex, as showed by tel22 DNA<sup>[51]</sup> (Figure 5.5b). The perturbations in G-quadruplex topology caused due to addition of ligand may be attributed to distortion of its structure,<sup>[52]</sup> and CD titration experiment could be employed to monitors these changes. Piperine is an optically inactive molecule and therefore it does not exhibit any circular dichroism (CD) spectrum. The interaction of Piperine to various G-quadruplex sequences was followed in the ultraviolet region. CD spectra of these sequences were not perturbed even after the addition of Piperine at twice the concentration of G-quadruplex DNA (D/N = 2.0). This observation suggested that upon binding of Piperine, globally the structure of DNA remains in G-quadruplex topology.<sup>[53]</sup> Thus, our CD results showed that binding of Piperine does not hamper the G-quadruplex topology formed by Pu24T, tel22 and ckit-21 DNA<sup>[53]</sup> and could indicate that it stabilizes G-quadruplex structure.

As observed from above experiments that Piperine has high affinity for Pu24T DNA sequence forming G-quadruplex structure over other G-quadruplex DNA structures. Thus, the interaction of Piperine with Pu24T G-quadruplex DNA was further explored in details. We have examined the presence of induced CD signal that indicated strong interaction between DNA and ligand. Induced CD signals were observed in the absorption region of ligand. At D/N = 0.0 no CD signal was seen at 364 nm (that is in the absorption range of Piperine). But with the addition of Piperine, a negative induced signal at ~364 nm was observed at D/N = 4.0 (Figure 5.6). The intensity of signal keeps on increasing with increasing the D/N ratio and saturated at D/N = 10.0 (Figure 5.6). Generally, the negative induced CD signal implies close interaction involving most likely an overlap of  $\pi$ - $\pi$  systems and indicates end-stacking<sup>[54]</sup> of ligand to G-quadruplex DNA<sup>[55]</sup>. Thus, the emergence of induced CD signal indicated that Piperine stabilizes Pu24T G-quadruplex DNA by binding via end stacking mode.

As of now it has been clear that Piperine binds to Pu24T G-quadruplex DNA and provides it stability, therefore, in order to understand the structural basis of this interaction, we have performed the detailed NMR studies as described in next section.

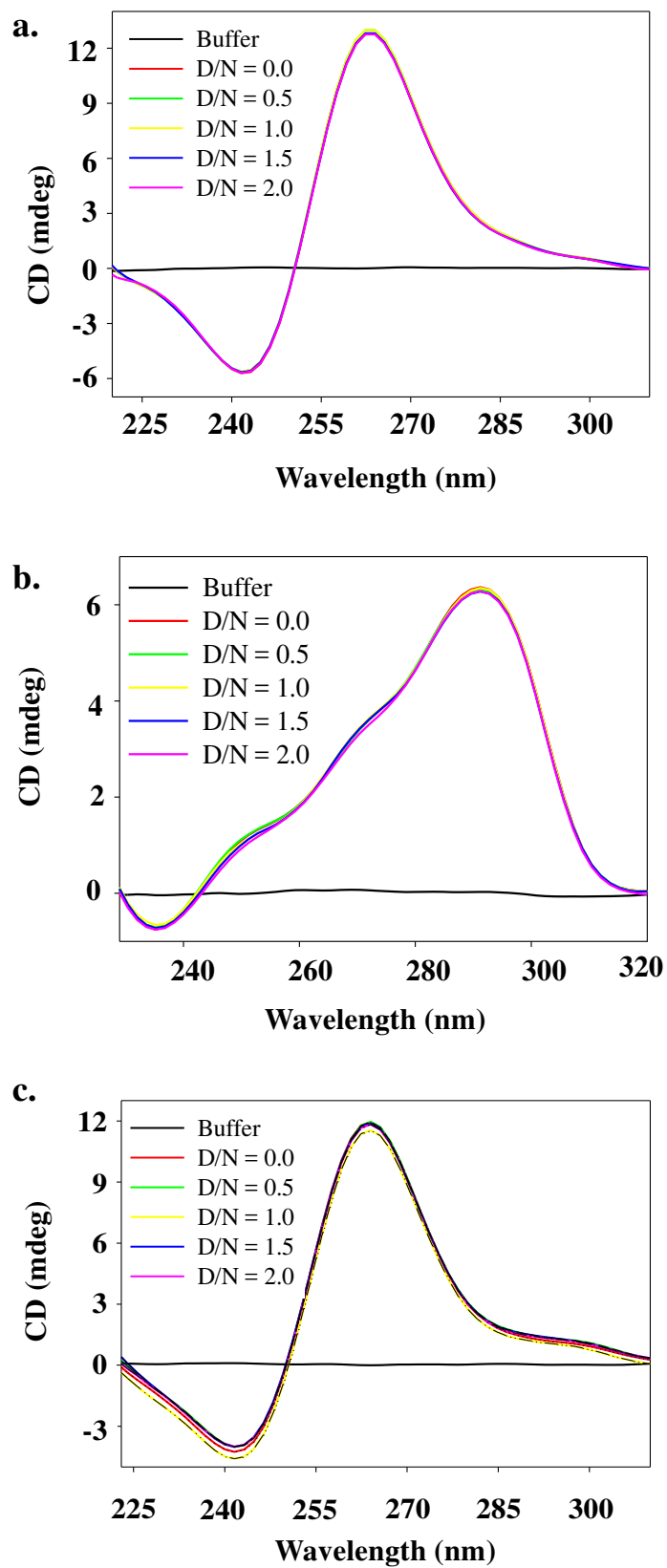


*Figure 5.5. Circular Dichroism titration spectrum for free G-quadruplex DNA (Red) (a) Pu24T (b) tel22 (c) c-kit21 and in the presence of Piperine as a function of increasing concentration of Piperine up to D/N ratio = 2.0.*

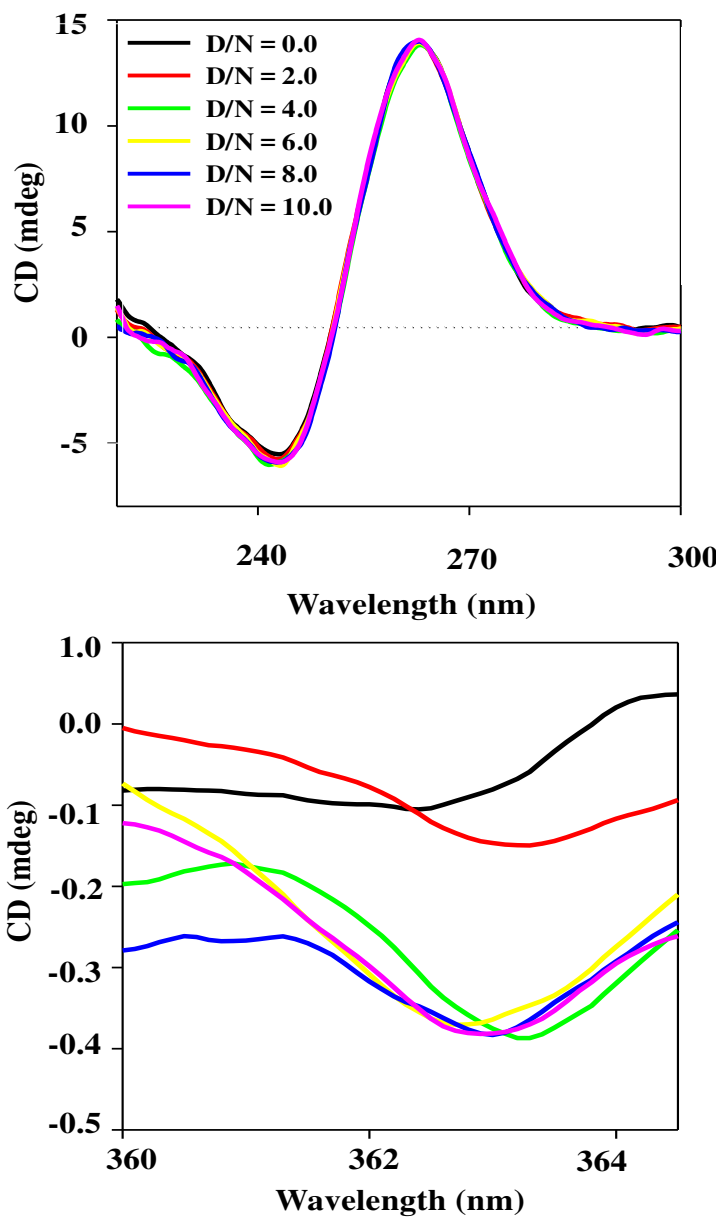


*Figure 5.6. Induced Circular Dichroism spectrum for free Pu24T (Black) and in the presence of Piperine as a function of increasing concentration of Piperine up to D/N ratio = 10.0. Bottom image showing magnified ICD signals.*

## 5.2.4 Nuclear Magnetic Resonance studies

### 5.2.4.1 One dimensional proton NMR studies

Nuclear magnetic resonance (NMR) is an appropriate method to probe the interactions between ligands and macromolecules. It is also unique amongst other biophysical techniques in providing information on the chemical nature of constituents present in sample and it is sensitive for changes in their environment. Employing this technique, we first wish to know which protons of Piperine are involved in the interaction with Pu24T DNA. This could be revealed by observing the chemical shift perturbations of ligand upon addition of DNA. Thus, we have performed 1D proton NMR titration experiment by incrementally adding Pu24T DNA to 400  $\mu$ M of Piperine solution. With the successive addition of DNA, broadening and separation of Piperine proton resonances were observed (Figure 5.7). These protons mainly include hydrogen atoms from conjugated system of Piperine like H7, H3, H5, H4 and H6. Thus, it shows that above mentioned protons takes part in interaction with Pu24T DNA. This could be possible only when Piperine molecule orients itself on Pu24T G-quadruplex structure in such a way that its conjugated system and aromatic ring will come in contact with G-tetrads of Pu24T and stacks on it.

#### 5.2.4.1.1 Assessment of G-quadruplex structure formation

The structural conformation of G-quadruplex DNA formed by Pu24T sequence in  $K^+$  solution was monitored by proton NMR. For the ease of analysis, the positions of the bases in this oligomer are designated as follows: d-(T<sup>1</sup><sub>p</sub> G<sup>2</sup><sub>p</sub> A<sup>3</sup><sub>p</sub> G<sup>4</sup><sub>p</sub> G<sup>5</sup><sub>p</sub> G<sup>6</sup><sub>p</sub> T<sup>7</sup><sub>p</sub> G<sup>8</sup><sub>p</sub> G<sup>9</sup><sub>p</sub> T<sup>10</sup><sub>p</sub> G<sup>11</sup><sub>p</sub> A<sup>12</sup><sub>p</sub> G<sup>13</sup><sub>p</sub> G<sup>14</sup><sub>p</sub> G<sup>15</sup><sub>p</sub> T<sup>16</sup><sub>p</sub> G<sup>17</sup><sub>p</sub> G<sup>18</sup><sub>p</sub> G<sup>19</sup><sub>p</sub> G<sup>20</sup><sub>p</sub> A<sup>21</sup><sub>p</sub> A<sup>22</sup><sub>p</sub> G<sup>23</sup><sub>p</sub> G<sup>24</sup><sub>p</sub>). One dimensional proton spectra of uncomplexed Pu24T DNA displayed well resolved 13 resonances in imino region of NMR spectra (10.5 ppm -12.0 ppm) that suggested the formation of G-quadruplex structure by this sequence. The assignment of nucleotide protons has been carried out by following the strategies adopted for standard B - DNA structures that is, sequential NOEs (base H8/H6)<sub>n</sub> - sugar (H1')<sub>n-1</sub>, (base H8/H6)<sub>n</sub> - sugar(H2'')<sub>n-1</sub>, (base H8/H6)<sub>n</sub> - sugar(H2')<sub>n-1</sub>; expected NOEs due to several short intra nucleotide distances<sup>[56]</sup> as well as NMR data of uncomplexed Pu24T as described in previous chapter. Thus, the position of each and every resonance was ascertained and unambiguous assignment of was performed as described in previous chapter (chapter 04).

#### 5.2.4.1.2 Temperature dependent one –dimensional proton NMR studies

We have also assessed the stability of Pu24T G-quadruplex DNA upon binding with

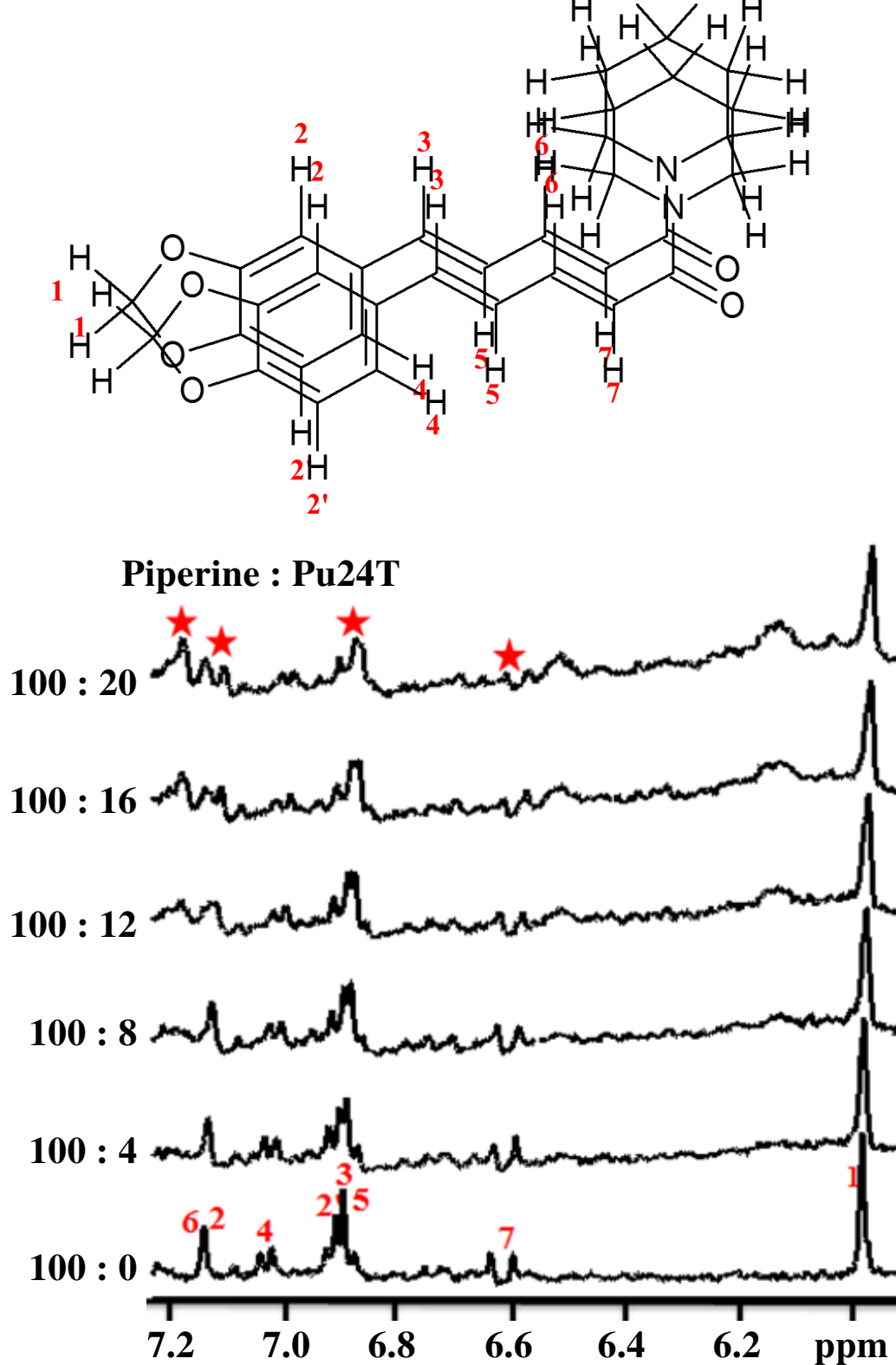


*Figure 5.7. One dimensional proton NMR titration of 400  $\mu$ M of Piperine with increasing concentration of Pu24T. Changes in perturbation of resonances were marked with asterisk. Chemical structure of Piperine is shown above the NMR spectra with numbered assigned protons.*

Piperine using temperature-dependent NMR studies. The rise in temperature causes breaking of hydrogen bonds, due to which proton resonances of DNA become broadened and sometimes they may disappear. However, if ligand stabilizes the G-quadruplex structure, sharp peaks were observed at higher temperatures as compared to free DNA. In our study, we have gradually increased the temperature by 5 degrees from 298K to 338K and NMR spectra were collected at each temperature for uncomplexed Pu24T DNA. It has been observed that with increase in temperature, the imino proton resonances of bases like G24, G8, G15 begin to broaden at 313 K (Figure 5.8a). Although, complete disappearance of resonances was not observed as melting temperature of Pu24T was higher than 338K. However, with the addition of Piperine at D/N = 1.0 and 2.0, sharpening and broadening of few imino proton resonances were observed (Figure 5.8b-c). In particular, resonances of G8, G24 imino proton can be seen as a sharp peaks upto 323K and then slightly broadened above this temperature. Also, the imino proton resonance of G15 also becomes sharp and clean at 323K in D/N 1.0 and 2.0 which was otherwise broadened in D/N = 0.0 upto 333K. Additionally, resonance of G18 imino proton was also clearly seen upto 338K after addition of Piperine in both the D/N ratios 1.0 and 2.0. Nevertheless, G18 base is a part of middle G-tetrad, but as seen from molecular dynamic simulation studies that Piperine molecule forms hydrogen bonds with G18 base (mentioned in later section). This could account for the observed changes in G18 imino proton upon addition of Piperine. Not only in imino region, there were changes in the chemical shifts and shape of resonance in base region (7.0 ppm - 8.5 ppm) of NMR spectra (Figure 5.9) The resonances of G8, G6, G24 base protons (H8) were broadened at 308K in D/N = 0.0, while at D/N = 1.0 and D/N = 2.0, these proton resonances were sharp upto 323K. Likewise, G15H8 proton resonance was broadened at 308K but it could be seen as separate peak upto 323K in presence of Piperine. All these results clearly show that binding of Piperine stabilizes the G-quadruplex structure formed by Pu24T DNA sequence. It is noteworthy to mention that all these protons of DNA belongs to those guanine nucleotides that takes part in the formation of upper and bottom G-tetrad of Pu24T G-quadruplex DNA. This result suggested that binding of Piperine stabilized Pu24T G-quadruplex structure that is in lined with our previous results from CD and UV melting data.

#### **5.2.4.1.3 One –dimensional proton NMR titration studies**

Further, we have also performed NMR titration experiment by incrementally adding Piperine to Pu24T DNA (Figure 5.10). The perturbations and broadening of DNA resonances were observed that indicated the complex formation of between Piperine and Pu24T DNA

T<sup>1</sup>GAG<sup>4</sup>GGT<sup>7</sup>GGT<sup>10</sup>GAG<sup>13</sup>GGT<sup>16</sup>GGGG<sup>20</sup>AAG<sup>23</sup>G<sup>24</sup>

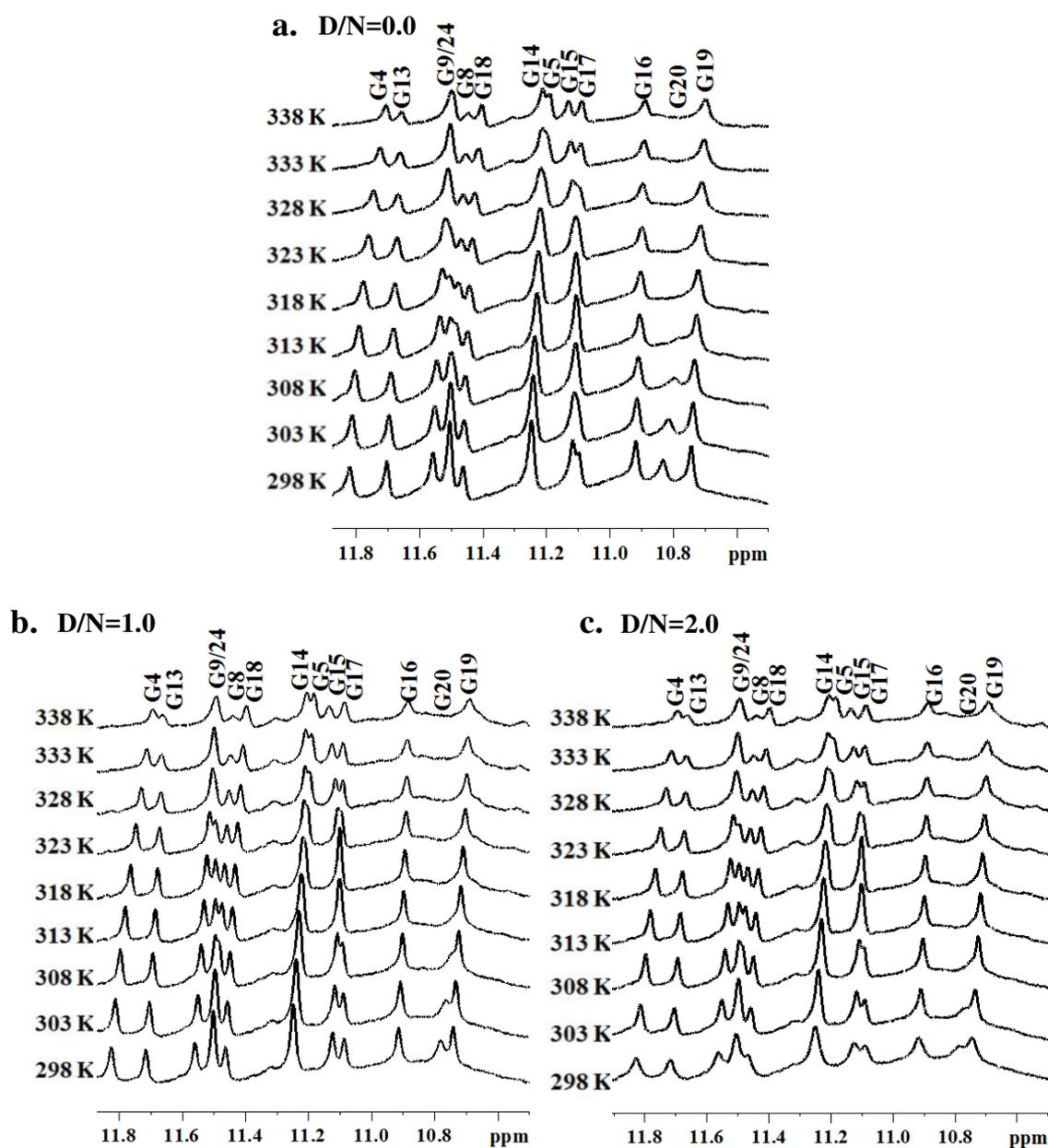


Figure 5.8. <sup>1</sup>H NMR spectra showing interaction of Piperine with Pu24T monitored by imino region as a function of temperature at various D/N ratio (a) 0.0 (b) 1.0 (c) 2.0.

T<sup>1</sup>GAG<sup>4</sup>GGT<sup>7</sup>GGT<sup>10</sup>GAG<sup>13</sup>GGT<sup>16</sup>GGGG<sup>20</sup>AAG<sup>23</sup>G<sup>24</sup>

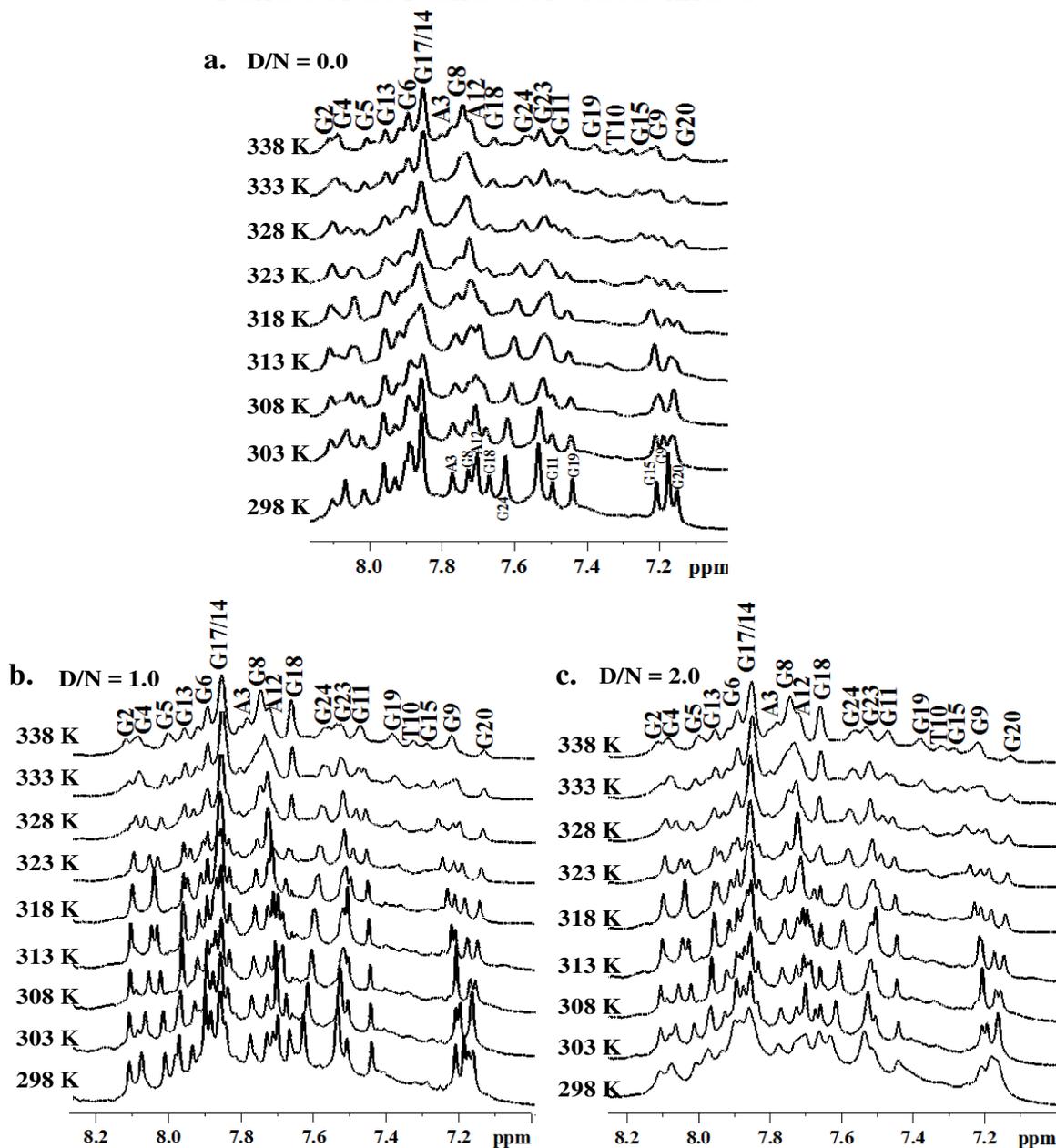
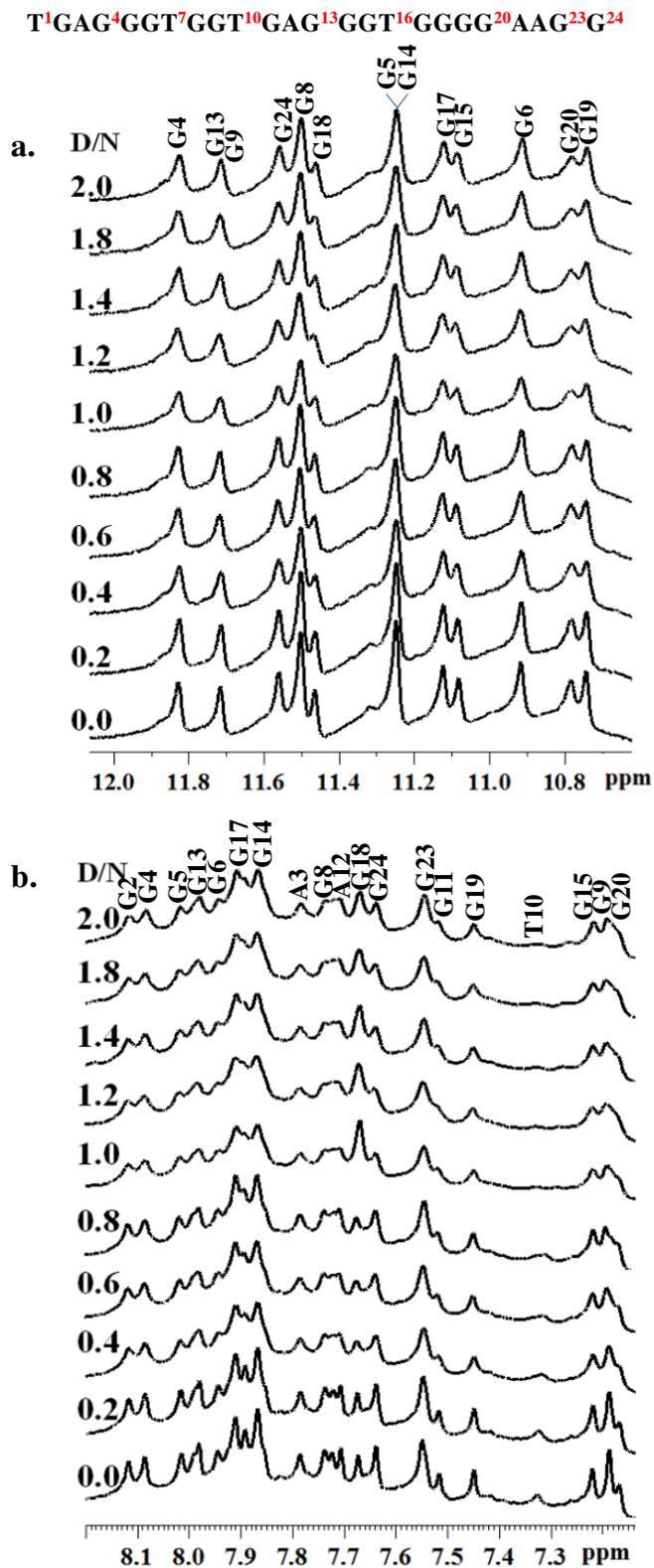
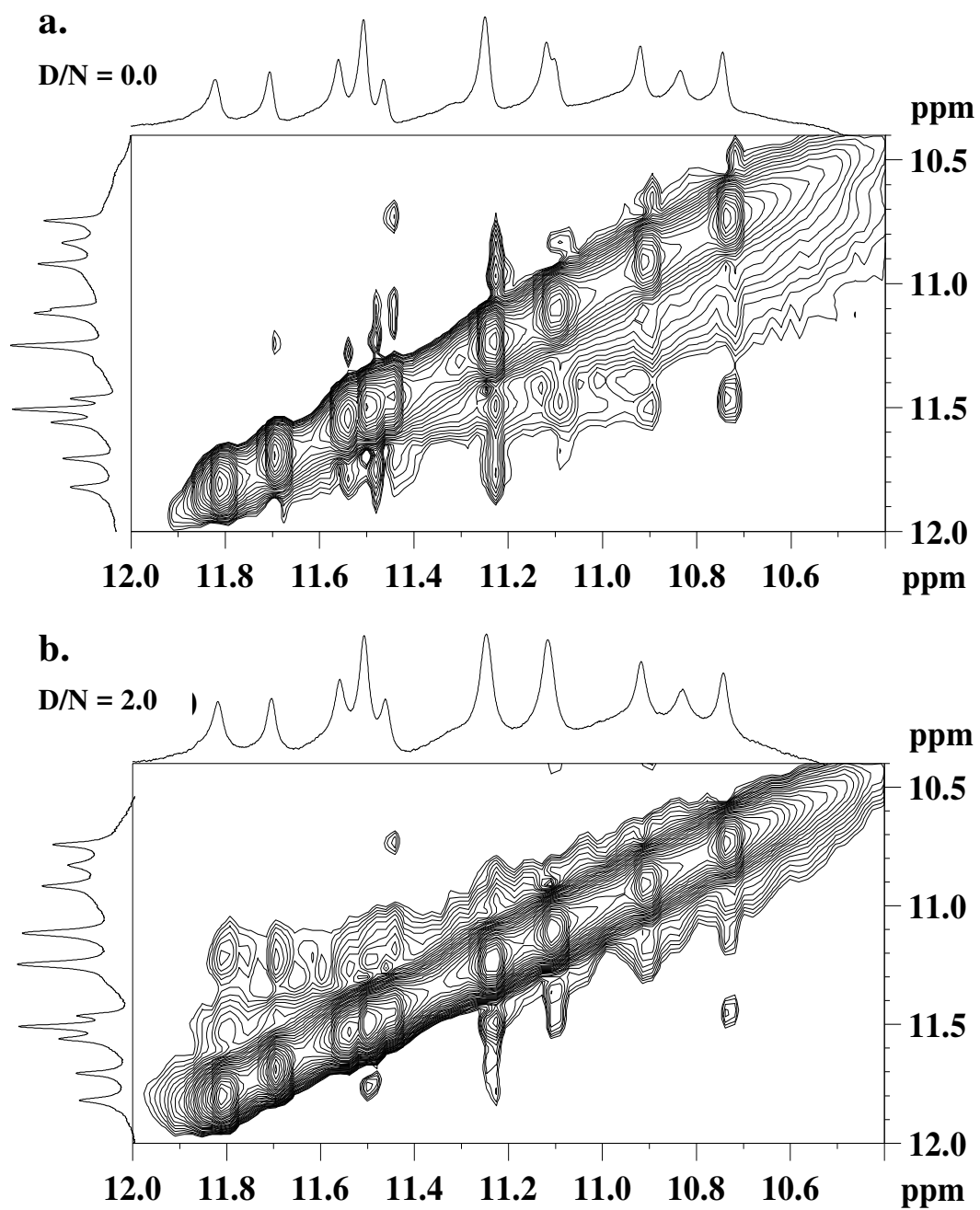


Figure 5.9. <sup>1</sup>H NMR spectra showing interaction of Piperine with Pu24T monitored by base region as a function of temperature at various D/N ratio (a) 0.0 (b) 1.0 (c) 2.0.



*Figure 5.10. One dimensional proton spectra for Piperine and Pu24T complex as a function of ligand/DNA (D/N) ratio at 298 K monitored by (a) Imino region (b) Base region.*



*Figure 5.11. Expansion of NOESY spectra showing imino region for Piperine and Pu24 DNA as a function of D/N ratio (a) D/N = 0.0 (b) D/N = 2.0 at 298 K.*

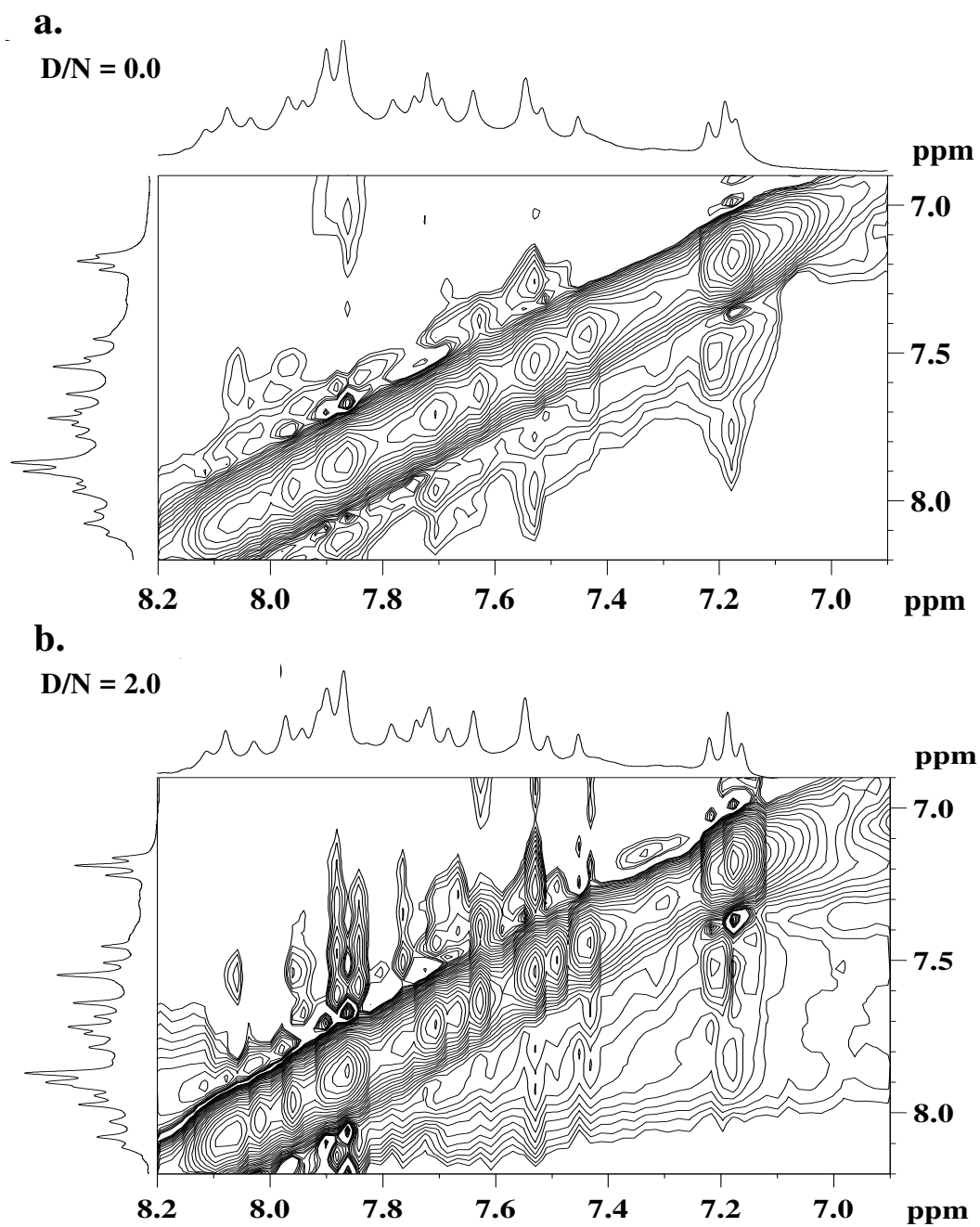


*Figure 5.12. Expansion of NOESY spectra showing base region for Piperine and Pu24 DNA as a function of D/N ratio (a)  $D/N = 0.0$  (b)  $D/N = 2.0$  at 298 K.*

However, a few changes were observed in the imino and base regions but we could not assign them unambiguously due to overlapping peaks. This renders difficulty for the distinction between the NOEs of ligand-ligand and ligand-Pu24T interactions.

Thus, unfortunately, no NOEs of interactions were identified to get a decisive NMR structure for the complex (Figure 5.11 and 5.12). Further, insight for this interaction was deduced by molecular docking and modelling experiment as mentioned in next section.

### 5.2.5 Docking and modelling studies

To get more clear understanding of the interaction of Piperine and Pu24T DNA, molecular docking studies were performed. The molecular structures of DNA as well as of ligand were first optimized using Discovery Studio 3.5 and docking was carried out by Autodock 4.0 using complete molecule of Pu24T in grid box. We have performed blind docking to know the preferential binding site of Piperine on Pu24T DNA. From docking result analysis, it was manifested that there were two separate sites on Pu24T for the possible binding of Piperine. Figure 5.13 shows the docked structures of Piperine with Pu24T DNA having the best binding energies at the two sites. The most privileged binding site for Piperine on Pu24T G-quadruplex DNA was found to be located below the bottom G-tetrad. At this location, Piperine binds to Pu24T DNA with binding energy of -7.18 kcal/mol (Site A) and has  $\pi$ - $\pi$  interactions with G6. As Piperine has planar structure, it is expected that it could get at both the ends of G-quadruplex structure. On further analysis, we have that second site is above the upper G-tetrad of Pu24T G-quadruplex DNA with binding energy of -5.45 kcal/mol (Site B). At this site also, Piperine was stacked by  $\pi$ - $\pi$  interactions with G17 base of Pu24T. It is also noteworthy that this G17 base and G6 base are involved in the formation of upper and bottom G-tetrads of Pu24T G-quadruplex DNA, respectively.

With this docked structure, we have performed unrestrained molecular dynamic simulation on Discovery Studio 3.5. The 100 ns unrestrained MD simulation was performed and throughout the simulation it has been found that both Piperine molecules remained bound to Pu24T G-quadruplex DNA. Simulation provides 100 iterations, of which, the conformation having lowest potential energy gave us a stable model of Piperine-Pu24T DNA. Figure 5.16a shows the model for Piperine - Pu24T complex obtained after simulation. In this model, each molecule of Piperine is located at both the terminal G-tetrads of G-quadruplex structure. On detailed analysis of this lowest potential energy model, we have observed that Piperine molecule is stacked on the upper and bottom G-tetrads of Pu24T DNA. This stacking was

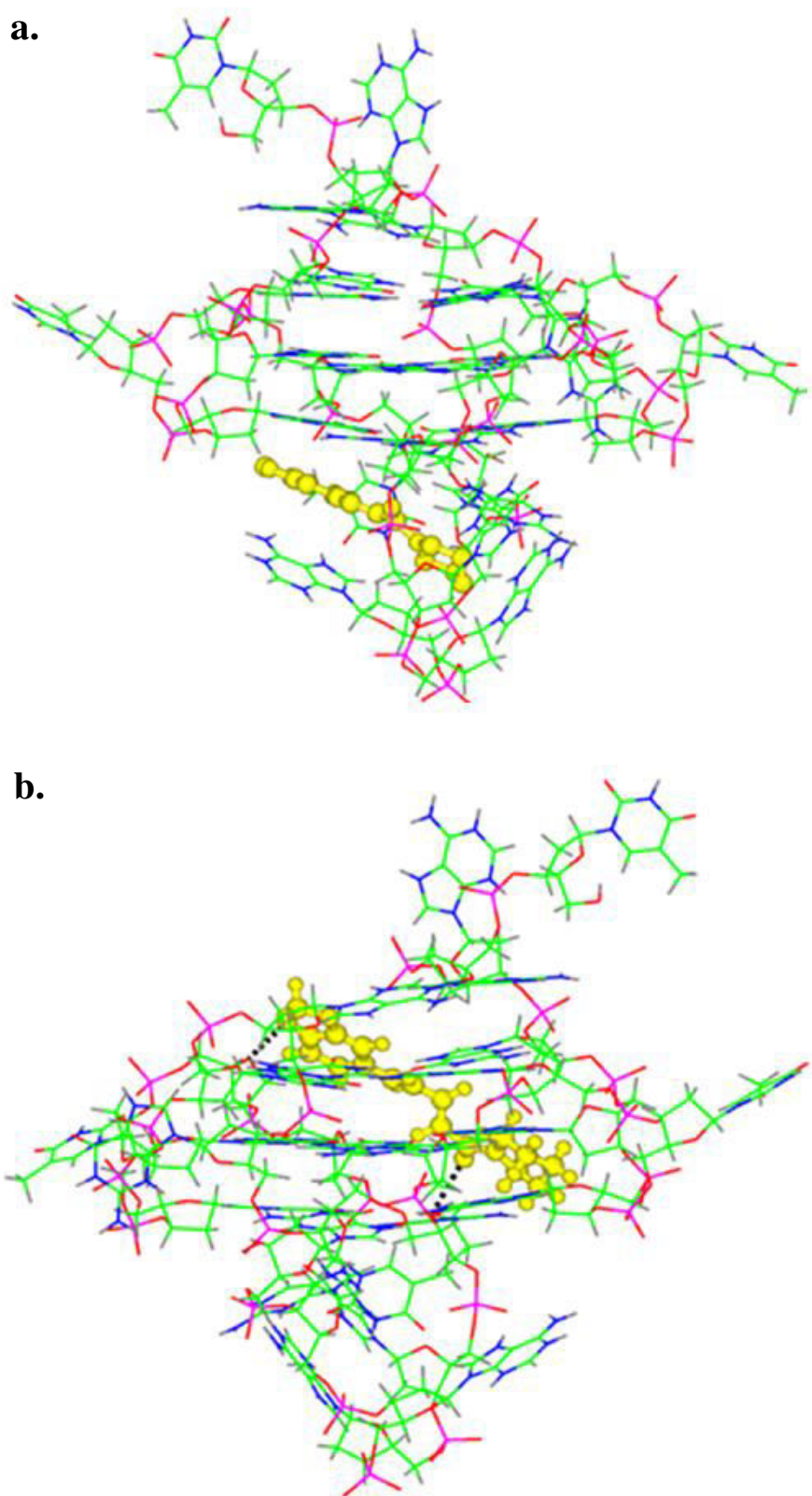


*Figure 5.13. Stable conformation of Piperine with Pu24T obtained from docking by Autodock 4.0 in which Piperine is shown in yellow color as ball stick representation. Black dotted lines showing hydrogen bonds between Piperine and Pu24T DNA.*

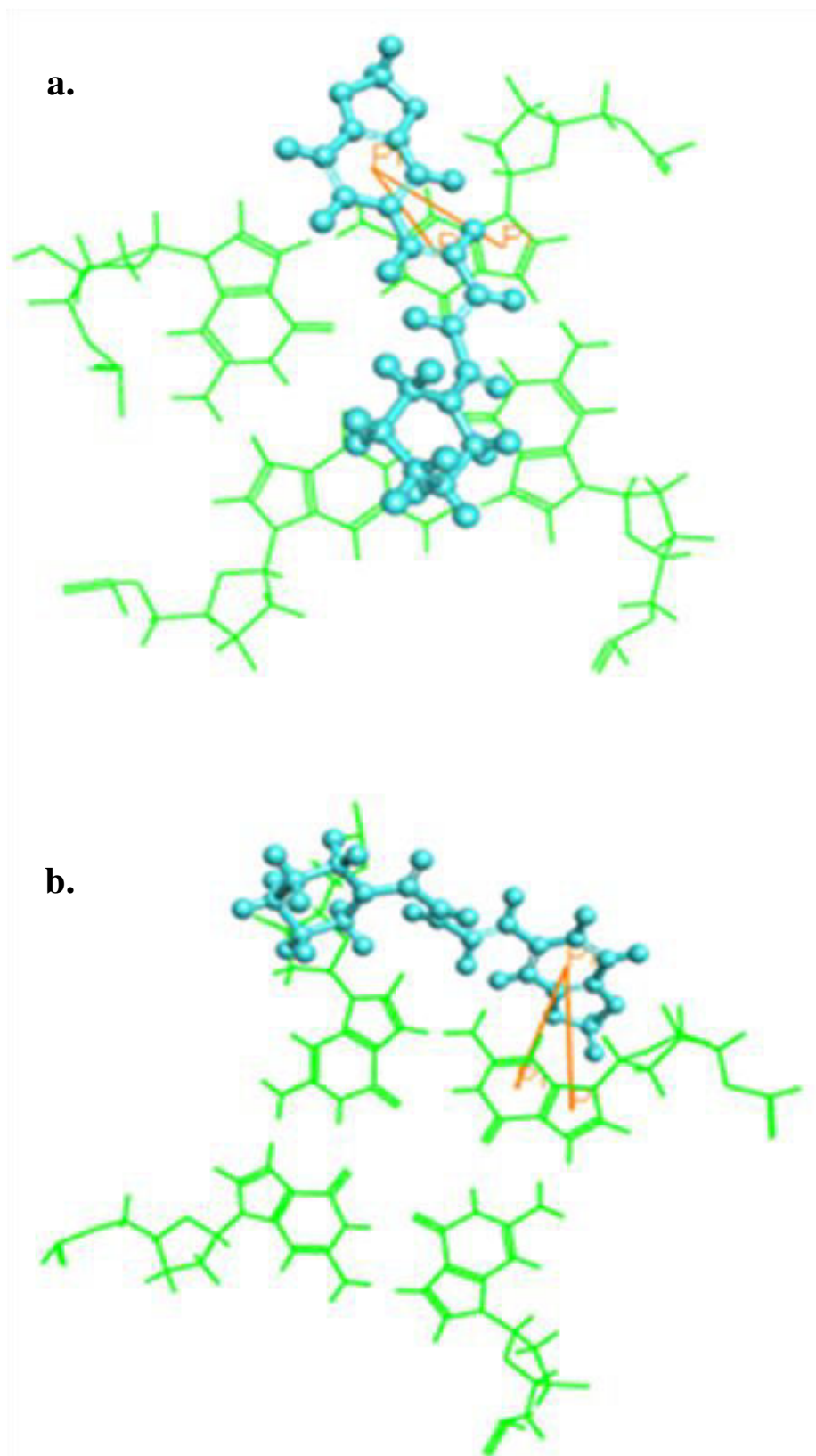


*Figure 5.14. Representation of docked structure of complex obtained from docking by Autodock 4.0 showing  $\pi$ - $\pi$  interactions (orange colored line) between Piperine (cyan) and G-tetrads (green) of Pu24T for both the sites (a) Top (b) Bottom.*

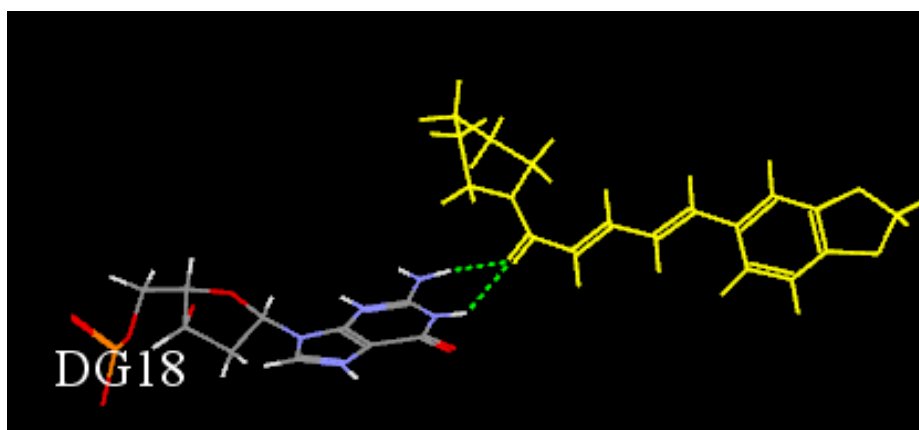


*Figure 5.15. Representation of hydrogen bond (green) formation between G18 nucleotide and Piperine molecule (Yellow) as obtained from molecular dynamic simulation studies.*

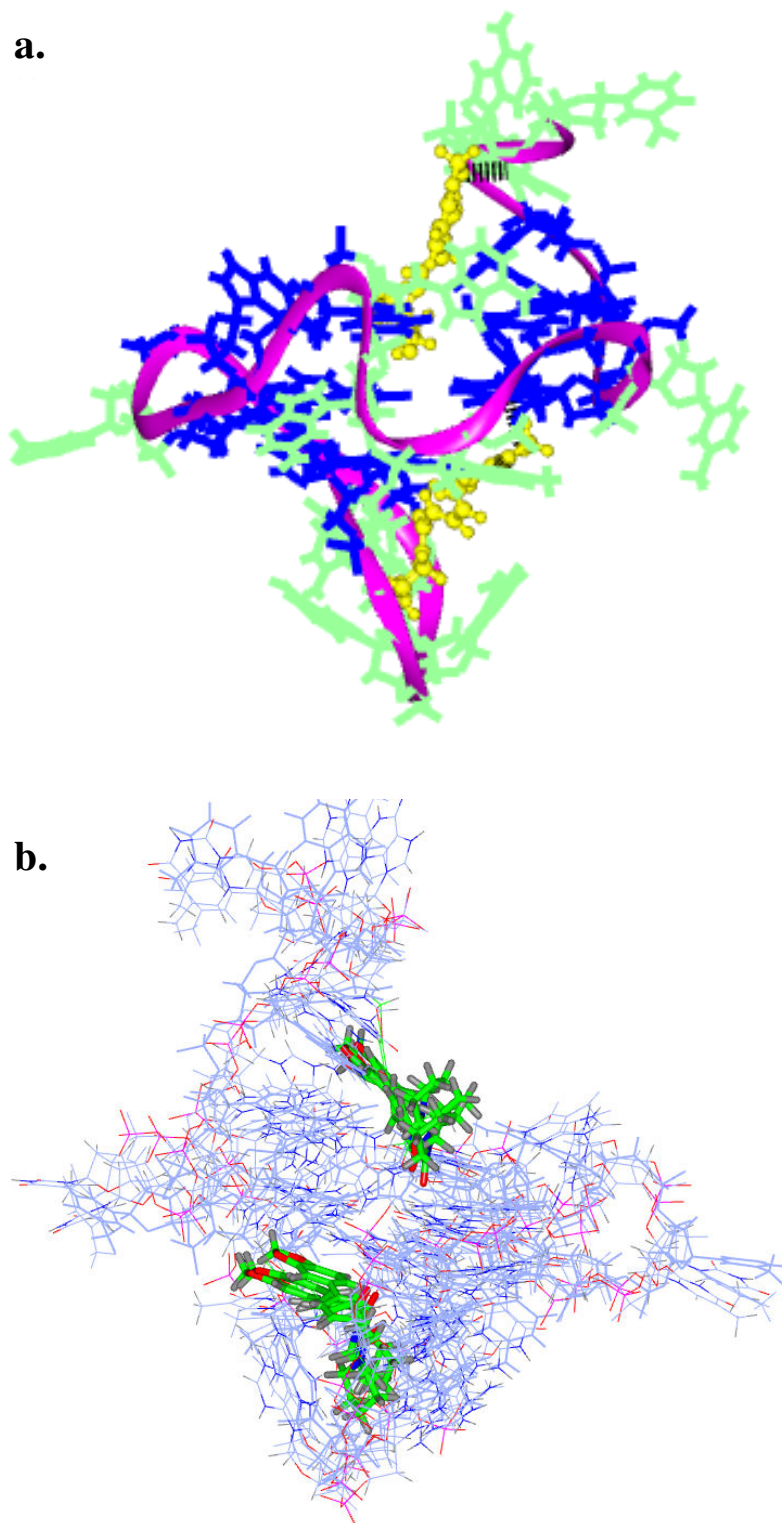


*Figure 5.16. (a) Lowest potential energy model of the complex obtained after molecular dynamic simulation. Black dashes showing hydrogen bond formed between Piperine (yellow) and Pu24T (G-tetrads are shown in blue color) (b) Ensemble of ten lowest energy structures after molecular dynamics simulation (Piperine: yellow color, Pu24T: ice blue color).*

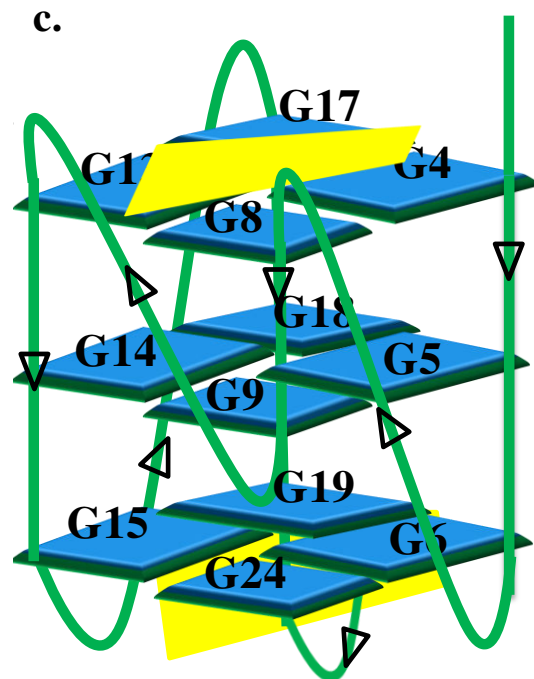


*Figure 5.16. (c) Schematic representation showing Piperine (yellow) stacking at the top G-tetrad and below the bottom G-tetrad of Pu24T DNA sequence forming G-quadruplex structure.*

also supported by hydrogen bond interaction for example, O9 of one of the Piperine molecule was hydrogen bonded with H22 of G18 base of Pu24T (Figure 5.15). The results of docking and simulation studies are in line with our experimental results that also suggest the Piperine binds to Pu24T at two sites that is at both the terminal G-tetrads and stabilizes the structure by formation of  $\pi$ - $\pi$  interactions and hydrogen bonding. Figure 5.16b shows the overlay of 10 lowest potential energy conformers obtained after unrestrained dynamic simulation. Figure 5.16c portrayed the schematic representation of model formed by Piperine - Pu24T-cmyc G-quadruplex DNA complex at D/N = 2.0.

It is always a requirement to assess the biological activity of drug; therefore Piperine's biological activity was also assessed as mentioned in next section.

## **5.2.6 Assessment of biological activity of Piperine**

### **5.2.6.1 Gel retardation assay**

In order to confirm the binding of Piperine to c-myc G-quadruplex DNA we have performed gel retardation assay. The formation of complex by binding of ligand to macromolecule will lead to retardation of its mobility on electrophoresis gel as compare to uncomplexed macromolecule. In our study, we have performed gel retardation assay by incubating 20  $\mu$ M of G-quadruplex DNA with increasing concentration of Piperine for 1hr at room temperature. We have observed retardation in the mobility of G-quadruplex DNA with the increasing concentration of Piperine. This observed shift in DNA bands corroborates the binding of Piperine to DNA and resulting in the formation of Piperine – DNA complex. This experiment was performed with all G-quadruplex DNA sequences used in this study and the maximum shift in mobility of DNA was observed for the complex formed between Pu24T DNA and Piperine followed by c-kit21 and then tel22 DNA (Figure 5.17). This result compliments the results obtained from biophysical analysis that suggests the highest affinity of Piperine for Pu24T DNA. The specificity of Piperine for G-quadruplex structure was also validated by performing this experiment with complimentary sequence of Pu24T DNA (5'-CCTTCCCCACCCTCACCACCCTCA-3') that does not form G-quadruplex structure. On incubating the same concentration of Piperine with this DNA sequence, no retardation in the mobility of DNA was observed that confirms the specificity of Piperine for G-quadruplex structure (Figure 5.18).

Further, we have performed DNA polymerase stop assay that confirms the stabilization of G-quadruplex structure formed by Pu24T DNA upon addition of Piperine as mentioned in next sub-section.

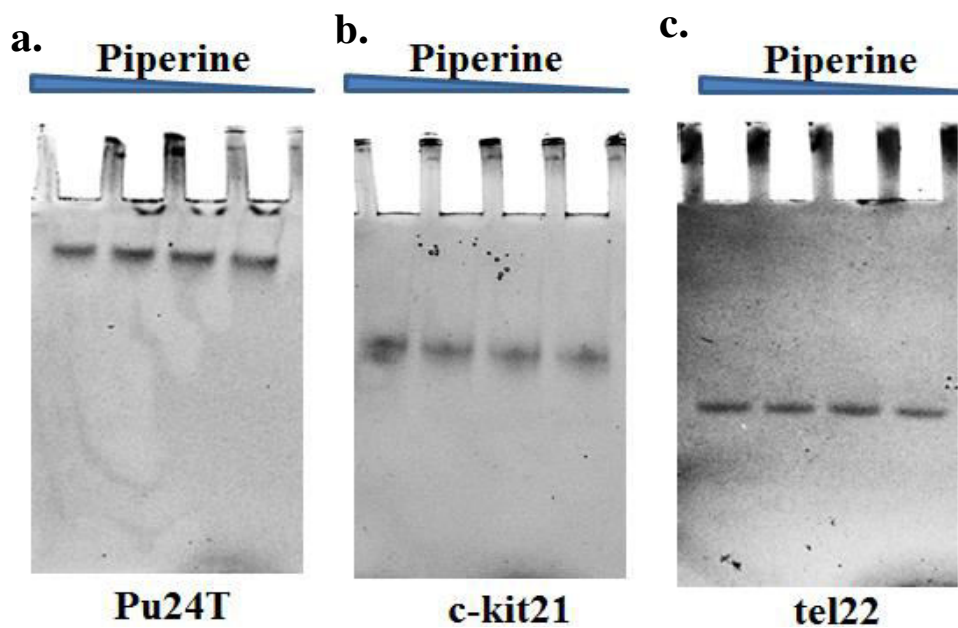


*Figure 5.17. Native PAGE image for gel retardation assay of (a) Pu24T (b) ckit21 DNA (c) tel22 G-quadruplex DNA incubated with increasing concentration of Piperine.*

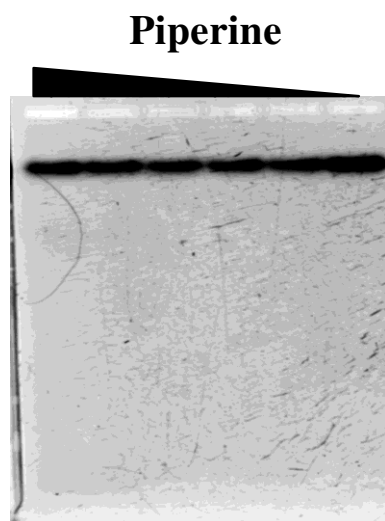


*Figure 5.18. Gel retardation assay of complimentary sequence of Pu24T that does not form G-quadruplex structure incubated with increasing concentration of Piperine. No significant shift in the mobility of DNA bands was observed.*

### 5.2.6.2 PCR stop assay

To amplify a DNA template, *Taq* Polymerase requires single stranded DNA. However, the presence of secondary structure in template DNA hinders its activity. G-rich sequences can also inhibit the process of DNA amplification by formation of stable intramolecular G-quadruplex structures. Ligands that stabilize G-quadruplex structure could lead to arrest of DNA synthesis process. In our study, we have utilized this principle to validate the stabilization of G-quadruplex structure by binding of Piperine. Pu24T DNA sequence was incubated with increasing concentration of Piperine and PCR is performed. A significant decrease in the intensity of PCR products were observed with increasing concentration of Piperine. This result indicates that Piperine stabilizes c-myc G-quadruplex DNA and thus blocks *Taq* Polymerase activity to amplify DNA (Figure 5.19).

Following this results, we have assessed the cytotoxic activity of Piperine on various cancer cell lines and explored its mechanism of action as described in next section.

### 5.2.7 Cytotoxic effects of Piperine on cancer cells

#### 5.2.7.1 Evaluation of apoptosis

In order to assess the cytotoxicity of Piperine in cancer cells, we have treated A549 cells with Piperine. It has been observed that Piperine induces concentration (Figure 5.20a) as well time-dependent (Figure 5.20b) apoptotic morphological changes in A549 cells. Cell counting data depicts reduced cell number, indicating anti-proliferative nature of molecule (Figure 5.20c-d). One of the major changes on the surface of apoptotic cells is the expression of phosphatidylserine (PS).<sup>[57]</sup> It is negatively charged phospholipid that is normally present in membrane leaflets on the cytosolic face. When cells undergo apoptosis, there is breaking of phospholipid asymmetry of their plasma membrane and they expose PS. Annexin V is a vascular protein that binds to phospholipids in a  $Ca_2^+$ -dependent way.<sup>[58-59]</sup> Annexin V preferentially binds to phospholipid species such as PS that are normally absent in the outer leaflet of plasma membrane but minimally binds to those that are constitutively present in the outer leaflet of plasma membrane such as phosphatidylcholine and sphingomyeline.<sup>[60]</sup> In early phase of apoptotic cell death when cell membrane remains intact, PS is translocate to the outer layer of the membrane.

Propidium iodide (PI) is a small fluorescent molecule that binds to DNA. It cannot passively cross the intact plasma membrane. PI uptake could be used to evaluate dead cells, in which plasma membranes become permeable. Thus, we evaluated the apoptotic response using Annexin V-FITC/PI labeling to characterize cytotoxicity profile of Piperine in A549

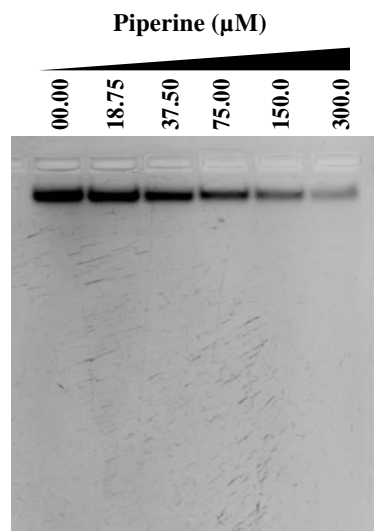


*Figure 5.19. PCR stop assay for Pu24T incubated with increasing concentration of Piperine.*

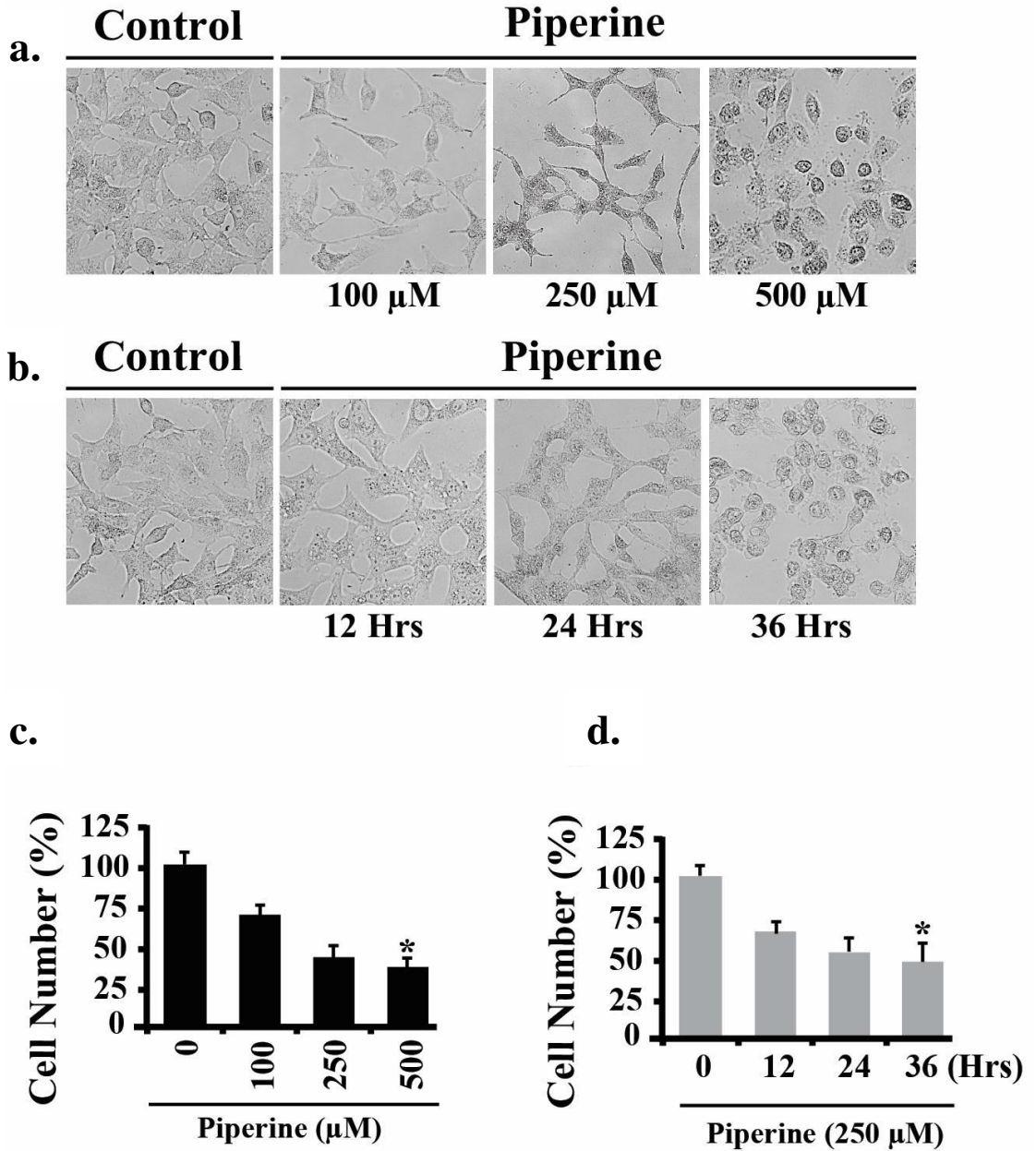


*Figure 5.20. (a-d) Exposure to Piperine results in reduced cell viability and apoptosis in A549 cells. (a-b) Bright field images for cells treated with Piperine in (a) concentration (b) time dependent manner. (c-d) Quantitative analysis of cell counting done using bright field images of cells treated with Piperine in (c) concentration (d) time dependent manner.*

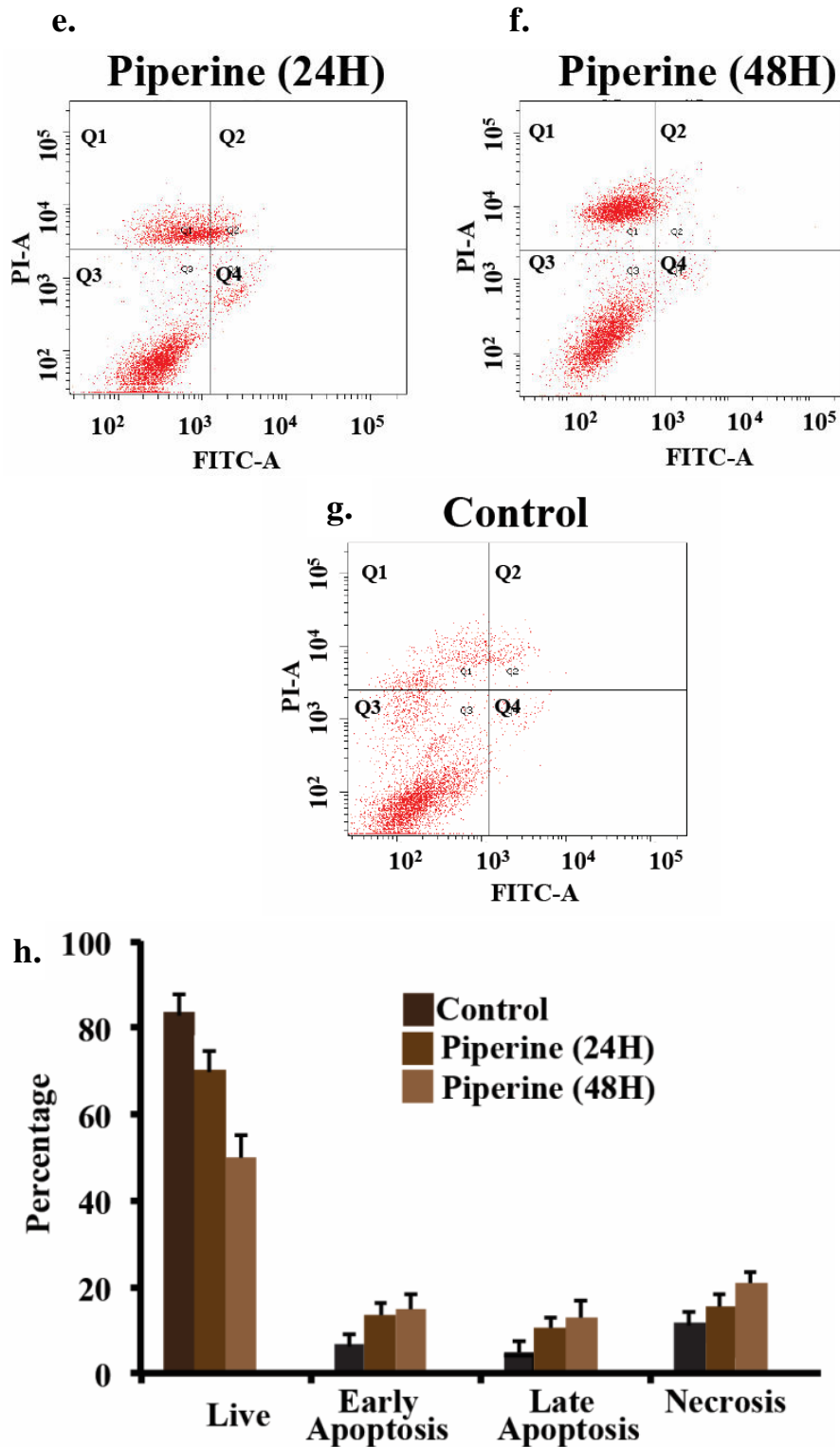


*Figure 5.20. (e-h) Apoptosis was assessed in A549 cells, by flow cytometry analysis, using Annexin V-FITC and Propidium Iodide double staining. Cells were treated with 250  $\mu$ M Piperine for (e) 24 hrs (f) 48 hrs (g) DMSO was used as control (h) Apoptosis analysis shown in bar graphs.*

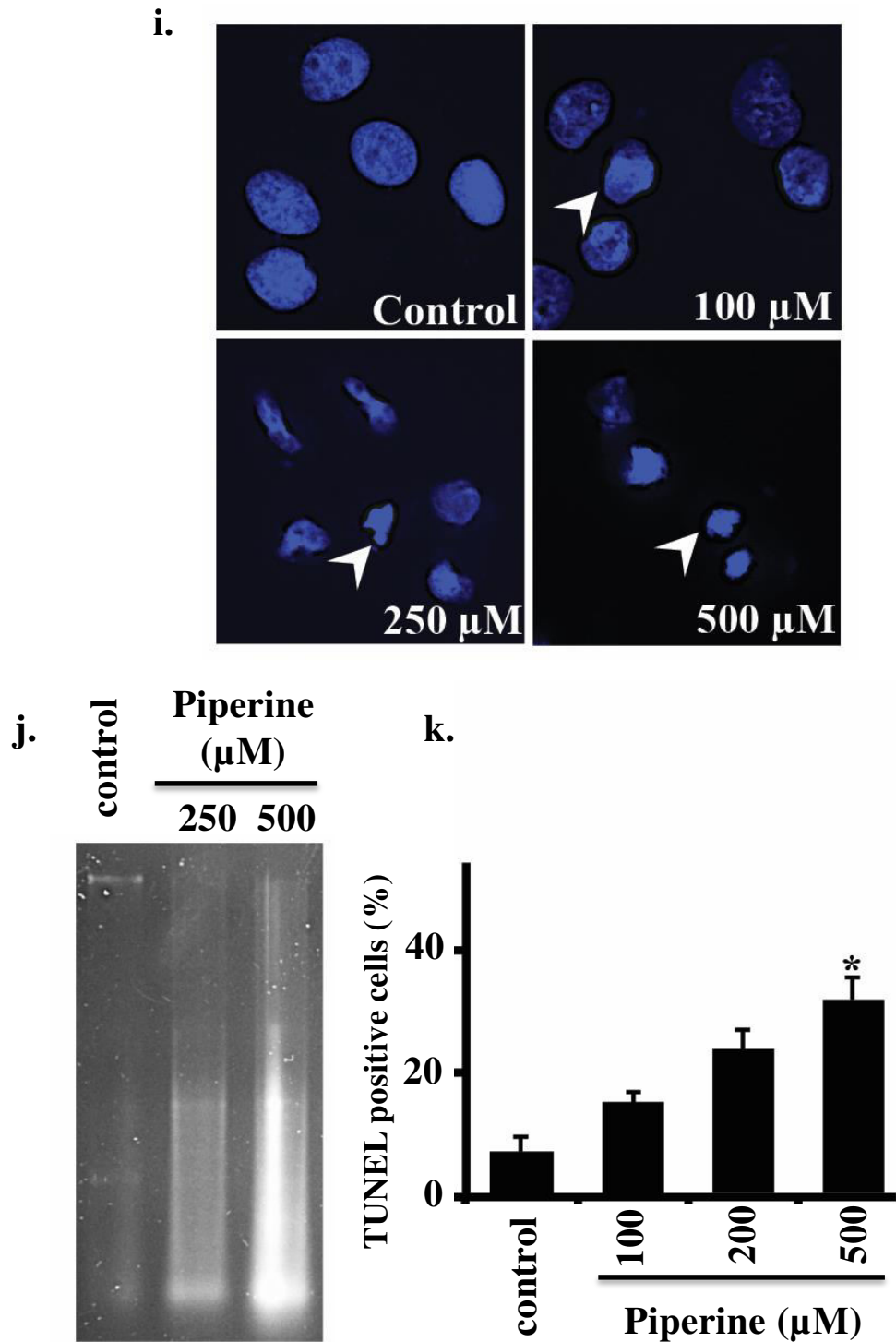


*Figure 5.20. (i-k) (i) Nuclear morphology of Piperine treated cells was observed using DAPI staining. (j-k) DNA fragmentation was assessed in Piperine treated cells as shown in agarose gel (j) TUNEL assay (k) DNA fragmentation confirmation*

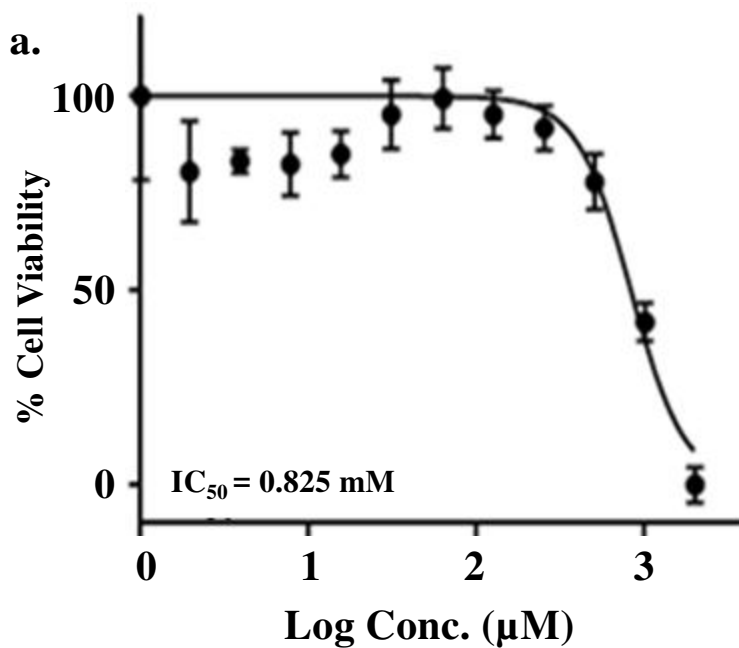


*Figure 5.21. (a) Cytotoxic effect of Piperine on MCF-7 cancer cell line. IC<sub>50</sub> value is mentioned at the bottom of plot.*

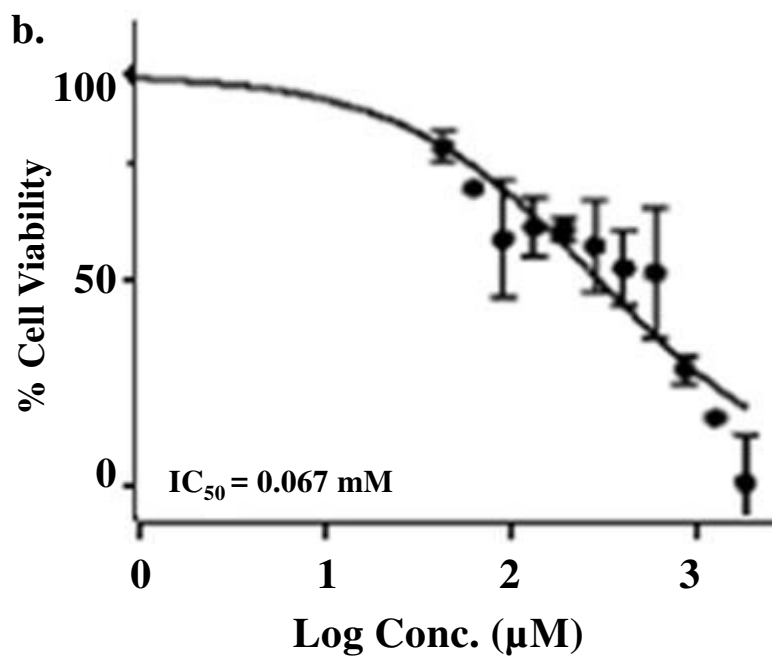


*Figure 5.21. (b) Cytotoxic effect of Piperine on PC3 cancer cell line. IC<sub>50</sub> value is mentioned at the bottom of plot.*

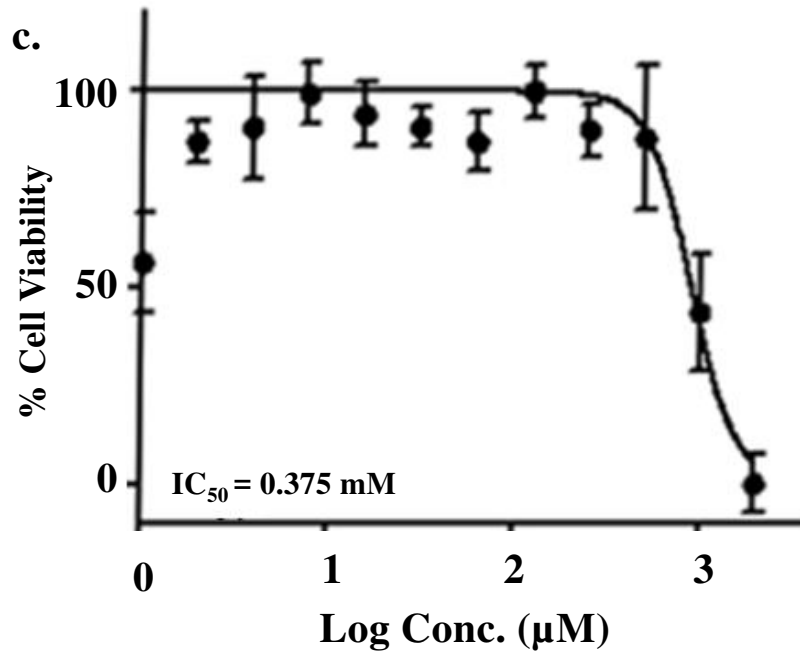


Figure 5.21. (c) Cytotoxic effect of Piperine on HepG2 cancer cell line.  $\text{IC}_{50}$  value is mentioned at the bottom of plot.

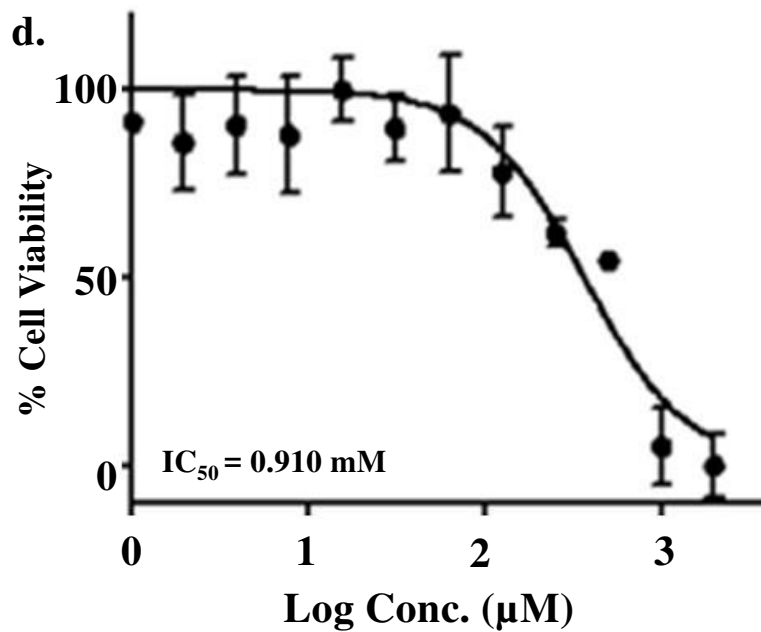


Figure 5.21. (d) Cytotoxic effect of Piperine on HeLa cancer cell line.  $\text{IC}_{50}$  value is mentioned at the bottom of plot.

cells. As shown in Figure 5.20 e-h, 250 $\mu$ M of Piperine results in gradual increase in cellular apoptosis in time dependent manner. Flow cytometric analysis of Annexin V stained cells resulted in increased apoptotic fraction in Piperine treated cells, as compared to control (Figure 5.20 e-h). As shown in Figure 5.20i, apoptotic characteristics, such as nuclear shrinkage and fragmentation, were observed in Piperine treated cells, when stained with DAPI. Further, DNA fragmentation (Figure 5.20j), an important apoptotic feature was confirmed by agarose gel electrophoresis and TUNEL analysis (Figure 5.20 k). This reduced cell number and apoptotic characteristics such as cytoplasmic and nuclear condensation, externalization of membrane phospholipid PS and DNA cleavage, were observed from various experiments on exposure of cells to Piperine.

In order to substantiate its cytotoxic effect on other cancer cell lines, we have performed MTT assay on HeLa, PC3, HepG2 and MCF-7 cell lines (Figure 5.21). We have found that Piperine shows concentration dependent cytotoxicity in all the cancerous cell lines used in this study that shows the potential of Piperine to inhibit various cancer cell growth.

#### **5.2.7.2 Semi- quantitative RT-PCR**

Reverse Transcription-Polymerase Chain Reaction (RT-PCR) is one of the sensitive and highly specific tools for the analysis of gene expression. This technique could be employed to compare relative or absolute levels of gene expression between control and treatment population. Therefore, we have also employed semi - quantitative RT-PCR to understand the effect of Piperine on down-regulation of *c-myc* gene (Figure 5.22). This will allow us to semi-quantitate the expression of *c-myc* gene relative to a constitutively expressed housekeeping gene,  $\beta$ -actin. As shown in Figure, a reduction in the level of *c-myc* mRNA in a dose-dependent manner (Figure 5.22) was observed and as it is clearly seen that  $\beta$ -actin mRNA is expressed likewise in both the control as well as in treated cells, thus, the reduction of mRNA level could be specific to *c-myc* gene.

### **5.3 Conclusion**

In this chapter, we have reported for the first time the binding of Piperine, a natural alkaloid, to various human G-quadruplex DNA sequences. We have probed this interaction of by employing various spectroscopic techniques like fluorescence, circular dichroism, UV-melting and NMR spectroscopy. Fluorescence titration data suggested that Piperine binds to all G-quadruplex DNA but shows highest affinity for G-quadruplex structure formed at *c-myc* promoter region (Pu24T). It also showed  $\sim 10^4$  folds specificity for G-quadruplex DNA

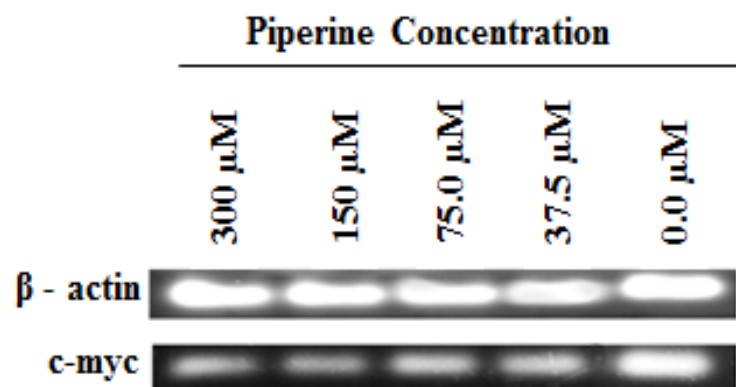


*Figure 5.22 Representative of semi-quantitative RT-PCR analysis.  $\beta$ -actin was used as internal control.*

over double stranded DNA. UV melting studies suggested that binding of Piperine stabilizes G-quadruplex structure that was further confirmed by CD titration experiment. Binding of Piperine does not causes perturbations in G-quadruplex structure even at D/N = 2.0 ratio. Induced CD band in absorption region of Piperine suggested the Piperine- Pu24T complex has strong binding interactions. Further, to know the solution structure of this complex, 1D and 2D NMR spectroscopy. Temperature dependent NMR titration data suggested the stabilization of Pu24T G-quadruplex upon binding of Piperine and supports our results of UV-meting and CD data. The addition of Piperine to Pu24T DNA causes perturbations in proton resonances of DNA particularly of those that were involved in formation of upper and lower G-tetrad. However, in 2D NMR experiment, we were unfortunate to find NOEs of interactions and we didn't have a conclusive NMR structure for the complex. Nevertheless, with the help of docking and molecular modelling studies, we proposed the model of Piperine - Pu24T complex. This model showed two different binding sites for Piperine are possible on Pu24T G-quadruplex structure. Of the both sites, the most privileged one is found to be located below the bottom G-tetrad, while the second site is above the upper G-tetrad. Piperine stacks at both of these sites via  $\pi$ - $\pi$  interactions and hydrogen bonds. Furthermore, in-vitro studies show that Piperine is cytotoxic to various cancer cells and causes apoptosis-mediated cell death. This first report on the interactions of Piperine with G-quadruplex DNA would encourage the studies for molecular aspects of its anti-cancer mechanism emphasizing its potential to down-regulate c-myc gene expression.

## 5.4 Methods

### 5.4.1 Reagents and cell lines

Piperine and other reagents used for buffer preparation such as NaCl, KCl, NaH<sub>2</sub>PO<sub>4</sub>, Na<sub>2</sub>HPO<sub>4</sub>, KH<sub>2</sub>PO<sub>4</sub> and K<sub>2</sub>HPO<sub>4</sub> (HPLC Grade) were purchased from Sigma Aldrich Chemicals Ltd. The solvents such as deuterium oxide, dimethyl sulphoxide (DMSO) were also procured from Sigma Aldrich Chemicals Ltd. All the reagents for PCR reaction like primers, dNTPs, *Taq* Polymerase was also obtained from Sigma Aldrich Chemicals Ltd.

Calf thymus DNA (CT-DNA), DNA sequence complimentary to Pu24T DNA: (d-5'-CCTTCCCCACCCTCACCACCCTCA-3') and the following three G-quadruplex DNA sequences:

cmyc: Pu24T(d-5'-TGAGGGTGGTGGAGGGTGGGGAAGG-3'),

tel22: (d-5'-AGGGTTAGGGTTAGGGTTAGGG-3'),

c-kit21: (d-5'-CGGGCGGGCGCGAGGAGGGG-3') were procured from Sigma Aldrich Chemicals Ltd., USA. Calf thymus DNA solution was prepared in the sodium phosphate buffer and its concentration was measured spectrophotometrically. For quadruplex formation, oligomers were dissolved in phosphate buffer (10 mM (K<sup>+</sup>), pH 7.0) with 50 mM KCl. The oligomer was annealed by heating at 90°C for 5 mins, followed by overnight incubation at room temperature to allow gradual cooling. All the biophysical experiments were performed in the above mentioned buffer otherwise stated separately.

Human lung cancer cell lines (A549), human prostate cancer cell lines (PC3), human liver cancer cell line (HepG2), Human cervical cancer cell line (HeLa) and human breast cancer cell lines (MCF-7) were purchased from National Centre for Cell Science (NCCS), Pune, India. Growth media like Dulbecco's modified Eagle's medium (DMEM), Ham's F12 medium, Minimum essential media Eagle (MEM) were purchased from Life Technologies (Gaithersburg, MD, USA). Cell culture reagents were purchased from Sigma. 4', 6-Diamidino-2-phenylindole (DAPI) was obtained from Life Technologies™. Phenol: Chloroform: Isoamyl alcohol mixture (25:24:1 v/v) was obtained from Himedia. DeadEnd™ fluorometric TUNEL system was obtained from Promega. FITC Annexin-V-Apoptosis Detection Kit I was purchased from BD Pharmingen™. Cells-to-cDNA™ II Kit (Ambion) was purchased from Invitrogen.

#### 5.4.2 Fluorescence titrations

Fluorescence titration experiment was performed on Synergy™ H1 multi-mode microplate reader using 96-well microplates at 25°C. The excitation and emission wavelengths for Piperine were obtained by performing its absorption and fluorescence scan diluted in potassium phosphate buffer. The readings were taken for Piperine: G-quadruplex DNA titration at emission wavelength of 486 nm when excited at the wavelength of 341 nm. Each sample was tested in duplicates in 75 µL reaction volume. 5-10 µM of G-quadruplex DNA and a final concentration of 100µM for CT-DNA were serially diluted; with the last well serve as blank (no DNA). Data were analyzed using SigmaPlot 12.0 software (Systat Software, Chicago, USA) according to the following equation that accounts for two receptor binding sites with two different affinities  $k_d1$  and  $k_d2$ :

$$f = \frac{B_{max1} \times abs(x)}{K_d1 \times abs(x)} + \frac{B_{max2} \times abs(x)}{K_d2 \times abs(x)} \quad (1)$$

$B_{max}$  = maximum number of binding sites.

$K_d$  = equilibrium binding constant.

### 5.4.3 Time-resolved fluorescence measurements

Time resolved fluorescence decays were collected on a Time-Correlated Single-Photon Counting (TCSPC) Spectrofluorometer (Horiba). A fixed wavelength Nano LED was used as the excitation source ( $k_{ex} = 375$  nm), and emission was detected at a different wavelength. The fluorescence emission of Piperine and its complex with G-quadruplex DNA were counted with a micro channel plate photo multiplier tube after passing through the monochromator and were further processed through a constant fraction discriminator (CFD), a time-to-amplitude converter (TAC) and a multi-channel analyser (MCA). The fluorescence decay was obtained and further analysed using DAS software, provided by FluoroLog-TCSPC instruments.

### 5.4.4 DNA thermal denaturation experiments

DNA denaturation experiments were carried out on a Perkin Elmer Lambda 35 spectrophotometer equipped with Peltier temperature programmer (PTP 6+6) and water Peltier system PCB-1500. Melting curves for DNA were collected at a heating rate of  $1^{\circ}\text{C}/\text{min}$ . in absence and presence of Piperine upto 2:1 Drug:DNA ratio. The normalized absorbance changes at 295 nm vs temperature were plotted.

### 5.4.5 Circular Dichroism

The Circular Dichroism (CD) experiment was performed on a J-815 Spectropolarimeter(JASCO) equipped with peltier junction temperature controller. A quartz cuvette with 0.2 cm path length was used to record the spectra of samples containing 20  $\mu\text{M}$  G-quadruplex and increasing concentrations of Piperine in 100 mM KCl, 10 mM phosphate buffer ( $\text{K}^+$ ) at pH 7.0. Spectra were recorded at 0.1 nm intervals from 200 nm to 350 nm with a 1 nm-slit width and averaged over three scans. Buffer CD spectra were subtracted from the CD spectra of DNA and the Drug-DNA complex.

### 5.4.6 Nuclear Magnetic Resonance

NMR experiments were conducted on AVANCE 500 MHz BioSpin International AG, Switzerland equipped with a 5 mm broad band inverse probe. NMR studies were performed in  $\text{H}_2\text{O} / \text{D}_2\text{O}$  solvent at 9:1 ratio. For Piperine titration experiment, Pu24T was added to 400 $\mu\text{M}$  Piperine solution upto D/N = 100:20 ratio and proton NMR spectra were collected at 298K for each titration step. For DNA titration experiment, 3.85mM of Pu24T-G-quadruplex DNA was prepared in 500  $\mu\text{L}$  potassium phosphate buffer and final concentration of Piperine

at D/N = 2.0 ratio was 7.7mM. NMR data were processed, integrated and analysed on Topspin (1.3 version) software. NMR samples were referenced with 3 - (Trimethylsilyl) propionic-2, 2, 3, 3-d<sub>4</sub> acid sodium salt (TSP).

#### 5.4.7 Docking and molecular dynamics simulation

The structure of G-quadruplex Pu24T (PDB code: 2MGN<sup>[61]</sup>) was taken as the starting model and the required replacements, addition of residues, optimization of G-quadruplex structure and Piperine structure using charm forcefield were performed on Discovery studio 3.5 The molecular docking studies were carried out on Autodock 4.0 in which G-quadruplex DNA was treated as rigid body. All the other parameters used were set to their default values. Pu24T and Piperine structures were converted to AD4 format files and Gasteiger charges were assigned to the atoms. The grid was set in such a manner that it covers complete DNA structure so that ligand can explore the whole conformational space. The Lamarckian genetic algorithm<sup>[62]</sup> was used for the search and the results were analyzed based on binding energy. For molecular dynamic (MD) simulation studies, the best conformation of Pu24T- Piperine complex obtained from docking studies was used as input. Second molecule of Piperine was placed manually in a way as obtained from docking studies. The complex was typed in charm forcefield<sup>[63]</sup> and solvated with periodic TIP3P<sup>[64]</sup> orthorhombic water box containing 2091 water molecules. This complex was first minimized then subjected to simulated annealing molecular dynamics by employing standard dynamic cascade. In this cascade, the system was heated to 700 K and equilibrated for 10ps under constant pressure. The production was done at 300 K for 100 ns in an NPT ensemble and long range electrostatics were treated with the Particle Mesh Ewald (PME) method<sup>[65]</sup> with a 14 Å cut-off radius counted the non-bonded distances. The SHAKE algorithm<sup>[66]</sup> was applied during the whole simulation runs in order to constrain the motion of Hydrogen bonds.

#### 5.4.8 Gel mobility shift assay

Gel mobility shift assay was performed by incubating 20µM G-quadruplex DNA with increasing concentrations of Piperine (0mM to 30.0mM) for 30 mins at room temperature. Products were resolved on 20% NATIVE polyacrylamide gel [29:1 acrylamide/bis(acrylamide)] prepared by polymerizing acrylamide in 1X TBE containing phosphate buffer (10 mM (K<sup>+</sup>), 50 mM KCl). Gel was visualized by EtBr staining and was analyzed on Image Quant LAS 4000 (GE Healthcare).

#### **5.4.9 Cell culture, DNA fragmentation, TUNEL assay, morphological evaluation and FACS analysis of apoptosis**

A549 cells were cultured in Dulbecco's modified Eagle's medium (Life Technologies, Gaithersburg, MD, USA), supplemented with 10% fetal bovine serum, 100 µg/ml streptomycin and 100 U/ml penicillin at 37 °C with 5 % CO<sub>2</sub> under incubator. Cells were seeded in different types of tissue culture plates and at a confluency of 60-70%, they were used for various experiments. For morphological evaluation of apoptosis, bright field images were taken of cells treated with different concentrations and for various time periods with Piperine. Dimethyl sulfoxide (DMSO) treatment was used as control. Following cell counting, to assess cell viability, above described experimental cells were mounted with DAPI for nuclear morphological analysis. DNA fragmentation was observed in Piperine treated cells using agarose gel electrophoresis and TUNEL staining. DNA was isolated from Piperine treated cells using phenol-chloroform method and TUNEL staining was performed as per manufacturer's instructions. For flow cytometric detection of apoptosis, cells were treated for different time periods with Piperine and stained with Annexin V-FITC and Propidium Iodide (PI), as per manufacturer's instruction. FACS data was collected using BD FACSAria™ III Cell-Sorting System (BD, Bioscience) and analysis was done with FACS Diva software (Becton Dickinson, USA). The cytotoxic effects of Piperine was also examined on other 04 cancer cell lines by performing MTT (3-(4, 5-dimethylthiazol-2-yl)-2, 5 diphenyltetrazolium bromide dye) assay. For semi-quantitative RT PCR analysis, PC3 cells were grown in 6-well tissue culture plates and at 60-70% confluency, cells were incubated with various concentrations (300.0, 150.0, 75.0 and 37.5µM) of Piperine for 24h at 37 °C in humidified 5% CO<sub>2</sub> incubator. Dimethyl sulfoxide (DMSO) treatment was used as control. Total RNA was prepared from treated and control cells and cDNA was prepared using Cells-to-cDNA™ II Kit (Ambion) according to the manufacturer's protocol. Reverse transcriptase reaction was performed on Mastercycler Nexus Gradient (Eppendorf). The thermal cycling condition was programmed as 45 min at 45°C, 10 min at 95°C for one single cycle. Semi – quantitative PCR was performed using gene specific primers with the following sequences:

c - MYC (forward): 5'-CTTCTCTCCGTCCTCGGATTCT- 3';  
c - MYC (reverse): 5'-GAAGGTGATCCAGACTCTGACCTT-3';  
β - actin (forward): 5'- GAGCTACGAGCTGCCTGAC-3';  
β - actin (reverse): 5'-AGCACTGTGTTGGCGTACAG-3'.

#### **5.5 References**

1. Sen D., Gilbert W. (1988), Formation of parallel four-stranded complexes by guanine-rich motifs in DNA and its implications for meiosis, *Nature*, 334, 364-366 (DOI: 10.1038/334364a0).
2. Huppert J.L., Balasubramanian S. (2005), Prevalence of quadruplexes in the human genome, *Nucleic Acids Res.*, 33, 2908-2916 (DOI: 10.1093/nar/gki609).
3. Wang Y., Patel D.J. (1993), Solution structure of the human telomeric repeat d[AG3(T2AG3)3] G-tetraplex, *Structure*, 1, 263-282 ((DOI: 10.1016/0969-2126(93)90015-9).
4. Yang D., Hurley L.H. (2006), Structure of the biologically relevant G-quadruplex in the c-MYC promoter, *Nucleosides Nucleotides Nucleic Acids*, 25, 951-968 (DOI: 10.1080/15257770600809913).
5. Maizels N. (2006), Dynamic roles for G4 DNA in the biology of eukaryotic cells, *Nat. Struct. Mol. Biol.*, 13, 1055-1059 (DOI: 10.1038/nsmb1171).
6. Zahler A.M., Williamson J.R., Cech T.R., Prescott D.M. (1991), Inhibition of telomerase by G-quartet DNA structures, *Nature*, 350, 718-720 (DOI: 10.1038/350718a0).
7. Shay J.W., Wright W.E. (2006), Telomerase therapeutics for cancer: challenges and new directions, *Nat. Rev. Drug. Discov.*, 5, 577-584 (DOI: 10.1038/nrd2081).
8. Siddiqui-Jain A., Grand C.L., Bearss D.J., Hurley L.H. (2002), Direct evidence for a G-quadruplex in a promoter region and its targeting with a small molecule to repress c-MYC transcription, *Proc. Natl. Acad. Sci. U. S. A.*, 99, 11593-11598 (DOI: 10.1073/pnas.182256799).
9. Rankin S., Reszka A.P., Huppert J., Zloh M., Parkinson G.N., Todd A.K., Ladame S., Balasubramanian S., Neidle S. (2005), Putative DNA Quadruplex Formation within the Human c-kit Oncogene, *J. Am. Chem. Soc.*, 127, 10584-10589 (DOI: 10.1021/ja050823u).
10. Dai J., Chen D., Jones R.A., Hurley L.H., Yang D. (2006), NMR solution structure of the major G-quadruplex structure formed in the human BCL2 promoter region, *Nucleic Acids Res.*, 34, 5133-5144 (DOI: 10.1093/nar/gkl610).
11. Sun D., Guo K., Rusche J.J., Hurley L.H. (2005), Facilitation of a structural transition in the polypurine/polypyrimidine tract within the proximal promoter region of the human VEGF gene by the presence of potassium and G-quadruplex-interactive agents, *Nucleic Acids Res.*, 33, 6070-6080 (DOI: 10.1093/nar/gki917).
12. Postel E.H., Mango S.E., Flint S.J. (1989), A nuclease-hypersensitive element of the human c-myc promoter interacts with a transcription initiation factor, *Mol. Cell. Biol.*, 9, 5123-5133 (DOI: 10.1128/mcb.9.11.5123).

13. Wiman K.G., Clarkson B., Hayday A.C., Saito H., Tonegawa S., Hayward W.S. (1984), Activation of a translocated c-myc gene: role of structural alterations in the upstream region, *Proc. Natl. Acad. Sci. U. S. A.*, 81, 6798-6802 (DOI: 10.1073/pnas.81.21.6798).
14. Mathad R.I., Hatzakis E., Dai J., Yang D. (2011), c-MYC promoter G-quadruplex formed at the 5'-end of NHE III1 element: insights into biological relevance and parallel-stranded G-quadruplex stability, *Nucleic Acids Res.*, 39, 9023-9033 (DOI: 10.1093/nar/gkr612).
15. Gonzalez V., Hurley L.H. (2010), The c-MYC NHE III(1): function and regulation, *Annu. Rev. Pharmacol. Toxicol.*, 50, 111-129 (DOI: 10.1146/annurev.pharmtox.48.113006.094649).
16. Ma D.-L., Chan D.S.-H., Fu W.-C., He H.-Z., Yang H., Yan S.-C., Leung C.-H. (2012), Discovery of a Natural Product-Like c-myc G-Quadruplex DNA Groove-Binder by Molecular Docking, *PLoS ONE*, 7, e43278 (DOI: 10.1371/journal.pone.0043278).
17. Wu P., Ma D.L., Leung C.H., Yan S.C., Zhu N., Abagyan R., Che C.M. (2009), Stabilization of G-quadruplex DNA with platinum(II) Schiff base complexes: luminescent probe and down-regulation of c-myc oncogene expression, *Chemistry*, 15, 13008-13021 (DOI: 10.1002/chem.200901943).
18. Ou T.M., Lu Y.J., Zhang C., Huang Z.S., Wang X.D., Tan J.H., Chen Y., Ma D.L., Wong K.Y., Tang J.C., Chan A.S., Gu L.Q. (2007), Stabilization of G-quadruplex DNA and down-regulation of oncogene c-myc by quindoline derivatives, *J. Med. Chem.*, 50, 1465-1474 (DOI: 10.1021/jm0610088).
19. Shirude P.S., Okumus B., Ying L., Ha T., Balasubramanian S. (2007), Single-Molecule Conformational Analysis of G-Quadruplex Formation in the Promoter DNA Duplex of the Proto-Oncogene C-Kit, *J. Am. Chem. Soc.*, 129, 7484-7485 (DOI: 10.1021/ja070497d).
20. Ashman L.K., Griffith R. (2013), Therapeutic targeting of c-KIT in cancer, *Expert. Opin. Investig. Drugs*, 22, 103-115 (DOI: 10.1517/13543784.2013.740010).
21. Tawani A., Kumar A. (2015), Structural Insight into the interaction of Flavonoids with Human Telomeric Sequence, *Sci. Rep.*, 5, 17574 (DOI: 10.1038/srep17574).
22. Pavan Kumar Y., Saha P., Saha D., Bessi I., Schwalbe H., Chowdhury S., Dash J. (2016), Fluorescent Dansyl-Guanosine Conjugates that Bind c-MYC Promoter G-Quadruplex and Downregulate c-MYC Expression, *Chembiochem*, 17, 388-393 (DOI: 10.1002/cbic.201500631).
23. Diveshkumar K.V., Sakrikar S., Rosu F., Harikrishna S., Gabelica V., Pradeepkumar P.I. (2016), Specific Stabilization of c-MYC and c-KIT G-Quadruplex DNA Structures by

- Indolylmethyleneindanone Scaffolds, *Biochemistry*, 55, 3571-3585 (DOI: 10.1021/acs.biochem.6b00120).
24. Srinivasan K. (2007), Black pepper and its pungent principle-piperine: a review of diverse physiological effects, *Crit. Rev. Food Sci. Nutr.*, 47, 735-748 (DOI: 10.1080/10408390601062054).
  25. Zarai Z., Boujelbene E., Ben Salem N., Gargouri Y., Sayari A. (2013), Antioxidant and antimicrobial activities of various solvent extracts, piperine and piperic acid from *Piper nigrum*, *LWT - Food Sci. Technol.*, 50, 634-641 (DOI: 10.1016/j.lwt.2012.07.036).
  26. Li S., Wang C., Li W., Koike K., Nikaido T., Wang M.W. (2007), Antidepressant-like effects of piperine and its derivative, antiepilepsirine, *J. Asian Nat. Prod. Res.*, 9, 421-430 (DOI: 10.1080/10286020500384302).
  27. Parmar V.S., Jain S.C., Bisht K.S., Jain R., Taneja P., Jha A., Tyagi O.D., Prasad A.K., Wengel J., Olsen C.E., Boll P.M. (1997), Phytochemistry of the genus *Piper*, *Phytochemistry*, 46, 597-673 (DOI: 10.1016/S0031-9422(97)00328-2).
  28. Mittal R., Gupta R.L. (2000), In vitro antioxidant activity of piperine, *Methods Find. Exp. Clin. Pharmacol.*, 22, 271-274 (DOI: 10.1358/mf.2000.22.5.796644).
  29. Shrivastava P., Vaibhav K., Tabassum R., Khan A., Ishrat T., Khan M.M., Ahmad A., Islam F., Safhi M.M., Islam F. (2013), Anti-apoptotic and anti-inflammatory effect of Piperine on 6-OHDA induced Parkinson's rat model, *J. Nutr. Biochem.*, 24, 680-687 (DOI: 10.1016/j.jnutbio.2012.03.018).
  30. Wadhwa S., Singhal S., Rawal S. (2014), Bioavailability Enhancement by Piperine: A Review, *Asian J. Biomed. Pharm. Sci.* 4, 1–8 (DOI: 10.15272/ajbps.v4i36.572 )
  31. Zutshi R.K., Singh R., Zutshi U., Johri R.K., Atal C.K. (1985), Influence of piperine on rifampicin blood levels in patients of pulmonary tuberculosis, *J. Assoc. Physicians India*, 33, 223-224.
  32. Johnson J.J., Nihal M., Siddiqui I.A., Scarlett C.O., Bailey H.H., Mukhtar H., Ahmad N. (2011), Enhancing the bioavailability of resveratrol by combining it with piperine, *Mol. Nutr. Food Res.*, 55, 1169-1176 (DOI: 10.1002/mnfr.201100117).
  33. Samuel M., Oliver S.V., Coetzee M., Brooke B.D. (2016), The larvicidal effects of black pepper (*Piper nigrum* L.) and piperine against insecticide resistant and susceptible strains of *Anopheles malaria* vector mosquitoes, *Parasit. Vectors*, 9, 238 (DOI: 10.1186/s13071-016-1521-6).
  34. Ferreira C., Soares D.C., Barreto-Junior C.B., Nascimento M.T., Freire-de-Lima L., Delorenzi J.C., Lima M.E., Atella G.C., Folly E., Carvalho T.M., Saraiva E.M., Pinto-da-

- Silva L.H. (2011), Leishmanicidal effects of piperine, its derivatives, and analogues on *Leishmania amazonensis*, *Phytochemistry*, 72, 2155-2164 (DOI: 10.1016/j.phytochem.2011.08.006).
35. Doucette C.D., Hilchie A.L., Liwski R., Hoskin D.W. (2013), Piperine, a dietary phytochemical, inhibits angiogenesis, *J. Nutr. Biochem.*, 24, 231-239 (DOI: 10.1016/j.jnutbio.2012.05.009).
36. Pradeep C.R., Kuttan G. (2004), Piperine is a potent inhibitor of nuclear factor-kappaB (NF-kappaB), c-Fos, CREB, ATF-2 and proinflammatory cytokine gene expression in B16F-10 melanoma cells, *Int. Immunopharmacol.*, 4, 1795-1803 (DOI: 10.1016/j.intimp.2004.08.005).
37. Zsila F., Hazai E., Sawyer L. (2005), Binding of the pepper alkaloid piperine to bovine beta-lactoglobulin: circular dichroism spectroscopy and molecular modeling study, *J. Agric. Food Chem.*, 53, 10179-10185 (DOI: 10.1021/jf051944g).
38. Zsila F., Matsunaga H., Bikádi Z., Haginaka J. (2006), Multiple ligand-binding properties of the lipocalin member chicken  $\alpha$ 1-acid glycoprotein studied by circular dichroism and electronic absorption spectroscopy: The essential role of the conserved tryptophan residue, *Biochim. Biophys. Acta*, 1760, 1248-1273 (DOI: 10.1016/j.bbagen.2006.04.006).
39. Suresh D.V., Mahesha H.G., Rao A.G., Srinivasan K. (2007), Binding of bioactive phytochemical piperine with human serum albumin: a spectrofluorometric study, *Biopolymers*, 86, 265-275 (DOI: 10.1002/bip.20735).
40. Haris P., Mary V., Haridas M., Sudarsanakumar C. (2015), Energetics, Thermodynamics, and Molecular Recognition of Piperine with DNA, *J. Chem. Inf. Model*, 55, 2644-2656 (DOI: 10.1021/acs.jcim.5b00514).
41. Balasubramanian S., Hurley L.H., Neidle S. (2011), Targeting G-quadruplexes in gene promoters: a novel anticancer strategy?, *Nat. Rev. Drug Discov.*, 10, 261-275 (DOI: 10.1038/nrd3428).
42. Monchaud D., Teulade-Fichou M.P. (2008), A hitchhiker's guide to G-quadruplex ligands, *Org. Biomol. Chem.*, 6, 627-636 (DOI: 10.1039/b714772b).
43. Koul S., Koul J.L., Taneja S.C., Dhar K.L., Jamwal D.S., Singh K., Reen R.K., Singh J. (2000), Structure-activity relationship of piperine and its synthetic analogues for their inhibitory potentials of rat hepatic microsomal constitutive and inducible cytochrome P450 activities, *Bioorg. Med. Chem.*, 8, 251-268 ([http://dx.doi.org/DOI: 10.1016/S0968-0896\(99\)00273-4](http://dx.doi.org/DOI: 10.1016/S0968-0896(99)00273-4)).

44. Wei C., Wang J., Zhang M. (2010), Spectroscopic study on the binding of porphyrins to (G(4)T(4)G(4))<sub>4</sub> parallel G-quadruplex, *Biophys. Chem.*, 148, 51-55 (DOI: 10.1016/j.bpc.2010.02.009).
45. Tysoe S.A., Morgan R.J., Baker A.D., Streckas T.C. (1993), Spectroscopic investigation of differential binding modes of .DELTA.- and .LAMBDA.-Ru(bpy)<sub>2</sub>(ppz)<sub>2</sub><sup>+</sup> with calf thymus DNA, *J. Phys. Chem.*, 97, 1707-1711 (DOI: 10.1021/j100110a038).
46. Islam M.M., Fujii S., Sato S., Okauchi T., Takenaka S. (2015), A Selective G-Quadruplex DNA-Stabilizing Ligand Based on a Cyclic Naphthalene Diimide Derivative, *Molecules*, 20, 10963-10979 (DOI: 10.3390/molecules200610963).
47. Phan A.T., Mergny J.L. (2002), Human telomeric DNA: G-quadruplex, i-motif and Watson-Crick double helix, *Nucleic Acids Res.*, 30, 4618-4625 (DOI: 10.1093/nar/gkf597).
48. Fernando H., Reszka A.P., Huppert J., Ladame S., Rankin S., Venkitaraman A.R., Neidle S., Balasubramanian S. (2006), A conserved quadruplex motif located in a transcription activation site of the human c-kit oncogene, *Biochemistry*, 45, 7854-7860 (DOI: 10.1021/bi0601510).
49. Katsuda Y., Sato S., Asano L., Morimura Y., Furuta T., Sugiyama H., Hagihara M., Uesugi M. (2016), A Small Molecule That Represses Translation of G-Quadruplex-Containing mRNA, *J. Am. Chem. Soc.*, 138, 9037-9040 (DOI: 10.1021/jacs.6b04506).
50. Chen X., Wang J., Jiang G., Zu G., Liu M., Zhou L., Pei R. (2016), The development of a light-up red-emitting fluorescent probe based on a G-quadruplex specific cyanine dye, *RSC Adv.*, 6, 70117-70123 (DOI: 10.1039/C6RA11152A).
51. Ambrus A., Chen D., Dai J., Bialis T., Jones R.A., Yang D. (2006), Human telomeric sequence forms a hybrid-type intramolecular G-quadruplex structure with mixed parallel/antiparallel strands in potassium solution, *Nucleic Acids Res.*, 34, 2723-2735 (DOI: 10.1093/nar/gkl348).
52. Zamiri B., Reddy K., Macgregor R.B., Pearson C.E. (2014), TMPyP4 Porphyrin Distorts RNA G-quadruplex Structures of the Disease-associated r(GGGGCC)<sub>n</sub> Repeat of the C9orf72 Gene and Blocks Interaction of RNA-binding Proteins, *J. Biol. Chem.*, 289, 4653-4659 (DOI: 10.1074/jbc.C113.502336).
53. Ranjan N., Andreasen K.F., Kumar S., Hyde-Volpe D., Arya D.P. (2010), Aminoglycoside binding to *Oxytricha nova* telomeric DNA, *Biochemistry*, 49, 9891-9903 (DOI: 10.1021/bi101517e).
54. Pagano B., Cosconati S., Gabelica V., Petraccone L., De Tito S., Marinelli L., La Pietra V., di Leva F.S., Lauri I., Trotta R., Novellino E., Giancola C., Randazzo A. (2012), State-

- of-the-art methodologies for the discovery and characterization of DNA G-quadruplex binders, *Curr. Pharm. Des.*, 18, 1880-1899 (DOI: 10.2174/138161212799958332).
55. Sabharwal N.C., Mendoza O., Nicoludis J.M., Ruan T., Mergny J.-L., Yatsunyk L.A. (2016), Investigation of the interactions between Pt(II) and Pd(II) derivatives of 5,10,15,20-tetrakis (N-methyl-4-pyridyl) porphyrin and G-quadruplex DNA, *J. Biol. Inorg. Chem.*, 21, 227-239 (DOI: 10.1007/s00775-015-1325-8).
56. Wuthrich K. (1986), NMR of Proteins and Nucleic Acids, Wiley, (ISBN: 978-0-471-82893-8).
57. Fadok V.A., Voelker D.R., Campbell P.A., Cohen J.J., Bratton D.L., Henson P.M. (1992), Exposure of phosphatidylserine on the surface of apoptotic lymphocytes triggers specific recognition and removal by macrophages, *J. Immunol.*, 148, 2207-2216.
58. Raynal P., Pollard H.B. (1994), Annexins: the problem of assessing the biological role for a gene family of multifunctional calcium- and phospholipid-binding proteins, *Biochim. Biophys. Acta*, 1197, 63-93 (DOI: 10.1016/0304-4157(94)90019-1).
59. Reutelingsperger C.P., Hornstra G., Hemker H.C. (1985), Isolation and partial purification of a novel anticoagulant from arteries of human umbilical cord, *Eur. J. Biochem.*, 151, 625-629 (DOI: 10.1111/j.1432-1033.1985.tb09150.x).
60. Andree H.A., Reutelingsperger C.P., Hauptmann R., Hemker H.C., Hermens W.T., Willems G.M. (1990), Binding of vascular anticoagulant alpha (VAC alpha) to planar phospholipid bilayers, *J. Biol. Chem.*, 265, 4923-4928.
61. Chung W.J., Heddi B., Hamon F., Teulade-Fichou M.P., Phan A.T. (2014), Solution structure of a G-quadruplex bound to the bisquinolinium compound Phen-DC(3), *Angew. Chem. Int. Ed.*, 53, 999-1002 (DOI: 10.1002/anie.201308063).
62. Morris G.M., Goodsell D.S., Halliday R.S., Huey R., Hart W.E., Belew R.K., Olson A.J. (1998), Automated docking using a Lamarckian genetic algorithm and an empirical binding free energy function, *J. Comput. Chem.*, 19, 1639-1662 (DOI: 10.1002/(SICI)1096-987X(19981115)19:14<1639::AID-JCC10>3.0.CO;2-B).
63. Brooks B.R., Brooks C.L., 3rd, Mackerell A.D., Jr., Nilsson L., Petrella R.J., Roux B., Won Y., Archontis G., Bartels C., Boresch S., Caflisch A., Caves L., Cui Q., Dinner A.R., Feig M., Fischer S., Gao J., Hodoscek M., Im W., Kuczera K., Lazaridis T., Ma J., Ovchinnikov V., Paci E., Pastor R.W., Post C.B., Pu J.Z., Schaefer M., Tidor B., Venable R.M., Woodcock H.L., Wu X., Yang W., York D.M., Karplus M. (2009), CHARMM: the biomolecular simulation program, *J. Comput. Chem.*, 30, 1545-1614 (DOI: 10.1002/jcc.21287).

64. Jorgensen W.L., Chandrasekhar J., Madura J.D., Impey R.W., Klein M.L. (1983), Comparison of simple potential functions for simulating liquid water, *J. Chem. Phys.*, 79, 926-935 (DOI: 10.1063/1.445869).
65. Darden T., York D., Pedersen L. (1993), Particle mesh Ewald: An N·log(N) method for Ewald sums in large systems, *J. Chem. Phys.*, 98, 10089-10092 (DOI: 10.1063/1.464397).
66. Ryckaert J.-P., Ciccotti G., Berendsen H.J.C. (1977), Numerical integration of the cartesian equations of motion of a system with constraints: molecular dynamics of n-alkanes, *J. Comput. Phys.*, 23, 327-341 (DOI: 10.1016/0021-9991(77)90098-5).



## Chapter 6

### Conclusions and Scope for future work

---

#### 6.1 Conclusions

In this thesis, we have studied G-quadruplexes structure forming DNA sequences found in human genome and explored their interaction with naturally available small molecules present in human diets. Appreciating the non-toxic effects of natural molecules and their potential role in providing beneficial effects to human health especially anti-cancer activity, we have explored their mechanism for exerting these effects to human cells via targeting G-quadruplex DNA and deduced the structural basis of these interactions.

Our first concern was to study the interaction of four flavonoids viz. Quercetin, Luteolin, Rutin and Genistein with human telomeric DNA sequence  $d(T_2AG_3T)_4$  forming G-quadruplex structure. In **chapter 3**, this interaction was explored by employing steady state and time resolved fluorescence titration studies and results suggested that Quercetin was the best candidate from a family of flavonoids. On one hand, it shows a highest affinity among other flavonoids used in study; on other hand it has high selectivity for G4 structure over duplex DNA. Further, we were interested to know how Quercetin binds to  $d(T_2AG_3T)_4$  DNA and confers stability to G-quadruplex structure. For this, we have employed NMR spectroscopy and simulation studies. With the help of 1D NMR and 2D NMR spectroscopy, all the protons of G-quadruplex DNA were assigned. NMR titration studies helped in calculating the structure of complex formed between Quercetin and  $d(T_2AG_3T)_4$  G-quadruplex DNA. The chemical shift perturbations allowed us to determine the binding sites of Quercetin on  $d(T_2AG_3T)_4$  DNA. We have observed 24 NOEs for H6, H8, H2' and H6' Quercetin protons with the base and sugar protons of the T1, T2 and T7 residues of  $d(T_2AG_3T)_4$  G-quadruplex DNA. With the obtained inter-molecular and intra-molecular NOEs, we have performed rMD simulations that suggested the intercalation of Quercetin chromophore at the T1/T2 or G6/T7 base step, which was stabilized by the stacking interactions. Temperature-dependent NMR studies clearly show that binding of Quercetin stabilizes the G-quadruplex structure. As observed at D/N = 0.0, the imino proton resonances start disappearing at 313 K and were completely lost at 323 K. However, at D/N = 2.0, these imino proton resonances can be seen upto 343 K. Stabilization of G-quadruplex structure was also determined by NOESY walk for the Quercetin –DNA complex in the NOESY spectra prove that the G-tetrad is intact and does not open to provide access to Quercetin. This result compliments the results of CD experiment in which we observed no changes when Quercetin

bound to DNA, even at D/N = 2:1 ratio. Furthermore, the stabilization of G-quadruplex structure was also evident by PCR stop assay. The observed decrease in the intensity of the PCR product with increasing concentration of Quercetin indicates that binding of Quercetin stabilize the biologically significant sequence of human telomeric DNA (Tel22) and blocks *Taq* polymerase activity of DNA amplification. This study highlights the structural aspects of the binding of flavonoids to G-quadruplexes formed by the human telomeric DNA sequence and also revealed the potential of flavonoids as useful candidates for anti-cancer therapeutics by regulating the telomeric G-quadruplex structure. The coordinates of the NMR model of the Quercetin and Tel7 complex have been deposited in the PDB as 2MS6.

Further, we wish to explore the potential of flavonoids for their interaction with other G-quadruplex DNA structures. Therefore, in **chapter 4**, we have extended my studies for the interaction of 09 flavonoids with biologically significant DNA sequence in *c-myc* promoter region forming G-quadruplex structure (Pu24T). In this study, steady state fluorescence titration studies and isothermal titration calorimetry studies were performed for the interaction of common dietary flavonoids, namely, Luteolin, Quercetin, Rutin, Genistein, Kaempferol, Puerarin, Hesperidin, Myricetin and Daidzein with Pu24T. The obtained results suggested that Quercetin was best candidate from family of flavonoids. On one hand, it shows a highest affinity among other flavonoids used in study; on other hand it has high specificity for G-quadruplex structure over duplex DNA. Moreover, Quercetin has high selectivity for Pu24T DNA over other G-quadruplex structures formed at different promoter regions of human genome. Using 1D and 2D NMR spectroscopy, proton of Pu24T G-quadruplex DNA were assigned and NMR titration studies helped in calculating the structure of complex formed between Quercetin and Pu24T. The perturbations in the resonances of Pu24T DNA upon addition of Quercetin allowed us to determine the sites of Quercetin binding Pu24T DNA. Further, we have observed 11 NOEs for H8 and H6' Quercetin protons with base, sugar and imino protons of guanine bases of Pu24T. Interestingly, these guanine residues take part in the formation of upper and bottom G-tetrad of Pu24T G-quadruplex DNA. Solution structure of this complex was deduced by performing rMD simulations studies that suggested the stacking of Quercetin at 5' and 3' G-tetrads of Pu24T G-quadruplex DNA structure and stabilize is structure via  $\pi$ - $\pi$  stacking. Stabilization of G-quadruplex structure upon binding of Quercetin was also confirmed by PCR stop assay that shows the inhibition of *Taq Polymerase* activity with increasing concentration of Quercetin. Further, the biological activity of Quercetin was assessed in HeLa cells that showed its subcellular

localization in nucleus. It inhibits the cell growth by inducing apoptosis and down-regulates c-myc gene expression in cancer cell. Our study provides favorable evidences for the interaction of Quercetin with c-myc G-quadruplex DNA and its stabilization upon binding; and revealed the potential of flavonoid, Quercetin, as suitable candidate for anti-cancer therapeutics by down regulating the c-myc gene expression. In this chapter we have reported the first solution structure for the Quercetin – Pu24T G-quadruplex DNA complex and the coordinates of the NMR model have been deposited in the PDB as 2N6C.

Apart from flavonoids, there are other groups of small molecules that are part of daily human diets and have been known for their anti-cancer activities, but till date their mechanism for exerting his effect have not been clear yet. One of such molecules is Piperine, a member of alkaloid family. Since several past decades, the potential of Piperine have been explored for providing beneficial effects to human health, yet its major cellular target is not known. In quest to discover this hidden mechanism, in **chapter 5**, we have probed the interaction of Piperine with various G-quadruplex DNA formed in human genome. Comprehensive biophysical studies suggested that Piperine showed specificity for G-quadruplex DNA over double stranded DNA, with highest affinity for G-quadruplex structure formed at c-myc promoter region (Pu24T). 1D and 2D NMR spectroscopy was performed to know the solution structure of Piperine- Pu24T complex. However, a few changes were observed in the imino and base regions but we could not assign them unambiguously due to overlapping peaks that renders difficulty for the distinction between the NOEs of ligand-ligand and ligand-Pu24T interactions. Thus, unfortunately, no NOEs of interactions were identified to get a decisive NMR structure for the complex. However, the docking studies showed that two different sites of binding sites are possible, the most privileged one is found to be located below the bottom G-tetrad having  $\pi$ - $\pi$  interactions with G6 base and second site is above the upper G-tetrad where Piperine was stacked by  $\pi$ - $\pi$  interactions with G17 base of Pu24T. Further, unrestrained molecular dynamic (MD) simulation studies for the obtained docked complex was performed and it gives a stable model for the Piperine - Pu24T complex in which each molecule of Piperine is located at both the terminal G-tetrads. Furthermore, in-vitro studies show that Piperine is cytotoxic to various cancer cells and causes apoptosis-mediated cell death. This first report on the interactions of Piperine with G-quadruplex DNA would encourage the studies for molecular aspects of its anti-cancer mechanism emphasizing its potential to down-regulate c-myc gene expression.

## 6.2 Future prospective

Increasing evidence has shown that DNA forming G-quadruplex structure play important role in biological processes and stabilization of these structures at telomere and various oncogenic promoter regions provides potential strategy as anticancer therapeutics. Although DNA sequences forming G-quadruplex structures have been targeted since several decades and the amount of research done in this field is impressive, yet not much have been explored for naturally available small molecules. In consideration to the beneficial effects of dietary small molecules of natural origin, some of them have been explored to interact and stabilize G-quadruplex structures. The research conducted in this thesis provides an in-depth investigation of the fundamental interactions of natural molecules with G-quadruplex DNA formed at various regions of human genome. This study provides solution structures for characterizing the novel binding interaction of small molecules and G-quadruplex structure and explored the mechanism of their anti- cancer effects. One of the major prospects to be addressed in future is a thorough understanding of the effect of these molecules on post transcriptional and translational modulations. This will be essential for validating and preceding this study for clinical translations of these natural ligands.

While targeting DNA G-quadruplex structures for anti-cancer therapeutics, there could also be other uses of these compounds. Apart from DNA, G-quadruplex structures are also known to be formed by RNA sequences. Literature has shown that transcribed RNA molecules adopt a stable secondary structure that determines the fate of RNA molecule. For example, secondary structures formed at 5' UTRs of mRNAs plays significant roles in post-transcriptional regulation of gene expression. Moreover, not only in human, G-quadruplex structures are also found in viruses. A very recent report suggested that G-quadruplex sequences found four of the conserved sequences of Zika virus are able to adopt stable, parallel- G-quadruplex structure and targeting this G-quadruplex with these molecules may provide a new approach for inhibiting viral replication. Additionally, as we have determined the stoichiometry of DNA- drug binding, this could be utilized for further designing and development of target specific drugs. This might be helpful in targeting various other diseases apart from cancer like neurodegenerative disease, bacterial, viral or parasitic diseases.